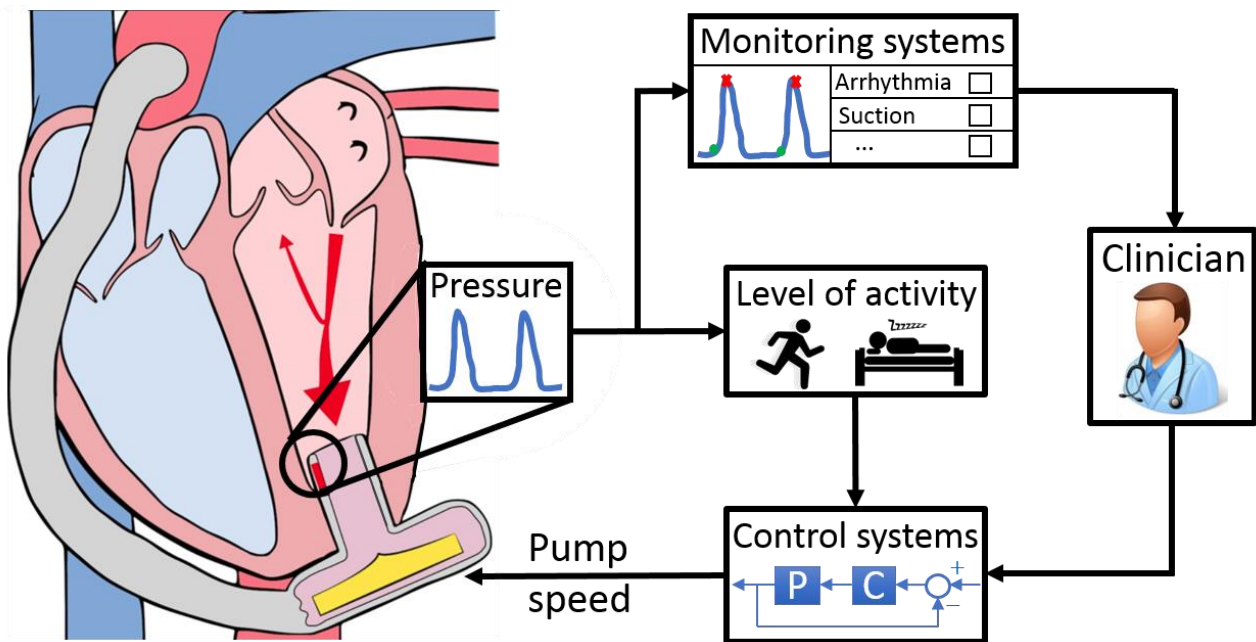


Diss. ETH No. 25148

Intelligent Rotary Blood Pumps with Physiological Response



Anastasios Petrou

2018

DISS. ETH No. 25148

**INTELLIGENT ROTARY BLOOD PUMPS
WITH PHYSIOLOGICAL RESPONSE**

A thesis submitted to attain the degree of

DOCTOR OF SCIENCES of ETH ZURICH
(Dr. sc. ETH Zurich)

presented by

Anastasios Petrou

MSc NTU Athens in Mechanical Engineering
born on 26.07.1991
citizen of
Greece

accepted on the recommendation of

Prof. Dr. Mirko Meboldt

Prof. Dr. med. Volkmar Falk

2018

Contents

ACKNOWLEDGEMENTS	V
ABSTRACT	VI
ZUSAMMENFASSUNG.....	VIII
NOMENCLATURE.....	X
1 INTRODUCTION	1
1.1 THE HEART FAILURE DISEASE	1
1.2 TREATMENT OPTIONS FOR HEART FAILURE.....	1
1.3 VENTRICULAR ASSIST DEVICES.....	2
1.3.1 <i>Evolution of the VAD technology</i>	2
1.3.2 <i>Promising outcomes of VAD therapy</i>	4
1.3.3 <i>Limitations of VAD therapy</i>	5
1.4 ZURICH HEART PROJECT	6
1.5 INTELLIGENT ROTARY BLOOD PUMPS.....	7
1.5.1 <i>Intuition for an intelligent rotary blood pump</i>	7
1.5.2 <i>Non-invasive monitoring and control approaches</i>	7
1.5.3 <i>Implantable sensors for VADs</i>	8
1.5.4 <i>Sensor-based monitoring and control approaches</i>	9
1.6 TESTING OF ALGORITHMS FOR BLOOD PUMPS	10
1.7 SCIENTIFIC CONTRIBUTION	10
2 A PHYSIOLOGICAL CONTROLLER FOR TVADS BASED ON SYSTOLIC LVP (PAPER I)	17
2.1 ABSTRACT	17
2.2 INTRODUCTION	17
2.3 MATERIALS AND METHODS	18
2.3.1 <i>Hybrid mock circulation</i>	18
2.3.2 <i>Systolic pressure as physiological index</i>	18
2.3.3 <i>Systolic pressure controller</i>	20
2.3.4 <i>Experiments</i>	21
2.4 RESULTS	23
2.4.1 <i>Baselines and nominal SP controller</i>	23
2.4.2 <i>Sensitivity of the SP controller on the controller parameters</i>	23
2.4.3 <i>Sensitivity of the SP controller on the contractility</i>	26
2.4.4 <i>Sensitivity of the SP controller on pressure sensor drift</i>	26
2.5 DISCUSSION.....	27
2.6 CONCLUSION	29
3 STANDARDIZED COMPARISON OF PHYSIOLOGICAL CONTROLLERS (PAPER II)	31
3.1 ABSTRACT	31
3.2 INTRODUCTION	31
3.3 MATERIALS AND METHODS.....	32
3.3.1 <i>Hybrid mock circulation</i>	32
3.3.2 <i>Selection of physiological controllers</i>	32
3.3.3 <i>Tuning process</i>	34
3.3.4 <i>Experiments</i>	34
3.3.5 <i>Evaluation</i>	35
3.4 RESULTS	37
3.5 DISCUSSION.....	41
3.6 CONCLUSION	43
3.7 ELECTRONIC MATERIAL.....	43

3.7.1	<i>Materials and Methods</i>	43
3.7.2	<i>Results</i>	45
4	IN VIVO EVALUATION OF PHYSIOLOGIC CONTROL ALGORITHMS FOR LVADS BASED ON LVV OR LVP (PAPER III)	51
4.1	ABSTRACT	51
4.2	INTRODUCTION	51
4.3	MATERIALS AND METHODS	52
4.3.1	<i>Anesthesia protocol</i>	52
4.3.2	<i>Surgical procedure</i>	52
4.3.3	<i>Physiologic controllers</i>	53
4.3.4	<i>Experiments</i>	54
4.3.5	<i>Data recording and extraction</i>	55
4.3.6	<i>Statistical analysis</i>	56
4.4	RESULTS	56
4.4.1	<i>Qualitative analysis of preload reduction</i>	56
4.4.2	<i>Hemodynamics during preload reduction</i>	56
4.4.3	<i>Statistical analysis of pump speed and pump flow</i>	57
4.4.4	<i>Preload sensitivity</i>	58
4.4.5	<i>Ventricular suction</i>	59
4.5	DISCUSSION	59
4.6	LIMITATIONS	61
4.7	CONCLUSION	61
5	RESPONSE OF A PHYSIOLOGICAL CONTROLLER FOR VADS DURING ACUTE PATHOPHYSIOLOGICAL EVENTS (PAPER IV)	63
5.1	ABSTRACT	63
5.2	INTRODUCTION	63
5.3	MATERIALS AND METHODS	64
5.3.1	<i>Hybrid mock circulation</i>	64
5.3.2	<i>Hemodynamic influence of intrathoracic pressure variations and arrhythmia</i>	65
5.3.3	<i>Extension of the numerical model</i>	66
5.3.4	<i>Simulation of Valsalva maneuver</i>	67
5.3.5	<i>Simulation of arrhythmia</i>	67
5.3.6	<i>Experiments</i>	67
5.3.7	<i>Pump control configurations</i>	68
5.4	RESULTS	68
5.5	DISCUSSION	72
6	COMPARISON OF LVAD FLOW ESTIMATORS (PAPER V)	75
6.1	ABSTRACT	75
6.2	INTRODUCTION	75
6.3	MATERIALS AND METHODS	76
6.3.1	<i>Pump flow estimators</i>	76
6.3.2	<i>Hybrid mock circulation</i>	79
6.3.3	<i>Dataset for parameter identification</i>	79
6.4	RESULTS	82
6.5	DISCUSSION	86
7	VISCOSITY PREDICTION IN A PHYSIOLOGICALLY CONTROLLED VAD (PAPER VI)	89
7.1	ABSTRACT	89
7.2	INTRODUCTION	89
7.3	MATERIALS AND METHODS	90
7.3.1	<i>Overview</i>	90

7.3.2	<i>Experiments on a hybrid mock circulation</i>	92
7.3.3	<i>Dataset generation</i>	92
7.3.4	<i>Model development process</i>	93
7.3.5	<i>Final Model</i>	94
7.4	RESULTS.....	95
7.4.1	<i>Models with Gaussian process</i>	95
7.4.2	<i>Final model: Stacked generalization with multi-scope models</i>	96
7.5	DISCUSSION.....	98
7.6	CONCLUSION.....	99
7.7	CORRIGENDUM:.....	99
8	A NOVEL MULTI-OBJECTIVE PHYSIOLOGICAL CONTROL SYSTEM FOR ROTARY LVADS (PAPER VII)	101
8.1	ABSTRACT.....	101
8.2	INTRODUCTION.....	101
8.3	MATERIALS AND METHODS.....	102
8.3.1	<i>Hybrid mock circulation</i>	102
8.3.2	<i>Experiments</i>	103
8.3.3	<i>Overview of control system</i>	103
8.3.4	<i>C1. Signal processing</i>	104
8.3.5	<i>C2. Estimators</i>	105
8.3.6	<i>C3. Controllers</i>	105
8.3.7	<i>Prioritization of the controllers</i>	107
8.4	RESULTS.....	108
8.4.1	<i>Signal processing (C1) and estimators (C2)</i>	108
8.4.2	<i>Control system</i>	108
8.5	DISCUSSION.....	112
8.5.1	<i>Limitations</i>	114
8.6	CONCLUSION.....	114
9	A VERSATILE HMC FOR HYDRAULIC INVESTIGATIONS OF CARDIOVASCULAR IMPLANTS (PAPER VIII)	115
9.1	ABSTRACT.....	115
9.2	INTRODUCTION.....	115
9.3	MATERIALS AND METHODS.....	116
9.3.1	<i>Hardware</i>	116
9.3.2	<i>Software</i>	117
9.3.3	<i>Active cardiovascular implant</i>	117
9.3.4	<i>Test case 1: BiVAD support during aortic valve insufficiency</i>	118
9.3.5	<i>Test case 2: TAH-configuration support during increase of the pulmonary vascular resistance</i>	119
9.3.6	<i>Test case 3: TCPC flow distribution during rest and exercise</i>	120
9.4	RESULTS.....	120
9.4.1	<i>Test case 1: BiVAD support during aortic valve insufficiency</i>	120
9.4.2	<i>Test case 2: TAH-configuration support during increase of the pulmonary vascular resistance</i>	121
9.4.3	<i>Test case 3: TCPC flow distribution during rest and exercise</i>	122
9.5	DISCUSSION.....	123
9.5.1	<i>Limitations</i>	124
9.6	CONCLUSION.....	125
10	CONCLUSION AND OUTLOOK	127
10.1	CONCLUSION.....	127
10.2	OUTLOOK.....	129
	REFERENCES.....	131

CURRICULUM VITAE143

Acknowledgements

This thesis constitutes the outcome of the research conducted within the Zurich Heart Project. The Zurich Heart Project is an interdisciplinary project among ETH Zurich, University Hospital Zurich and German Heart Institute Berlin. The part of my research was funded by Stavros Niarchos Foundation. Thus, I am grateful to the initiators of this project and my funding organization for making it possible for me to conduct my research in a very interesting topic and under exceptional conditions. Of course, special thanks for this go to my Professor Mirko Meboldt for accepting me in his group and providing me his consultancy and the freedom to develop my ideas. I would also like to thank my co-examiner and leader of the Zurich Heart Project, Professor Volkmar Falk, for accepting to be my co-examiner and his continuous valuable feedback during the meetings of the Zurich Heart team.

Next, I would like to express my gratitude to my predecessors in this research field, Dr. Gregor Ochsner and Dr. Raffael Amacher for introducing me into the topic and transferring me a great amount of knowledge. Their exceptional research was my inspiration and offered a very solid basis to build up my own research. The daily interaction with Dr. Ochsner also helped me substantially to shape and evolve my character.

Many thanks go to my colleagues in the Biomedical group of Product Development Group Zurich. Particularly, to my group leader Dr. Marianne Schmid Daners for her continuous support with the projects and the manuscripts and for the fact that she was continuously ensuring that I stay focused on my research. Also, to my office mates Martin Batliner, Stefan Boës and Seraina Dual for all the good moments we spent together and for making the working hours even more joyful. We conducted many fruitful discussions which helped my way of thinking and collaborated in several projects with great communication.

I owe my thanks to Dr. Marcus Granegger for all the interesting discussions, his valuable feedback and for broadening my horizons in the field of ventricular assist devices. I also want to thank my close collaborators from other institutes: Dr. Panagiotis Pergantis from German Heart Institute Berlin, Nicholas Cohrs from Functional Material Laboratory of ETH Zurich, and Dominik Siallagan from the Children's National Medical Center of Washington, DC, for the fruitful collaborations and the manuscripts we wrote together.

I also wish to thank all my students for teaching me so much during our interaction and for supporting the results of this thesis. Especially, Marcial Monn, Menelaos Kanakis, Jongseok Lee, Daniel Kuster, and Luca Arpagaus who had major contributions in some of the published studies. Also, thanks to Sara Mettler and Dario Fenner for their technical support in the development of the testbench and to Ms. Brigitte Rohrbach for the valuable contributions with the revision of the manuscripts as well as Dr. Bente Thamsen for the critical revision of parts of the current thesis.

Finally, special thanks go to my family and my girlfriend for providing me with psychological support during this work and for helping me sustain a good work-life balance.

Abstract

Ventricular assist devices (VADs) have been established as a viable treatment for heart failure and are currently used as an alternative to heart transplantation. More than 6,000 VADs are implanted every year, 95% of which are rotary VADs. A main disadvantage of the rotary VADs is that they operate at constant speed. Thus, they do not adapt to the varying perfusion requirements of the VAD patients. That may lead to critical conditions, such as ventricular suction or overload due to over- and underpumping, respectively, which in turn may result in severe, life-threatening complications, such as right heart failure or arrhythmia. Furthermore, not only the lack of continuous pump-speed control but also the non-existing monitoring of hemodynamics prevent the clinicians from applying and adapting the desired therapeutic protocol continuously.

The Zurich Heart Project envisions the development of a blood pressure sensor, which will be integrated at the pump inlet cannula, to provide a continuous measurement of the ventricular pressure. The goal of the current thesis was to develop and evaluate control and monitoring algorithms that only rely on such a pump inlet pressure (PIP) sensor to meet various objectives and reduce the complications occurring during VAD therapy. For this purpose, a novel multi-objective, physiological control system for a rotary left VAD (LVAD) was developed and evaluated within this thesis.

The aim of such a system was to meet the following control and monitoring objectives: (1) Physiological pump flow adaptation to the varying perfusion requirements. (2) Aortic valve (AV) opening for a predefined time to prevent AV insufficiency, while controlling the level of LVAD support (partial vs full). (3) Augmentation of the aortic pulse pressure to achieve a better LV washout. (4) Safe operation such that LV suction, overload, and pump backflow are prevented. (5) Monitoring of the LV pre- and afterload conditions as well as the cardiac rhythm to enable a better supervision of the therapy by the clinicians. Objectives (2), (3) and (5) were implemented and evaluated within one study (Paper VII), while objectives (1) and (4) required extensive investigations leading to six different studies (Papers I-VI).

To meet objective (1), a new pump-flow-adaptation controller for LVADs was developed (Paper I). The controller relied on the systolic pressure (SP) at the pump inlet to determine the varying perfusion requirements, thus named as SP controller. Its performance was evaluated experimentally and compared with the clinical standard of the constant speed (CS) operation, as well as with another five of the most promising pump-flow-adaptation controllers presented in literature (Paper II). Cardiovascular conditions with varying physiological requirements and LV contractility were simulated on a hybrid mock circulation (HMC), while a simulated pressure sensor drift was implemented. All controllers, including the SP controller, presented a greater preload sensitivity than the CS operation, thus imitating the response of a physiological circulation. The SP controller showed high sensitivity to contractility, but also high robustness against sensor drift, while over- and underpumping events were eliminated.

To validate the pump-flow-adaptation controllers under more realistic conditions, eight acute animal experiments were conducted (Paper III). The SP controller and an earlier presented volume-based controller, named preload-responsive speed (PRS) controller, were evaluated and compared with the CS operation. The potential of these pump-flow-adaptation controllers to reduce suction events and increase perfusion during increased preload in a clinical setting was validated. Thus, the SP controller or a preload-based, i.e., based on end-diastolic pressure can be used to meet objective (1).

The in-vivo experiments showed that pump-flow-adaptation controllers alone might not be sufficient to fully eliminate critical flow conditions. That finding was validated in vitro by simulating acute pathophysiological events, such as Valsalva maneuver and premature ventricular contractions (Paper IV). For this purpose, suction and overload detection and release controllers were developed (Paper VII) to meet objective (4) of the multi-objective control system. To prevent pump backflow events, the signal of pump flow had to be estimated to provide an input for the backflow controller.

A new pump flow estimator was developed, which constitutes a modification of an existing approach (Paper V). A systematic comparison study with in-vitro and in-vivo experiments supported the development of this approach, which improved the performance of the estimator in negative flows. To further improve the reliability of the estimator, a novel machine learning model to accurately and continuously predict the viscosity during VAD support of a pathological circulation based on the pump inlet pressure and pump-intrinsic signals

was developed (Paper VI). Such a model also promises the early detection of possible bleeding or pump thrombosis events, which are directly related to the blood viscosity, thus enhancing the patient monitoring.

Having developed and validated algorithms to meet objectives (1) and (4), the final multi-objective control and monitoring system was realized (Paper VII). Features from the PIP were extracted to classify the opening status of the AV with a machine learning model (objective (2)). The EDP, the mean aortic pressure (MAP) and the SP per beat were detected to fulfill objective (5). A sinusoidal speed modulation synchronized to the heartbeat was implemented to meet objective (3). In-vitro experiments proved the high preload sensitivity of the control system, while regulating the opening time of the aortic valve, thus controlling the loading of the LV. A threefold increase in the aortic pulse pressure was achieved compared to a CS operation, while preventing critical flow conditions. Thus, the required objectives were met by harmonically combining various controllers.

Finally, a new HMC was developed, to investigate the potential of physiological control for biventricular assist device (BiVAD) and total artificial heart (TAH) support cases (Paper VIII) and compare them with the CS operation. Critical conditions were prevented only with physiological control, and future implementation of the multi-objective control system developed also for BiVAD cases should be considered. Such a multi-objective control system gives the clinicians the possibility to apply personalized therapeutic protocols and to better supervise of the progress of the therapy. Thus, the risk of myocardial atrophy may be reduced, as well as the adverse events that occur due to wrong speed settings. Future in-vivo studies should be conducted to investigate the robustness of the system and to prove the potential promised.

Zusammenfassung

Herzpumpe (Ventricular Assist Devices, VADs) haben sich als praktikable Therapie bei Herzinsuffizienz etabliert und werden derzeit als Alternative zur Herztransplantation eingesetzt. Jährlich werden mehr als 6.000 VADs implantiert, von denen 95% rotative VADs sind. Ein wesentlicher Nachteil der Rotor-basierenden VADs ist, dass sie mit konstanter Drehzahl betrieben werden. Sie passen sich somit nicht an die unterschiedlichen Perfusionsanforderungen der VAD-Patienten an. Das kann zu kritischen Zuständen führen, wie z.B. Ventrikelsaugen oder Überlastung durch Über- bzw. Unterpumpen, was wiederum zu schweren, lebensbedrohlichen Komplikationen wie rechtsventrikuläre Insuffizienz oder Arrhythmie führen kann. Darüber hinaus verhindern nicht nur die fehlende kontinuierliche Pumpendrehzahlregelung, sondern auch die fehlende Überwachung der Hämodynamik, dass die Ärzte das gewünschte Therapieprotokoll kontinuierlich anwenden und anpassen.

Das «Zurich Heart Project» sieht die Entwicklung eines Blutdrucksensors vor, der an der Einlasskanüle der Pumpe integriert wird, um eine kontinuierliche Messung des Ventrikeldrucks zu ermöglichen. Das Ziel der aktuellen Arbeit war die Entwicklung und Evaluierung von Regelungs- und Überwachungsalgorithmen, die nur auf Basis eines solchen Sensor arbeiten, um verschiedene Ziele zu erreichen und die Komplikationen, die während einer VAD-Therapie auftreten, zu reduzieren. Zu diesem Zweck wurde im Rahmen dieser Arbeit ein neuartiges multiobjektives, physiologisches Regelungssystem für eine rotierende linke VAD (LVAD) entwickelt und evaluiert.

Ziel eines solchen Systems war es, die folgenden Regelungs- und Überwachungsziele zu erreichen: (1) Physiologische Anpassung der Pumpendurchflussmenge an die unterschiedlichen Perfusionsanforderungen. (2) Öffnen der Aortenklappe (AV) für eine vordefinierte Zeit, um eine AV-Insuffizienz zu verhindern, während das Niveau der LVAD-Unterstützung kontrolliert wird (partiell vs. voll). (3) Erhöhung des Aortenpulsdrucks, um eine bessere LV-Auswaschung zu erreichen. (4) Sicherer Betrieb, so dass LV-Ansaugen, Überlastung und Pumpenrückfluss verhindert werden, und (5) Überwachung der LV-Vor- und Nachlastbedingungen sowie des Herzrhythmus, um eine bessere Überwachung der Therapie durch die Kliniker zu erreichen. Die Ziele (2), (3) und (5) wurden innerhalb einer Studie (Paper VII) umgesetzt und evaluiert, während die Ziele (1) und (4) umfangreiche Untersuchungen erforderten, die zu sechs verschiedenen Studien führten (Papers I-VI).

Um das Ziel (1) zu erreichen, wurde ein neuer Pump-Durchfluss-Anpassungsregler für LVADs entwickelt (Paper I). Der Regler stützte sich auf den systolischen Druck (SP) am Pumpeneintritt, um die unterschiedlichen Perfusionsanforderungen zu bestimmen, daher auch als SP-Regler bezeichnet. Das Verhalten des Reglers wurde experimentell evaluiert und mit dem klinischen Standard des Konstantdrehzahlbetriebes (CS-Betrieb) sowie mit weiteren fünf der vielversprechendsten Pump-Durchfluss-Anpassungsregler aus der Literatur verglichen (Paper II). Herz-Kreislauf-Erkrankungen mit unterschiedlichen physiologischen Anforderungen und LV-Kontraktilität wurden auf einem Hybrid Mock Circulation (HMC) Prüfstand simuliert, ausserdem wurde eine simulierte Drucksensor-Drift implementiert. Alle Regler, einschließlich des SP-Reglers, zeigten eine höhere Vorlastempfindlichkeit als der CS-Betrieb und imitierten damit die Reaktion eines physiologischen Kreislaufs. Der SP-Regler zeigte eine hohe Empfindlichkeit gegenüber Kontraktilität, andererseits eine hohe Robustheit gegenüber Sensordrift, während Über- und Unterpumpvorgänge verhindert werden konnten.

Um die Pump-Durchfluss-Anpassungsregler unter realistischeren Bedingungen zu validieren, acht akute Tierversuche durchgeführt (Paper III). Der SP-Regler und ein früher vorgestellter volumenbasierter Regler, genannt PRS-Regler (preload-responsive speed), wurden evaluiert und mit dem CS-Betrieb verglichen. Das Potenzial dieser Pump-Durchfluss-Anpassungsregler zur Reduzierung von Ansaugen und zur Erhöhung der Perfusion bei erhöhter Vorspannung im klinischen Umfeld wurde validiert. Somit kann der SP-Regler oder ein preload-basierter, d.h. auf enddiastolischem Druck (EDP) basierender Regler verwendet werden, um das Ziel zu erreichen (1).

Die In-vivo-Experimente zeigten, dass Pump-Flow-Anpassungsregler allein nicht ausreichen, um kritische Strömungsverhältnisse vollständig zu eliminieren. Dieser Befund wurde in vitro validiert, indem akute pathophysiologische Ereignisse wie Valsalva-Manöver und vorzeitige ventrikuläre Kontraktionen simuliert wurden (Paper IV). Zu diesem Zweck wurden Ansaug- und Überlasterkennungs- und Präventionsregler

entwickelt (Papier VII), um das Ziel (4) des multiobjektiven-Regelungssystems zu erreichen. Um Rückflussereignisse zu vermeiden, musste das Signal des Pumpendurchflusses mit Schätzalgorithmen ermittelt werden, welcher wiederum als Eingang für den Rückflussregler diene.

Ein neuer Pumpendurchfluss-Schätzer wurde entwickelt, der eine Modifikation eines bestehenden Ansatzes darstellt. Eine systematische Vergleichsstudie mit In-vitro- und In-vivo-Experimenten unterstützte die Entwicklung dieses Ansatzes (Paper V), der die Leistung des Schätzers bei negativen Strömungen verbesserte. Um die Zuverlässigkeit des Schätzers weiter zu verbessern, wurde ein neuartiges maschinelles Lernmodell zur genauen und kontinuierlichen Ermittlung der Viskosität während der VAD-Unterstützung einer pathologischen Zirkulation basierend auf dem Pumpeneingangsdruck und pumpeneigenen Signalen entwickelt (Paper VI). Ein solches Modell verspricht auch die Früherkennung von möglichen Blutungen oder Pumpthrombosen, die in direktem Zusammenhang mit der Blutviskosität stehen und somit die Patientenüberwachung verbessern.

Nach der Entwicklung und Validierung von Algorithmen zur Erreichung der Ziele (1) und (4) wurde das finale multiobjektive Regelungs- und Überwachungssystem realisiert (Papier VII). Merkmale aus dem Pumpeneinlassdruck wurden extrahiert, um den Öffnungsstatus mit einem maschinellen Lernmodell zu klassifizieren (Ziel (2)). Der EDP, der mittlere Aortendruck (MAP) und der SP pro Herzschlag wurden ermittelt, um das Ziel (5) zu erreichen. Eine sinusförmige, auf den Herzschlag synchronisierte Drehzahlmodulation wurde implementiert, um das Ziel (3) zu erreichen. In-vitro-Experimente zeigten die hohe Vorlastempfindlichkeit des Regelsystems bei gleichzeitiger Regelung der Öffnungszeit der Aortenklappe und damit der Beladung des LV. Im Vergleich zu einer CS-Betrieb wurde eine Verdreifachung des Aortenpulsdrucks erreicht, wobei kritische Strömungsverhältnisse vermieden wurden. So konnten die geforderten Ziele durch die harmonische Kombination verschiedener Regler erreicht werden.

Als Letztes wurde eine neue HMC entwickelt, um das Potenzial der physiologischen Regler für biventrikuläre (biventricular assist devices, BiVAD) und total totale künstliche (TAH) Herzunterstützungssysteme (Paper VIII) zu untersuchen und mit der CS-Betrieb zu vergleichen. Kritische Zustände konnten nur durch physiologische Kontrolle verhindert werden, und die zukünftige Implementierung des multiobjektiven Regelungssystems auch für BiVAD-Fälle sollte in Betracht gezogen werden. Ein solches multiobjektives Regelungssystem gibt den Ärzten die Möglichkeit, personalisierte therapeutische Protokolle anzuwenden und den Fortschritt der Therapie besser zu überwachen. So kann das Risiko einer Myokardatrophie reduziert werden, ebenso wie die Nebenwirkungen, die durch falsche Drehzahlseinstellungen auftreten. Zukünftige In-vivo-Studien sollten durchgeführt werden, um die Robustheit des Systems zu untersuchen und das versprochene Potenzial nachzuweisen.

Nomenclature

Acronyms and Abbreviations

AI	Afterload impedance
AoP	Aortic pressure
BiVADs	Biventricular assist devices
CO	Cardiac output
CS	Constant speed
EDP	End-diastolic pressure
EDV	End-diastolic volume
HF	Heart failure
HH	Healthy heart
HMC	Hybrid mock circulation
HR	Heart rate
IIR	Infinite impulse response
IOP	Inlet-outlet pressure
ITP	Intrathoracic pressure
LV	Left ventricle
LVP	Left ventricular pressure
LVV	Left ventricular volume
MCL	Mock circulation loop
PF-EDP	Pump flow-end-diastolic pressure
PRS	Preload responsive speed
PS	Pump speed
PVCs	Premature ventricular contractions
RV	Right ventricle
SP	Systolic pressure
SPPC	Suction-prevention physiologic controller
tVAD	Turbodynamic ventricular assist device
VM	Valsalva maneuver
ΔP	Pump-pressure difference
ΔRPM	Maximum minus minimum pump speed

1 Introduction

1.1 The heart failure disease

The heart constitutes a vital organ of the human body, as it pumps blood through the vessels of the circulatory system to provide oxygen, nutrients and support the metabolism process. Heart failure (HF) is a very complex disease that deteriorates this pumping ability of the heart and thus leads to inadequate perfusion. This disease presents many abnormalities at both cellular and organ level. As an example, changes in the size of the myocyte lead to changes of the wall thickness and the cardiac mass. Based on the ejection fraction, the natriuretic peptide levels and the presence of structural heart disease or diastolic dysfunction, three types of HF have been derived: 1) HF with reduced ejection fraction (systolic HF), 2) HF with preserved ejection fraction (diastolic HF), and 3) HF with mid-range ejection fraction.

HF disease constitutes the major cause of death worldwide, consecutively over the last 15 years. In 2015, around 27% of all deaths worldwide (56.4 million, as reported by the World Heart Organization) were due to ischemic heart disease and strokes. Figure 1.1 depicts the percentages of people suffering from HF for several countries and continents. More than 26 million people worldwide suffer from HF, which corresponds to approximately 1-2% of the population. Furthermore, HF is rising rapidly, even in developing countries. As an example, 5.7 million people have currently HF in the US, which is projected to increase up to 8 million by 2030, i.e. a 46% increase [1].

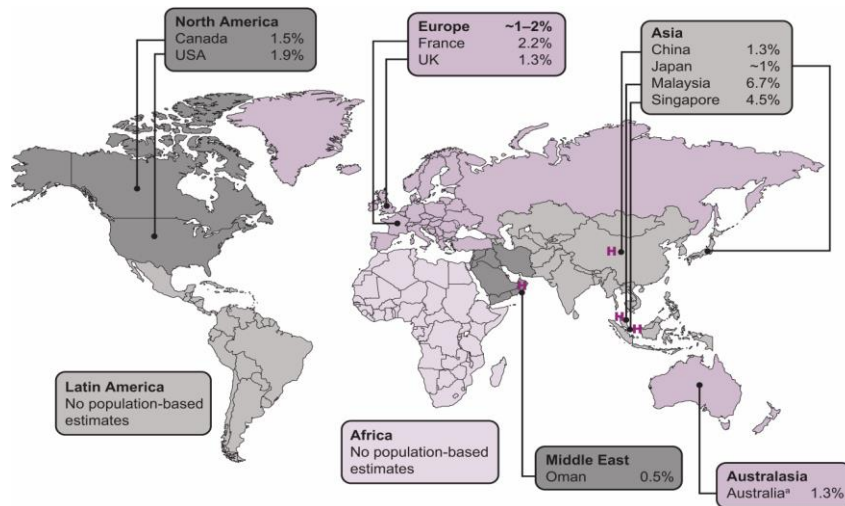


Figure 1.1: Percentage of people suffering from heart failure for different countries and continents (source: www.escardio.org).

1.2 Treatment options for heart failure

Because of the big numbers of HF occurrence, which led to its definition as a global pandemic, the treatment options are of great importance and concern a great amount of the total health expenditure (\$31 billion in 2012 in the US [1]). The first treatment method that doctors follow is the optimal medical therapy. This method includes a combination of medications, such as inotropes and beta blockers, based on the level and type of disease. These drugs aim at decreasing the workload of the heart, while enabling a physiological perfusion and, ultimately, relieving the HF symptoms. Unfortunately, this treatment option lowers the quality of life (QoL) of the patients as their mobility is constrained, while it is considered medically and economically unfeasible, especially for the end-stage HF patients.

If medical therapy does not suffice, various surgical interventions or medical devices are considered to treat the HF. Such can be a coronary bypass surgery, heart valve repair or replacement and implantation of cardioverter-defibrillators or pacemakers. When even these actions do not improve the condition of the

1.3 Ventricular assist devices

patient or the patient is from the beginning diagnosed with end-stage HF, heart transplantation (HTx) remains the gold standard treatment. HTx dramatically improves the survival and QoL of HF patients.

Figure 1.2 shows the number of heart transplantations that took place worldwide per year and location from 1982 to 2011. Even today, this number remains below 5,000 and proves that there is a great shortage of donor hearts worldwide that leads to long waiting time. In the US, 50,000-100,000 patients would need directly a donor heart [2].

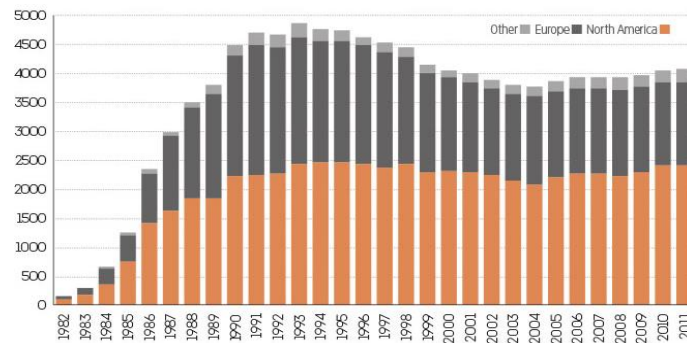


Figure 1.2: Number of heart transplantation by year and location.

(source: <https://www.theneweconomy.com/technology/hundreds-of-lives-transformed-by-syncardias-artificial-heart>)

The limited outcomes and QoL with only medical therapy and the lack of donor hearts led to the development of a new medical device, named as ventricular assist device (VAD). VADs are mechanical blood pumps, which are implanted mainly at the left ventricle (LV) of the heart and are connected to the aorta through an anastomosis. Thus, they pump in parallel to the diseased heart and support the propulsion of the oxygenated blood to the rest of the body. They were primarily used by the clinicians to keep the HTx-candidates alive until a donor organ is available (Bridge-to-Transplant). Nowadays, due to the technological improvements that followed over the years, VADs can even be used as an alternative therapy to HTx (Destination Therapy).

The following chapter provides a short overview of the history of VADs as well as the current status of the outcomes of the therapy. The limitations are also presented to frame the gap that this thesis addresses.

1.3 Ventricular assist devices

The development of mechanical circulatory support (MCS) systems started in 1953 with the first heart lung machine. In 1963, Dr. Michael DeBakey implanted the first left VAD (LVAD), which was pneumatically driven. Dr. Denton Arthur Cooley conducted the first total artificial heart (TAH) implantation in 1969 [3] and the focus during these early years of MCS development was mainly on TAHs that replace the native, diseased heart. However, the high rates of severe complications shifted the focus towards MCS devices that are simpler and support the native LV only. Thus, the era of LVADs was initiated and led to the development of several devices that can be categorized into three generations and used for different treatment goal, i.e., bridge-to-transplantation (BTT), destination therapy (DT) or bridge-to-recovery (BTR). Figure 1.3 depicts the evolution of LVAD concepts and their generation associated.

1.3.1 Evolution of the VAD technology

First-generation LVADs were characterized by their principle of operation that aims at mimicking the pumping behavior of the native heart. A chamber was filled with blood until an external force from a pneumatical or electrical actuator was applied to eject the blood to the systemic circulation. Such volume displacement pumps were the Novacor LVAS (formerly WorldHeart, Oakland, CA, USA and acquired by HeartWare International, Inc., Framingham, MA, USA in 2012), the EXCOR (Berlin Heart, Berlin, Germany), and the Thoratec PVAD and HeartMate XVE (Abbott Laboratories, formerly Thoratec Corporation, Pleasanton, CA, USA). These LVADs were equipped with one-way valves to prevent backflow. That allowed them to store volume for a desired time during the cardiac cycle, thus controlling how much the LV is unloaded and how strong the stored blood will be ejected. These are key characteristics for controlling the pre- and

afterload of the LV. Initially, they were used as a BTT with the first successful BTT treatment reported in 1984 [4]. However, the first-generation LVADs were accompanied by several complications such as bleeding, infections, device failure, thrombosis [4] and low quality of life. Some reasons were the low durability due to the multiple mechanical parts and valve degradation, the large size, the big noise emissions and the paracorporeal placement. To encounter these limitations, the development of the second-generation devices was initiated.

The second-generation devices were rotary blood pumps, which aim at supporting the pumping capacity of the LV. Such devices were the HeartAssist 5 (ReliantHeart Inc., Houston, TX, USA), the Jarvik 2000 (Jarvik Heart Inc., New York, NY, USA), the HeartMate II (Abbott Laboratories, Chicago, IL, USA), and the EVAHEART (Evaheart Inc., Houston, TX, USA). These systems consist of three main components: the intracorporeal or extracorporeal pump which incorporated a rotating impeller, the percutaneous driveline, and the peripherals, which include the controller and the batteries. The onset of the new era of the second-generation devices was highlighted through a clinical study by Slaughter et al. [5], who showed that the survival rates with HeartMate II were by 30% higher than with HeartMate XVE, while achieving a better QoL for the patients with higher mobility and less adverse events. Their smaller size, lack of noise, better durability and less infections susceptibility were the main reasons for these outcomes. Another milestone study that proved the superiority of second-generation over first-generation devices, but also over the optimal medical treatment, was the REMATCH study [6]. The number of implantations of rotary blood pumps was continuously increasing between 2006 and 2014, while implantation of pulsatile pump became rare [7]. HeartMate II constitutes the most successful device, with respect to number of implantations (over 20,000) and has received BTT and DT approvals from FDA since 2008 and 2010, respectively.

Despite this superiority, outcomes with second-generation devices are still limited [7]. The occurrence of bleeding remains high due to the high dose of anticoagulants on the one hand but also impairment of the coagulation system presumably due to the supraphysiologic shear stresses in the pumps [8]. Infections, pump thrombosis and strokes still occur and constitute life-threatening events and reasons that lower the QoL of the patients and sustain the high costs of the therapy due to the required rehospitalizations [9]. The VAD community focused on ways to restrict these limitations, and the third-generation devices were the result of this effort.

The third-generation LVADs were presented as devices with improved hemocompatibility due to their advanced bearing systems. Sophisticated designs were developed to enable fully rotor levitation, such that any mechanical contact between the rotor and the stationary parts is avoided. The theory behind was that a fully levitated rotor would yield reduced shear stress and critical flow situations, such as stagnation. Such devices are the INCOR (Berlin Heart GmbH., Berlin, Germany), the VentrAssist (Ventricor – sales have stopped), the HVAD (Medtronic Inc., FL, USA), the Levacor (WorldHeart – sales have stopped), and the HeartMate 3 (Abbott Laboratories, Chicago, IL, USA). Despite the technological advancements incorporated within these devices, serious adverse events occur at the same frequency as with the second-generation LVADs. That proved that reducing blood damage constitutes a very complex, multifactorial step forward. The main improvement observed especially with the HeartMate III was the elimination of de novo pump thrombus [10], which is probably a result of the wide clearances (greater than 250 μ m) that yield better wash-out. Furthermore, the active magnetic levitation technology of HeartMate III led to thinner and more flexible drivelines which allow better treatment of infections (re-tunnelling or replacement without pump exchange) [11].

Novel concepts of LVADs are currently under development, such as the CorWave LVAD (CorWave SA, Clichy, France) and the TORVAD (Windmill Cardiovascular Systems Inc., Austin, TX, USA), which promise less shear stress. Furthermore, a rotary device for RVAD cases or pediatrics from VADovations, Inc. (Oklahoma City, Oklahoma, US) has presented promising results against hemolysis and large protein degradation. It remains to be seen whether these concepts, as well as several others which are under development from new or existing companies, will bring substantial improvements in the clinical environment.

In summary, second-generation VADs brought a revolution in HF treatment and almost fully replaced the first-generation ones. Third-generation VADs brought great technological advancements but poor improvement with respect to clinical outcomes, compared to second-generation VADs [12], [13]. Future technologies seem to focus on the important deficits of current systems, but their feasibility and reliability in clinical practice has not yet been validated. The following chapter highlights the important clinical outcomes reported over the last years with VAD therapy.

1.3 Ventricular assist devices

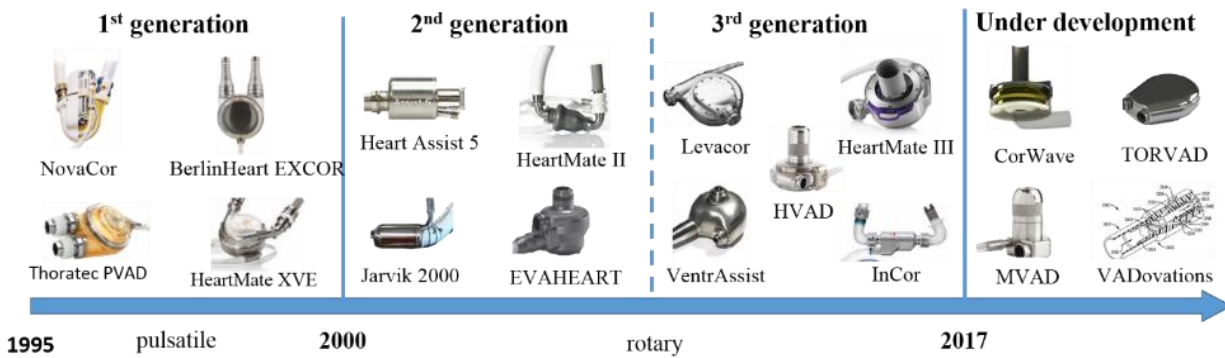


Figure 1.3: Historical evolution of ventricular assist devices.

1.3.2 Promising outcomes of VAD therapy

Various milestone-studies have proved the promising outcomes of VAD therapy over the years. The first important milestone study, the REMATCH study in 2001 [6], proved the better survival rates of VAD therapy compared to optimal medical therapy. Figure 1.4 depicts this superiority of VAD therapy based on several studies conducted. According to Rose et al. [6], survival rate on the pulsatile HMI after one and two years of support was 52% and 29%, respectively, whereas the survival with optimal medical therapy was 23% and 8% for one and two years, respectively. In 2009, Slaughter et al. [5] proved clinically the superiority of continuous-flow over pulsatile-flow pumps. Patients supported by HeartMate II had a more than 60% survival rate at 2 years compared to those with HeartMate XVE, from whom only 24% survived (Figure 1.4). Thus, it became clear that the evolution of the VAD technology further improved the survival rates and according to the latest (eighth) Intermacs report [10], the first- and second-year survival rates have reached up to 80% and 70%, respectively. These superior results have been validated by several studies, which are included in Figure 1.4. Currently, the survival rates of VAD therapy equal those of patients following HTx [14]. The number of VAD implantations increased at around 10,000 per year, while patient survival has exceeded the 10 years and the QoL has significantly improved. Despite that, the cost of the therapy is still considered very high compared to HTx [15].

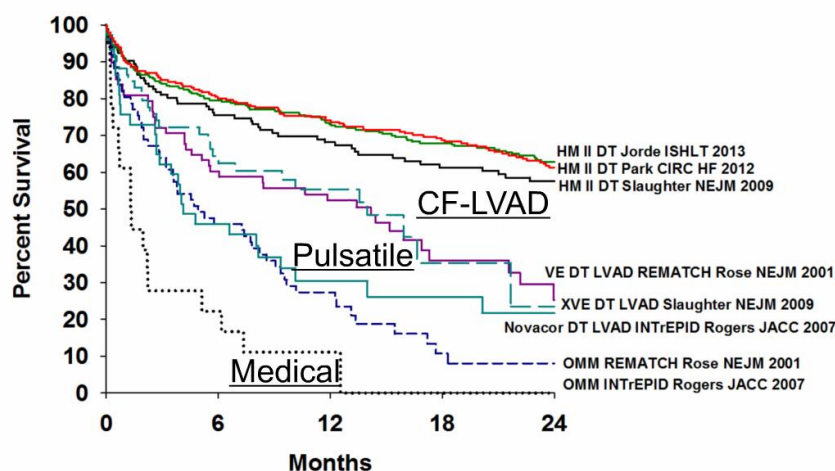


Figure 1.4: Survival rates of heart failure patients when following a destination therapy (DT) with continuous-flow LVAD (CF-LVAD) versus pulsatile LVADs or optimal medical management (OMM) for 24 months. Figure initially published by Jorde et al. [16].

Another positive outcome of VAD therapy is the occurrence of myocardial recovery [17], which constitutes the most desirable outcome of the HF therapy because the VAD could be explanted again and the patient would be considered healed. Since many years, it had been observed that VAD support may lead to the reversal or improvement of several aspects of HF, such as morphological hypertrophy [18], beta-adrenergic responsiveness [19] and contractile dysfunction [20]. The reversal of structural remodeling is widely observed in patients with dilated cardiomyopathy especially during the first six months of the therapy, due to the better

unloading of the LV by the VAD. Several patients have also reached the point of reversal of the functional remodeling, which is associated with an increased contractility and leads to pump explantation. Such cases constitute a milestone for the HF treatment as they altered the belief about the chronic HF from an irreversible, progressive disease to a potentially treatable one.

However, only 1-3% of the VAD patients present full recovery. From those who follow device explantation, about 40% present recurrent remodeling. All these facts support the opinion that there is few understanding about the biological “driving motors” of recovery and the optimal timing for weaning. That has led to a diversity among clinics regarding strategies to promote recovery, as well as methods to monitor the recovery and decide for VAD explantation. A recent study, the RESTAGE HF [21], aims at further investigating the potential of recovery by combining several strategies, such as medication and patient selection. Despite the enthusiasm with the continuously improving outcomes of VAD therapy and the remarkable experience of recovery, high costs [15] of the therapy and still-occurring adverse events hamper the further spread of this treatment option and have constrained the number of annual implantations [10] and the patient QoL. These adverse events are described in more detail in the following Chapter.

1.3.3 Limitations of VAD therapy

Many adverse events occur during VAD therapy and may lead to severe complications, frequent readmissions and even death. Neurologic events, such as strokes, constitute the main cause of death followed by multi-system organ failure and infections. Device malfunction and right heart failure (RHF) have also a small risk for death [10]. Further adverse events that have high rates of occurrence but do not directly lead to death are gastrointestinal bleeding (GIB), arrhythmias and aortic valve regurgitation. In the next paragraph, some of these adverse events are further described.

The stroke rate is approximately 10-15% in the first year of LVAD support, while with HVAD it increased up to 30% at 2 years, according to the ENDURANCE trial [12]. Strokes can be either ischemic or hemorrhagic. An important factor for strokes is the level of anticoagulation. It is believed that by maintaining an INR (the ratio of the time that the patient's plasma clots to that of a normal sample) between 1.5 and 2.5 and providing the proper medication, the risk of thrombosis and, therefore, of stroke may be mitigated. An increased mean arterial pressure (MAP) that exceeds 90 mmHg increases also the risk of strokes [22].

Pump thrombosis, i.e. the formation of a thrombus within the pump as a reaction of the coagulation system, may also lead to death, unless it is treated with medication or more drastically with LVAD replacement or HTx. Malposition of the inflow cannula or deformation of the outflow graft, low LVAD flows, small gaps and high heat losses constitute reported reasons for thrombogenicity. Pump thrombosis is usually associated with increased hemolysis.

Infections constitute a permanent threat during VAD therapy that increases considerably the first-year mortality [23]. Infections are independent of the device and may be the reason for almost half of the readmissions [24]. The driveline that penetrates through the skin is the most common site of infection. Antibiotics and surgical procedures may follow to treat the infection.

Arrhythmias, i.e. irregular cardiac rhythm, constitute the third-most-frequent adverse event, occurring in almost 30% of the LVAD patients. It is presented as ventricular tachycardia/fibrillation (VT/VF). Arrhythmias greatly increased with rotary LVADs due to the high occurrence of suction events. Suction occurs due to overpumping, i.e., when the pump speed does not adapt to decreased preloads of the LV. The LV wall collapses, the septum may touch the VAD cannula and VT may be triggered. Despite that, heart rate does not influence the cardiac output during rotary VAD support, as rotary VADs do not depend on systole and diastole, thus no negative influence on hemodynamics is considered. However, arrhythmias may initiate other symptoms, such as RHF [22], or even thromboembolism [25] and lead to readmissions or, even worse, death.

RHF is one of the most important adverse events and its occurrence varies from 5-50% of the patients who followed LVAD implantation [26], [27]. It can lead to severe complications that require rehospitalization with prolonged intensive care stay, while the risks of bleeding, renal insufficiency and mortality increase [27], [28]. Currently, much research is focused on RHF as there are many aspects to be investigated with respect to reasons of the failure, early or late monitoring and treatment. Many studies tried to identify risk predictors and scores for RHF, however, a metaanalysis study proved that none of these indices can robustly predict RHF [29]. Several researches have indicated the increased blood flow post-LVAD implantation to increase the RV

1.4 Zurich Heart Project

loading and lead to RHF. Great pressure differences between RV and LV, for example during overpumping conditions, lead to septum shift and increased RV volumes that compromise RV contractility [29].

Treatment strategies for RHF start with medication (vasodilators, inotropes). If RHF develops early in the postoperative phase short-term MCS is usually considered. For late or persistent RHF and unsuccessful medical therapy, a right VAD (RVAD) is the only option, which leads to a biventricular support configuration (BiVAD). Thus far, the outcome of BiVAD support is significantly worse compared to LVAD support. Due to the absence of a specific, small, clinically evaluated device for RVAD support, the implantation is delayed until end-organ failure is irreversible, which leads to very high mortality rates. During the last years, the 1-year survival rate has stagnated at approximately 55% [7]. An alternative treatment option for biventricular failure is the total artificial heart (TAH), which is a single device with two integrated pumps. In contrast to BiVAD systems, the native heart of the patient is explanted to create space for the TAH. In 2014, approximately 50 TAHs were implanted in the U.S. [3]. The 1-year survival rate of TAH patients is approximately 60% and, therefore, also lower compared to LVAD patients.

Aortic valve insufficiency (AI), i.e. the leakage of the aortic valve each time the left ventricle relaxes, may cause problems in LVAD patients by limiting the end-organ perfusion and overloading the LV due to excessive regurgitant flow. A systemic review showed that 25% of the LVAD patients of the studies analyzed developed AI, which was increasing by 4% every month of support. A closed aortic valve was concluded to play an important role on development of AI. Excessive aortic root dilation, due to commissural fusion resulted from loss of pulsatility and constantly elevated aortic pressure [30], may also lead to malformation of the aortic valve and reach the point of AI. Mild AI can be compensated with diuretics and vasodilators for afterload reduction, but more severe symptoms require surgical intervention for repair or even replacement [31].

Bleeding constitutes a major adverse event, observed in about 20% - 45% of rotary LVAD patients [32] with low, however, death rate. This percentage is twice as big as with pulsatile LVAD patients due to the high levels of anticoagulation required. GIB is the most severe form of bleeding and requires readmission followed by several diagnostic tests and blood transfusions that lower the QoL of the patients and, unfortunately, do not achieve a successful treatment. The reasons for bleeding are controversial and many researchers try to identify them and address them. A study suggested that 31% of GIB is due to arterio-venous malformations [33].

The influence of limited pulsatility with rotary LVADs on bleeding has led to a debate within the research community [34], [35]. It is believed that the low pulsatility may lead to hypoperfusion and hypoxia, similar to the Heyde's syndrome [36]. Hypoxia, in turn, results in vascular dilation and angiodysplasia which is considered a major factor of bleeding. Additional factors proposed are the high shear stress during rotary LVAD support that induce platelet dysfunction [37], as well as the protein ADAMTS-13, which has been proven to lead to degradation of von Willebrand factor (vWf), which, in turn, has been associated with bleeding events [38]. Other risk factors can be advanced age, prior GIB, high INR and low number of platelets [39]. Several protocols have been proposed to prevent or treat bleeding. These include manipulation of the medication therapy (holding anticoagulants, administering proton pump inhibitors, lowering INR) or of the pump setting (decreasing pump speed to open the aortic valve and create pulsatility). A study showed that an open AoV and greater pulsatility are associated with less bleeding [40] but this was opposed from another study [39].

Taking into consideration the limitations of the VAD therapy, it is intuitive to believe that the limited physiological and biological footprint of current rotary LVADs constitutes the major factor that causes these complications and adverse events. On the effort to encounter these limitations, the "Zurich Heart Project" was initiated in Zurich, Switzerland. A short overview of this project is presented in the next section.

1.4 Zurich Heart Project

Zurich Heart Project constitutes a multidisciplinary and inter-institutional collaboration, involving the University of Zurich (UZH), the University Hospital Zurich (USZ), the German Heart Institute Berlin (DHZB) and ETH Zurich. Figure 1.5 illustrates this collaboration and the labs that are involved in this effort. Aims of the project are the development of new technologies for the treatment of HF and the improvement of the physiological and biological footprint of current VADs. For this purpose, many resources have been devoted towards a more biological interface between blood cells and the device, while other groups focus on a more physiological interaction between the device and the circulation. This thesis, as highlighted in Figure 1.5, is part of the latter direction. It investigates the potential of algorithms relying on signals from implantable sensors, to enable better monitoring and a more physiological response of the pump speed. Since this research

field had been greatly researched over the last decades, a summary of the state-of-the-art in sensors and algorithms is provided in the next section.

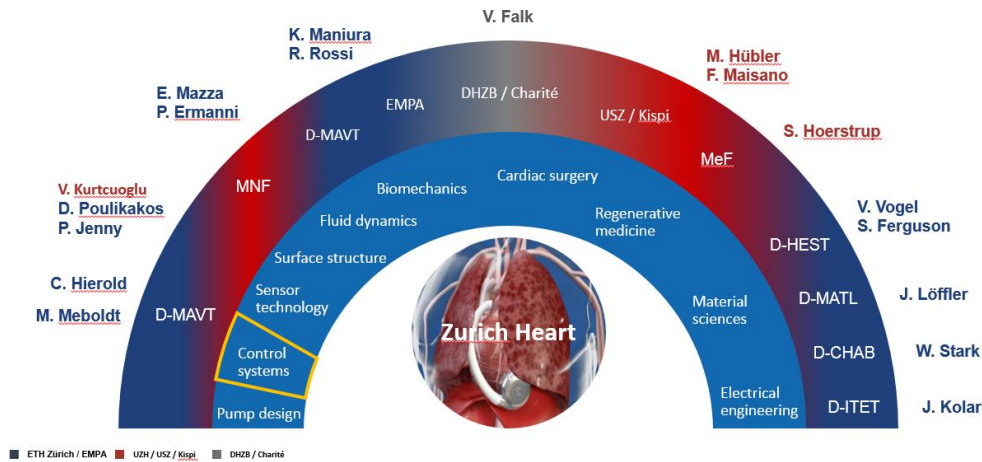


Figure 1.5: Illustration of the organization of the Zurich Heart Project. Control systems for VADs (marked in orange) constitutes the focus of this thesis.

1.5 Intelligent rotary blood pumps

1.5.1 Intuition for an intelligent rotary blood pump

The idea of a smart MCS system started many years ago. After the first TAH was developed, the intuition to have a smart device that imitates the human heart followed intuitively. For this purpose, the imitation of the Frank-Starling mechanism [41], which describes the cardiac output response of a healthy human heart during preload changes, was the goal from the beginning. Further ideas focused on applying a pulsatile speed modulation on rotary VADs such that the pulse pressure increases and resembles better the human heart. However, all these efforts remained in research level. Currently, LVADs operate at a fixed pump speed, except the HeartMate III that uses a fixed, periodic speed profile. Recent clinical studies from Medical University of Vienna have proven that such approaches are very likely to create critical flow condition in VAD patients, due to over- or underpumping, and primarily lead to suction, backflow, and overload, respectively, and, at a later stage, cause complications (see Section 1.3.3).

1.5.2 Non-invasive monitoring and control approaches

The lack of reliable telemetric systems for continuous monitoring of the patients after discharge from a healthcare facility hinders the prediction or immediate detection of adverse events, which would allow their treatment at an early stage. Thus, their treatment relies mostly on the awareness of the patients and their caregivers. To counteract this deficiency, non-invasive monitoring algorithms for various hemodynamic information have been proposed [4]–[8], which are mainly based on the estimated pump flow from pump intrinsic signals. Their implementation in clinical practice for continuous monitoring of the interaction between the human heart and the VAD can provide the clinical personnel with significant information, leading to a significant improvement of the patient outcomes.

Pump flow can be either measured or estimated from the pump intrinsic signals. Devices with implantable flow sensors, such as the aVAD from ReliantHeart, Inc. (Houston, TX, USA) [3], have entered the clinical practice, while other companies, such as the HVAD from Medtronic, Inc. (Minneapolis, MN, USA), still prefer estimation techniques. Acquiring the pump flow signal is very important as it has proven to contain much hemodynamic information [4] and clinicians may use it for multiple purposes. For adjusting the pump speed during hospitalization, clinicians also observe the mean pump flow. Changes in mean pump flow can be

1.5 Intelligent rotary blood pumps

associated with pump thrombosis, RHF or great preload changes, as it occurs during dehydration or bleeding [5]. Changes in HCT will lead in turn to changes in pump flow and thus alarm the clinical personnel for a closer supervision of the patient. Furthermore, changes in flow pulsatility are used by the clinicians as an indicator for changes of the contractility of the patients. Apart from the application in clinical practice, the research community has presented several studies with algorithms that show the potential of the pump flow for various monitoring and control objectives. Such algorithms aim at detecting suction events [6], arrhythmia [7], changes in the contractility of the LV of the patient [8], the status of the aortic valve [9] and preventing backflow events [10]. Moreover, algorithms that estimate the preload of the LV and enable the physiological adaptation of clinical VADs have been proposed and even evaluated with clinical trials [11].

Several research groups have worked on the development of a reliable, pump-flow estimator. Both in-vitro and in-vivo studies have been conducted to evaluate the estimators. Tsukiya et al. [42] were the first to investigate the use of pump-intrinsic signals as inputs for a static model that estimates the pump flow. This model-based approach constituted later the basis of Kitamura et al. [43] and Granegger et al. [44], who extended it with the dynamic model of the pump. The estimator developed by Granegger et al. [44] outperformed the one used clinically on HVAD system and achieved the smallest estimation error. A group of researchers [45]–[48] followed a more empirical approach with autoregressive exogenous (ARX) models to derive the relationship between pump-intrinsic signals and flow. Giridharan et al. [49] developed an Extended Kalman Filter (EKF) which uses soft sensors to estimate flow rate and head pressure. In addition, few studies increased the non-invasive input space of pump speed and power, by adding the blood viscosity, which has proven to greatly affect the performance of the estimator [48], [50]. Thus, the continuous monitoring of HCT is regarded quite beneficial for a reliable pump flow estimation.

Only few methods to detect HCT changes have been proposed. Clinicians currently analyze the log files of the pump current of the devices to detect changes in blood viscosity or the onset and occurrence of adverse events, such as pump thrombosis [51], [52]. Low-flow alarms or power spikes constitute potential indicators for the early detection of complications [53], but they cannot provide a direct level of emergency until exact values of HCT are measured, which can only happen during the hospitalization of the patient. Hijikata et al. [54] proposed the only approach in research, thus far, for viscosity estimation. However, this approach has only been evaluated at fixed, pump-speed settings and constant physiological requirements of the circulation, while it only applies for pumps with contactless, active, magnetic bearing.

Pump current variations, which are currently used clinically, may not be solely correlated with changes in viscosity. In the case of applied artificial pulsatility, as already implemented clinically at Heartmate III (Abbott Laboratories Inc., Illinois, US), or physiological control, which is considered as a future technology for improving VAD-therapy [55], the pump current will continuously vary due to the varying desired pump speed. Thus, in such cases, only monitoring the pump current will not suffice to monitor changes in viscosity or to detect possible adverse events.

1.5.3 Implantable sensors for VADs

Several implantable sensors for measuring blood pressure, volume or pump flow continuously have been researched over the last decades. However, small success has been reported in clinical practice. Only the implantable flow sensors have been integrated into VAD systems, as discussed in the previous section. Despite this success, several drawbacks prevent the companies of the most frequently implanted devices to incorporate such a technology into their VAD systems. A biocompatible, durable and accurate blood pressure sensor has not yet been developed but it is likely to be realized in the near future [56]. Several sensors for VADs are currently under development [56], whereas a left atrial pressure sensor, has been tested with VAD patients as well [57]. Furthermore, the first FDA approved implantable pressure sensor for the pulmonary arterial pressure (CardioMEMS™ HF System, Abbott AG, Illinois, US) has recently been realized and is in clinical use, even with LVAD patients [58]. Regarding LV volume sensors, patents and applications for measuring the blood conductance or admittance within the LV and deriving the LV volume have been developed since many years ago. However, none of these managed to be evolved into a reliable, longterm device, applicable in the field of VADs. A new concept for integrating an industrial pressure sensor at the pump inlet cannula [59] and new concepts for measuring LV volume [60] have been developed within the research group of Zurich Heart

Project. The state of development among pressure and volume sensors has been described in more detail by Tchanchaleishvili et al. [57] and Dual et al. [60], respectively.

1.5.4 Sensor-based monitoring and control approaches

Driven by the assumption that a physiologically controlled LVAD can prevent some of the life-threatening conditions described in paragraph 1.3.3, and following the progress in sensor technologies, various concepts of physiological controllers have been developed over the last decades [61].

In the beginning, most control approaches used non-invasive signals as inputs, such as the estimated pump flow [61]. The drawbacks of these approaches are the limited robustness and accuracy of the estimators [62], as well as the limited correlation of these signals with the Frank-Starling mechanism of the healthy heart. To overcome these drawbacks, recent approaches are based on invasive signals, such as the LV pressure, the aortic pressure, the LV volume, or the measured pump flow [63]. These approaches also claim to aim at imitating the Frank-Starling mechanism of the healthy heart by estimating or measuring the preload condition of the LV.

Most physiological controllers published can be divided into three groups, based on their concept. The first group consists of controllers that rely on the measurement of preload [64]–[66], for instance EDV, EDP, or left atrial pressure (LAP) to regulate the pump speed. The second group consists of controllers which use indirect information of the preload by measuring a signal which is believed to correlate with preload [67]–[69], for instance the pump flow or pressure pulsatility. Such controllers present a high sensitivity to contractility changes, which is not the case for the controllers of the first group. The third group includes controllers, which aim at maintaining the cardiac output in a physiological range [70]–[77], for instance by controlling the pump speed such that the mean aortic pressure remains within a predefined range. Figure X illustrates these three categories with examples.

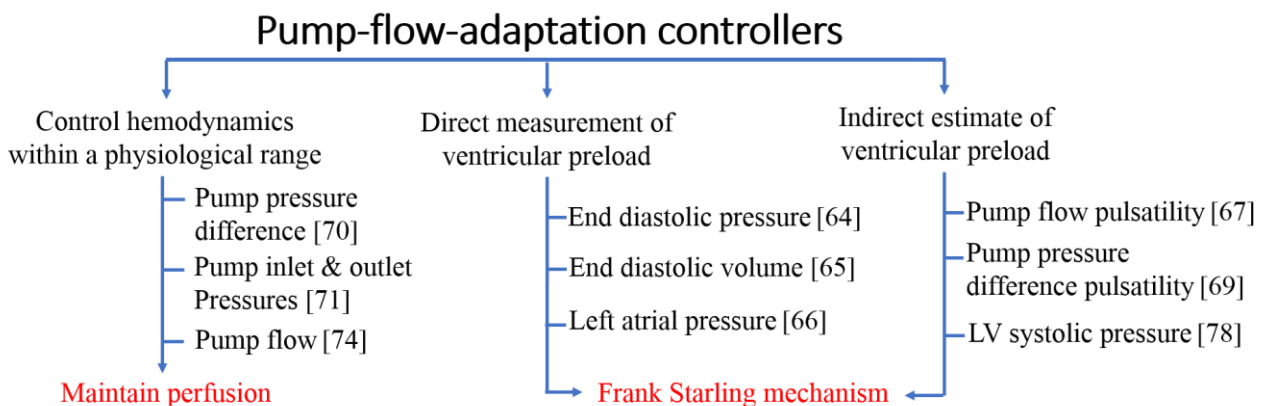


Figure 1.6: Categorization of the pump-flow-adaptation controllers based on their control input and objective.

Most of the controllers of these three groups have been evaluated with in-silico and in-vitro experiments, which include variations of the pre- and afterload conditions, as well as of the contractility of the pathological circulation. Their gain parameters are usually tuned manually, based on the desired performance. In the original studies, the physiological controllers were compared with the clinical standard of the constant-speed (CS) operation [65], [78]. Only Mansouri et al. [64], Lim et al. [79], and Pauls et al. [80] extended this protocol. In the first study, authors compared their controller with a previously developed, and based on pump flow pulsatility [81]. In the second study, in-silico exercise and head-up-tilt experiments were conducted to compare controllers representing the third group of Figure 1.6. Finally, Pauls et al. [80] reported the broadest comparison study on a mock circulation with eight invasive pump-flow-adaptation controllers.

All these in-vitro studies have shown promising results about the potential of physiological control in the clinical practice. However, only few have been validated in animal models with acute studies [82], [83], while none of them has been evaluated during a chronic experiment, and only one controller has been evaluated in humans [84]. Although no feedback controllers have been implemented for longterm in clinical practice, some

1.6 Testing of algorithms for blood pumps

companies made some steps forward and incorporated in their devices feedforward controllers. Such controllers are for detecting suction, based on the estimated or measured pump flow, and release it by decreasing the pump speed to a predefined setpoint. Additionally, they have implemented algorithms to enable an aortic valve opening or to augment the aortic pulse pressure of the patients. The latter has been investigated extensively, on the effort to restore a physiological, arterial pulse pressure during rotary-LVAD support. Amacher et al. [85] investigated in vitro the effect of different periodic speed signals and phase shifts to the heart beat, on the hemodynamics of an LVAD-assisted pathological circulation.

Most of the monitoring and control algorithms proposed are developed to achieve one specific objective, e.g. pump flow adaptation. Only few approaches have been presented in literature, which aim at combining various indices and fulfilling various objectives. The first such approach was presented by Bullister et al. [71], who used the pump inlet and outlet pressures and the heart rate as inputs to their pump-flow-adaptation controller. Additional algorithms were incorporated into their system to detect suction and pump backflow. Arndt et al. [69]^{Error! Reference source not found.} developed an approach to estimate the pump pressure difference, which was then correlated to preload changes, suction events, and classification of full or partial support. Karantonis et al. [86] used the pump speed signal as input for a classification and regression tree to detect five different states of the LV, i.e., backflow, ventricular ejection, closed aortic valve, and intermittent or continuous suction. Amacher et al. [87] developed the most sophisticated approach so far, which can compute the optimal waveform of the LVAD speed based on a predefined objective function. For their study, a trade-off function between maximum aortic valve flow and minimum stroke work was applied. Drawback of the approach is the continuous requirement of many hemodynamic parameters to run the optimization algorithm.

1.6 Testing of algorithms for blood pumps

The development of algorithms for VADs requires extensive testing to prove their performance under various conditions, and to ensure the desired performance in a clinical environment. At the early stage of development, in-silico environments are preferred. They consist of a numerical model of the human blood circulation and an analytical model of a blood pump that supports the circulation. They offer the possibility to conduct a great variation of experiments, which must be carefully designed and conducted to mimic as good as possible the clinical scenarios. The next step concerns in-vitro experiments, where a physical model of a blood pump is used and thus the algorithms are applied at a real device. In this case, the components of the numerical model of the circulation can be partially mimicked with hardware components (semi-hybrid mock loops), where e.g. a vessel resistance is represented and adjusted by a valve. Another approach for in-vitro testing uses the whole numerical model in software form and a hydraulic interface is constructed to realize the interaction between the physical device and the modelled circulation (hybrid mock loops). Water-glycerin mixtures are usually used as blood analog. Similar to in-silico testing, in-vitro testing allows the evaluation of the performance of the algorithms under various conditions and in short time.

To incorporate the effect of blood and come closer to real conditions, ex-vivo [88] and in-vivo experiments with animal hearts and models, respectively, have been conducted. Such experiments are considered more complex and expensive but, on the other hand, more realistic. In current thesis, both in-vitro and acute, in-vivo (pig models) experiments were conducted.

1.7 Scientific contribution

This thesis was conducted within the frame of the Zurich Heart Project. The main goal was to investigate the potential that the integration of a pressure sensor at the pump inlet would bring for improving the physiological behaviour of the VADs and, ultimately, the QoL of the VAD patients. Figure 1.7 illustrates the desired outcome of being able to adapt the pump speed with regard to the specific therapeutic strategy and the physiological requirements, as well as to monitor the condition of the LV and the cardiovascular system continuously. Furthermore, the limits of what can be achieved with the pump inlet pressure as a signal and the

requirements for such a sensor had to be identified. First, as this research field has been in focus from several researchers over the last years, this work also aimed at investigating and analyzing the state-of-the-art technologies and at comparing them with the developments of the thesis. Second, after deciding on the most robust and appropriate algorithms, the author envisioned a multi-objective control and monitoring system which will lead to intelligent rotary blood pump with physiological response.

The major objectives that such a system would have to fulfill are: (1) physiological pump flow adaptation to the varying perfusion requirements, (2) aortic valve (AV) opening for a predefined time, (3) augmentation of the aortic pulse pressure, (4) safe operation such that LV suction, overload, and pump backflow are prevented, and (5) monitoring of the LV pre- and afterload conditions as well as the cardiac rhythm. Thus, the goals of physiological pump flow adaptation and elimination of critical flow conditions can be realized. By increasing the arterial pulsatility, patients may benefit with better washout of the left ventricle and less stiffening of the aortic wall. The control of the status of the AV is of great importance to prevent AV insufficiency, while better controlling the level of LVAD support (partial vs full). Such control strategies allow the clinicians to apply with reliability their therapeutic strategies and to adapt the continuously based on the hemodynamic parameters which are monitored.

In the following paragraphs, the studies that include the evaluation of the state-of-the-art algorithms as well as the new developments which, ultimately, led to the final result of the multi-objective control and monitoring system are described. The goal of these paragraphs is to summarize the scientific contribution of this thesis by first framing the research gaps or questions, and then answering them in the form of published studies.

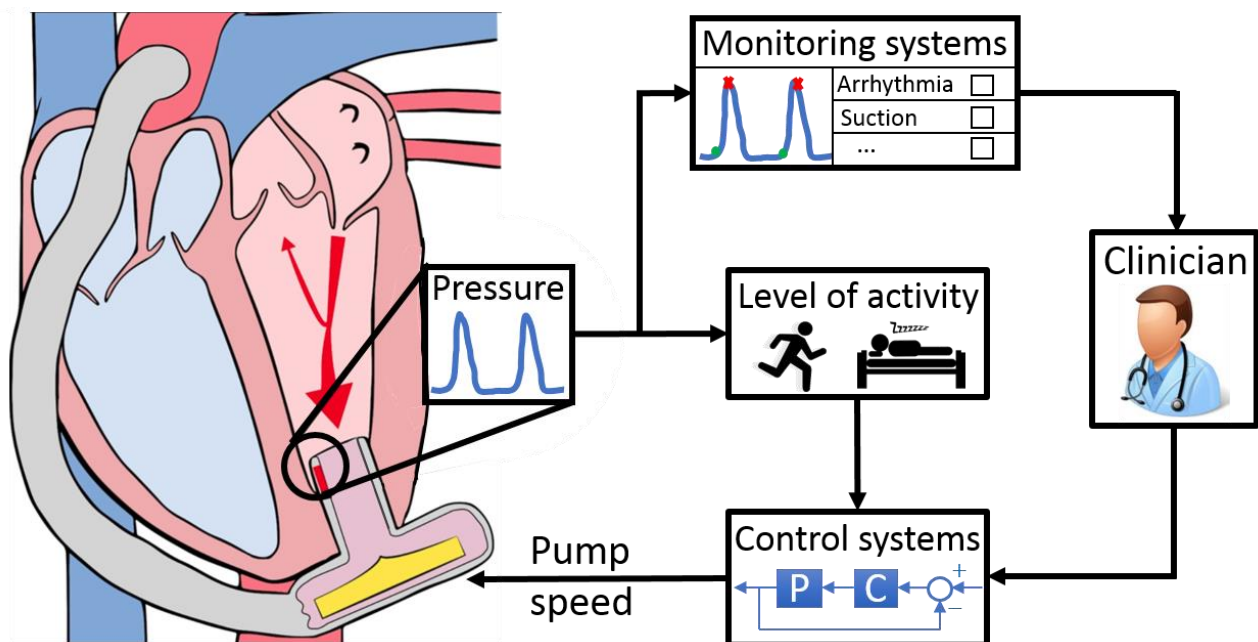


Figure 1.7: The concept of a pressure sensor integrated at the inlet cannula of a ventricular assist device. The pressure signal measured constitutes the input for various algorithms that enable a continuous monitoring of several hemodynamic parameters. Additional algorithms control the VAD speed to meet various objectives and adapt it to the physiological requirements of the circulation. (Figure derived by www.micro.mavt.ethz.ch/research/advanced-microsystems/ventricular-assist-devices.html and modified)

This thesis started with the demand for a control algorithm that would have the pump inlet pressure as an input to adapt the pump speed to the perfusion requirements of a VAD-supported circulation. Two additional important requirements were set from the beginning: First, the algorithm should only rely on the pump inlet pressure, without requiring additional implantable sensor technologies. Second, it should be reliable against possible sensor drift that may occur during long-term implantation. To the knowledge of the author, this requirement hadn't been addressed by any controller earlier proposed in literature. To address these

1.7 Scientific contribution

requirements, a new concept of a pressure-based pump-flow-adaptation controller was developed, which relied on the systolic pressure (SP) at the pump inlet [78] (study presented in Chapter 2).

- [78] A. Petrou, G. Ochsner, R. Amacher, P. Pergantis, M. Rebholz, M. Meboldt, and M. Schmid Daners, “A Physiological Controller for Turbodynamic Ventricular Assist Devices Based on Left Ventricular Systolic Pressure,” *Artif. Organs*, vol. 40, no. 9, pp. 842–855, 2016.

The SP controller, as named, constitutes a simple control structure. In-vitro experiments with varying pre- and afterload conditions proved its potential to adapt the pump flow to the varying physiological requirements of a pathological circulation. This performance was barely influenced by excessive sensor drift of up to ± 25 mmHg. Another benefit of this concept is that its initial calibration post-implantation would not change the routine of the clinicians. However, the study revealed the sensitivity of the controller during contractility changes, which may lead to over- or underpumping when contractility greatly increases or decreases, respectively. A recalibration of the controller would then be required. To the best of the author’s knowledge, that controller was the first to rely on the pump inlet pressure signal only and to perform robustly against high sensor drifts. Its implementation would not change the current calibration steps that clinicians follow when defining the constant speed.

The next question was to determine the advantage of the SP controller over all the others that exist in literature. To answer this question, a systematic experimental a comparison study was performed in vitro [63] (presented in Chapter 3).

- [63] A. Petrou, J. Lee, S. Dual, G. Ochsner, M. Meboldt, and M. Schmid Daners, “Standardized Comparison of Selected Physiological Controllers for Rotary Blood Pumps: In Vitro Study,” *Artif. Organs*, vol. 42, no. 3, 2017.

Thus far, only one in-vitro comparison study among eight pump-flow-adaptation controllers had been reported [80], where the influence of contractility changes and sensor drift were not investigated while an equal tuning of the controllers was not presented clearly. The best controllers of that study, together with another four controllers from literature, including the SP controller [78] and the volume-based PRS controller, which was earlier developed in our group [65], were gathered and evaluated in depth [63]. The selected controllers used one or more of the pump inlet or outlet pressures, the pump flow and the LV volume signals as control inputs. A main challenge of this comparison study was to ensure equal testing conditions. For this purpose, the loop-shaping method was used to select gains with the same objectives for each controller, which was a unique part of the study. The study included variations of the pre- and afterload conditions as well as the contractility of a VAD-supported, pathological circulation. Each of these experiments was repeated for different levels of sensor drift, for each of the possible sensors used. The occurrence of possible critical flow conditions, such as LV suction and overload were reported. Results proved the great potential of preload-based controllers, such as the PRS controller, to adapt to varying physiological requirements and contractility changes, but they may be less robust when sensor drift occurs. The SP controller, despite the known sensitivity in contractility changes, seemed to cover most of the requirements for a safe clinical implementation by responding physiologically to pre- and afterload variations even during high sensor drifts. That comparison study proved experimentally the theoretical foundations by Tchanchaleishvili et al. [89] regarding the potential of preload-based pump-flow-adaptation controllers.

To validate the findings in vivo under realistic physiological and pathophysiological conditions, acute in-vivo experiments with 10 pig models were conducted. The SP and PRS controllers were evaluated, which had been developed in our group, and compared with the clinical standard of the CS operation [83] (Chapter 4).

- [83] G. Ochsner, M. J. Wilhelm, R. Amacher, A. Petrou, N. Cesarovic, S. Staufert, B. Röhrnbauer, F. Maisano, C. Hierold, M. Meboldt, and M. S. Daners, “In Vivo Evaluation of Physiologic Control Algorithms for Left Ventricular Assist Devices Based on Left Ventricular Volume or Pressure,” *ASAIO J.*, vol. 63, no. 5, pp. 568–577, 2017.

Pre- and afterload variation experiments were conducted, with the use of a heart-lung machine and an occlusive balloon catheter, respectively. Low, high and normal gains were implemented, which were defined in vitro, while the DP2 blood pump served as an LVAD. No suction events were reported when the LVAD was controlled by the SP controller, while during two experiments the PRS controller yielded suction but for 2-3 heartbeats and then, it was released. Several suction events occurred during the CS operation, when preload was decreasing. Both SP and PRS controllers were able to adapt the pump flow during the variations as desired. These results validated the initial in-vitro findings [63],[78], and proved the potential of such pump-flow-adaptation controllers to prevent suction and overload, thus realizing a more physiological perfusion for the circulation.

Despite the realistic conditions that an in-vivo environment offers, it limits the variety of the experiments compared to an in-vitro environment, where the hemodynamic parameters can take any desired value. In contrast, several effects may be missing from the in-vitro environments, such as the effect of breathing on the hemodynamics due to the changes of the intrathoracic pressure, as observed by the in-vivo data. The incorporation of the influence of the intrathoracic pressure allowed the simulation of pathophysiological scenarios which may occur at a daily basis, such as strain (Valsalva maneuver) or coughing. Including the simulation of arrhythmia in the form of premature ventricular contractions based on Amacher et al. [90], a new study (Chapter 5) was conducted to investigate the desired response of a pump-flow-adaptation controller during such acute, pathophysiological events [91].

- [91] A. Petrou, P. Pergantis, G. Ochsner, R. Amacher, T. Krabatsch, V. Falk, M. Meboldt, and M. S. Daners, "Response of a physiological controller for ventricular assist devices during acute patho-physiological events: an in vitro study," *Biomed. Eng. / Biomed. Tech.*, vol. 62, no. 6, pp. 623-633, 2017.

Results showed that even with a pump-flow-adaptation controller, critical flow conditions, such as backflow and suction may occur. The latter, was also observed during the in-vivo study. That new testing protocol allows for testing and improving potential safety controllers that focus on such critical flow conditions. The results derived, raised the motivation for a multi-objective control system which will prevent such conditions.

To prevent backflow events, which are assumed to further induce blood damage, the signal of the pump flow is required. Although implantable pump flow sensors have already been used in VAD systems, the idea of the current thesis was to use a pump inlet pressure sensor only. Thus, the author focused on the development of a pump flow estimator, based on the available signals. As described in paragraph 1.5.3, several concepts for pump flow estimators have been developed. Each of these non-invasive estimators, which rely on pump-intrinsic signals and the HCT measurement, have been developed and evaluated from different groups, under different tests, testing environments and using various pumps. Therefore, a direct comparison and selection of a concept was difficult. Furthermore, few studies have evaluated these estimators with varying pump speed and physiological requirements, as well as with a very controlled viscosity of the working medium.

For this purpose, the first systematic comparison study with flow estimators was designed, using the in-vitro [63] and in-vivo [83] experiments from the previous studies conducted (Chapter 6). The goal of the study was to identify the potential of each estimator and their limitations when used as input for control approaches. For the in-vitro measurements, a new viscosity control system was used, which allowed to evaluate them under the same viscosity [92]. A motor-model-based approach [44], an Extended Kalman Filter approach [49], an approach that uses the hydraulic model of the pump and one that combines the motor and the hydraulic models were developed for this study [93].

- [93] A. Petrou, D. Kuster, J. Lee, M. Meboldt, and M. Schmid Daners, "Comparison of flow estimators for ventricular assist devices: an in-vitro and in-vivo study," *Submitt. Ann Biomed Eng*, 2018.

1.7 Scientific contribution

All these approaches rely on the relationship between pump current and flow, which is considered linear. However, based on the design of the VAD impeller, this relationship can be characterized by non-linearities, which influence the performance of the estimator negatively. For the blood pump that was used in all presented studies, the DP2 (Xenios AG, Heilbronn, Germany), this non-linearity started close to 0 L/min and below, making it difficult to use the estimated pump flow for developing a robust backflow controller. Results showed that by using a single pump inlet pressure, no significant improvements can be achieved. Based on the estimation errors achieved, the reference flow of the backflow controller was identified such that backflow is prevented, as well as the reliability of the flow-based indices for monitoring purposes. With this study, the estimator, which would be incorporated to the multi-objective control system was concluded.

In the previous study [93], the estimators were also evaluated for a varying HCT value, thus investigating the influence of HCT on the estimation error. As it was already known, changes in HCT lead to a less reliable estimator, unless its value is continuously updated. Nowadays, HCT can only be measured by the clinical personnel when the VAD patient visits the healthcare center. That was the motivation for the next study (Chapter 7), which was focused on the development of a viscosity prediction algorithm [94].

[94] A. Petrou, M. Kanakis, S. Boes, P. Pergantis, M. Meboldt, and M. Schmid Daners, "Viscosity prediction in a physiologically controlled ventricular assist devices:," *IEEE Trans Biomed Eng*, 2018.

For this purpose, pump-intrinsic signals, estimated pump flow and the pump inlet pressure were used as input for a machine-learning model. This model was based on Gaussian processes for regression, while a modification of the stacked generalization process was developed to combine the performance of three different models. Ultimately, a mean absolute error of 1.8% in HCT was achieved, when evaluating the model with unseen data that included several variations of the pump speed and the physiological requirements. This model was a first step towards the online prediction of the HCT, which remains to be seen.

The next study (Chapter 8) constitutes the major contribution of the current thesis, as it presents the realization of the multi-objective control (MOC) system which only relies on the pump inlet pressure [95].

[95] A. Petrou, M. Monn, M. Meboldt, and M. Schmid Daners, "A Novel Multi-objective Physiological Control System for Rotary Left Ventricular Assist Devices," *Ann Biomed Eng*, pp. 1–12, 2017.

The results and algorithms developed from all previous studies were used to meet some of the objectives, such as the physiological pump flow adaptation and the prevention of suction, backflow and overload. Apart from these objectives, that MOC system also aimed at: regulating the status of the aortic valve, augmenting the aortic pulse pressure inlet pressure. To realize these objectives, signal-processing algorithms were developed to extract several features from the pump inlet pressure. These features also allowed the monitoring of the LV pre- and afterload conditions, by estimating the mean aortic pressure, as well as the cardiac rhythm.

Pre-, afterload and contractility variations were conducted in vitro to evaluate the performance of the control system. Results proved the physiological adaptation of the pump flow, following the preload changes, while the aortic pulse pressure yielded a threefold increase compared to a CS operation. The status of the aortic valve was detected with an overall accuracy of 86% and was controlled as desired. This was the first study to present an aortic-valve-opening controller and report its evaluation with in-vitro experiments. Previous multi-objective control systems consisted of a pump-flow-adaptation controller and a suction detection and release controller, as described in Section 1.5.4. The novel multi-objective control system developed within this thesis constitutes the first to include that many control objectives which are applied harmonically and validated in vitro. With the in-vitro results acquired [95], the proposed system showed its potential for a safe physiological response to varying perfusion requirements, while offering important hemodynamic indices for patient monitoring during LVAD therapy. More important, such a system promises a reduction of the risk for myocardial atrophy and allows the continuous implementation and monitoring of personalized therapeutic protocols that would promote the myocardial recovery, the most desired outcome of LVAD therapy.

The final study of the thesis (Chapter 9) differed from the previous ones, as it focused on the investigation of the importance of physiological control during BiVAD or TAH support, which constitute potential treatment options for biventricular failure. As described in section 1.3.3, this is a quite common disease, especially post-

LVAD implantation. Current BiVAD systems operate at a CS, thus leading to several complications and presenting poor outcomes, whereas TAH systems are quite complex and present low reliability which leads to low survival rates as well. For the purposes of this study [96], a new HMC for evaluating BiVADs and TAHs was developed, relying on the existing know-how from an earlier developed HMC for LVADs within our group [97]. Numerical models for a circulation with biventricular failure and without the native heart were developed and used for the HMC developed.

[96] A. Petrou, M. Granegger, M. Meboldt, and M. Schmid Daners, “A versatile hybrid mock circulation for hydraulic investigations of active and passive cardiovascular implants,” *Under review in ASAIO J*, 2018.

A preload-based, pump-flow-adaptation controller, similar to the one used at the multi-objective control system developed, was implemented in two HVADs which were used for BiVAD and TAH configurations. For the BiVAD case, aortic valve insufficiency experiments were simulated, while the HVADs were either operating at a constant speed or controlled by the pump-flow-adaptation controller. For the TAH case, an increase of the pulmonary vascular resistance was applied while the HVADs were controlled similar to the BiVAD case. The results of the experiments indicated the potential of physiological control during BiVAD or TAH support to prevent suction or overload events, which may occur during CS operation. The HMC developed was able to generate realistic, pathophysiological waveforms, while all hemodynamic conditions were simulated by only adapting the software. The latter constitutes a great advantage of our HMC compared to other HMCs developed, where significant hardware changes are required to perform experiments with different type of devices.

This characteristic of versatility led to the exploitation of the HMC for additional experiments that simulate a Fontan circulation from rest to exercise conditions, where Fontan grafts usually fail. A total-cavopulmonary-support (TCPC) geometry was derived from a patient with MRI and reproduced with 3D printing techniques. This physical model of the TCPC was interacting with the numerical model of the Fontan circulation through the hydraulic interface of the HMC. To the best knowledge of the author, no such sophisticated testing environment has been presented for evaluating BiVAD, TAH and Fontan cases without modifying the hardware of the setup, while no study has reported tests with a TCPC in a hardware-in-the-loop setup. This study showed that the TCPC geometry influences the flow distribution between left (LPA) and right pulmonary artery, which was unbalanced and 10% higher in LPA and led to higher pressures [96].

The HMC developed constitutes a reliable testing environment for the initial development steps of BiVAD and TAH devices and their control algorithms. Its versatility offers the possibility to test several active or passive cardiovascular implants, such as artificial valves. With Fontan experiments, we proved that the HMC together with rapid prototyping methods may enhance the design of anatomic structures and improve their geometry before implantation to achieve better hemodynamics.

In addition to the contributions of the current thesis, the author collaborated with colleagues and other institutes for the following projects. The most important collaboration was the study with the acute in-vivo experiments, which has already been described and constitutes a whole chapter (Chapter 4) of this thesis. A fruitful collaboration was realized with Children’s National Medical Center, Washington, DC. The HMC developed [96] and presented in Chapter 9 was used for validating their studies with computational fluid dynamics that aim at the preoperative optimization of patient-specific grafts for achieving better Fontan hemodynamics [98]. Another study on our HMC was together with the group of Functional Materials of ETH Zurich, who developed a silicon TAH using 3D printing and injection molding techniques [99]. My contribution included the evaluation of the silicon TAH when supporting a human blood circulation. Furthermore, I supported my colleagues Rebholz et al. [100] with the in-silico evaluation of a pulsatile LVAD operating at high-frequency and with identifying the required stroke volume of such a device. In another study with Dual et al. [60], the recordings from the in-vivo trials [83] were analyzed and a correlation between the changes in R-wave magnitude and the LV end-diastolic volume (EDV) was derived, constituting the R-wave magnitude a potential feature for estimating EDV. Finally, together with my colleagues, we developed the first control system for controlling the viscosity of the working medium of our HMC [92]. The influence of fluid

1.7 Scientific contribution

viscosity on the measured performance of each VAD was investigated. This viscosity control system was used in most of my studies and allowed to conduct unique experiments with high fidelity, especially when evaluating flow estimator [93] and developing the HCT prediction model [94]. These studies are not included in the current thesis and the reader can find more information within the provided references.

- [60] S. A. Dual, G. Ochsner, A. Petrou, R. Amacher, M. J. Wilhelm, M. Meboldt, and M. Schmid Daners, “R-Wave Magnitude: a Control Input for Ventricular Assist Devices,” in *Proceedings of the 8th International Workshop on Biosignal Interpretation*, pp. 18-21, 2016.
- [92] S. Boës, G. Ochsner, R. Amacher, A. Petrou, M. Meboldt, and M. Schmid Daners, “Control of the Fluid Viscosity in a Mock Circulation,” *Artif. Organs*, vol. 15, no. 12, 2017.
- [98] D. Siallagan, Y.-H. Loke, L. Olivieri, J. Opfermann, C. S. Ong, D. De Zelicourt, A. Petrou, M. Schmid Daners, M. Meboldt, K. Nelson, L. Vricella, J. Johnson, N. Hibino, and A. Krieger, “Virtual surgical planning, flow simulation and 3D electro-spinning of patient-specific grafts to optimize Fontan hemodynamics,” *Submitt. Publ. J Thorac Cardiovasc Surg*, vol. 155, no. 4, pp. 1734-1742, 2018.
- [99] N. H. Cohrs, A. Petrou, M. Loepfe, M. Yliruka, C. M. Schumacher, A. X. Kohll, C. T. Starck, M. Schmid Daners, M. Meboldt, V. Falk, and W. J. Stark, “A Soft Total Artificial Heart-First Concept Evaluation on a Hybrid Mock Circulation,” *Artif. Organs*, vol. 41, no. 10, pp. 948-958, 2017.
- [100] M. Rebholz, R. Amacher, A. Petrou, M. Meboldt, and M. Schmid Daners, “High-frequency operation of a pulsatile VAD – a simulation study,” *Biomed. Eng. / Biomed. Tech.*, vol. 62, no. 2, pp. 161–170, 2016.

2 A Physiological Controller for tVADs Based on Systolic LVP (Paper I)

2.1 Abstract

The current paper presents a novel physiological feedback controller for turbodynamic ventricular assist devices (tVADs). This controller is based on the recording of the left ventricular (LV) pressure measured at the inlet cannula of a tVAD thus requiring only one pressure sensor. The LV systolic pressure (SP) is proposed as an indicator to determine the varying perfusion requirements. The algorithm to extract the SP from the pump inlet pressure signal used for the controller to adjust the speed of the tVAD shows robust behavior. Its performance was evaluated on a hybrid mock circulation. The experiments with changing perfusion requirements were compared with a physiological circulation and a pathological one assisted with a tVAD operated at constant speed. A sensitivity analysis of the controller parameters was conducted to identify their limits and their influence on a circulation. The performance of the proposed SP controller was evaluated for various values of LV contractility, as well as for a simulated pressure sensor drift. The response of a pathological circulation assisted by a tVAD controlled by the introduced SP controller matched the physiological circulation well, while over- and underpumping events were eliminated. The controller presented a robust performance during experiments with simulated pressure sensor drift.

2.2 Introduction

The blood propulsion by the healthy heart provides all tissue of the human body with oxygen and nutrients and removes waste products. The heart's hydraulic output is regulated by various interacting mechanisms, which ensure that the perfusion meets the continuously varying requirements [101]. In case of heart failure, the severe left ventricular (LV) dysfunction impairs the cardiac contraction and consequently, reduces the cardiac output (CO). Heart failure constitutes a common, costly and even fatal condition, mainly in developed countries [102]. The treatment of heart failure depends on the severity of the disease [103]. For severe heart failure, heart transplantation remains the gold standard treatment. However, this treatment is limited by a donor heart shortage and therefore, the long-term application of mechanical circulatory support systems has been increasing [7], [104].

Ventricular assist devices (VADs) constitute such a mechanical circulatory support system. VADs are mechanical blood pumps, which support the pumping function of the failing heart. Most VADs are implanted in the LV and pump blood into the aorta, in parallel to the remaining heart [105]. VAD technology has improved over the last decades and nowadays, their performance in terms of survival is comparable to that of heart transplantations [106]. However, adverse events still occur at a high rate [7] and require further technological improvements in future systems. One limitation of today's VADs is their constant speed operation, which may lead to over- and underpumping situations as the perfusion requirements change. Adverse events that are presumably promoted by over- and underpumping are hemolysis and thromboembolic events due to suction, as well as right heart failure or lung edema caused by volume or pressure overloading [107]–[109]. Consequently, the physiological adaptation of VADs is a promising technological enhancement to improve the outcome of the VAD therapy.

A variety of control strategies for VADs has been developed to achieve physiological adaptation [61]. The two major challenges in the development of a physiological controller are the selection of the sensory feedback signal and the design of an algorithm, which adjusts the pump speed based on this measurement. Many controllers are based on pump intrinsic signals, like the motor current, the pump speed or the heart rate (HR), which can be calculated from the motor current waveform [110]–[113]. Other physiological controllers based on either measured or estimated flow [114]–[116], atrial pressure [117], pump pressure head [118]–[120], end-diastolic volume (EDV) [65], or end-diastolic pressure (EDP) [121], [122] have been developed, evaluated and published.

2.3 Materials and Methods

Most of them try to imitate the Frank-Starling mechanism [101], which describes how the CO of a healthy heart depends on after- and preload. In case of a pathological heart, this mechanism is unable to meet the perfusion requirements due to the impaired functioning of the LV. Even though the flow of a VAD also depends on the after- and preload, its sensitivity differs greatly from the Frank-Starling mechanism. The current paper presents a novel physiological controller for turbodynamic VADs (tVADs), which imitates the Frank-Starling mechanism based on the measured pump inlet pressure (PIP) using the systolic pressure (SP) of the PIP signal as input to the controller. From here on, we refer to it as SP controller.

The SP controller proved a physiological adaptation of the tVAD's speed during after- and preload variations and followed the perfusion requirements of a simulated patient well. The algorithmic steps to extract the SP from the PIP and the adjustment of the tVAD speed are presented. The relationship between the LV SP and the LV filling as well as the sensitivity of the SP controller's parameters and the influence of the LV contractility and the pressure sensor drift were analyzed.

2.3 Materials and Methods

2.3.1 Hybrid mock circulation

All experiments were conducted on the hybrid mock circulation (HMC) presented in [97]. The HMC mimics the cardiovascular system by a numerical model [123] that is connected to the tVAD by a numerical-hydraulic interface. A non-implantable mixed-flow turbodynamic blood pump (Deltastream DP2, Medos Medizintechnik AG, Stolberg, Germany) that allows implementing various control approaches substitutes the tVAD in order to conduct all the experiments. Various pathophysiological scenarios have been simulated to test physiological control algorithms [65]. Unstressed venous volume, arterial resistance, LV contractility and HR can be varied independently. In order to imitate a pathological circulation with the HMC, the contractility of the LV was reduced, and the HR was increased. The specific settings for each experiment are described in the Experiments Section.

2.3.2 Systolic pressure as physiological index

In the following paragraphs, we analyze the possibility to use the SP as a measure for preload. For this purpose, pressure-volume (PV) loops of a physiological circulation, a pathological circulation without tVAD support and a pathological circulation assisted by a tVAD operated at constant speed were generated using the HMC. For each case, we investigated the dependence of SP on the after-, preload and contractility. Figure 2.1 depicts all these PV loops, which are qualitatively validated by [124], [125].

In a physiological circulation, the SP is mainly determined by the afterload and by the contractility of the LV [101]. Afterload refers to the pressure or the resistance against which the heart must work to eject blood during systole. During isovolumetric contractions, the intraventricular pressure increases until the aortic valve opens, and the ejection phase starts. Additionally, the arterial compliance and resistance as well as the resistance of the aortic valve influence the SP. Figure 2.1A shows the dependence of the SP on the afterload, whereby the SP increases as afterload increases and decreases as afterload decreases, respectively. Figure 2.1B shows that preload changes affect the SP similarly to afterload changes. A preload increase (EDV increase) results in an increase of stroke volume (SV) and correspondingly CO, resulting in an aortic pressure (AoP) increase and consequently in an SP increase [125]. A preload reduction will have the opposite effects, i.e., decreased SV, CO, AoP and SP. Figure 2.1C shows the dependence of the SP on the contractility. A contractility increase, results in a small increase in SP, while the EDV decreases, and vice versa.

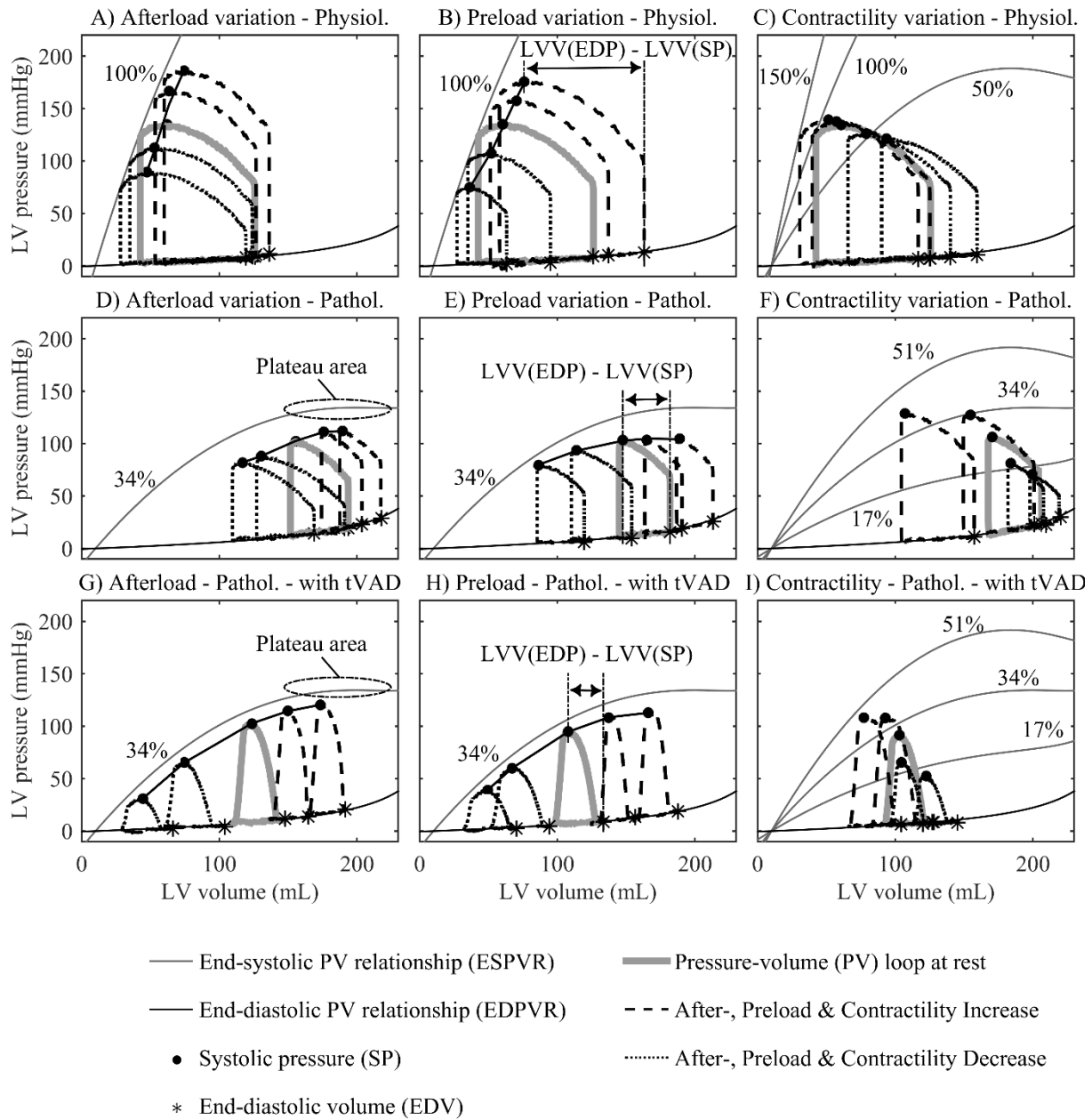


Figure 2.1: Panels A), D) and G) show pressure-volume (PV) loops for five different afterload values. Panels B), E) and H) show PV loops for five different preload values. Panels C), F) and I) show PV loops for five different contractility values. Panels A), B) and C) depict the PV loops of a physiological (Physiol.) circulation; panels D), E) and F) depict the PV loops of a pathological (Pathol.) circulation; panels G), H) and I) depict the PV loops of a pathological circulation assisted with a constant speed tVAD. The systolic pressure (SP) and end-diastolic volume (EDV) values are measured and marked for all PV loops. In the pathological circulation the left ventricular (LV) contractility is reduced and therefore, small changes of SP values are detected during increased after- and preload. The end-systolic and end-diastolic PV relationship curves are illustrated, as well as their plateau area. The contractility values expressed in percentage of the normal physiological contractility (100%) are indicated alongside the ESPVR curves. The difference between the LV volume at end-diastolic pressure (EDP) and the LV volume at SP ($LVV(EDP) - LVV(SP)$) is indicated by two dash-dotted vertical lines.

Figure 2.1D – 2.1F show the PV loops of a pathological circulation where the contractility of the simulated heart was reduced, during after-, preload and contractility variations. Due to the decreased contractility, the slope of the end-systolic-pressure-volume relationship (ESPVR) curve decreased as well [125]. Thus, smaller intraventricular pressures for the same after- and preload conditions are generated (Figure 2.1D, 2.1E) compared to the physiological circulation (Figure 2.1A, 2.1B). Additionally, during both after- and preload

increase, the heart is unable to further increase its intraventricular pressure and the influence on the SP is limited (Figure 2.1D and 2.1E). Figure 2.1D depicts this limitation through the plateau area of the ESPVR curve [125]. During contractility variations the pathological heart responds similarly to the physiological, i.e., the SP decreases during a contractility decrease and vice versa. Figure 2.1G-2.1I show the same after-, preload and contractility variation experiments conducted with a pathological circulation assisted with a tVAD set at a constant speed, which yields to 5 L/min at rest. In that case, the influence of all variations on the shape of the PV loops is different, because the continuous unloading of the LV with the tVAD reduces the SV [124], [125].

The influence of afterload on the SP is still large, however, the shape of the PV loops in Figure 2.1G show that this is not a direct influence. Unlike the PV loops in Figure 2.1A, those in Figure 2.1G show a great variation of the EDV, i.e., the LV filling. This means that the afterload has a direct effect on the filling of the LV, which in turn dictates the SP. This effect can be explained by the reduced and almost constant SV. Vertical lines in the panels B, E and H in Figure 2.1 indicated the difference between the EDV and the LV at maximum pressure. Clearly, with a small SV this difference is also small under tVAD support. In this case, as long as the filling is below the indicated plateau area, the SP directly depends on the LV filling and can therefore be seen as a measure of preload. Figure 2.1I shows that the contractility of the LV also influences the SP, which can therefore not be viewed as contractility independent.

We developed our controller according to the behavior of SP during after- and preload variations. The limitation of such a controller during contractility variations is addressed and discussed in the Results and Discussion section. The use of the SP value as physiological index for a tVAD controller requires that the PV loops of the LV remain below the plateau area and above the suction area (as depicted in Figure 2.1G and 2.1H). This requirement can be fulfilled by using a physiological controller to regulate the pump speed. The following section presents the algorithmic steps of such a controller.

2.3.3 Systolic pressure controller

We developed a controller for tVADs based on SP to restore the physiological hemodynamics, by increasing the tVAD assistance to the LV, when SP increases and vice versa. The SP controller is a proportional controller, which adapts the pump speed proportionally to the SP. The measured PIP is the input to the controller, and the desired pump speed (N_{des}) is the output. Figure 2.2 shows the structure of the SP controller. It consists of two parts: First, the PIP is low-pass filtered with a first-order infinite impulse response (IIR) filter. The maximum pressure, i.e. the SP, is detected within a fixed time interval of 2 seconds to ensure that an SP value is detected even for low heart rates. Second, the SP control algorithm is executed according to:

$$N_{des} = k_{sp} (SP - SP_{ref}) + N_{ref} \quad (2.1)$$

where k_{sp} is the proportional gain (rpm/mmHg), SP_{ref} is the SP obtained during calibration (mmHg) and N_{ref} is the pump speed during calibration (rpm). The controller linearly relates a signal that varies with after- and preload variations (the SP) to the pumping work by controlling the N_{des} , and thus imitates the Frank-Starling mechanism.

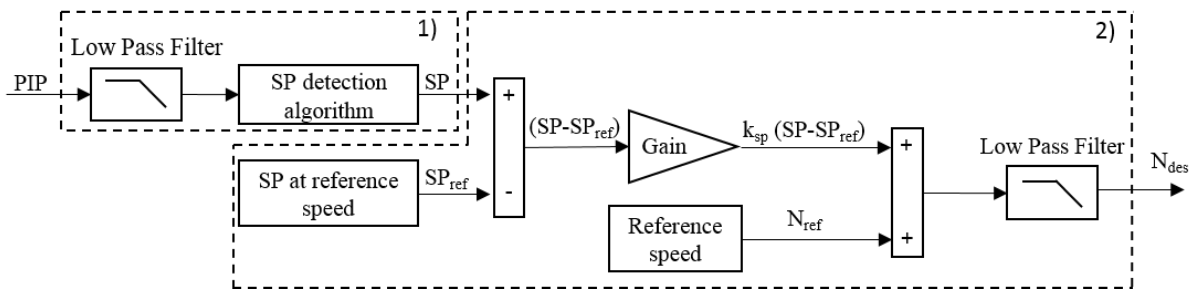


Figure 2.2: Structure of the SP controller. First, the systolic pressure (SP) is extracted and its difference from the reference systolic pressure SP_{ref} is calculated. Second, the resulting SP difference is multiplied by the proportional gain k_{sp} of the controller and the product is added to the reference speed of the controller in order to define the desired pump speed N_{des} . The reference speed N_{ref} and the corresponding systolic pressure SP_{ref} are obtained during the patient specific calibration process.

For this study, the parameters N_{ref} and SP_{ref} of the SP controller were identified with the following calibration process. First, we manually identified the constant pump speed that yielded a desired CO at rest. The chosen speed was saved as N_{ref} and the corresponding SP was saved as SP_{ref} . The gain k_{sp} was not identified during the calibration process, but defined by conducting an in vitro sensitivity analysis, which is presented in the Experiments and Results Sections.

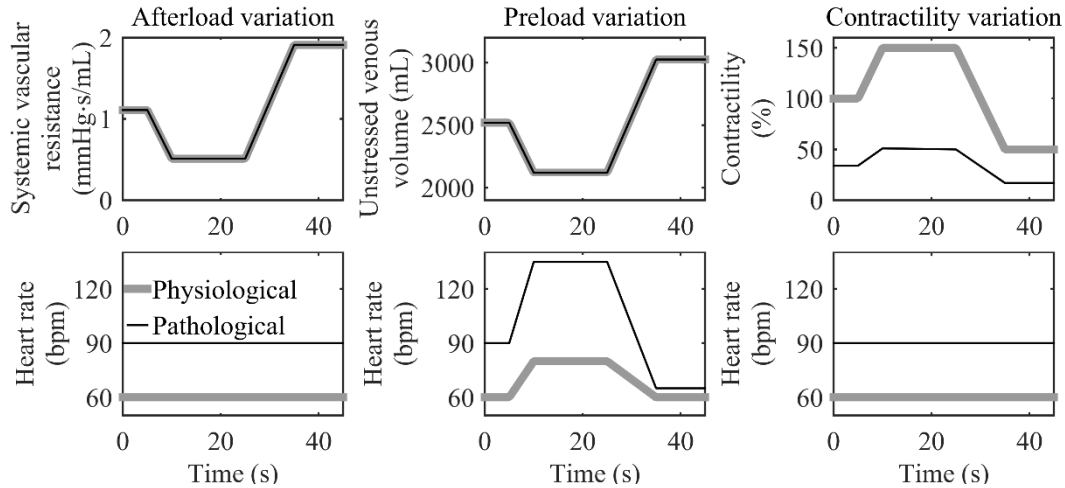


Figure 2.3: Defined cardiovascular parameters for the after-, preload and contractility variation experiments. During the preload variation experiment, the systemic vascular resistance was controlled by the baroreflex; during the afterload variation experiment, the unstressed venous volume was controlled by the CO autoregulation. The contractility was maintained at 34% or 100% for both variations. For the contractility variations experiments, both, systemic vascular resistance and unstressed venous volume were fixed at the values attained in the resting condition (corresponding to $0 \text{ s} < t < 5 \text{ s}$ of after- and preload variation).

2.3.4 Experiments

Figure 2.3 depicts the prescribed variations of cardiovascular parameters for our experiments. The parameters for after- and preload variations correspond to the variations presented in [65], with a wider range of parameters. We additionally conducted experiments with a varying contractility. Specifically, we varied the HR, the unstressed venous volume, the systemic vascular resistance and the contractility in order to represent the after-, preload and contractility variations. The experiments were designed not to mimic a specific daily situation, but to allow for an independent investigation of the effects of the after-, preload and contractility variations on the performance of the SP controller. In addition, the focus of the experiments was on fast and wide-ranging variations of cardiovascular parameters, which are challenging for a desired physiological VAD controller.

For each experiment, the HMC ran for 20 s with a constant pump speed and fixed physiological parameters to allow the system to reach steady state at the resting condition. Then, one of the experiments was started. The duration of after- and preload variations was 45 s. For the contractility variation experiment, the duration was increased to 100 s to reach steady state after each variation. During the experiments, the LV pressure was continuously measured (PN2009, IFM Electronic GmbH, Essen, Germany). This measurement was given as an input to the SP controller.

Table 2.1 lists the specific configurations used for the experiments. We conducted four different studies to evaluate these configurations. Each study included the comparison of different configurations of Table 2.1 and experiments of Figure 2.3. Table 2.2 lists the studies conducted, as well as the corresponding configurations tested, and the variations applied. Configurations C1-C7 and C10-C11 were evaluated under after-, preload and contractility variations whereas C8 and C9 were only evaluated under after- and preload variations and the contractility were held constant. Further investigations of the performance of the SP controller included various configurations, which are listed in Table 2.3 in the Results section.

Table 2.1: Settings of the different experiment configurations.

Configuration (#)	Predefined Parameters			Variables obtained during calibration process		Contractility during after- and preload variations (%)	Sensor Drift (mmHg)
	tVAD support	CO at rest (L/min)	Controller Gain - k_{sp} (rpm/mmHg)	Reference Speed - N_{ref} (rpm)	Reference SP - SP_{ref} (mmHg)		
C1	-	5	-	-	-	100	-
C2	Constant speed	5	-	4180	-	34	-
C3	SP controller	5	40	4180	91	34	0
C4	SP controller	4.5	40	3750	102	34	0
C5	SP controller	5.5	40	4500	73	34	0
C6	SP controller	5	10	4180	91	34	0
C7	SP controller	5	220	4180	91	34	0
C8	SP controller	5.85	40	4180	118	60	0
C9	SP controller	4.7	40	4180	32	10	0
C10	SP controller	5.28	40	4180	91	34	+15
C11	SP controller	4.87	40	4180	91	34	-15

CO, cardiac output; SP, systolic pressure; tVAD, turbodynamic ventricular assist device

All four studies, listed in Table 2.2, are described below:

1) Baselines and nominal SP controller:

Comparison of the performance of a pathological circulation assisted with the nominal SP controller (C3) with the performances of a physiological circulation (C1) and with a pathological circulation assisted with a tVAD running at constant speed (C2). The gain k_{sp} was set to 40 rpm/mmHg, and the desired CO was chosen to be 5 L/min, which yielded a reference speed N_{ref} of 4180 rpm during calibration.

2) Sensitivity of the SP controller on the controller parameters:

The second study analyzes the performance of the SP controller for different values for the controller parameters. Particularly, the influence of the SP controller's gain k_{sp} and reference speed N_{ref} on the CO and the SP were investigated. The high and low values for the N_{ref} were chosen such that a CO of 5.5 and 4.5 L/min, respectively, resulted at rest. The high and low values for k_{sp} were identified based on different limits. The high gain was identified by gradually increasing it, until strong CO oscillations were observed during the experiments, which occurred at $k_{sp} = 220$ rpm/mmHg. The low gain was identified by gradually decreasing it, until the pump operates close to suction (SP close to 0 mmHg), which occurred at $k_{sp} = 10$ rpm/mmHg. Both configurations C6 and C7 were compared to the nominal SP controller C3.

3) Sensitivity of the SP controller on the contractility:

The third study investigated the influence of various contractility conditions on the circulation assisted with a tVAD controlled with the SP controller, during after- and preload variations. Both experiments were conducted for different constant contractility values from 10% to 60%. The RMS values with respect to the nominal SP controller at a 34% contractility (C3) were calculated.

4) Sensitivity of the SP controller on sensor drift:

The performance of the nominal SP controller during all three variations was evaluated when the pressure sensor is affected from drift. The drift was simulated by adding or subtracting a constant offset to the actual LV pressure measurement. The maximum offset was ± 25 mmHg.

Table 2.2: List of conducted studies, tested configurations and applied variations.

Study	Description	Configurations tested	Preload variation	Afterload variation	Contractility variation
1	Baselines and nominal SP controller	C1-C3	✓	✓	✓
2A	Sensitivity of the SP controller on the controller parameters	C3-C5	✓	✓	✓
2B		C3, C6, C7	✓	✓	✓
3	Sensitivity of the SP controller on the contractility	C8, C9	✓	✓	×
4	Sensitivity of the SP controller on sensor drift	C10-C11	✓	✓	✓

2.4 Results

2.4.1 Baselines and nominal SP controller

Figure 2.4 shows the result of the baselines and SP controller performance. Three configurations are compared; the physiological circulation (C1), the pathological circulation assisted with a constant speed tVAD (C2) and the pathological circulation assisted with a tVAD controlled by the SP controller (C3). The CO response of the circulation supported by the SP-controlled tVAD is similar to that of the physiological circulation. In contrast, when the tVAD is operated at constant speed, the CO response is attenuated, and suction events occur (at $t > 38$ s during preload variation and at $20 \text{ s} < t < 28$ s during afterload variation). When the contractility increases, the CO of C1 and C2 remains almost constant, while it slightly increases when the SP controller is applied. During the contractility decrease, the CO of C1 decreases while the EDP increases up to 12 mmHg. With C3, the CO decreases even more than with C1, while the EDP increases up to 25 mmHg. Study 1 in Table 2.3 shows the CO RMS values of C2 and C3 configurations with respect to C1. The CO RMS values of C3 for after- and preload variation experiments are closer to zero compared to C2, proving the more physiological response of the pump when the SP controller is applied. However, the C2 configuration presents better CO results (based on RMS values) than the C3 during the contractility variations.

Figure 2.5 shows the PV loops of C3 during all three experiments. The LV volume remains within a physiological range and the SP varies according to the LV filling in both after- and preload variation experiments. During the strong contractility variations, this is not the case. Figure 2.6 depicts the detection of the SP from the PIP signal during the preload variation according to the detection algorithm presented in the Materials and Methods section. The SP value is reliably detected every 2 s. A delay is introduced due to the filtering and the fixed time interval used.

2.4.2 Sensitivity of the SP controller on the controller parameters

Figure 2.7 shows a comparison of two configurations with a different value for the reference speed (C4 and C5) in comparison with the nominal SP controller (C3) during the preload experiment. SP signals show that no overpumping events (suction) occurred in both cases despite the maladjustment of the reference speed. Figure 2.8 shows a comparison of two configurations with a different value for the controller gain (C6 and C7) in comparison with the nominal SP controller (C3) during the preload experiment. With $k_{sp} = 220$ rpm/mmHg (C7), CO and pump speed oscillations occurred during the preload increase, which indicates small stability margins. In contrast, with $k_{sp} = 10$ rpm/mmHg (C6), the controller dictates small speed changes only, which resulted in very low SP values during the preload decrease at $t > 40$, similar to the constant speed operation of the tVAD (C2). The calculated RMS values for various reference speeds and gain parameters with respect to the nominal SP controller are listed in Table 2.3. The CO RMS values for the two reference speeds tested in C6 and C7 do not differ much. However, we observed more aortic valve flow when the reference speed was low (C4). The speed, and in turn CO, oscillations shown in Figure 2.8 during the preload variation, were also observed during the afterload and the contractility variation. However, they already occurred at lower

2.4 Results

controller gains, namely at $k_{sp} = 140$ rpm/mmHg during the afterload variation and at $k_{sp} = 80$ rpm/mmHg during the contractility variation. Suction only occurred at controller gain values below 10 rpm/mmHg.

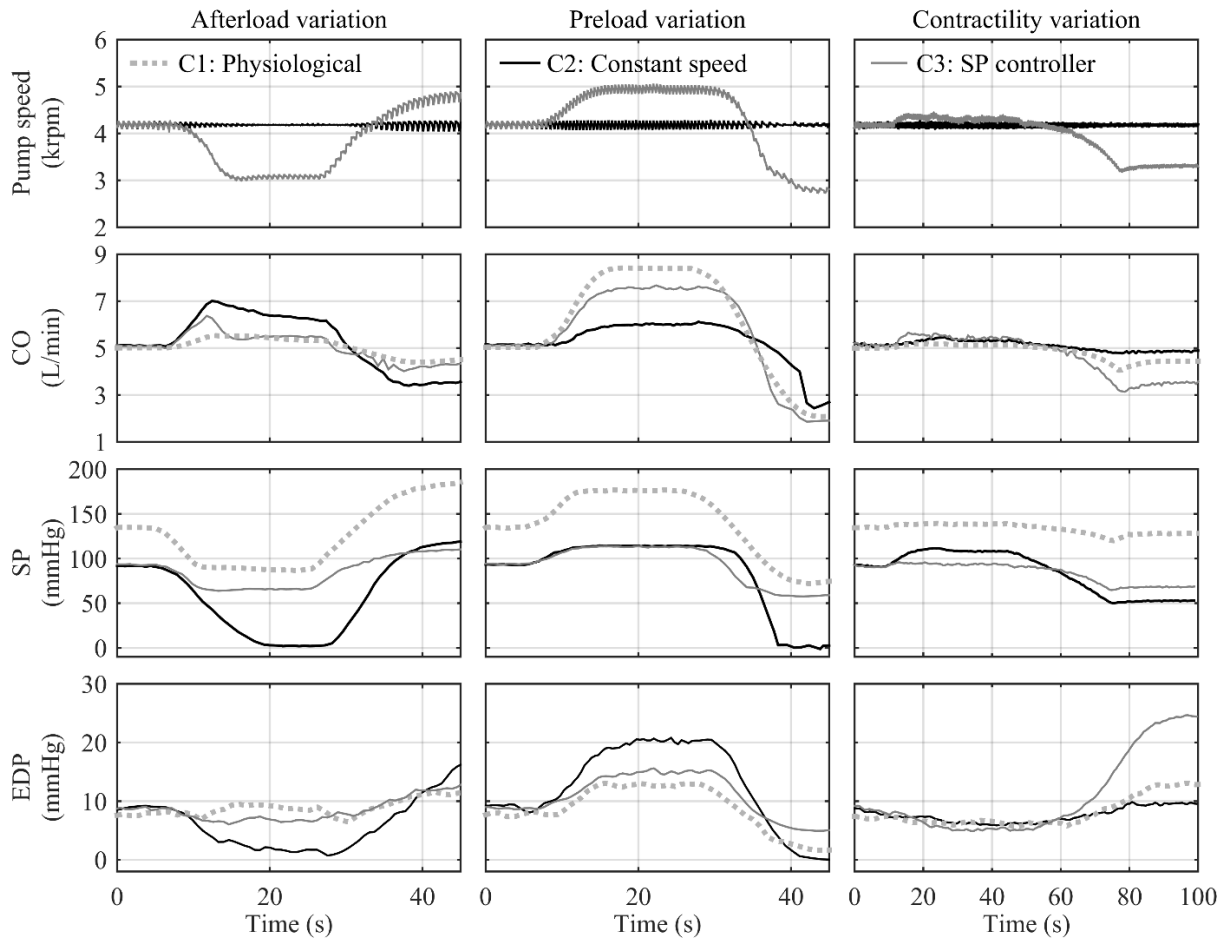


Figure 2.4: Experimental results of Study 1. After-, preload and contractility variation experiments for the physiological circulation (C1), the pathological circulation assisted with a constant speed tVAD (C2), and the pathological circulation assisted with a tVAD controlled by the SP controller (C3). The resulting signals for pump speed, cardiac output (CO), systolic pressure (SP) and end-diastolic pressure (EDP) are depicted.

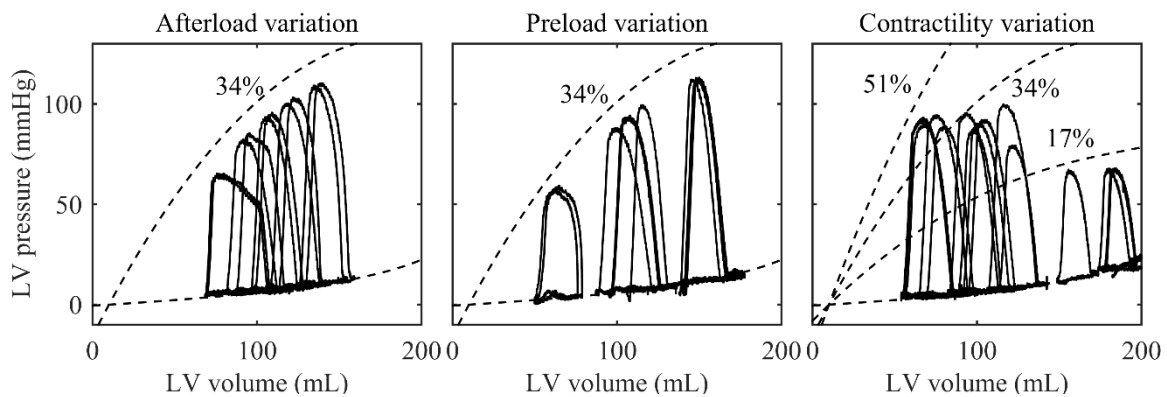


Figure 2.5: Pressure-volume loops during after-, preload and contractility variation experiments for the pathological circulation assisted with a tVAD controlled by the SP controller (C3). The dashed lines indicate the end-systolic and end-diastolic pressure-volume relationship curves for different contractility values, which are indicated in percent of the physiological contractility.

Table 2.3: Calculated root mean square values for cardiac output in liters/minute for all Studies conducted, all after-, preload and contractility variations implemented and configurations evaluated. For Study 1 the configurations are compared with the physiological circulation (C1), whereas for the Studies 2A, 2B, 3 and 4 the configurations are compared with the nominal SP controller (C3). All labelled configurations (e.g. C3) are also presented in a figure above.

Study 1	<i>Baselines and nominal SP controller</i>										
	Physiological (C1)			Constant speed (C2)				Nominal SP controller (C3)			
Afterload variation	0			0.86				0.29			
Preload variation	0			1.61				0.58			
Contractility variation	0			0.31				0.54			
Study 2A	<i>Reference Speed N_{ref} (rpm)</i>										
	3750 (C4)			4180 (C3)				4500 (C5)			
Afterload variation	0.42			0				0.39			
Preload variations	1.02			0				1.04			
Contractility variation	0.64			0				0.82			
Study 2B	<i>Gain parameter k_{sp} (rpm/mmHg)</i>										
	0	10 (C6)	20	40 (C3)	60	80	100	120	140	200	220 (C7)
Afterload variation	0.65	0.36	0.24	0	0.17	0.33	0.46	0.74	0.88	-	-
Preload variation	1.24	1.05	0.55	0	0.28	0.61	0.47	0.86	0.81	0.88	1.08
Contractility variation	0.78	0.46	0.24	0	0.27	0.56	-	-	-	-	-
Study 3	<i>Contractility parameter (%)</i>										
	10 (C9)	15	20	25	30	35	40	45	50	55	60 (C8)
Afterload variation	0.39	0.33	0.21	0.21	0.12	0.06	0.14	0.22	0.28	0.35	0.4
Preload variation	1.11	0.88	0.64	0.36	0.23	0.18	0.31	0.64	0.93	1.19	1.46
Contractility variation	-	-	-	-	-	-	-	-	-	-	-
Study 4	<i>Pressure sensor drift (mmHg)</i>										
	-25	-20	-15 (C10)	-10	-5	0 (C3)	5	10	15 (C11)	20	25
Afterload variation	0.61	0.39	0.35	0.23	0.14	0	0.12	0.2	0.24	0.3	0.33
Preload variation	1.38	1	0.64	0.38	0.16	0	0.34	0.47	0.67	0.78	0.93
Contractility variation	0.7	0.59	0.47	0.33	0.23	0	0.1	0.24	0.36	0.49	0.53

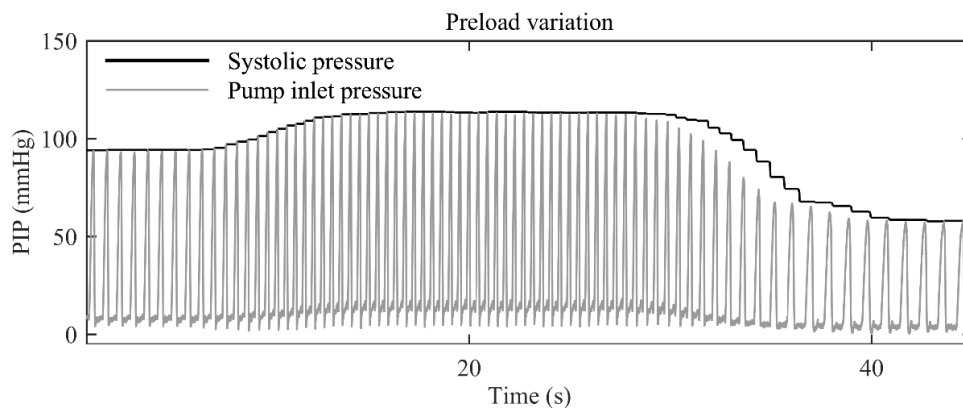


Figure 2.6: The Pump inlet pressure (PIP) and the extracted systolic pressure (SP) during the preload variation experiment.

2.4 Results

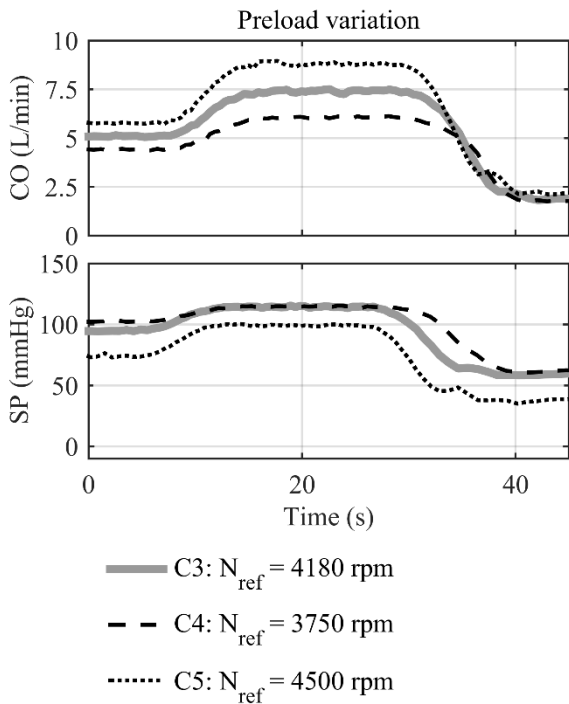


Figure 2.7: Sensitivity analysis of the SP controller reference speed N_{ref} (C4, C5) in comparison with the nominal SP controller (C3).

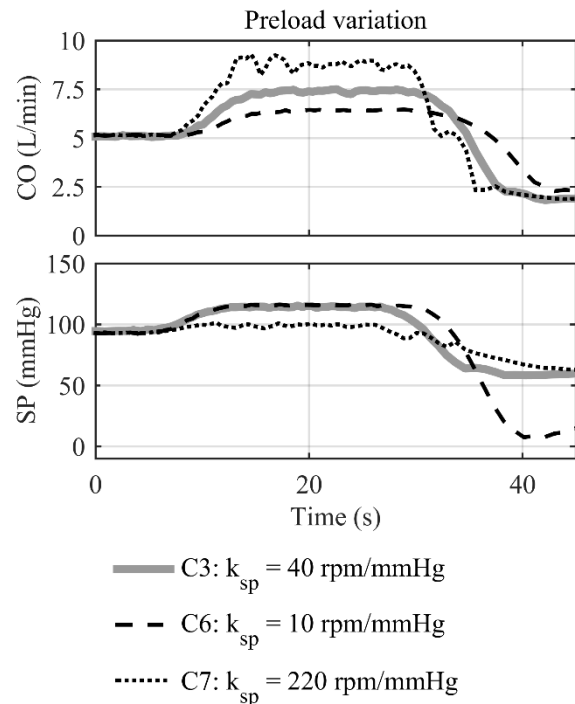


Figure 2.8: Sensitivity analysis of the SP controller gain k_{sp} (C6, C7) in comparison with the nominal SP controller (C3).

2.4.3 Sensitivity of the SP controller on the contractility

Figure 2.9 shows the influence of the contractility on the performance of the nominal SP controller during the preload variation. The contractility is increased from 34% (C3) to 60% (C8) (e.g. myocardial recovery) and decreases from 34% (C3) to 10% (C9) (e.g. progressive heart failure). The contractility increase (C8) led to an increase of the CO up to nearly 10 L/min during the preload increase, which even exceeded the CO of the physiological circulation (Figure 2.4, CO panel of Preload variation). The contractility decrease (C9), led to a reduced CO during the preload increase. Furthermore, the pump was operating close to suction (minimum SP = 5 mmHg at $t > 40$ s) during the preload decrease. The CO RMS values of all contractility values tested for both after- and preload variations are listed in Table 2.3, Study 3. The contractility variations mainly influenced the performance of the nominal SP controller during the preload variations. Suction events (LV pressure < 0 mmHg) did not occur for any tested contractility value during both experiments.

2.4.4 Sensitivity of the SP controller on pressure sensor drift

Figure 2.10 shows the effect of a sensor drift on the CO and the SP during the preload variation. The sensor drift is implemented by a constant offset in the LV pressure measurement. An offset of ± 15 mmHg, only has a small effect on the resulting CO. And even with ± 25 mmHg, no suction events occurred. Study 4 in Table 2.3 lists the calculated CO RMS values for various values for the sensor drift with respect the values obtained with 0 mmHg offset. A drift of -25 mmHg led to a CO RMS value greater than 1 L/min.

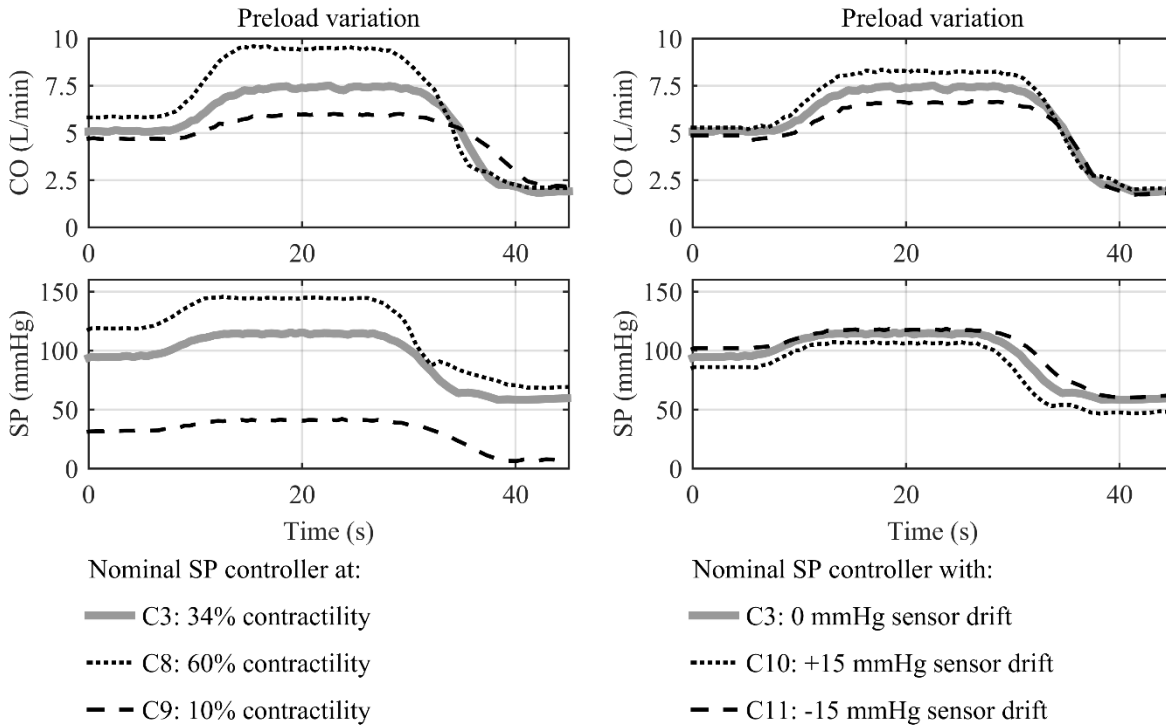


Figure 2.9: Influence of contractility increase and decrease on the performance of the SP controller. The figure shows how CO and SP change when the contractility of a specific pathological LV increases (C8) or decreases (C9).

Figure 2.10: Influence of sensor drift on the performance of the SP controller. The figure shows how CO and SP change when the measurement of the pressure sensor is affected by a drift of ± 15 mmHg.

2.5 Discussion

A tVAD operated at constant speed is able to restore the hemodynamics of a patient suffering from severe heart failure to a physiological range. However, variations of the physiological requirements can lead to over- or underpumping. Figure 2.4 shows that the SP controller is able to avoid such events and yield a physiological adaptation of the CO. The performance of the SP controller is based on the strong dependence of the SP on after- and preload, when a tVAD assists a pathological circulation. During contractility variations, the SP controller (C3) behaved similar to the physiological circulation (C1), with respect to CO changes, but more aggressively, i.e., greater CO changes were observed when the contractility was changed.

We can categorize most published physiological controllers in three groups, according to their concept. The first group consists of controllers that are directly based on preload [65], [121], [126], i.e., they use a measure of preload as the input to the controller, for instance EDV, EDP, or left atrial pressure (LAP). These controllers are independent of the contractility. The second group consists of controllers, which rely on an estimate of preload [116], [118], [127], for instance the pump flow or pressure pulsatility. These algorithms depend on preload as well as contractility, but they also aim at imitating the response of the native heart, i.e., the Frank-Starling mechanism. The third group consists of controllers, which aim at maintaining the perfusion [70]–[77] in a physiological range for instance through measurements of mean arterial pressure, EDP, pump flow or pump pressure difference. The SP controller can be assigned to the second group, as the SP, just like most pulsatility indices, depends on preload as well as contractility.

In [128], the authors evaluated various physiological controllers from these three groups in vitro. Their results show that among the pressure controllers, those based on EDP present the best physiological performance [121], [122]. The performance of the pump-flow-pulsatility-based controller [116] is slightly inferior, but still good [121], [128]. The SP controller is based on the estimation of the preload condition of

the LV and therefore, it lacks preload sensitivity compared to direct preload-based controllers [65], [121], [122].

However, the novelty of the SP controller has a few advantages over most other controllers. First, only one pressure sensor at the inlet cannula of the pump is required in order to implement the controller, while the other pressure-based controllers require an additional sensor to measure either the pump flow [121] or the pressure at the outlet of the pump (aortic pressure) [118], [119], [122], [129]–[131]. Thus, the SP controller keeps the complexity of the system low. Second, sensor drift constitutes a major problem of implantable pressure sensors [132] and the SP controller is very robust towards this drift. Figure 2.5 shows that SP undergoes large variations (55 to 110 mmHg) during after- and preload variations and therefore the influence of noise and sensor drift on the performance of the SP controller is small. Figure 2.10 and Study 4 in Table 2.3 justify this statement by showing the influence of the sensor drift on the CO. In contrast, EDP undergoes small variations during after- and preload variations (Figure 2.4), which makes it quite sensitive when sensor noise or drift are present. Third, the SP is the maximum value of the LV pressure signal, which is, compared to EDP, easier to extract.

The SP controller is simple in structure. It has only three parameters to be defined: the reference speed N_{ref} , the reference SP SP_{ref} and the gain k_{sp} . The reference speed can be adjusted in the same way as it is done in current clinical practice [133]. For the SP controller, the physician will adjust an initial pump speed according to his or her clinical guidelines. For every tVAD, the N_{ref} will be different and based on the pressure-speed-flow characteristics. After choosing the reference speed, the SP_{ref} is automatically extracted, stored and used in the control algorithm. Figure 2.7 shows that the performance of the SP controller when controlling the DP2 can be influenced by setting different reference speeds. For the DP2, a range of the N_{ref} between 3500 rpm and 4500 rpm results in a good physiological performance without suction events.

In our study, we proposed a value of 40 rpm/mmHg for the gain, which represents a physiological performance and large stability margins. Table 2.3 and Study 2B show that within a gain range from 20 rpm/mmHg to 60 rpm/mmHg the CO RMS value for all experiments is lower than 0.55 L/min and suction can be prevented. This gain and its margins would need to be redefined, when the SP controller is implemented on a clinically used tVAD. However, contractility variation study (Study 3) showed that in case of a very low contractility (below 10%, i.e., ejection fraction < 10%) the SP controller with a gain of 40 rpm/mmHg will be unable to change the tVAD speed sufficiently and suction events may occur.

The occurrence of suction due to contractility variations could be avoided with a separate suction detection algorithm [120], which runs in parallel with the SP controller. Suction events are detected by such an algorithm and a separate algorithm to release suction is activated. A suction detection could also be implemented for a constant speed tVAD. However, the lack of physiological adaptation would still be present.

The parameter k_{sp} represents the gain from the SP to the pump speed. Due to the small stroke volume of tVAD supported patients, the contractility can be regarded as the gain from EDV to SP, defined by the slope of the ESPVR. The overall gain from EDV to pump speed is therefore the multiplication of k_{sp} and the contractility. For the overall gain from EDV to pump speed to be approximately constant, large variations of the contractility therefore require an adaptation of k_{sp} . Methods to assess the contractility or detect contractility variations based on pump flow or LV pressure have been proposed [134]–[136], which could also be implemented in the SP controller to detect contractility changes or even to automatically adapt k_{sp} . However, such an adaptation requires a thorough investigation, which is not in the scope of the current paper.

During an isolated acute contractility decrease, the SP controller decreased the pump speed causing a reduced pump support to the native heart, which in turn led to a strong increase in EDP (Figure 2.4). The EDP increased due to the blood accumulation in the pulmonary circulation ultimately leading to a condition of decompensated heart failure. Such a response of the SP controller is regarded as undesirable and constitutes a limitation of the controller. However, changes in contractility are typically related to changes in after- and preload. The Frank-Starling mechanism and Anrep effect [125] (contractility increase following an afterload increase) are known manifestations of this interdependence and constitute parts of the compensatory mechanisms of the heart.

The systolic dysfunction seen in the dilated cardiomyopathies constitutes a result of reduced contractility. Genetic or acquired pathophysiological and biochemical disorders, such as ischemia, toxins, inflammation, infection and tachycardia can lead to an acute or chronic reduction of contractility and heart failure. All these causes of decreased contractility can theoretically cause either a net reduction in the preoperative myocardial contractility or a relative reduction of the increased post-LVAD contractility, compromising the unloading of the LV. In our study, we investigated the response of the SP controller against acute complications (Figure 2.4, Table 2.3), which could cause an abrupt decrease, like acute ischemia, inflammation (septic heart) or

tachycardia. Such cases are life threatening and must be treated in the hospital anyway and, therefore, not through the response of the SP controller.

In a possible clinical implementation, the SP controller must perform properly during all clinical conditions. Arrhythmic events, such as premature ventricular contractions [90], are frequently observed in VAD patients. Furthermore, acute and strong variations in their LV pressure due to breathing or strain events may occur during their daily life. The performance of the SP controller has been investigated under such conditions and none of the aforementioned conditions caused a problem for the SP controller. Suction events were avoided, and a physiological CO response was observed.

In this study, we do not address the lack of a pressure sensor at the inlet of the clinically used tVADs. A biocompatible, durable and accurate blood pressure sensor has not yet been developed but is likely to be realized in the near future [132], [137]–[139]. Furthermore, the first implantable blood pressure sensor was approved by the Food and Drug Administration (FDA) after a premarket approval application (PMA) in 2014 [140]. This pressure sensor developed by St. Jude Medical, named CardioMEMS HF System, aims at monitoring the pressure of the pulmonary artery in heart failure patients and includes a method to recalibrate the pressure measurement in case of sensor drift. In addition, several groups have recently focused on the development of physiological controllers for tVADs based on pressure measurements [126], [141].

The goal of the current study is to present the structure of a new physiological controller for tVADs. The controller was evaluated *in vitro* and it showed promising improvements over the constant speed operation of the tVAD. Acute *in vivo* experiments have recently been conducted using the exact structure of the nominal SP controller (C3) in order to further evaluate its performance and improve upon its limitations. However, the results of these experiments are not in the scope of the current paper.

2.6 Conclusion

The systolic pressure (SP) controller enables a physiological adaptation of the speed of a turbodynamic ventricular assist device (tVAD) to the perfusion requirements of a patient. The desired speed for the tVAD is generated based on a measurement of the pump inlet pressure. *In vitro*, a mimicked pathological circulation assisted with a tVAD controlled by the SP controller performed similarly to a physiological circulation with respect to the cardiac output. At the same time, over- and underpumping were eliminated. Physiological control is believed to improve the quality of life of tVAD patients and to reduce adverse event rates by providing appropriate perfusion of the organs. Therefore, the SP controller will in the future promote the tVAD treatment as a viable alternative to heart transplantation.

3 Standardized Comparison of Physiological Controllers (Paper II)

3.1 Abstract

Various physiological controllers for left ventricular assist devices (LVADs) have been developed to prevent flow conditions that may lead to left ventricular (LV) suction and overload. In the current study, we selected and implemented six of the most promising physiological controllers presented in literature. We tuned the controllers for the same objectives by using the loop-shaping method from control theory. The in-vitro experiments were derived from literature and included different preload, afterload and contractility variations. All experiments were repeated with an increased or decreased contractility from the baseline pathological circulation and with simulated sensor drift. The controller performances were compared with an LVAD operated at constant speed (CS) and a physiological circulation. During preload variations, all controllers resulted in a pump flow change that resembled the cardiac output response of the physiological circulation. For afterload variations, the response varied among the controllers, whereas some of them presented a high sensitivity to contractility or sensor drift, leading to LV suction and overload. In such cases, the need for recalibration of the controllers or the sensor is indicated. Preload-based physiological controllers showed their clinical significance by outperforming the CS operation and promise many benefits for the LVAD therapy. However, their clinical implementation in the near future for long-term use is highly dependent on the sensor technology and its reliability.

3.2 Introduction

Over the last decade, left ventricular assist device (LVAD) therapy has become a viable alternative to heart transplantation for heart failure (HF) patients. The great technological improvements on LVADs contribute to continuously improving the survival rates of the LVAD patients [7]. However, several adverse events, such as strokes, right ventricular (RV) failure, and bleeding still follow LVAD therapy and lead to life-threatening complications [7] and rehospitalization of the patients. The limited adaptation of the LVAD flow is considered as one of the limitations of the current clinical devices that are operated at constant speed (CS) and represents one possible cause for some of these adverse events. For instance, when the LVAD flow is higher than the venous return, ventricular suction may occur, i.e., the left ventricle (LV) empties and the LV wall collapses. This overpumping condition may damage the myocardium and, ultimately, lead to hemolysis and thrombosis [142]. In contrast, when the LVAD flow is lower than the venous return, the LV is overloaded and a congestion of the pulmonary circulation may occur [61].

Driven by the assumption that a physiologically controlled LVAD can prevent some of these life-threatening conditions, various concepts of physiological controllers have been developed over the last decades [61]. In the beginning, most concepts were based on non-invasive signals, such as the estimated pump flow [128]. However, it has been proven that estimators lack robustness and accuracy [128]. Recent approaches are based on invasive signals, such as the LV pressure, the aortic pressure, the LV volume, or the measured pump flow [65],[71],[78],[81],[82],[143],[144]. Most of these approaches claim to aim at imitating the Frank-Starling mechanism of the healthy heart by estimating or measuring the preload condition of the LV. Pauls *et al.* [80] conducted in-vitro experiments with several physiological controllers and showed that preload-based controllers, particularly those based on the LV end-diastolic pressure, can effectively prevent LV suction and overload. A recent review on physiological controllers supports these results regarding the physiological performance of preload-based physiological controllers [145]. Despite the promising results of physiological controllers over the last years, only few have been evaluated in animal models [73],[83] while only one has been evaluated in humans [144]. All studies were acute, and no chronic experiment has been reported so far.

A variety of physiological controllers based on invasive signals have been presented in literature. The majority of them have been tested in silico or in vitro under experiments that include preload, afterload and contractility variations. The gain parameters of these controllers were tuned manually, based on their desired performance. In the original studies, the physiological controller was compared with the clinical standard of

3.3 Materials and methods

the constant-speed (CS) operation [65],[78]. In addition to the CS operation, Mansouri *et al.* [81] compared their controller with one that was based on pump flow pulsatility [81]. The experiments they implemented represented exercise, blood loss, and contractility reduction scenarios. Lim *et al.* [147] conducted an in-silico comparison study with exercise and head-up tilt experiments, but only with non-invasive controllers. Furthermore, Pauls *et al.* [80] compared the performance of seven invasive physiological controllers on a mock circulation. Their experiments included acute changes of pulmonary (PVR) and systemic (SVR) resistances, as well as variations of venous return and contractility of a pathological circulation. For that study, the controllers were tuned by minimizing the two-norm of the tracking error of the controllers. Among the controllers tested, only three were able to avoid LV suction and overload during all the pre- and afterload variations. Their respective control concepts are a constant inlet pressure [71] a constant afterload impedance [143], and a Starling-like approach based on the end-diastolic pressure [141].

The aim of the current study is to evaluate the safe and physiological performance of selected physiological controllers under various clinical conditions, which are emulated in vitro. These conditions include variations of the physiological requirements of the circulation, LV contractility changes and occurrence of sensor drift, all without any recalibration of the controller. The influence of such conditions on the response of the controllers was investigated with respect to complications like LV suction, LV overload, or even pump speed oscillations. The selected controllers, described in the Materials and Methods section, have presented a remarkable performance in previous studies, but they have never been compared among each other. Compared to previous studies, we introduce a new method for tuning physiological controllers with the help of a numerical model of the human cardiovascular system. This method ensures equal tuning objectives for all controllers. With this standardized test, we aimed at evaluating the performances of these controllers. To our knowledge, such a comparison has not been published before. For the implementation of a physiological controller in the clinical environment the quality and limitation of the controllers need to be assessed and the ultimate controller is to be identified and developed.

3.3 Materials and methods

3.3.1 Hybrid mock circulation

All experiments were conducted on a hybrid mock circulation (HMC) earlier developed in our group and described in detail by Ochsner *et al.* [97] This HMC is based on the hardware-in-the-loop concept and consists of three parts, namely a numerical model of the human cardiovascular system [123] including the emulation of ventricular suction [148], the LVAD and the numerical-hydraulic interface, which allows a real-time interaction of the real LVAD, and the simulated circulation. The numerical-hydraulic interface consists of two pressure-controlled reservoirs, which represent the LV and the aorta, and a flow probe. For our study, a non-implantable, mixed-flow turbodynamic blood pump [149] (Deltastream DP2, Xenios AG, Heilbronn, Germany), which is clinically used for extracorporeal membrane oxygenation or extracorporeal circulatory life support, was used as an LVAD, which was modified such that the pump speed can be controlled as desired. The same speed-controller loop of the electric motor of the LVAD was used to track the desired speed computed by the physiological controllers. For our experiments, we ran the HMC until steady state was reached and then started the test scenarios. The numerical model was executed with MATLAB/Simulink running on Real-Time Windows Target (The Mathworks Inc., Natick, MA, USA) and all signals were recorded at 5 kHz. We used a glycerol-water mixture with a viscosity of 2.8 mPa·s at 22 °C for all the experiments to mimic a blood hematocrit of 32%. This viscosity was controlled based on an earlier developed control system [92].

3.3.2 Selection of physiological controllers

Six different physiological controllers were evaluated, which aim at adapting the pump flow to the LVAD-patient physiological requirements. Thus, no pulsatile speed controllers were included in the study, as their influence on the hemodynamics of a circulation has been investigated in detail in previous studies [85]. The selection of the controllers was mainly based on ensuring a reliable redevelopment of the controllers. Thus, we neglected controllers that did not provide sufficient information. Furthermore, we tried to include a variety of concepts that have been presented to outperform the CS operation or other controllers in previous comparison studies. Particularly, two of the implemented controllers [71], [143] (described below) were

selected due to their outperformance against another five controllers and the CS operation presented in the comparison study of Pauls et al. [80]. The other four controllers were selected due to their clear outperformance over the CS operation that they presented when published [65], [70], [78], [81], while they offered a reasonable concept variability. For the case of controllers presented in [65], [78], they have been previously developed in our group and, therefore, we have a deep insight of both, while they have been successfully evaluated in vivo [83]. Each principle is described below. Figure 3.1 depicts a schematic overview of the structure of the physiological controllers used in the current study, whereas Table 3.1 lists all of their parameters. Each controller is split into two parts, the reference generator part and the feedback controller part.

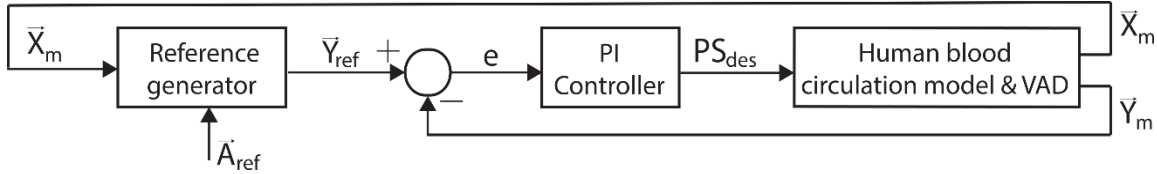


Figure 3.1: A general, schematic description of all physiological controllers of the study. \vec{X}_m measured signals, \vec{Y}_m measured control inputs, \vec{Y}_{ref} computed reference control inputs, \vec{A}_{ref} user-defined inputs, e error, PI proportional-integral, PS_{des} , desired pump speed, LVAD left ventricular assist device.

- *Inlet-outlet pressure (IOP) controller*
The IOP controller constitutes a cascaded control arrangement [71]. Measured aortic pressure and heart rate (HR) are used to define the setpoint of the minimum LV diastolic pressure (LVDPmin). This setpoint is then used to control the pump speed based on the measured LVDPmin, within a 3-s moving window. For our study, we refer to this controller as inlet-outlet pressure (IOP) controller.
- *Afterload-impedance (AI) controller*
The AI controller uses the LV pressure signal as input and calculates the reference mean flow based on a numerical three-element Windkessel model that is evaluated in real time [143]. A proportional-integral (PI) controller is used to control the pump speed to match the pump flow to the reference pump flow. Although the authors developed the controller based on the estimated LV pressure, for our study, we use the measured LV pressure to avoid the estimation error introduced.
- *Pump flow and end-diastolic pressure (PF-EDP) controller*
The PF-EDP controller also consists of a cascaded control loop, which uses the EDP to compute a desired pump flow [81]. For this purpose, a polynomial function to fit the Frank-Starling curves is used instead of the linear function proposed by Salamonsen *et al.* [150] and used in the study of Pauls *et al.* [80]. A PI controller is then applied to match the measured pump flow to the desired one. We refer to it as the PF-EDP controller.
- *Suction-prevention physiological controller (SPPC)*
The SPPC controller uses the pump-pressure difference (ΔP) and the difference between the maximum and minimum pump speed (ΔRPM) within a heartbeat as controller inputs [70]. The ΔRPM is used to identify and prevent suction events. The goal of this controller is to maintain the ΔP and ΔRPM above a user-defined threshold through PI gain-scheduled controllers and, ultimately, to provide a physiological adaptation and suction prevention.
- *Preload responsive speed (PRS) controller*
The PRS controller is based on the measurement of the end-diastolic volume (EDV) to calculate the desired hydraulic power output of the LVAD and to control the speed [65]. This controller constitutes a P controller.
- *Systolic pressure (SP) controller*
The SP controller is based on the systolic inlet cannula pressure and uses the SP as a surrogate to estimate the preload condition of the LV at a specific contractility [78]. This controller constitutes a P controller.

3.3 Materials and methods

Table 3.1 lists the control parameters for each controller whose calculation is described in the following section. The reference generator differs for each controller. Its output consists of the computed reference control inputs (\vec{Y}_{ref}) for each measured control input (\vec{Y}_m). This reference value is either computed by an equation based on measured signals (\vec{X}_m) or defined directly by the user (\vec{A}_{ref}). The inputs, the outputs, and the method to compute the outputs are also summarized in Table 3.1.

3.3.3 Tuning process

The parameters of the controllers were tuned based on four control objectives: 1) pump speed at rest (Exp. 1 of Table 2) that yields an equal cardiac output (CO) close to 5.0 L/min, 2) reference tracking of the flow with zero steady-state error, 3) phase margin of more than 60°, and 4) crossover frequency as high as possible. For the SP and PRS controllers, only the objective 1) was applied, because their tuning process has been described earlier [65],[78]. Both use P controllers and the error between reference and measured signals is not designed to decrease over time. Therefore, the reference tracking does not constitute a control objective for them. Their reference tracking results are provided in the supplementary material. In contrast, the IOP, the PF-EDP, the AI and the SPPC controllers were tuned according to all four objectives. The parameters of the reference generator are adapted to meet objective 1), while the parameters of the feedback controller are adapted to meet the objectives 2), 3) and 4). These parameters are the proportional gain k_p and the integrator gain k_I , which are part of the transfer function $K(s)$ of the PI controllers given by Eq. (3.1):

$$K(s) = k_p + \frac{k_I}{s} \quad (3.1)$$

We first derived a linear-discrete autoregressive exogenous (ARX) model of the used numerical model of the cardiovascular system. Then, the loop-shaping method was applied to find the PI gain parameters [151]. A description of the derivation process of the linear model and the implementation of the loop-shaping method are included in the supplementary material. In Figure 3.2, plots A – H show the loop gains achieved, while the plots I – L show the reference tracking performance when a change of the reference setpoint is applied manually. A good reference tracking is achieved with zero steady-state error and no limit cycles at rest (Exp. 1 of Table 2). The calculated parameters of the controllers are presented in Table 3.1.

3.3.4 Experiments

We conducted various experiments to compare the physiological controllers when they control an LVAD which assists a pathological circulation. A pathological circulation was simulated by reducing the LV ejection fraction (EF) to 30%. The experiments were selected from a wide range of experiments proposed in literature. **Error! Reference source not found.** lists all experiments, the parameters which varied during the simulated experiments, as well as their sources. Experiments 2, 3 and 4 of **Error! Reference source not found.** represent wide-ranging variations of cardiovascular parameters which allow for a complete evaluation of the concepts of the physiological controllers and do not refer to specific clinical scenarios. Experiments 5 and 6 include simultaneous variations of cardiovascular parameters and represent the clinical scenarios from rest to exercise and from sleep to awake condition, respectively. A detailed description of the values of the PVR, the SVR, the unstressed venous volume (UVV), the HR, the contractility, and the time intervals during all experiments is provided in the supplementary material.

All experiments listed in **Error! Reference source not found.** were repeated with an increased and a decreased contractility of the circulation and with a simulated constant sensor drift (i.e., an offset applied to the measured signal). Changes in contractility may occur due to the progression of HF or a recovery of the myocardium [152]. Pressure-sensor drift may occur due to changes at the material properties of the sensor, for instance [153]. For this purpose, all experiments (except Exp. 4) were repeated with increased and decreased LV contractility of 51% and 17%, respectively. These values represent an EF of 44% (LV remodeling) and 13% (severe HF), respectively.

Little information is available in literature regarding sensor drift. Troughton et al. [154] reported a pressure sensor drift of 4.7 mmHg after 3 months with HF patients. In our study, in order to identify the acceptable sensor drift limits for each pressure-based controller, we implemented offset values of ± 5 , ± 15 , ± 25 mmHg.

In the cases where the pump inlet and outlet pressure sensors were required, such as in SPPC and IOP controllers, the drift was arbitrarily implemented only at the pump inlet pressure measurement to avoid too large a combination of experiments. For volume sensors, we implemented a drift of ± 10 , ± 25 , ± 50 mL. Because no long-term, implantable volume sensor is available, we chose the drift to be in the range of inaccuracies of volume measurements observed and considered as acceptable in clinical studies [155]. The tuning and calibration parameters of the controllers listed in Table 3.1 were kept constant during all experiments.

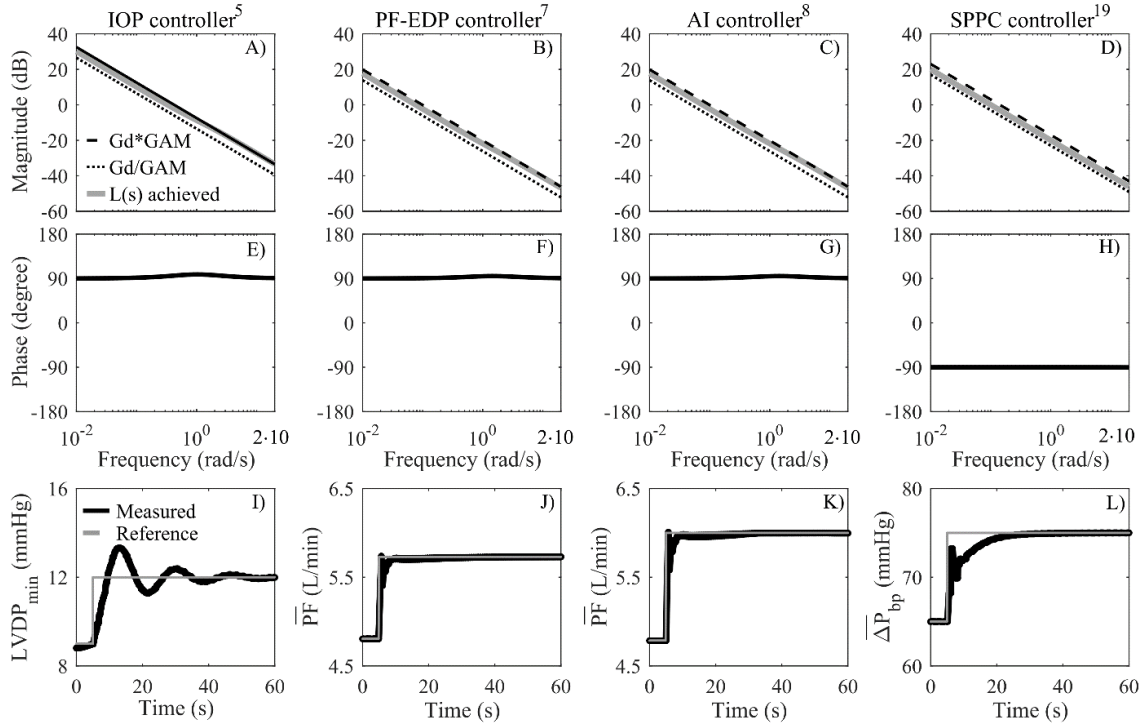


Figure 3.2. Plots A – H show the loop gains achieved, while plots A – D additionally depict the stability margins (black lines, G_d desired loop shape, GAM loop-shaping accuracy. Plots I – L depict the reference tracking achieved for each controller. In I) the minimum left ventricular diastolic pressure ($LVDP_{min}$) is being tracked, in J – K the mean pump flow (\overline{PF}) and in L) the mean pump head pressure ($\overline{\Delta P}_{bp}$). *IOP* inlet-outlet pressure controller, *PF-EDP* pump flow-end-diastolic pressure controller, *AI* afterload-impedance controller, *SPPC* suction-prevention and physiological controller.

3.3.5 Evaluation

We evaluated the impact of various physiological controllers on a pathological circulation. Here, we first report the change in pump speed (PS) and pump flow (PF) (ΔPS , ΔPF , respectively) between the initial steady-state PS and PF and the one achieved after the variations for the pathological circulation assisted by an LVAD controlled by the different controllers. Furthermore, the change in CO (ΔCO) is depicted for the HH as a comparison. The time-varying signals of PS, PF, CO, mean arterial pressure (MAP), and EDP are presented for Exp. 2a and 2b. The occurrence of LV suction and overload is identified among all the experiments of the study and summarized in a table. LV suction is defined when LV EDP equals 0 mmHg and LV overload when LV EDP is above 20 mmHg. Additionally, the pre- and afterload sensitivity of each controller and the HH were calculated and included within the supplementary material.

3.3 Materials and methods

Table 3.1: Content of the reference generator (Figure 3.1) and the proportional-integral controller for each physiological controller. The resulting values of the tuned objectives are also listed.

Controller	Reference generator			Proportional-Integral (PI) controller			Results of tuning objectives		
	User-defined Inputs \vec{A}_{ref}	Measured signals \vec{X}_m	Computed reference control inputs \vec{Y}_{ref}	Method	Measured control inputs \vec{Y}_m	Proportional gain k_p	Integral Gain k_I	CO (L/min)	Crossover frequency (Hz)
IOP [71]	LVDP _{min,ref} = 9 mmHg HR _{ref} = 100 bpm AoP _{ref} = 100 mmHg	HR, AoP	EDP _{ref} ,	Outer loop control	LVDP _{min}	100 rpm/mmHg	90 rpm/mmHg·s	4.82	0.04
AI [143]	R* = 0.95 mmHg·s/mL	LVP	\overline{PF}_{ref}	Three-element Windkessel model [143]	PF	30 rpm·s/mL	40 rpm/mL	4.80	0.01
PF-EDP [81]	$K_{PF}(EDP) = 11$	EDP	\overline{PF}_{ref}	Polynomial Function [81]	PF	30 rpm·s/mL	40 rpm/mL	4.81	0.01
SPPC [70]	$\overline{\Delta P}_{bp,ref} = 60$ mmHg $\Delta RPM_{ref} = 20$ rpm	-	$\overline{\Delta P}_{bp}$ ΔRPM_{ref}	-	ΔP ΔRPM	[40, 25, 40, 70, 140, 40, 35] rpm/mmHg [10, 5, 3, -20, -0.1]	[20,18,10,25,50, 8, 8] rpm/mmHg·s [5,3,1.5,-3,-0.1] s ⁻¹	4.80	0.15
SP [78]	SP _{ref} = 90 mmHg, PS _{ref} = 3900 rpm	-	SP _{ref}	-	SP	40 rpm/mmHg	0	4.80	-
PRS [65]	EDV _{ref} = 80 mL HR _{ref} = 90 bpm	-	EDV _{ref}	Calculation of hydraulic pump power [65]	EDV	0.01 J/mL	0	4.80	-

CO cardiac output, LVDP_{min} minimum left ventricular diastolic pressure, HR heartrate, AoP aortic pressure, R* systemic resistance, $K_{PF}(EDP)$ scaling factor [81], ΔP pump pressure difference, ΔRPM maximum minus minimum pump speed, SP systolic pressure, EDV end-diastolic volume, EDP end-diastolic pressure, PF pump flow rate, PS pump speed, ref reference, *des* desired, *e* error between measured and reference signals, CS constant-speed operation, IOP inlet-outlet pressure controller, PF-EDP pump flow-end-diastolic pressure controller, AI afterload-impedance controller, SPPC suction-prevention and physiologic controller, SP systolic-pressure controller, PRS preload-responsive controller.

Table 3.2. List of all experiments including the description of the variations with the respective literature reference. For each experiment, the varied parameters of the circulation together with the time interval for their variation are presented. The exact values of the parameters throughout the experiments are listed in the supplementary material.

Exp	Description	Parameters	Units	Variation	HR (bpm)	TI (s)
1	Baseline (rest) [78]	-	-	-	90	-
2a	Preload increase [78]	UVV	(mL)	+ 500	90 to 135	5
2b	Preload decrease [78]			- 500		
3a	Afterload decrease [78]	SVR	(mmHg·s/mL)	- 0.6	90	5
3b	Afterload increase [78]			+ 0.8		
4a	Contractility increase [78]	EF	(%)	+ 14	90	15
4b	Contractility decrease [78]			- 17		
5	Rest to exercise [80]	SVR	(mmHg·s/mL)	- 0.53	60 to 80	10
		PVR	(mmHg·s/mL)	- 0.05		
		UVV	(mL)	+300		
6	Sleep to wake [67]	SVR	(mmHg·s/mL)	- 0.5	60 to 80	10
		EF	(%)	+ 17		

Exp experiment, *HR* heartrate, *TI* time interval, *SVR* systemic vascular resistance, *PVR* pulmonary vascular resistance, *UVV* unstressed venous volume, *EF* ejection fraction.

3.4 Results

Figure 3.3 illustrates the ΔPS and ΔPF for Exp. 2a - 4b and the various LVAD control modes of the study, when the LVAD assists a pathological circulation. For these experiments, the controllers started from identical initial conditions (at rest – Exp.1). The red dashed line represents the ΔCO of the HH. During Exp. 2a (preload increase), the PS remained constant with the CS operation and almost unchanged with the SPPC controller. As a result, the respective ΔPF increased by less than 1 L/min. All other controllers increased the PS. The ΔPF due to the PRS and the IOP controllers was similar to the ΔCO of the HH (close to 3 L/min), whereas the other controllers increased the PF by approximately 2 L/min. For Exp. 2b, all physiological controllers decreased their PS. The PRS and SP controllers resulted in greater PF changes (more than 3 L/min) than the others (less than 2.5 L/min).

During Exp. 3a and 3b, the IOP and SPPC controllers resulted in small PS and in turn PF changes, the latter being similar to the CS operation. The other controllers (PF-EDP, AI, PRS and SP), decreased the PS and PF during Exp. 3a by around 1000 rpm and 2 L/min, respectively. Furthermore, although they increased the PS by around 1000 rpm during Exp. 3b, the PF even decreased due to the increased afterload. During Exp. 4a (contractility increase), the PS and PF slightly increased with the AI and SP controllers, as happened with the CO of the HH, while they decreased with the rest controllers. During Exp. 4b (contractility decrease), all controllers kept the PS and PF unchanged, similarly to the CO response of the HH, except for the AI and SP controllers which decreased the PS by approximately 1000 rpm and in turn the PF by 2 L/min.

Figure 3.4 depicts the change in PS and PF for Exp. 5 and 6. Here, the initial conditions of the circulation are different, as we defined them according to Pauls et al. [80] (Exp. 5) and Mansouri et al. [121] (Exp. 6). Therefore, each controller had a different PS and PF at “Start”. During Exp. 5, the IOP and the SPPC controllers increased the PS by approx. 1500 rpm which in turn yielded a PF of up to 10 L/min, which equals the resulted CO of the HH. The PRS controller followed with a slightly less PS and PF increase of approx. 1000 rpm and 3 L/min, respectively. The other controllers did not increase the PS or even decreased (AI controller) and the PF increased by 1 to 2 L/min only due to additional work of the pathological heart. Changes in LV stroke work and CO for Exp. 2-6 are provided in the supplementary material.

During Exp. 6, the initial conditions (decreased contractility due to sleep) led to a decreased PS and PF with the SPPC, the AI and the SP controllers compared to the CS operation. The PF-EDP, the IOP and the PRS controllers increased the PS and generated, as a result, a higher PF which was close to 4.5 L/min. At the end of the variation, these controllers decreased the PS but the PF remained almost unchanged due to the

3.4 Results

contractility increase. The other controllers increased the PS and in turn the PF due to the afterload increase. All controllers, except the AI, resulted in a PF close to the CO of the HH.

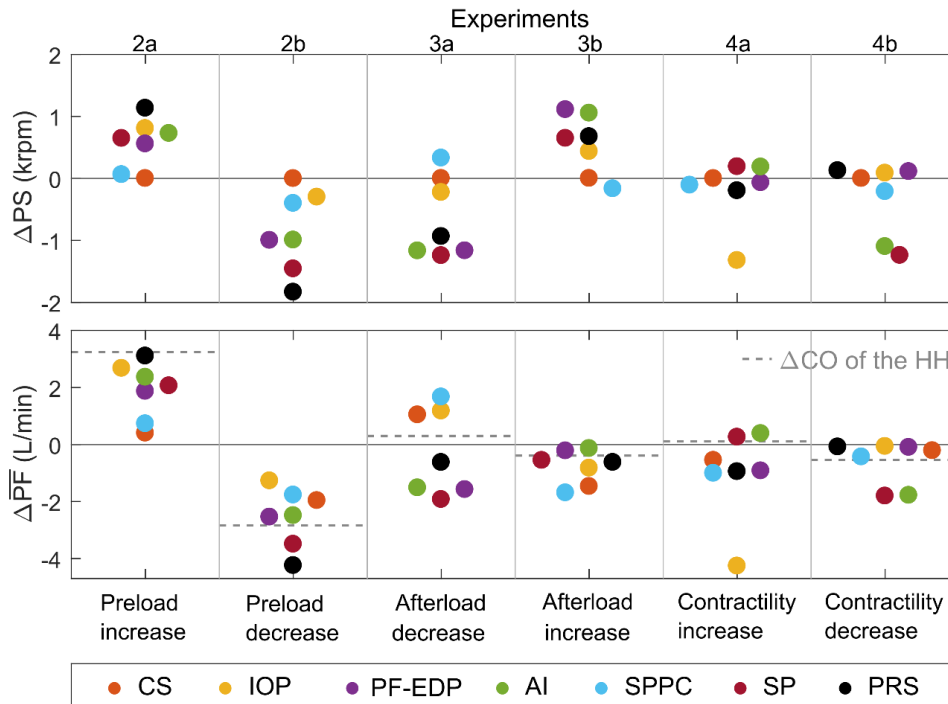


Figure 3.3. Change in pump speed (ΔPS) and mean pump flow ($\Delta \overline{PF}$) between the initial steady-state PS and PF and the ones attained after the variations of Exp. 2a - 4b for a pathological circulation assisted by an LVAD with and without physiological control. The corresponding change in cardiac output (ΔCO) of a healthy heart (HH) is depicted in dashed-red line. CS constant-speed operation, IOP inlet-outlet pressure controller, PF-EDP pump flow-end-diastolic pressure controller, AI afterload-impedance controller, SPPC suction-prevention and physiological controller, SP systolic-pressure controller, PRS preload-responsive controller.

Figure 3.5 depicts the signals of the pump speed, the PF, the CO, the MAP and the EDP of all controllers during the preload variation experiments (Exp. 2a and 2b). The HH performance is also depicted through the CO, the MAP and the EDP signals. During preload variations, the pump speed and PF signals show that the response of all physiological controllers were similar to that of the HH during the variations. The CO signal shows that the PRS controller matched almost exactly the perfusion of the HH. In contrast, the performance of the SPPC controller matched with that of the CS controller. During preload increase (Exp. 2a), EDP increased above 20 mmHg with the SPPC controller and the CS operation. Furthermore, during the preload decrease (Exp. 2b), EDP equaled 0 mmHg with the CS operation, while it was close to 0 mmHg, i.e., close to suction with the IOP and the SPPC controllers. All other results that are presented in the same way as Figure 3.5 are provided in the supplementary material.

Figure 3.6 depicts the repetition of Exp. 2a and 2b, but with a decreased EF by 13% (left side) and with a simulated sensor drift of +5 mmHg and +25 mL for pressure and volume measurements, respectively (right side). The signals of the PS, the PF, the CO, the MAP and the EDP are depicted. When EF decreased, the performance of the IOP and the PRS controllers was similar to their baseline case with an EF of 30% (Figure 3.5). The response of the PF-EDP controller was also similar to its baseline case with 30% EF, apart from the preload decrease phase ($t > 30$ s), where pump speed and in turn CO oscillations were observed. All other controllers presented an underpumping condition compared to the baseline case (Figure 3.5). This is justified by the lower than the initially calibrated pump speed of 3900 rpm, which in turn led to less than 5 L/min initial PF and CO ($t = 0$ s). Furthermore, similarly to the CS operation, the EDP increased above 20 mmHg during the preload increase. During the preload decrease, the IOP controller and the CS operation led to 0 mmHg EDP, while with the other controllers, this was not the case.

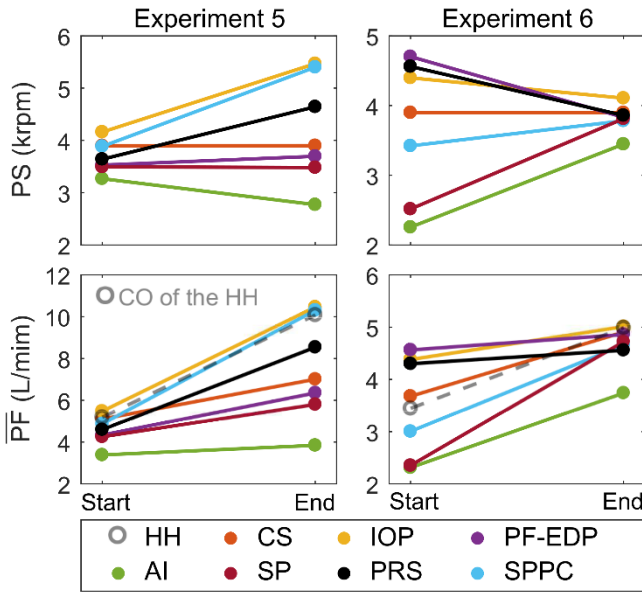


Figure 3.4. Change in pump speed (PS) and mean pump flow (\overline{PF}) between the initial steady-state PS and PF and the ones attained after the variations of Exp. 5 (rest to exercise) and 6 (sleep to wake) for a pathological circulation assisted by an LVAD with and without physiological control. The corresponding change in cardiac output (CO) of a healthy heart (HH) is depicted in dashed-red line and red circles. *CS* constant-speed operation, *IOP* inlet-outlet pressure controller, *PF-EDP* pump flow-end-diastolic pressure controller, *AI* afterload-impedance controller, *SPPC* suction-prevention and physiological controller, *SP* systolic-pressure controller, *PRS* preload-responsive controller.

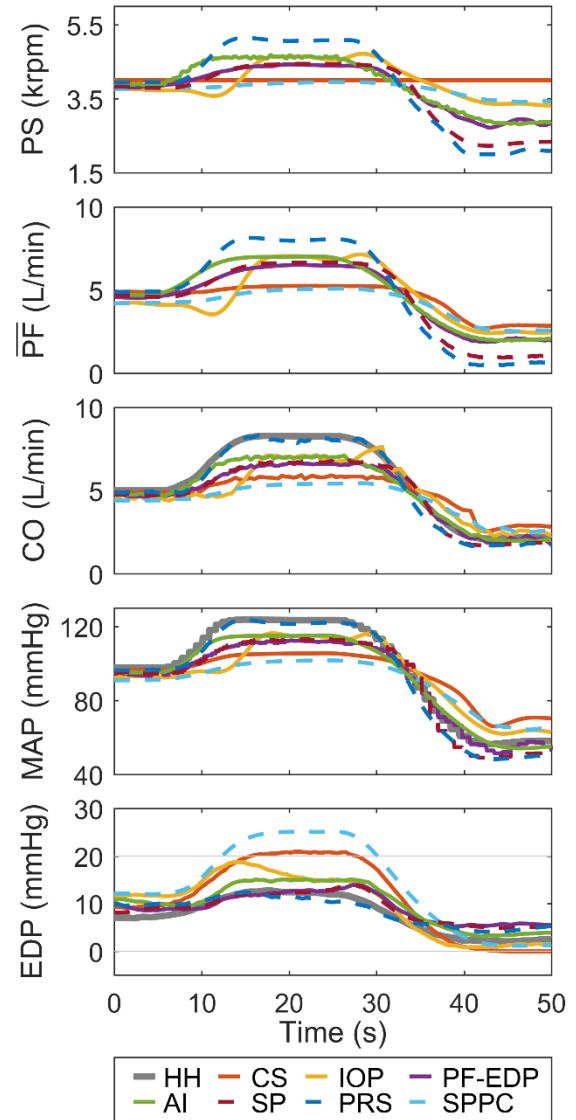


Figure 3.5: Performance of each controller of the study during preload variations (Exp 2). The pump speed (PS), the mean pump flow (\overline{PF}), the cardiac output (CO), the mean arterial pressure (MAP), and the end diastolic pressure (EDP) are depicted. The thresholds of 20 and 0 mmHg are illustrated in EDP plot. *CS* constant speed operation, *IOP* inlet-outlet pressure controller, *PF-EDP* pump flow-end diastolic-pressure controller, *AI* afterload-impedance controller, *SPPC* suction-prevention and physiological controller, *SP* systolic-pressure controller, *PRS* preload-responsive controller.

3.4 Results

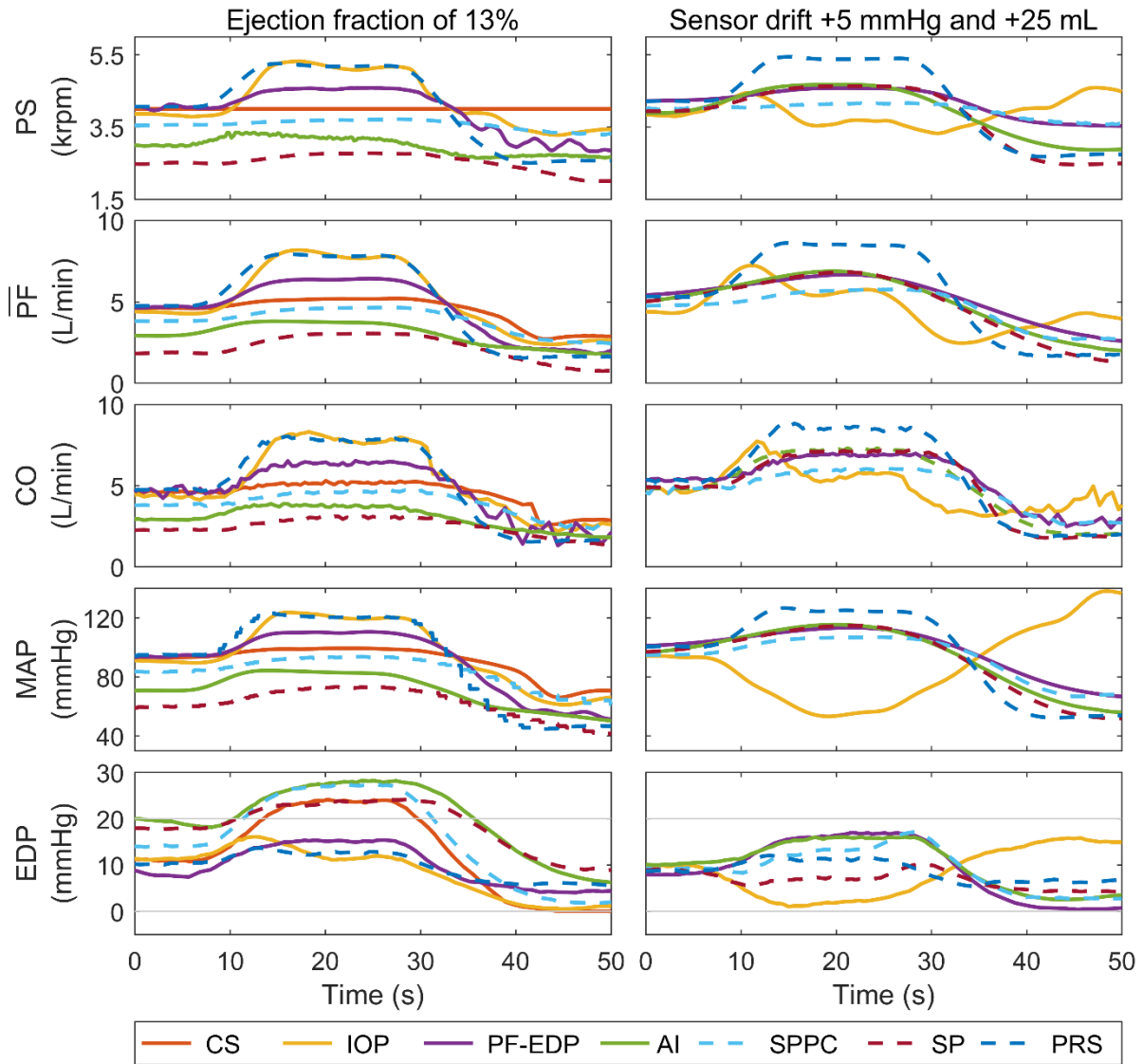


Figure 3.6: Performance of each controller of the study during the preload variation experiment (Exp. 2a and 2b). Left, the ejection fraction of the circulation is decreased to 13%. Right, the sensor drift of +5 mmHg for the pressure sensor and +25 mL for the volume sensor are simulated (right). The signals of the pump speed (PS), the mean pump flow (\overline{PF}), the cardiac output (CO), the mean arterial pressure (MAP) and the end-diastolic pressure (EDP) are depicted. The thresholds of 20 and 0 mmHg are illustrated in EDP plot. CS constant-speed operation, IOP inlet-outlet pressure controller, PF-EDP pump flow-end-diastolic pressure controller, AI afterload-impedance controller, SPPC suction-prevention and physiological controller, SP systolic-pressure controller, PRS preload-responsive controller.

Compared to the baseline case with no drift (Figure 3.5), the positive sensor drift influenced all the physiological controllers during the preload increase by increasing the pump speed attained. Thus, the PF, the CO, and the MAP were larger than the baseline as well. On the contrary, as a result of the higher PF due to the sensor drift, the EDP remained below the 20-mmHg threshold with all controllers. During the preload decrease, the sensor drift had a negative effect on the performance of the IOP, the PF-EDP, and the SPPC controllers. Suction events occurred ($EDP = 0$ mmHg) as the pump speed was higher than in the baseline case. No suction occurred with the AI, the SP, and the PRS controllers.

The influence of changes of contractility and sensor drift on the performance of the controllers during the experiments (see Table 3.1) is summarized in Table 3.3. The cases of LV suction (S) and LV overload (O) are identified for every controller at each experiment. However, only the failure limits are listed, i.e., when a controller has failed with a pressure sensor drift of +5 mmHg, it also fails for +15 mmHg, but the latter is not listed for reason of space limitations. According to Table 3.3, LV suction and overload occur with the CS

operation, the AI, the SPPC and the SP controllers when contractility variations occur. In contrast, the IOP, the PF-EDP, and the PRS controllers are mainly not influenced by contractility changes. Furthermore, the performance of the IOP, the PF-EDP and the SPPC controllers is influenced from inlet pressure sensor drift, while for the other physiological controllers, this is not the case.

Table 3.3: Summary of the performance of all controllers with respect to left ventricular suction (S) and overload (O). The results correspond to experiments of **Error! Reference source not found.** but with three different ejection fractions (13%, 30%, 44%) and with simulated sensor drift (± 10 , ± 25 , ± 50 mL for the PRS controller, ± 5 , ± 15 , ± 25 mmHg for the other controllers, respectively).

Exp	Manipulation	CS	IOP [71]	PF-EDP [81]	AI [143]	SPPC [70]	SP [78]	PRS [65]
2	EF (%)	13: O 30: S 44: S	✓	✓	13: O	13: O	3: O	✓
	D (mmHg, mL)	n/a	+5: S -15: O	+15: S -15: O	✓	+5: S	✓	✓
3	EF (%)	13: O	✓	✓	13: O	13: O 30: S 44: S	13: O	✓
	D (mmHg, mL)	n/a	+5: S -15: O	+15: S -15: O	✓	+5: S	✓	✓
4	EF (%)	n/a	n/a	n/a	n/a	n/a	n/a	n/a
	D (mmHg, mL)	n/a	+15: S -5: O	+15: S -15: O	✓	-15: O	✓	✓
5	EF (%)	✓	✓	13: O	13: O 30: O	13: O	13: O	✓
	D (mmHg, mL)	n/a	+15: S -15: O	-15: O	✓	✓	✓	✓
6	EF (%)	30: O	✓	✓	30: O	13: O 30: O	30: O	✓
	D (mmHg, mL)	n/a	+5: S	+15: S -5: O	✓	✓	✓	✓

Exp experiment, *CS* constant-speed controller, *IOP* inlet-outlet pressure controller, *PF-EDP* pump flow-end-diastolic pressure controller, *AI* afterload-impedance controller, *SPPC* suction-prevention and physiologic control, *SP* systolic-pressure controller, *PRS* preload-responsive controller, *EF* ejection fraction, *D* simulated sensor drift, ✓ no suction or overload occurred, *n/a* not applicable

3.5 Discussion

In the used numerical model of the human cardiovascular system [156] and during preload variations, all physiological controllers indicated a similar change of PS and PF to the CO response of a HH. The number of PS and PF change varied among the controllers due to the different concepts, the parametrization, and the sensitivities to preload changes of each controller. Due to the limited physiological adaptation, the CS operation and the SPPC controller led to LV suction and overload (Figure 3.5). During combined pre- and afterload variations (Exp. 5), the LVAD controlled by either of the IOP, the SPPC, or the PRS controller had a PF adaptation which resembled the CO adaptation of the HH (Figure 3.4). During Exp. 5, the PS was slightly increased with the SP controller, it even decreased with the AI controller, and it remained unchanged in CS operation. Therefore, the PF increase (Figure 3.4) was mainly the result of the additional work of the pathological heart, which may lead to LV overload. The results of the LV SW (provided in the supplementary material) present the cases where the LV SW was greatly increased.

The contractility of the heart of an LVAD patient can significantly vary over time [152]. For AI, SPPC and SP controllers this would lead to LV suction or overload (Table 3.3). During Exp. 4a (contractility increase),

3.5 Discussion

all physiological controllers kept the PS and PF almost unchanged, except for the IOP controller who greatly decreased them. In general, a PS decrease would be considered as desired during contractility increase, as the more the heart recovers, the less it needs the LVAD assistance. In contrast, the reverse reaction is desired when the contractility decreases, such as during Exp. 4b. Even though the HH decreases the CO (Figure 3.3), the goal of a physiological controller should be to keep the CO stable. For this purpose, the assistance to the LV from the LVAD should be increased. This was not the case for the SP and AI controllers, while the other controllers kept the PF almost unchanged. This result is also depicted during Exp. 2 under 13% EF (Figure 3.6). The AI, the SPPC and the SP controllers decreased the pump speed when contractility decreased and thus, led to a lower CO than that of the HH. Because of this underpumping condition, an LV overload occurred.

The current study showed that sensor drift influences the performance of the controllers investigated (Table 3.3). Even though it is not widely explored in the development of physiological controllers, sensor drift constitutes one of the obstacles that hampers a possible clinical implementation of physiological controllers, and the consequence of the sensor drift consequences to the circulation need to be investigated. Results depicted in Figure 3.3-Figure 3.5 and in Table 3.3 show that physiological controllers based on EDP, such as the IOP and the PF-EDP, present a very physiological response and a high preload sensitivity. However, their performance may be influenced by high drift and thus may lead to suction and overload (Figure 3.6, Table 3.3). A high sensitivity to sensor drift was also observed in the case of the SPPC controller, while the AI and the SP controllers were less affected by drift (except for Exp. 6 with less than -5 mmHg of drift). No critical flow conditions were observed with the PRS controller for the drift of LV volume sensor implemented and with the numerically modeled pathological circulation used. However, due to the lack of data of any long-term use of volume sensors, the correctness of the drift applied remains to be reevaluated in the ongoing research. Particularly, the effect of remodeling should be considered, which is very dominant during the first period of the LVAD treatment.

All the physiological controllers investigated in this study required an invasive signal, such as pump flow, LV pressure (or pump inlet pressure), or LV volume. The state of development among pressure and volume sensors has been described by Tchanchaleishvili et al. [89] and Dual et al. [60], respectively. Pump flow sensors are known in clinical practice as they have already been used with LVADs, e.g. the one by ReliantHeart Inc. Therefore, they can be considered to be directly accessible for use in physiological control systems. The number of sensors required for control purposes differ among the physiological controllers. Only the SP and PRS controllers require a single sensor for their implementation, which keeps the complexity of the system lower than for the others. The AI and the PF-EDP controllers require both pump flow and pump inlet pressure sensors, while the SPPC and the IOP controllers require pump inlet and outlet pressure sensors. While these additional sensors increase the number of parameters of the controllers that have to be tuned and calibrated, they may provide additional useful information concerning the circulation and improve the monitoring of the LVAD patients [157].

We conducted an extensive in-vitro comparison study of where some of the most promising physiological controllers, which were carefully implemented, evaluated and compared. The use of the loop-shaping method offered a standardized comparison. A 2-norm minimization function of the error signals in the time domain was previously proposed to compute the PI gains for different control algorithms [80]. Yet, the current work uses the loop-shaping design instead to obtain more insight into the system dynamics, to reach robust stability and performance levels, while providing a performance level similar to that of the time domain. The resulted gains are related to the used rotary blood pump. The study could be repeated for any pump type, after defining the new gains with the proposed method, without affecting the main conclusions regarding pros and cons of each concept for physiological control.

We acknowledge that, in general, the existing in-vitro environments do not perfectly mimic the human circulation, but they serve well for various experiments with physiological controllers. Of course, we encourage the community to repeat such a study with a different in vitro environment and additional physiological controllers that are considered promising. The experiments conducted are likely to represent various clinical scenarios. However, further research and improvement of the human physiology models should be considered in future studies to incorporate clinical scenarios and different LVAD-patient models even more accurately (e.g. Petrou et al. [91], Fresiello et al. [158]).

3.6 Conclusion

The response of the physiological controllers during preload, afterload, and contractility variations as well as sensor drift was evaluated. In the end, all controllers investigated responded similar to the HH during preload variations and outperformed the CS operation. But, they presented different sensitivity to afterload and contractility variations and sensor drift, which in some cases led to critical flow conditions. In such cases, either sensor calibrations (such as with the IOP and the PF-EDP controllers during sensor drift) or offset corrections (such as with the AI and the SP controller during contractility changes). This requirement for calibration calls for a correct monitoring. This study proves the power of preload-based controllers (e.g. IOP, PF-EDP, PRS controller), which has been theoretically reported by Tchantchaleishvili et al. [89]. They clearly outperformed the CS operation, thus indicating the benefits that physiological control may bring in the clinical environment. Furthermore, our study reveals the complexity and the uncertainties around the clinical implementation of physiological controllers. By analyzing various aspects of each approach, we are gaining knowledge on the required improvements of the existing physiological controllers and, ultimately, design a safe and physiological control system.

3.7 Electronic material

3.7.1 Materials and Methods

Experiments

Table 3.4: List of the exact values of the varied parameters applied to the experiments (Exp) of the main manuscript (**Error! Reference source not found.**) and the description of the variation with the respective literature reference. The varied parameters of the circulation are the systemic vascular resistance (SVR), the pulmonary vascular resistance (PVR), the unstressed venous volume (UVV), the heartrate (HR), and the contractility relative to the contractility of a physiological circulation. The representative clinical conditions of each experiment as well as their source are defined.

Exp	Description	Time (s)	SVR (mmHg·s/mL)	PVR (mmHg·s/mL)	UVV (mL)	HR (bpm)	Contractility (%)
1	Baseline	40	Fixed at 1.11	Fixed at 0.1	Fixed at 2520	Fixed at 90	Fixed at 34
2a, 2b	Wide-ranging preload variations [78]	[0, 5, 10, 25, 35, 45]	Fixed at 1.11	Fixed at 0.1	[2520, 2520, 2020, 2020, 3025, 3025]	[90, 90, 135, 135, 65, 65]	Fixed at 34
3a, 3b	Wide-ranging afterload variations [78]	[0, 5, 10, 25, 35, 45]	[1.11, 1.11, 0.51, 0.51, 1.91, 1.91]	Fixed at 0.1	Fixed at 2520	Fixed at 90	Fixed at 34
4a, 4b	Recovery or heart failure progression [78]	[0, 5, 20, 40, 70, 100]	Fixed at 1.11	Fixed at 0.1	Fixed at 2520	Fixed at 90	[34, 34, 51, 51, 17, 17]
5	Rest to exercise [80]	[0, 5, 15, 120]	[0.98, 0.98, 0.45, 0.45]	[0.08, 0.08, 0.03, 0.03]	[2520, 2520, 2020, 2020]	[60, 60, 80, 80]	Fixed at 34
6	Sleep to wake [67]	[0, 5, 10, 30]	[1.65, 1.65, 1.11, 1.11]	Fixed at 0.1	Fixed at 2520	Fixed at 60	[15, 15, 34, 34]

Tuning Process

We used the loop-shaping method to define the proportional-integral (PI) gain parameters of the inlet-outlet pressure (IOP) [71], the pump flow–end-diastolic pressure (PF-EDP) [81] and the afterload-impedance (AI) [143] controllers, as well as the suction prevention physiological controller (SPPC) [70]. The objectives that had to be met are described in the main manuscript. The loop gain is defined by Eq. (3.7.1):

$$L(s) = G(s)K(s) \quad (3.7.1)$$

where $G(s)$ is the transfer function of the plant. The derivation of the linear plant $G(s)$ is described in detail in the Section ARX model of the numerical model. The deviation of the magnitude of the loop gain $L(s)$ from the magnitude of a desired loop gain $L_{\text{des}}(s)$ was minimized. The $L_{\text{des}}(s)$ was chosen as a type one pure integrator Eq. (2), where ω_c is the crossover frequency which approximately corresponds to the closed-loop bandwidth.

$$L_{\text{des}}(s) = \frac{\omega_c}{s} \quad (3.7.2)$$

The L_{des} exhibits the slope of -20 dB/decade at all frequencies, ensuring that $|L(j\omega \rightarrow 0)| \rightarrow \infty$ for reference tracking with zero steady-state error and that $|L(j\omega \rightarrow \infty)| \rightarrow 0$ for noise rejection and robustness towards model uncertainty. The ω_c is selected at least ten times smaller than the sampling rate of each controller to avoid the limit cycle and ensure that $|L(j\omega)| \ll 1$ for frequencies requiring high performance. As the sampling rate, we used the change rate of the reference signals of each controller, as proposed by their authors. The parameters of the PI controller were computed for the desired loop shape by using the MATLAB (Mathworks Inc., Natick, MA, USA) function named “loopsyn”. Figure 3.1 of the main manuscript depicts the loop gains obtained and the reference tracking performance of the IOP, the PF-EDP, the AI, and the SPPC controllers. Figure 3.7 presents the reference tracking performance of the PRS and SP controllers.

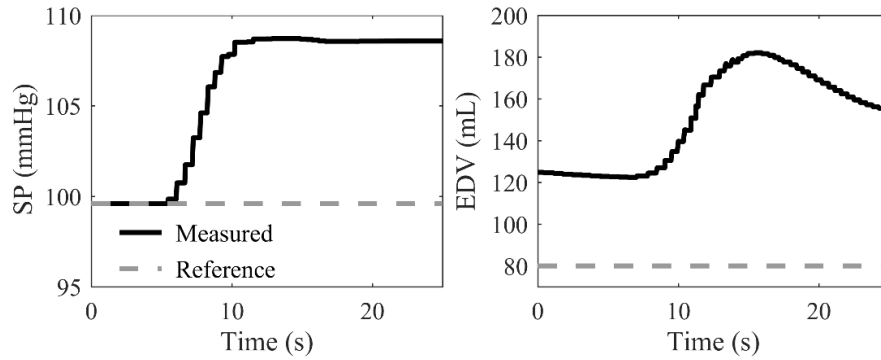
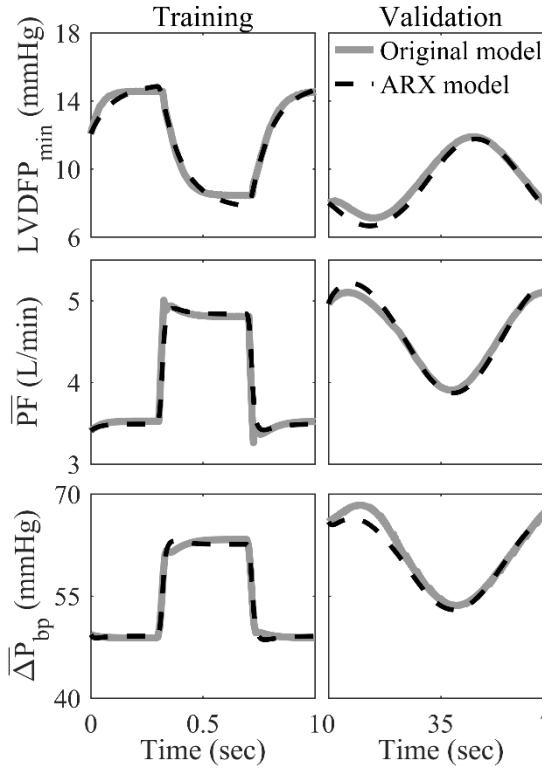


Figure 3.7: Reference tracking results for the systolic pressure (SP) and preload responsive speed (PRS) controller. The control inputs of the SP and end-diastolic volume (EDV) are depicted. For both controllers, the reference values are being defined after a cardiac output of 4.8 L/min was achieved.

ARX model of the numerical model

This section describes the derivation of the linear plant model $G(s)$ using the system identification techniques. As the controller synthesis described in the current work requires a linear plant model $G(s)$, the nonlinear model of the LVAD and mock circulation was approximated linearly around the desired equilibrium, which is the flow rate level reached for the experiment at rest. Despite the existence of many states, a SISO model was constructed with the motor speed as an input signal and the measured reference signal as an output signal. The control architecture of the algorithms evaluated in this study justifies the use of such SISO models.

A system identification procedure requires sets of training and validation data. An experiment at rest (Exp. 1 – Table 3.4) with a constant motor speed of 3,900 rpm with an added pseudorandom binary sequence (PRBS) signal was used as the training data. The sinusoidal motor speed was used for the validation process. Figure 3.8 presents the corresponding results at a frequency of 0.16 rad/s. A maximum of 0.9 rad/s was identified as the maximum acceptable frequency to estimate the original model. The “arx” function of MATLAB was used to construct the linear plant model. Table 3.5 lists the ARX model parameters.


Table 3.5: Parameters of the ARX model

Plant	Coefficients	
	a0	b0
Minimum LVDFP	-1	$1.4e-06$
Mean pump flow rate	-0.99	$-9.5e-07$
Pump pressure difference	-0.99	$6.1e-06$
		0.13
		0.05

Figure 3.8: Training (left) and validation (right) results of the ARX model of the numerical model of the cardiovascular system during the implementation of square-wave motor speed profiles. The signals of the minimum left ventricular diastolic filling pressure ($LVDFP_{min}$), the mean pump flow (\overline{PF}), and the pump pressure difference ($\overline{\Delta P}_{bp}$) are depicted.

3.7.2 Results

Pre- and afterload sensitivity

The pre- (PS) and the afterload sensitivities (AS) of the controllers and of the healthy heart (HH) were calculated from Exp. 2a and 3a (Table 3.4) and based on the equations presented in Pauls et al. [80], i.e., $PS = \Delta PF_{mean} / \Delta EDP$ and $AS = \Delta PF_{mean} / \Delta MAP$, respectively. The Δ denotes the differential value, PF_{mean} is the mean pump flow, and MAP is the mean arterial pressure. Table 3.6 shows the PS and AS of each controller as well as that of the HH. The PS of the PRS controller ($0.46 \text{ L}\cdot\text{min}^{-1}\cdot\text{mmHg}^{-1}$) is closer to the PS of the HH ($0.74 \text{ L}\cdot\text{min}^{-1}\cdot\text{mmHg}^{-1}$), while the AI, the IOP, the SP and the PF-EDP follow with sensitivity values from 0.28 to $0.19 \text{ L}\cdot\text{min}^{-1}\cdot\text{mmHg}^{-1}$, respectively. For the SPPC controller and the CS operation, the PS is below $0.06 \text{ L}\cdot\text{min}^{-1}\cdot\text{mmHg}^{-1}$. The PRS controller presents the minimum AS, which is closer to that of the HH. The other controllers have a similar afterload sensitivity of approximately $0.03 \text{ L}\cdot\text{min}^{-1}\cdot\text{mmHg}^{-1}$, except for the SPPC controller whose AS at $0.06 \text{ L}\cdot\text{min}^{-1}\cdot\text{mmHg}^{-1}$ is slightly higher.

3.7 Electronic material

Table 3.6: Preload (PS) and afterload sensitivity (AS) of each controller of the study including the values of the healthy heart.

	PS (L·min ⁻¹ ·mmHg ⁻¹)	AS (L·min ⁻¹ ·mmHg ⁻¹)
HH	0.74	0.008
CS	0.03	0.03
IOP	0.25	0.03
PF-EDP	0.19	0.03
AI	0.28	0.03
SPPC	0.06	0.06
SP	0.20	0.04
PRS	0.46	0.01

CS constant-speed operation, IOP inlet-outlet pressure controller, PF-EDP pump flow-end diastolic-pressure controller, AI afterload-impedance controller, SPPC suction-prevention and physiological controller, SP systolic-pressure controller, PRS preload-responsive controller, HH healthy heart.

Time-varying signal for Exp. 3

Figure 3.9 depicts the performance of the controllers during afterload variations (Exp 3). Here, an inverse response of the SPPC controller compared to the other controllers and a delayed response of the IOP controller are observed from the PS signal. With the PF-EDP, AI, and SP controllers, a greater change in PF was observed than with the PRS controller. Despite that, all four of them matched well the CO of the HH. The SPPC controller led to 0 mmHg EDP (suction) during the afterload decrease, while similarly to the CS operation it exceeded the 20-mmHg EDP threshold during the afterload increase.

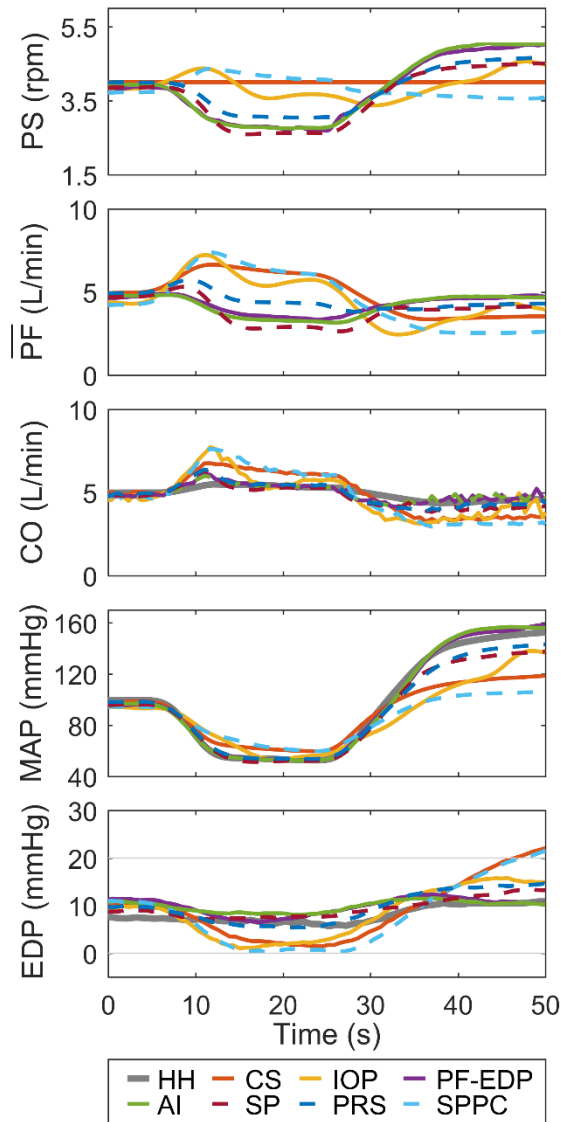


Figure 3.9: Performance of each controller of the study during afterload (Exp 3) variations. The pump speed (PS), the mean pump flow (\overline{PF}), the cardiac output (CO), the mean arterial pressure (MAP), and the end diastolic pressure (EDP) are depicted. The thresholds of 20 and 0 mmHg are illustrated in EDP plot. CS constant-speed operation, IOP inlet-outlet pressure controller, PF-EDP pump flow-end diastolic-pressure controller, AI afterload-impedance controller, SPPC suction-prevention and physiological controller, SP systolic-pressure controller, PRS preload-responsive controller.

Time-varying signal for Exp. 5 and 6

Figure 3.10 presents the same signals as Figure 3.9, but for the rest-to-exercise (Exp. 5) and sleep-to-wake (Exp. 6) experiments. During exercise, the IOP, SPPC and PRS controllers increased their pump speed and flow and matched well the CO, MAP, and EDP of the HH. In contrast, the other controllers (CS, PF-EDP, SP) kept their speed almost constant or even decreased it (AI controller). In these cases, the CO increased only due to the additional work by the heart and could not match the CO of the HH. This lower perfusion led to lower MAP values than in the HH case. Furthermore, it led to EDP values which are close to 20 mmHg, while for the case of the AI controller EDP exceeded the value of 20 mmHg.

During the sleep-to-wake experiment, the initially decreased contractility (15%) resulted in lower initial pump speeds with the SPPC, the AI, and SP controllers than those obtained with the CS operation. The low speeds, i.e., the limited assistance from the LVAD to the LV, in turn led to greater EDP values than those of the HH, which exceeded the 20-mmHg threshold. In case of the PRS, the PF-EDP, and the IOP controllers the

3.7 Electronic material

initial pump speed remained close to the one defined in the calibration. As a result, the EDP remained below 20 mmHg. The increase in contractility and decrease in afterload that occurred after 15 s caused the controllers to converge at almost the same pump speed and in turn pump flow and CO.

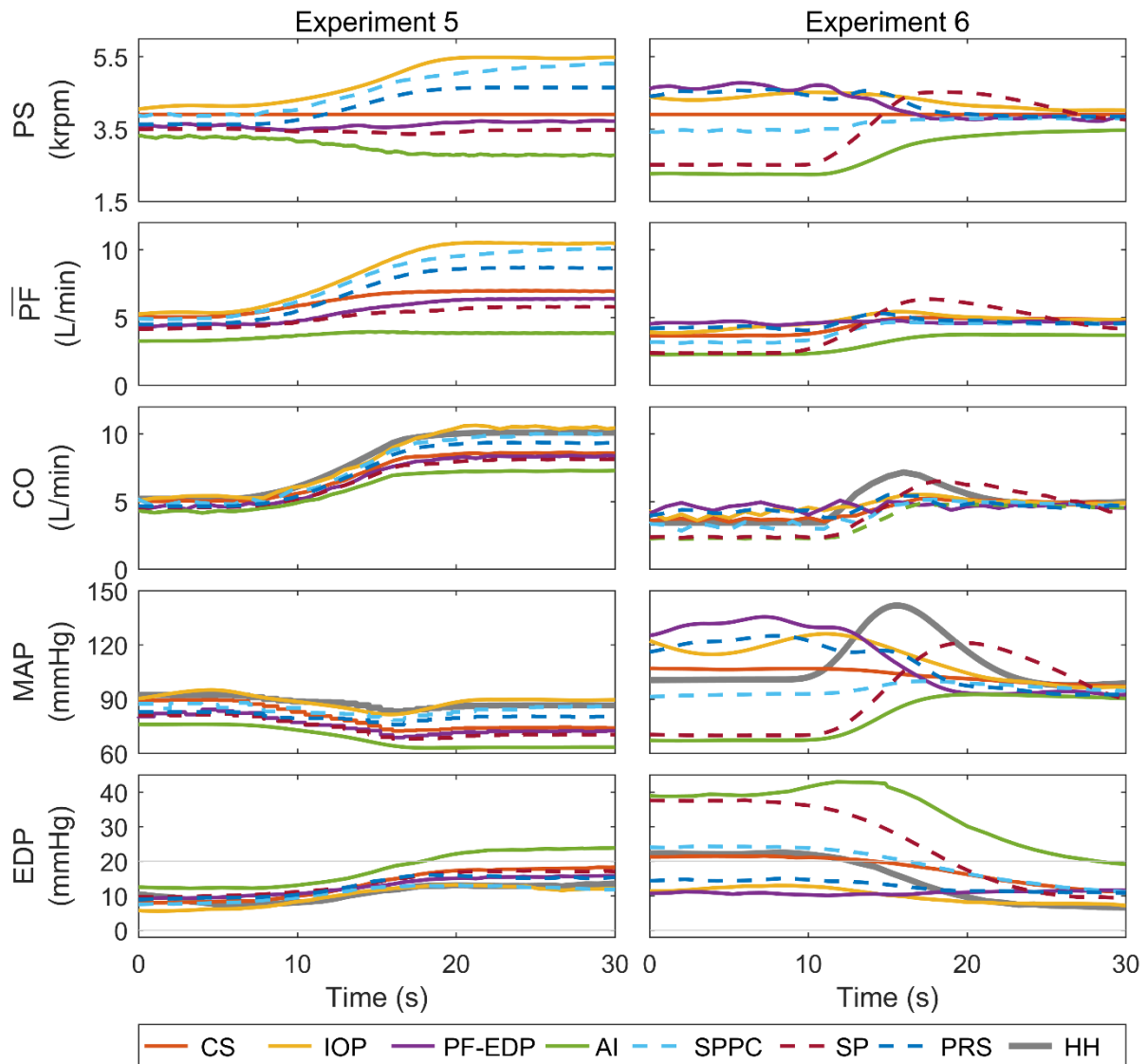


Figure 3.10: Performance of each controller of the study during the exercise experiment (Exp 5 - left) and the waking-up experiment (Exp 6 - right). The pump speed (PS), the mean pump flow (\overline{PF}), the cardiac output (CO), the mean arterial pressure (MAP), and the end diastolic pressure (EDP) are depicted. The thresholds of 20 and 0 mmHg are illustrated in EDP plot. CS constant-speed operation, IOP inlet-outlet pressure controller, PF-EDP pump flow-end-diastolic pressure controller, AI afterload-impedance controller, SPPC suction-prevention and physiological controller, SP systolic-pressure controller, PRS preload-responsive controller.

Change in CO for Exp. 2 – 6

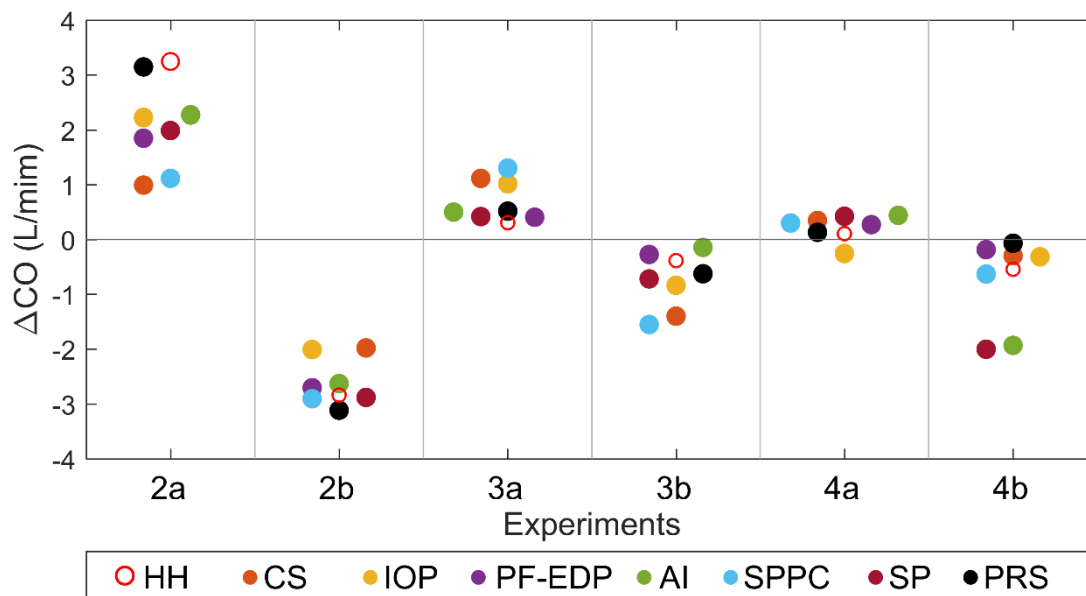


Figure 3.11: Change in cardiac output (ΔCO) between the initial steady-state CO and the CO attained after the variations of Exp. 2a - 4b for the healthy heart (HH) and the pathological circulation assisted by a physiologically controlled LVAD. CS constant-speed operation, IOP inlet-outlet pressure controller, PF-EDP pump flow-end-diastolic pressure controller, AI afterload-impedance controller, SPPC suction-prevention and physiological controller, SP systolic-pressure controller, PRS preload-responsive controller.

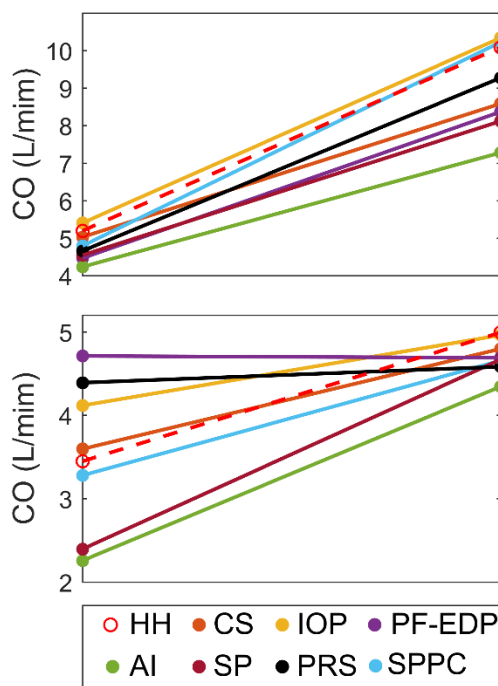


Figure 3.12: Change between the initial steady-state cardiac output (CO) and the CO attained after the variations of Exp. 5 (rest to exercise) and 6 (sleep to wake) for the healthy heart (HH) and the pathological circulation assisted by a physiologically controlled LVAD. CS constant-speed operation, IOP inlet-outlet pressure controller, PF-EDP pump flow-end-diastolic pressure controller, AI afterload-impedance controller, SPPC suction-prevention and physiological controller, SP systolic-pressure controller, PRS preload-responsive controller.

Left ventricular stroke work for Exp. 2 – 6

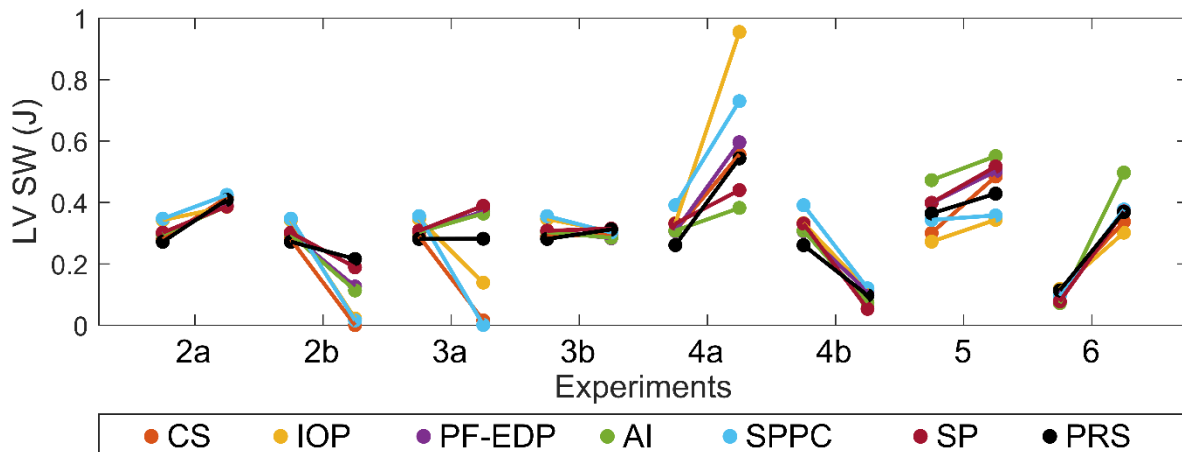


Figure 3.13: Changes between the initial steady-state left ventricular stroke work (LV SW) and the resulting LV SW after the variations of all experiments (Table 3.4) for a pathological circulation assisted by a physiologically controlled LVAD. CS constant-speed operation, IOP inlet-outlet pressure controller, PF-EDP pump flow-end-diastolic pressure controller, AI afterload-impedance controller, SPPC suction-prevention and physiological controller, SP systolic-pressure controller, PRS preload-responsive controller.

4 *In Vivo* Evaluation of Physiologic Control Algorithms for LVADs Based on LVV or LVP (Paper III)

4.1 Abstract

Turbodynamic left ventricular assist devices (LVADs) provide a continuous flow depending on the speed at which the pump is set, and do not adapt to the changing requirements of the patient. The limited adaptation of the pump flow to the amount of venous return can lead to ventricular suction or overload. Physiological control may compensate such situations by an automatic adaptation of the pump flow to the volume status of the left ventricle. We evaluated two physiological control algorithms in an acute study with eight healthy pigs. Both controllers imitate the Frank-Starling law of the heart and are based on a measurement of the left ventricular volume or pressure, respectively. After implantation of a modified Deltastream DP2 blood pump as an LVAD, we tested the responses of the physiological controllers to hemodynamic changes and compared them with the response of the constant speed mode. Both physiological controllers adapted the pump speed such that the flow was more sensitive to preload and less sensitive to afterload, as compared to the constant speed mode. As a result, the risk for suction was strongly reduced. Five suction events were observed in the constant speed mode, one with the volume-based controller, and none with the pressure-based controller. The results suggest that both physiological controllers have the potential to reduce the number of adverse events when used in the clinical setting.

4.2 Introduction

Despite great technical and clinical improvements, left ventricular assist device (LVAD) therapy is still affected by many adverse events like strokes, right ventricular (RV) failure, bleeding, hemolysis, or driveline infection [7]. Some of these adverse events are thought to be promoted by the non-physiological response of the LVAD operated at constant speed. However, whereas the direct hemodynamic effects are well understood, the clinical consequences of these are mainly assumptions: When the pump flow is higher than the blood return to the heart, the LV is emptied by the pump, and eventually, ventricular suction, i.e., a collapse of the ventricular walls, occurs. Ventricular suction presumably promotes hemolysis and thrombus formation due to flow stasis and damage to the myocardium which may be sucked onto the pump inlet [159]. In addition, excessive unloading of the LV may lead to a septum shift, which impairs the functioning of the RV and may cause a tricuspid valve insufficiency, which in turn may lead to RV failure [160]. In contrast, when the pump flow is lower than the blood return and the LV itself is too weak to generate more flow, the LV is overloaded and a congestion of blood in the left atrium (LA) and the pulmonary circulation occurs [61]. LV overload may additionally injure the already failing LV due to a consecutive increase in wall tension. Furthermore, the increased pulmonary pressure due to the congestion of blood may in extreme cases lead to lung edema and imposes an excessive load on the RV. Physiological control may have the potential to reduce the number of adverse events by adaptation of the pump speed and, thus, prevention of suction or overload.

Many physiological controllers have been analyzed *in silico* or *in vitro* and were presented in the literature, but only few controllers were also tested *in vivo*. The *in vivo* studies can be subdivided into four categories: First, studies which collected *in vivo* data, e.g. during a pump speed ramp, and then proposed a physiological controller after the analysis of this data [161]–[167]. Second, studies with suction detection and prevention algorithms [168]–[173]. Third, studies in which the pump speed is pulsed in synchrony with the cardiac cycle [164], [174]–[180]. And fourth, studies with physiological controllers activated *in vivo* (animals or human patients) [82], [84], [115], [181]–[183]. Of all four categories, only the last represents the case of a closed feedback loop, which is an important difference, because feedback can lead to instability. No chronic *in vivo* experiments with activated physiological controllers are found in the literature.

4.3 Materials and methods

We have also presented two physiological controllers in previous in vitro studies: The preload responsive speed (PRS) controller adjusts the pump speed based on a measurement of the LV volume [65], whereas the systolic pressure (SP) controller adjusts the pump speed based on a measurement of the LV pressure [78]. The purpose of both controllers is the imitation of the Frank-Starling law of the heart, which states that the flow generated by the healthy ventricle mainly depends on its preload [101]. The pressure-flow characteristics of a turbodynamic LVAD operated at constant speed differs greatly from that of a healthy heart. Compared to a healthy LV, the sensitivity of an LVAD to afterload is higher and the sensitivity to preload is lower [184]. This small preload sensitivity is the reason why the adaptation of the pump flow to the venous return is limited and suction or LV overload can occur. By adapting the pump speed and indirectly the pump flow to the preload, the physiological controllers aim at preventing suction or LV overload and all their negative consequences.

We conducted acute in vivo experiments with eight healthy pigs to compare our two physiological controllers for LVADs with the constant speed (CS) mode. For this purpose, we induced hemodynamic changes, while the LVAD was operated in one of the three control modes. Using a heart-lung machine (HLM) and an occlusive balloon catheter placed in the descending aorta, we applied acute pre- and afterload changes and observed changes of the pump speed, the pump flow, and multiple hemodynamic variables. The goal of the study was to investigate whether the physiological controllers react to the induced hemodynamic changes as defined by the Frank-Starling law and whether they work robustly in vivo.

4.3 Materials and methods

The experiments were conducted with eight pigs ($m = 91.13 \pm 9.69$ kg). The animal housing and all procedures and protocols were approved by the Cantonal Veterinary Office (Zurich, Switzerland) under the license number 152/2013. Housing and experimental procedures were in accordance with the Swiss animal protection law and also conform to Directive 2010/63 EU of the European Parliament and of the Council of September 22, 2010 on the Protection of Vertebrate Animals used for Experimental and other Scientific Purposes and also conform to the Guide for the Care and Use of Laboratory Animals.

4.3.1 Anesthesia protocol

After loss of postural reflexes following premedication with ketamine (20 mg/kg), azaperone (1.5 mg/kg) and atropine (0.75 mg), the anesthesia was deepened by a bolus injection of propofol (1-2 mg/kg bodyweight), and the animals were intubated. Anesthesia was then maintained with 2-3% isoflurane and propofol (2-5 mg/kg/h). Amiodarone (2-3 mg/kg bolus iv) was administered as anti-arrhythmic therapy in order to stabilize the heart rhythm. Pain management included fentanyl (0.02 mg/kg/h) constant rate infusion (CRI) for the duration of the procedure. After the animals were put on cardio-pulmonary bypass, isoflurane was discontinued, and anesthesia was maintained by co-administration of propofol (5 mg/kg/h) and fentanyl (0.02 mg/kg/h) CRI. Vital parameters, reflexes, blood-gases and acid-base balance were monitored during the whole procedure. After completion of the experimental procedure, the animals were euthanized by an overdose of Na-pentobarbital.

4.3.2 Surgical procedure

After induction of anesthesia and placement of the animal in supine position, the chest was draped in sterile fashion. Following midline skin incision over the sternum, a median sternotomy was performed. The pericardium was opened. After administration of heparin 300 IE/kg, the aortic arch and right atrium were cannulated (Opti22 OptiSite Arterial Cannula and TFM324L Venous Cannula, Edwards Lifesciences, Irvine, CA, USA) for connection with the HLM (Stöckert SIII, Sorin Group Deutschland GmbH, Munich, Germany). The extracorporeal circulation was started, keeping normothermic conditions. The ascending aorta was completely mobilized for the placement of the flow probe (T-208/24PAU, Transonic Systems, Inc., Ithaca, NY, USA). Three ultrasound crystals (UDG, Sonometrics Corp., London, Canada) were positioned on the LV for volume measurements by using custom-designed, 3D-printed crystal holders. The two short-axis crystals were placed in a midventricular position next to the left anterior descending and posterior descending arteries. One of the long-axis crystals was positioned at the lateral base of the left ventricle, as counterpart for the

second long-axis crystal that was attached to the inflow cannula of the LVAD. Figure 4.1 illustrates the placement of the crystals, the flow probe, and the HLM tubing.

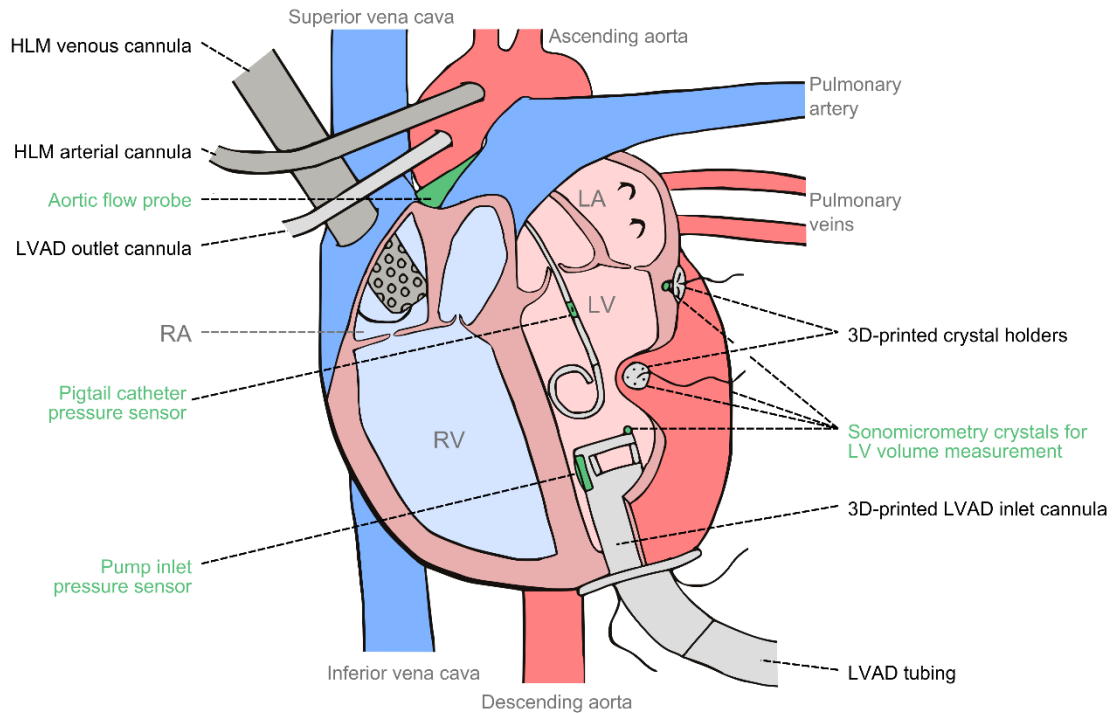


Figure 4.1: Illustration of the heart with all implanted cannulas and sensors. The four sonomicrometry ultrasound crystals were placed to measure the long and the short axis of the LV. Custom-designed, 3D-printed crystal holders were used to keep three of the crystals fixed in an intramural position; the fourth crystal was placed on the inlet cannula of the LVAD. The pigtail catheter for LV pressure measurement was used in case the pump inlet pressure sensor failed. HLM: heart-lung machine, LVAD: left ventricular assist device, RA: right atrium, RV: right ventricle, LA: left atrium, LV: left ventricle.

A modified Deltastream DP2 (Medos Medizintechnik AG, Stolberg, Germany) extracorporeal blood pump was used as an LVAD. The motor and the controller of the Deltastream DP2 pump were replaced with industrial components (EC 32, maxon motor ag, Sachseln, Switzerland / Accelus ASP-090-09, Copley Controls Corp., Canton, MA, USA), such that the pump speed could be controlled as desired. An arterial cannula (Opti22 OptiSite, Edwards Lifesciences, Irvine, CA, USA) was inserted into the ascending aorta, between flow probe and cannula of the HLM, serving as outflow graft for the LVAD. Figure 4.2 shows the inflow cannula that was specifically designed for the experiments and 3D-printed with Polyamide 12 (Materialise NV, Leuven, Belgium). The inflow cannula contains a through-wall recess for a non-medical grade, digital, barometric pressure sensor KP253 (Infineon Technologies AG, Neubiberg, Germany). The sensing surface of the sensor is in direct contact with the blood flow while the electrical interconnects on the backside were protected by a sealing compound (1-2577 Conformal Coating, Dow Corning Corp., Midland, MI, USA).

4.3.3 Physiologic controllers

In previous publications, we have presented physiological control algorithms based on a measurement of the LV volume or LV pressure together with promising in vitro results [65], [78]. The working principle of both controllers has been described in detail and is therefore only briefly summarized here. The purpose of both controllers is the imitation of the Frank-Starling law, i.e., the adaptation of the pump flow to the preload of the failing heart.

The PRS controller is operated in the simplified version, where the heart rate is not extracted, but is assumed to be constant at 60 bpm. Five steps are required to compute the desired pump speed PS_{des} based on the measured LV volume. First, the LV volume signal is low-pass filtered with a second-order infinite impulse

4.3 Materials and methods

response (IIR) filter with bandwidth of 2.7 Hz to remove measurement noise. Second, the end-diastolic volume (EDV) is extracted from the LV volume signal by identifying the maximum value from a 1.5 s sliding window. Third, the desired hydraulic power of the pump (PP_{des}) is computed by $PP_{des} = k_{prs} * (EDV - EDV_0)$, where $k_{prs} = 10 \text{ J/L}$ is the controller gain and the offset EDV_0 is obtained during calibration. Fourth, PS_{des} is computed from PP_{des} using a static, nonlinear mapping, which takes into account the efficiency of the pump and the influence of the cannulae on the resistance to flow. And fifth, the desired pump speed is again low-pass filtered with a first-order IIR filter with a bandwidth of 0.16 Hz.

The SP controller requires four main steps to compute the desired pump speed PS_{des} based on the measured LV pressure. First, the LV pressure signal is low-pass filtered with a first-order IIR filter with bandwidth of 15.9 Hz to remove measurement noise. Second, the systolic pressure SP is extracted from the LV pressure by identifying the maximum value from a 2 s sliding window. Third, PS_{des} is computed by $PS_{des} = k_{sp} * (SP - SP_0) + PS_0$ where $k_{sp} = 40 \text{ rpm/mmHg}$ is the controller gain, and the offset SP_0 as well as the reference pump speed PS_0 are obtained during calibration. And fourth, the desired pump speed is again low-pass filtered with a first-order IIR filter with a bandwidth of 0.32 Hz.

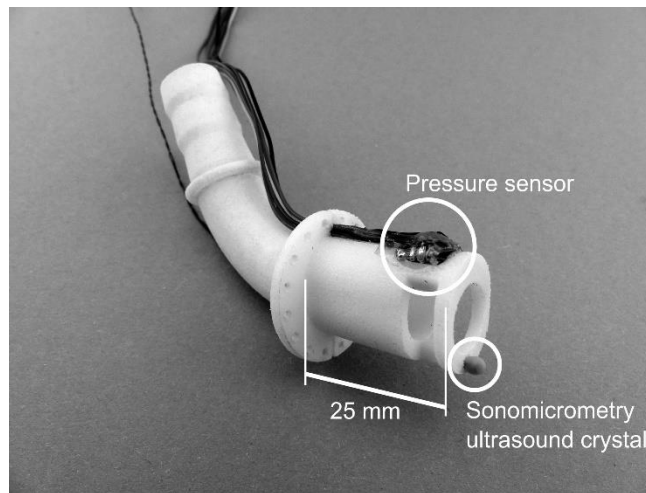


Figure 4.2: 3D-printed LVAD inlet cannula with integrated sensors.

For implantation of the LVAD inflow cannula, four felt-supported 3-0 Prolene (Ethicon Inc., Somerville, NJ, USA) U-stitches were placed around the left ventricular apex. After incision of the apex, a muscular cylinder was excised. The inflow cannula was inserted through the apical hole and fixed to the apex by placing the Prolene sutures through the implant ring of the cannula. The outflow and inflow cannulae were connected to the tubing of the LVAD under careful deairing. The LVAD was started at 2000 rpm and the speed was increased while the flow through the HLM was decreased accordingly. A minimal flow of 0.5 L/min was maintained through the HLM to prevent flow stasis. As last steps, a pigtail catheter (Ventri-Cath 510 PV Loop Catheter, Millar Instruments Inc., Houston, TX, USA) was inserted through the carotid artery into the LV to measure the LV pressure, and a Reliant Stent Graft Balloon Catheter (Medtronic, Minneapolis, MN, USA) was placed through the femoral artery into the descending aorta for afterload variations.

Finally, depending on the selected controller, the respective computed desired pump speed PS_{des} is fed to the speed controller of the electric motor of the LVAD. Both physiological controllers were implemented in Matlab/Simulink and executed on Real-Time Windows Target (The Mathworks Inc., Natick, MA, USA).

4.3.4 Experiments

Three different manipulations were applied to simulate hemodynamic changes: a preload reduction, a preload increase, and an afterload increase. The preload was reduced and increased by draining or infusing 500 mL of blood using the HLM. After the preload reduction experiment, the 500 mL were infused back into the pig before another 500 mL were infused to simulate the preload increase. The afterload was increased by inflating the balloon catheter in the descending aorta.

Figure 4.3 shows an overview of the experimental protocol. With each of the eight pigs, two identical blocks of experiments were conducted (A and B). At the beginning of each block, the volume loading of the pig was

adjusted to achieve acceptable flow and pressure levels, and the controllers were calibrated. For the calibration, the pump was set to the CS mode and the speed was manually adjusted such that the mean flow through the aortic valve was approximately 0.5 L/min and no suction occurred. The identified pump speed was taken as the reference speed for the entire block. Then, both physiological controllers were automatically calibrated, i.e., the parameter EDV_0 of the PRS controller and the parameters SP_0 and PS_0 of the SP controller were set such that PS_{des} of both controllers corresponded to the reference speed identified before. The experiments were then started by randomly selecting one of the three controllers and starting with the first manipulation.

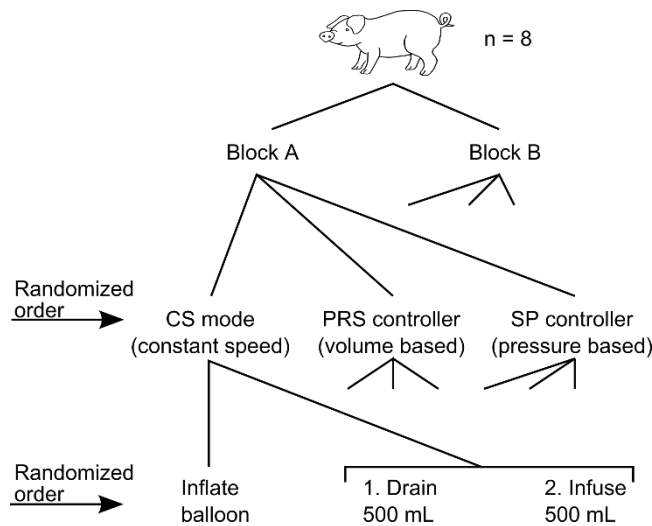


Figure 4.3: Overview of the study protocol. With all eight pigs, the same experiments were conducted once in Block A and once in Block B. In each block, both physiological controllers and the CS mode were tested with all three manipulations, yielding 18 manipulations per pig. The PRS controller is based on LV volume; the SP controller is based on LV pressure.

4.3.5 Data recording and extraction

Table 4.1 lists all signals that were recorded continuously at 500 Hz during the experiment. The carotid arterial pressure was recorded using the ACQ-7700 System (DSI Ponemah; Valley View, OH, USA); all other signals except the LV pressure were recorded using an MF624 input/output card (Humusoft s.r.o, Prague, Czech Republic) and Matlab Real-Time Windows Target (The Mathworks Inc., Natick, MA, USA). The signals from the two recording systems were synchronized during post processing using a manual trigger signal that was recorded on both systems. Because of its digital interface, the LV pressure sensor (KP253) was acquired at 200 Hz using an Arduino Due development board (Arduino S.R.L, Scarmagno, Italy), which fed the signal to the PC running Matlab Real-Time Windows Target, where it was upsampled to 500 Hz and recorded. The LV pressure sensor failed in Pigs 2 and 5, and in this case we switched to the pressure measurement of the pigtail catheter as input for the SP controller. Because these two sensors are not placed at the exact same position, they do not measure the same signal. Differences were observed during suction, when the inlet cannula pressure showed negative pressure spikes, but not for the systolic pressure that is used as input for the SP controller. The LV volume was obtained by measuring the short and long axes of the LV with ultrasound crystals and computing the volume with an ellipsoid model.

For further analysis, steady-state sections before and after each manipulation were extracted. These sections were identified manually and had a duration of at least 10 s. The gray shaded rectangles in Figure 4.4 indicate the identified steady-state sections for three preload reduction manipulations. With an automatic algorithm, the individual heartbeats within those sections were identified and beat-by-beat mean values were extracted and stored. From these values, the mean values for the entire section were computed for the following signals: pump speed, pump flow, aortic valve flow and carotid arterial pressure. The total cardiac output (CO) was computed by adding the mean aortic valve flow and pump flow signals. In addition, the beat-by-beat end-diastolic pressure (EDP) was identified as the pressure on the bottom right corner of the LV pressure-volume loop, and the stroke work was extracted by computing the area inside the pressure-volume loop.

Table 4.1: Recorded signals

Signal	Abbreviation	Sensor
Left ventricular pressure	LVP	KP253, Infineon Technologies AG, Neubiberg, Germany (Pigs 1, 3, 4, 6, 7, and 8) <i>or</i> Ventri-Cath 510 PV Loop Catheter / MPVS Ultra PV Loop System, Millar Instruments Inc., Houston, TX, USA (Pigs 2 and 5)
Carotid arterial pressure	CARP	DTXPlus DT-NN, Argon Medical Devices Inc., Plano, TX, USA
Left ventricular volume	LVV	UDG, Sonometrics Corp., London, Canada
Pump speed	PS	Encoder HEDL 5540, maxon motor ag, Sachseln, Switzerland
Pump flow	PF	TS410/ME-11PXL, Transonic Systems, Inc., Ithaca, NY, USA
Aortic valve flow	AVF	T-208/24PAU, Transonic Systems, Inc., Ithaca, NY, USA

4.3.6 Statistical analysis

For each manipulation (preload reduction, preload increase, and afterload increase) we conducted statistical tests to compare the physiological controllers with the CS mode of the LVAD. We computed the change in pump speed ΔPS and the change in pump flow ΔPF from before to after the manipulation. Then we used a paired t-test to compare each physiological controller with the CS mode. We conducted eight tests per manipulation and applied a Bonferroni correction to counteract the problem of multiple tests, yielding a significance level of $p = 0.05/8 = 0.00625$.

4.4 Results

In total, 144 preload and afterload manipulations were planned (18 manipulations in 8 pigs) and 139 were conducted completely. The other 5 manipulations were either not conducted or aborted due to a very low perfusion. Of these 139 manipulations, 19 were excluded, because no steady-state sections could be identified before or after the manipulation. The remaining 120 manipulations were used for further analyses.

4.4.1 Qualitative analysis of preload reduction

Figure 4.4 shows the results of the preload reduction experiment for Pig 5, Block A with the CS mode and both physiological controllers. The first row shows how both physiological controllers reduce the pump speed in response to the reduced preload, while it is kept constant in the CS mode. The pump flow shown in the second row decreases with all three control modes, however, in the CS mode it returns to the initial value after 10 s. The small oscillations in the pump speed are caused by the mechanical ventilation, which influences the LV pressure and volume signals.

4.4.2 Hemodynamics during preload reduction

Figure 4.5 shows the mean values of the pump speed, the pump flow, the stroke work, the CO, the EDP, and the carotid arterial pressure before and after the preload reduction experiment from Block A for all eight pigs. The purpose of this figure is to show the hemodynamic state of all pigs and the variability between them, as well as the magnitude of the change induced by draining 500 mL of blood. Qualitatively, differences between the CS mode and the physiological controllers can be observed for the pump speed and pump flow signals. When the pump is operated in CS mode, the pump speed remains constant and the changes in pump flow are small. With both physiological controllers, the pump speed is reduced and the reduction in pump flow is more pronounced. Quantitative values and a statistical analysis are provided in the subsequent paragraphs. For the stroke work, the CO, the EDP, and the carotid arterial pressure, the qualitative analysis shows no difference between the CS mode and the physiological controllers. The differences between the two physiological controllers are also small for all signals and are overshadowed by the inter-animal variability.

The results for the pre- and afterload increase experiments can be found in the supplementary material, processed in the same manner as the results presented in Figure 4.5.

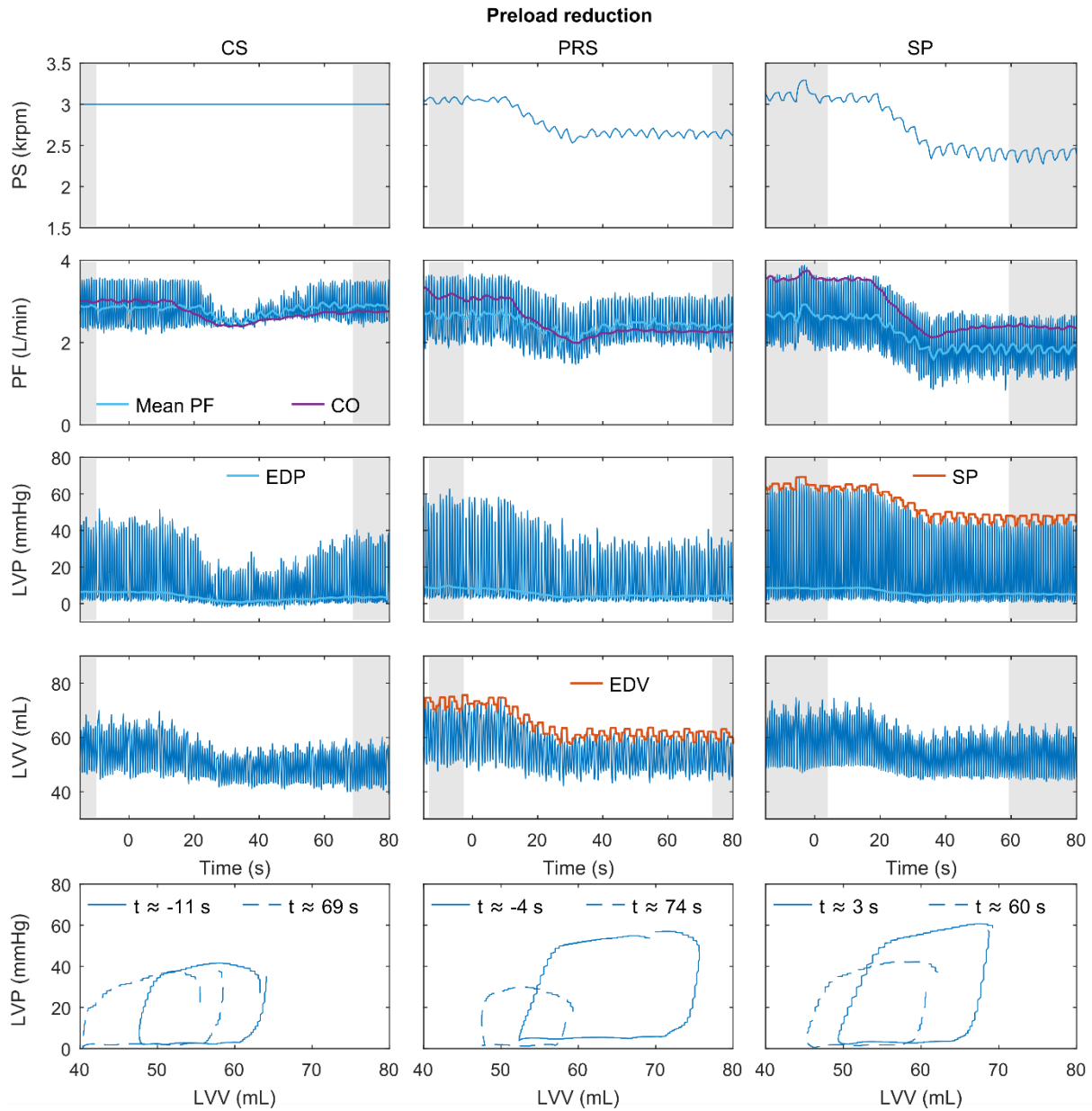


Figure 4.4: Example results of the preload reduction experiment (Fig 5, Block A) with the CS mode and both physiological controllers. The figure shows the pump speed (PS), the pump flow (PF), the cardiac output (CO), the LV pressure (LVP), the end-diastolic pressure (EDP), and the LV volume (LVV) signals. The end-diastolic volume (EDV) and the systolic pressure (SP) signals plotted in red are the respective input signals to the physiological controllers. The shaded gray areas indicate the steady-state sections that were used to calculate the mean values before and after the manipulations. The preload reduction was started at $t = 0$ s in all three cases.

4.4.3 Statistical analysis of pump speed and pump flow

Figure 4.6 provides a quantitative analysis of the differences between the CS mode and the physiological controllers with a statistical analysis of the change of the pump speed and pump flow signals during the three manipulations. The pump speed analysis generates five statistically significant results distributed over all manipulations and both controllers. The p-value of all comparisons is small and all speed changes except of one (afterload increase, SP controller, Block A) go in the expected direction. Three pump flow comparisons

4.4 Results

are statistically significant; none of them for the preload increase manipulation. Table 4.2 lists the mean and standard deviation of ΔPS and ΔPF over both blocks for each manipulation and each control mode. While both controllers react similarly to preload changes, the reaction of the SP controller to the afterload increase is stronger.

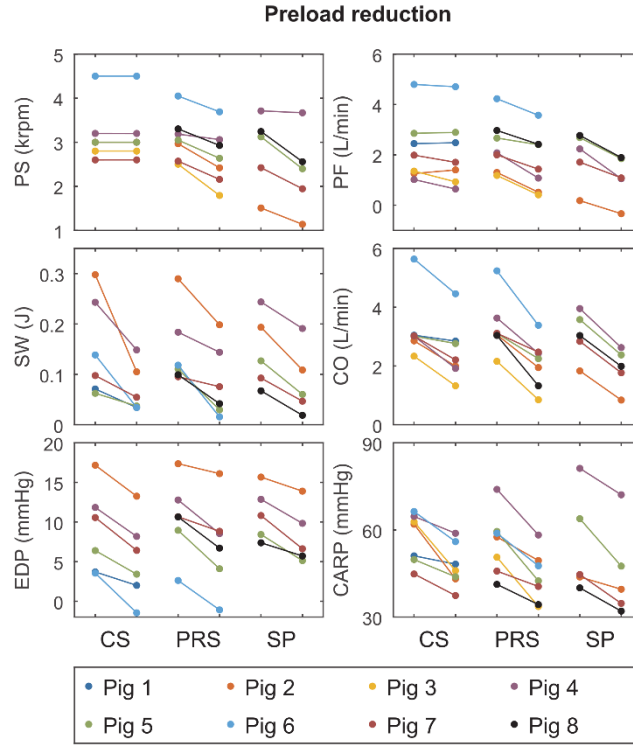


Figure 4.5: Hemodynamic changes during the preload reduction experiment for Block A and all eight pigs. Each panel shows the change of one signal for the constant speed (CS) mode on the left-hand side, the PRS controller in the middle, and the SP controller on the right-hand side. The figure shows six signals, the pump speed (PS), the pump flow (PF), the stroke work (SW), the cardiac output (CO), the end-diastolic pressure (EDP), and the carotid arterial pressure (CARP). Same figures but for pre- and afterload increase experiments can be found in the supplementary material of paper.

Table 4.2: Mean and standard deviation over both blocks

Manipulation	CS mode		PRS controller		SP controller	
	ΔPS (rpm)	ΔPF (L/min)	ΔPS (rpm)	ΔPF (L/min)	ΔPS (rpm)	ΔPF (L/min)
Preload reduction	0	-0.13 ± 0.21	-496 ± 265	-0.68 ± 0.35	-408 ± 198	-0.60 ± 0.28
Preload increase	0	0.10 ± 0.29	241 ± 104	0.36 ± 0.26	279 ± 146	0.39 ± 0.29
Afterload increase	0	-0.57 ± 0.45	263 ± 149	-0.17 ± 0.25	860 ± 373	0.74 ± 0.39

4.4.4 Preload sensitivity

In order to investigate whether the reaction of the two controllers to the preload changes is appropriate, we extracted the preload sensitivity of the LVAD as the change in pump flow divided by the change in preload $\Delta PF / \Delta EDP$. A physiological preload sensitivity value is reported by Salamonsen et al. [184] as 0.21 ± 0.03 L/min/mmHg. The values we obtained from the preload reduction experiment are 0.03 ± 0.08 L/min/mmHg for the CS mode, 0.21 ± 0.29 L/min/mmHg for the PRS controller, and 0.26 ± 0.13 L/min/mmHg for the SP controller.

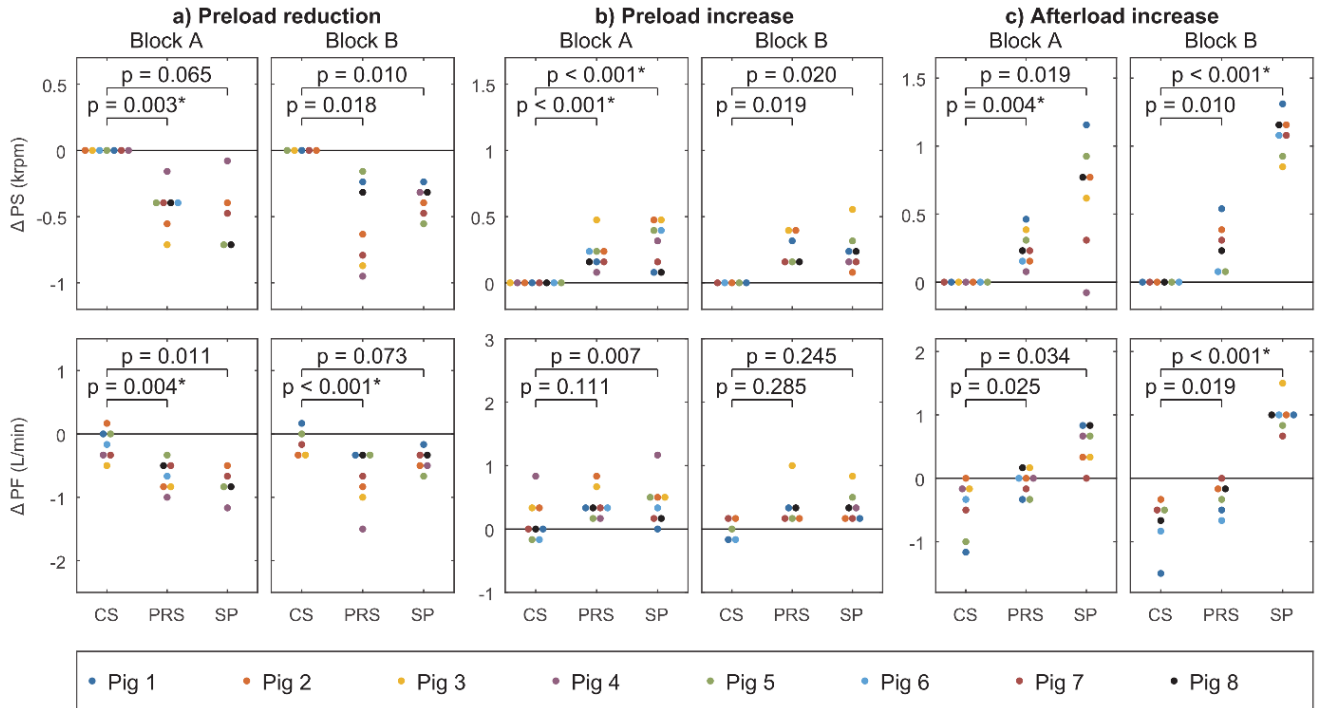


Figure 4.6: Change of the pump speed (ΔPS) and pump flow (ΔPF) during the preload reduction, the preload increase, and the afterload increase experiments. The values of the PRS and the SP controllers were compared to the values obtained with the constant speed (CS) mode using a paired t-test with a significance level of 0.00625.

4.4.5 Ventricular suction

In total, 34 preload reduction experiments were conducted with the pump inlet pressure sensor active and ventricular suction was observed six times: five times with the CS mode and once with the PRS controller. Table 4.3 lists all suction cases to provide an overview of the hemodynamic conditions that prevailed before the preload reduction experiments were started. During suction, all signals were highly transient, and no steady-state phase could be identified. Two cases can also be found in Figure 4.5, but the corresponding steady-state sections were identified after the suction events.

Table 4.3: Suction cases

Case	Control Mode	Pig	Block	Pump flow before suction (L/min)	End-diastolic pressure before suction (mmHg)	Duration of suction (s)
1 ³	CS	3	A	1.35	n/a ¹	5
2	CS	3	B	1.24	n/a ¹	6
3	CS	4	B	2.21	12.37	7 ²
4 ³	PRS	6	A	4.23	2.62	2
5	CS	8	A	2.94	7.56	9
6	CS	8	B	2.75	10.22	5

¹EDP could not be extracted reliably for Pig 3 due to the round shape of the PV loop.

²then aborted and volume reinfused.

³these experiment can be found in Figure 4.5.

4.5 Discussion

The study results show clearly that both the PRS controller as well as the SP controller react to preload changes in the expected direction and thereby imitate the Frank-Starling law of the heart. The panels a) and b) in Figure 4.6 show that in response to a preload reduction (increase), both controllers reduce (increase) the

4.5 Discussion

pump speed, resulting in a reduced (increased) pump flow. The question if the reaction is adequately strong is answered with the preload sensitivity values listed in the Results section paragraph titled “Preload sensitivity”. Even though these numbers are affected by a high variance, they indicate that the preload sensitivity of the controllers is similar to that of the native heart. The reaction of the controllers to the preload increase is weaker than that to the preload reduction (see Table 4.2). We believe that this difference can be explained by the high contractility of the healthy LV, which can fully compensate for the preload increase by increasing the aortic valve flow, which in turn prevents the controllers to increase the pump flow substantially. A categorization of the two controllers in comparison with others presented in literature can be found in a previous publication [78].

Most physiologic controllers are designed to prevent suction however, their reaction can be too weak, or too slow such that suction may still occur. The findings of this study suggest that our physiological controllers are able to prevent suction effectively. The one suction event observed with the PRS controller was released after only two heartbeats, which indicates that the controller did not fail completely in this case. For a clinical application, the physiological controllers will be extended by an additional suction detection system as proposed in the literature [170]. In addition, a similar system would intervene when the pump speed is very low or very high over a longer time, indicating sensor drift or a similar malfunction. However, in the current study we only tested the core algorithm of the control system.

The results of the current study show that the PRS controller also reacts to afterload changes in the expected manner, i.e., as defined by the Frank-Starling law. Figure 4.6c) shows that when the afterload is increased, the PRS controller increases the pump speed to counteract the decrease in pump flow. The question if the reaction is adequately strong is easier to answer compared to the preload reduction, because we want the pump flow to be insensitive to afterload. With the PRS controller, this goal is achieved, as the change in pump flow almost goes to zero ($\Delta PF = -0.17 \pm 0.25$ L/min) compared to -0.57 ± 0.45 L/min with the CS mode. In contrast, the reaction of the SP controller to an afterload increase is too strong, which results in an increase in pump flow by 0.74 ± 0.39 L/min. This overreaction is clearly undesirable as it may lead to excessive arterial pressures. However, previous in vitro studies have shown that with a weak LV and under LVAD support, the SP is less influenced by the afterload [78]. We therefore assume that with a failing instead of a healthy LV, the reaction of the SP controller to afterload changes would be more adequate. In general, it remains to be determined if the imitation of the Frank-Starling law without taking the perfusion into account explicitly represents the optimal physiological control system.

One important outcome of this study is the proof of the robustness of both physiological controllers: No experiment had to be aborted because of a controller problem. In fact, we conducted two identical blocks of experiments (A and B) with each pig and did not observe any substantially different results. The sensors we used to measure the LV volume and pressure can only be used for acute experiments, but they proved to be sufficiently accurate, i.e., the accuracy requirements for future biocompatible sensor systems are moderate. Clearly, the development of reliable, long-term stable implantable sensors is absolutely critical for the success of physiological control. Before the second block, we recalibrated both physiological controllers. This procedure was necessary, because the hemodynamics changed continuously, and the controller settings rendered inappropriate after some time. Whereas the hemodynamic changes during an acute experiment are presumably different from those observed in LVAD patients, a chronic study with a physiological controller is required to answer the question of how much recalibration is required. Both physiological controllers also worked well during arrhythmic periods, which were observed in two of the eight pigs.

The controller gains need to be selected carefully as a compromise between performance and stability. When the gains are too low, the difference to the CS mode is negligible; when the gains are too high the controllers can become unstable. Both controller gain values were selected based on in vitro experiments. The gain of the PRS controller additionally allows a physiological interpretation as the slope of the preload recruitable stroke work [65], [78]. In preliminary in vivo experiments, we had tested higher and lower gain values. Sustained oscillations could be observed with gain values around $k_{prs} = 20$ J/L and $k_{sp} = 80$ rpm/mmHg, which indicates that the stability margins with the normal gains are approximately two. With low gains, i.e., $k_{prs} = 5$ J/L and $k_{sp} = 20$ rpm/mmHg, no substantial difference to the CS mode could be observed.

Therefore, we believe that the presented values represent a reasonable compromise between a high gain margin and a good preload sensitivity.

Although the current study shows that the reaction of the controllers is physiological, it does not allow a statement on their effectiveness in human patients. The results in Figure 4.6 show that the stroke work, the CO, the EDP, and the carotid arterial pressure are all not substantially affected by the presence of physiological control. This outcome can be well explained by the healthy pig model that was used. Only Schima et al. [84] have tested a physiological controller in human patients and they reported a significant increase in pump flow and significant decrease in pulmonary arterial pressure in response to physical exercise. The PRS and the SP controller are expected to achieve a similar response in human patients. However, while those results show that physiological control can improve the hemodynamics, only long-term clinical experience will show if the number of adverse events can be reduced.

4.6 Limitations

The main limitation of the presented study is the use of a healthy animal model. Due to the high contractility of the healthy LV, the preload sensitivity of the combined heart-LVAD system was very high. Consequently, the hemodynamics of our model differ substantially from those of a patient suffering from heart failure. However, both physiological controllers have already been evaluated in vitro with a HF model [65], [78]. We expect a similar behavior of the controllers in a HF animal model. Furthermore, this study represents the first approach to test the two physiological controllers in vivo and due to the complexity, we decided not to use pharmacological agents to reduce the contractility or to alter the afterload. Future studies however, will have to be conducted with a heart failure animal model that is more complex but represents the clinical situation more accurately.

Another limitation concerns the LV pressure and volume sensors we used. Not only the ellipsoid model, but also the placement of the sonomicrometry ultrasound crystals introduced uncertainty on the measured LV volume. However, the offset of the LV volume had no influence on the closed-loop system with the PRS controller. Furthermore, the lack of long-term stability of both pressure and volume sensors constitutes a yet unsolved problem, which hampers the chronic in-vivo or even clinical implementation of physiological control. Nevertheless, both sensors served for the purpose of the study, i.e., for deriving short-term recordings during the acute animal trials and, eventually, evaluating the physiological controllers.

4.7 Conclusion

This study shows that both the PRS controller as well as the SP controller work robustly in vivo and adapt the pump flow according to the Frank-Starling law of the heart, which strongly reduces the risk of ventricular suction or overload. The effectiveness of the two controllers in reacting to hemodynamic changes is promising. Integrated in an LVAD, they may be able to fulfill the needs of physiological adaptation in the clinical setting. Future work is necessary to develop completely integrated, long-term stable and biocompatible sensor systems feeding the controller with the required LV volume or pressure signal.

5 Response of a Physiological Controller for VADs during Acute Pathophysiological Events (Paper IV)

5.1 Abstract

The current paper analyzes the performance of a physiological controller for turbodynamic ventricular assist devices (tVADs) during acute pathophysiological events. The numerical model of the human blood circulation implemented on our hybrid mock circulation was extended in order to simulate the Valsalva maneuver (VM) and premature ventricular contractions (PVCs). The performance of an end-diastolic volume (EDV)-based physiological controller for VADs, named preload responsive speed (PRS) controller was evaluated under VM and PVCs. A slow and a fast response of the PRS controller were implemented by using a three-seconds moving window and a beat-to-beat method, respectively, to extract the EDV index. The hemodynamics of a pathological circulation, assisted by a tVAD controlled by the PRS controller were analyzed and compared with a constant speed support case. Results show that the PRS controller prevented suction during the VM with both methods, while with constant speed this was not the case. On the other hand, the pump flow reduction with the PRS controller led to low aortic pressure, while it remained physiological with the constant speed control. Pump backflow was increased when the moving window was used but it avoided sudden undesirable speed changes, which occurred during PVCs with the beat-to-beat method. In a possible clinical implementation of any physiological controller, the desired performance during frequent clinical acute scenarios should be considered.

5.2 Introduction

Implantable ventricular assist devices (VADs) have become a viable solution for the ever-growing population of heart failure patients. The continually improving clinical outcome of the VAD-therapy [185] play an important role on this result. According to data presented in [7], which was derived from more than 15,000 patients, the one- and two-year survival rates with turbodynamic VADs (tVADs) currently reach 80% and 70%, respectively, while the quality of life remains improved after two years compared to pre-implantation. More than 90% of the VAD patients receive a tVAD. Although a reduction of adverse events has been reported during the last years, complications of this therapy such as hemolysis, cardiac arrhythmias, pump thrombosis, gastrointestinal bleeding, right ventricular (RV) failure and left ventricular (LV) overloading, still pose a problem. Despite the increased durability of newer generations of pumps, a stable incidence of device malfunction and exchange due to all causes is evident [7], [186].

Several research groups [61], [65], [69]–[71], [81], [143], [187] have proposed physiological control as a solution to reduce or even eliminate over- and underpumping events, which are presumably related to adverse events, such as hemolysis, pump thrombosis and RV failure. These control strategies are based on various signals, such as the LV pressure (LVP), the LV volume (LVV), the aortic pressure (AoP), or the pump flow. Their goal is to adjust the speed and ultimately the blood flow of a tVAD such that the resulting cardiac output (CO) meets the perfusion requirements of the circulation. By matching the pump flow to the hemodynamic status of the patient, adverse events related to over- and underpumping can be prevented and the physiological adaptation of the CO is restored.

All physiological controllers extract one or more indices from either a measured or an estimated signal of the heart-tVAD system. These indices are fed into a control system which adjusts the desired speed of the tVAD. In [81], [143] the authors implemented a beat-to-beat extraction algorithm for their control indices, namely the end-diastolic pressure (EDP) and mean pump flow, respectively. In [65], [69]–[71] the authors proposed signal processing algorithms, which extract the indices of the end-diastolic volume (EDV), the pump pressure difference, the pump speed pulse, or the EDP over a time window with a predefined fixed length. Particularly, in [71] and [55] a moving window with a length of three seconds of their measured signals was implemented in order to extract their respective control inputs, whereas Wang et al. [70] proposed a moving

5.3 Materials and Methods

one-second time window. The suction detection algorithm developed in [69] uses a moving maximum search algorithm for the identification of the diastolic level of the pulsation of the pump differential pressure. Additionally, authors in [67] used low-pass filtering methods, such as the nonlinear morphological filter, in order to feed their controller with the required mean pump flow.

The controller presented in [55] was evaluated by *in vitro* experiments, which represent wide-range variations of cardiovascular parameters and simulate resting or exercising conditions. Similar experiments for testing physiological controllers either *in silico* or *in vitro* are presented in [69], [81], [187], [188]. In contrast, authors in [79] investigated the response of several physiological controllers during more sudden changes in hemodynamic parameters. These changes were related to exercise (CO increase) and head-up tilt (CO decrease), simulated through a detailed numerical model [189]. Additional cases that lead to such sudden changes are related to pathophysiological events like respiration (deep ex- or inspiration), strain (Valsalva or Mueller maneuver, coughing or heavy lifting) or arrhythmia.

Approaches to simulate such pathophysiological events either numerically or by manipulating mechanical components have been proposed. In [190], the authors presented a numerical model of a human circulation that incorporates the influence of the intrathoracic pressure (ITP) and can therefore potentially simulate respiration and Valsalva maneuver (VM). However, the simulation of these events and their use for evaluating physiological controllers was not in the scope of their study. A study focused on VM simulation has been presented in [191], however without investigating a VAD-assisted circulation. In [192], the authors simulated VM in their mock circulation loop (MCL), which is built for evaluating biventricular assist devices (BiVADs). They were able to reproduce VM by manipulating the mechanical valves of their MCL, which represented the systemic and pulmonary vascular resistances, in order to apply a resistance increase, thereby emulating the influence of an increase of the ITP. These simulations were later used to evaluate physiological controllers for BiVAD support cases [141]. Amacher et al. [90] simulated premature ventricular contractions (PVCs) in order to evaluate arrhythmia detection algorithms, when a pulsatile speed mode of a tVAD, synchronized to the heart cycle, is implemented.

The current paper describes how our numerical model of the human blood circulation [97] was extended to simulate specific pathophysiological events, namely PVCs and VM, by manipulating the heart rate (HR) and the ITP. For both extensions, we focused on the hemodynamics in the LV of a pathological circulation assisted by a tVAD, which was either controlled by one of several configurations of the preload responsive speed (PRS) controller [55] or set at a constant speed. The core algorithm of the PRS controller remained unchanged, but the EDV extraction algorithm was modified, to influence the aggressiveness of the controller. The pros and cons of fast and slow response during PVCs and VM were analyzed and compared to the clinical case of the constant speed control. The potential of the proposed extended human blood circulation model for testing new control algorithms is indicated and possible complications of standalone physiological controllers discussed. The need for additional algorithmic features that will support the core of the physiological controller is highlighted to guarantee preventing undesired over- and underpumping events.

5.3 Materials and Methods

5.3.1 Hybrid mock circulation

We conducted experiments on a hybrid mock circulation (HMC) based on the hardware-in-the-loop concept, which has been developed in our group [97]. Figure 5.1 shows a picture of the hardware part of the HMC, while its caption defines the parts and their manufacturer. In our experiments, a non-implantable mixed-flow turbodynamic blood pump that allows implementing various control approaches substituted the tVAD (c). The pump is connected to two pressure-controlled reservoirs (a), (b) and a backflow pump (d) ensures that the fluid level in the two reservoirs remains constant during the experiments. The fluid level is measured by infrared range finders (h) and fed to the backflow pump-controller. The pressure in each reservoir is controlled using one proportional solenoid inlet valve and two proportional solenoid outlet valves (g) per reservoir, a vacuum receiver (i) and a vacuum pump (j), and one fluid-pressure (e) sensor per reservoir.

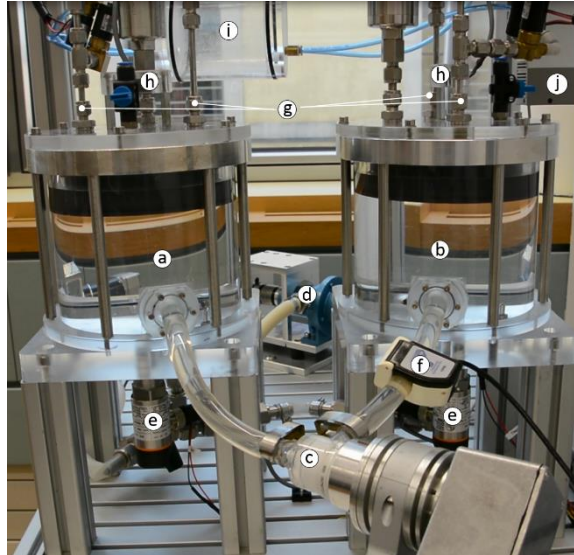


Figure 5.1: Picture of the hardware part of our hybrid mock circulation consisting of two pressure-controlled reservoirs (a) and (b), a blood pump head (Deltastream DP2, Xenios AG, Heilbronn, Germany) (c) equipped with an encoder (ME22, PWB Encoders GmbH, Eisenach, Germany) and an industrial motor controller (Accelus, ASP-090-09, Copley Controls Corp., Canton, MA), a backflow pump (Moyno 500 Pumps-200 Series, Moyno, Inc., Springfield, OH) (d), two fluid-pressure sensors (PN2009, IFM Electronic GmbH, Essen, Germany) (e), one ultrasonic flow probe (TS410/ME-11PXL, Transonic Systems, Inc., Ithaca, NY) (f), one proportional solenoid inlet valve (PVQ33-5G-23-01F, SMC Pneumatics, Tokyo, Japan) and two proportional solenoid outlet valves (PVQ33-5G-40-01F, SMC Pneumatics) per reservoir (g), two fluid-level sensors (GP 2Y0D810Z0F, Sharp, Osaka, Japan) (h), a vacuum receiver (i) and a vacuum pump (ZL112-K15LOUT-E26L-Q, SMC Pneumatics) (j).

The reference signals for the pressure controllers of the two reservoirs are computed in real-time by a validated numerical model of the human blood circulation [123], based on the measured pump flow (f). This numerical model consists of lumped-parameter elements. Thus, the veins of the upper and lower limb circulation, the inferior vena cava etc. are implemented with one classic Windkessel model, which does not allow an implementation of the ITP on the vessels and organs of the thorax separately. Therefore, the numerical model was extended for the current investigation as described below.

5.3.2 Hemodynamic influence of intrathoracic pressure variations and arrhythmia

In order to define the required modifications of the existing numerical model, the hemodynamic influence of ITP variations and PVCs had to be identified. For this purpose, the response of both a physiological and a pathological circulation during these events was analyzed based on clinical studies and is presented below.

The VM causes an increase in the ITP without hyperinflation of the lungs. In the physiological circulation, increased ITP causes a decrease in the RV preload and RV filling, leading to a decrease in LV preload and CO. In the pathological circulation, the decrease of CO is significantly smaller or even inverted compared to the healthy heart. That happens due to the blood pooling in the pulmonary vascular system which can compensate the decrease in LV preload, thus preserving the LV EDV. The preserved LV EDV, in combination with the decrease in the LV afterload in the failing heart, is responsible for the altered influence of VM on CO and AoP in heart failure [193]–[195]. Similar ITP changes are observed during coughing, strain, bowel movement, heavy lifting etc. [195].

Arrhythmias cause abrupt changes in the CO. Bradycardia causes a decrease in the CO and an overload of the cardiopulmonary system. Tachycardia, both ventricular and supraventricular, impairs the diastolic filling of the ventricles, leading to a decrease of the CO. Extrasystoles cause a decrease in both LV and RV EDV by generating PVCs and disrupting the diastolic phase. Arrhythmias in the setting of left VAD therapy can lead to suction events because of a decrease in LV preload, for instance during bradycardia or tachycardia, leading to a reduction of the RV SV or directly in LV EDV during extrasystoles [194].

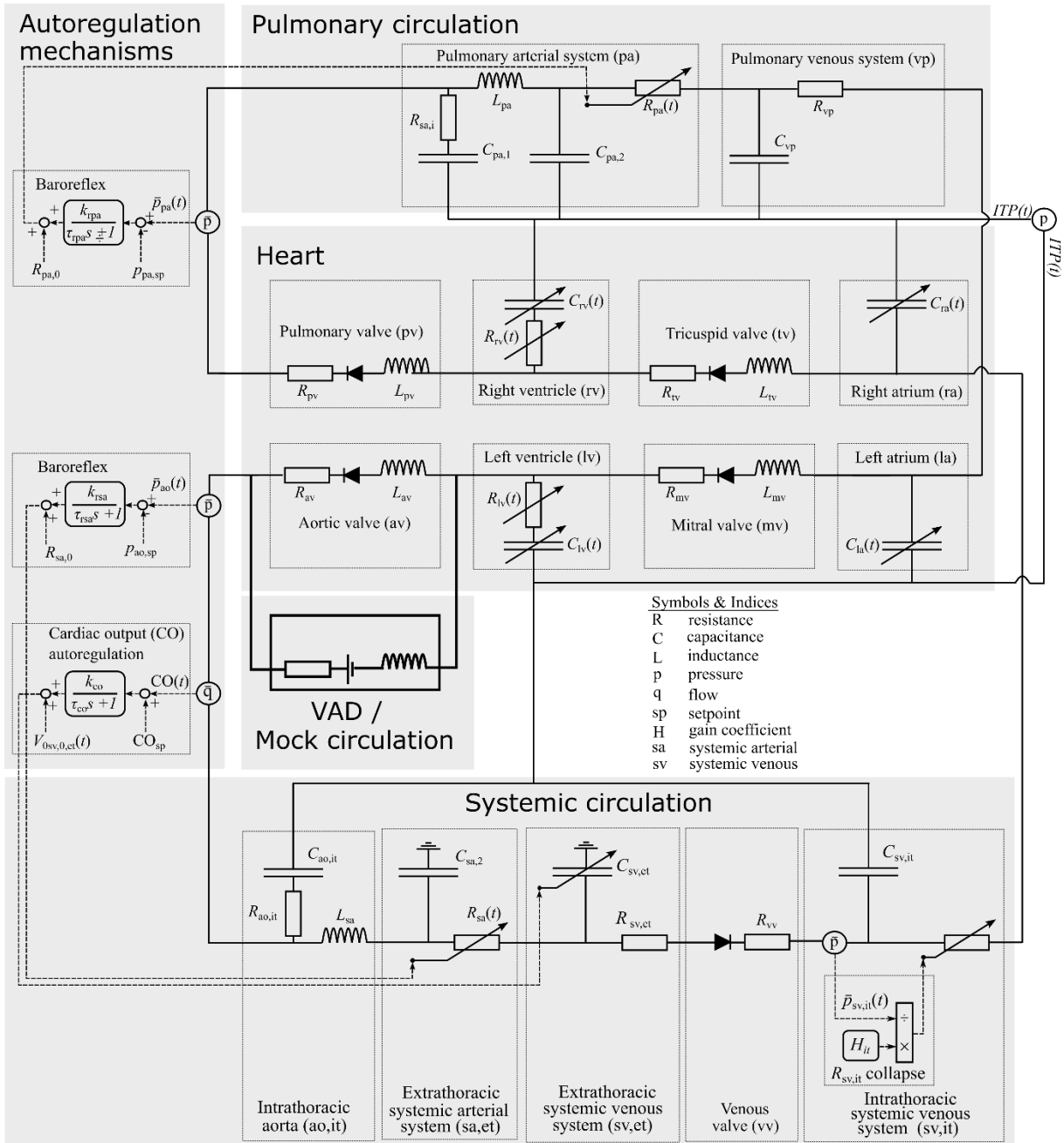


Figure 5.2: Electrical analog of the extended numerical model of the human blood circulation to include the influence of the intrathoracic pressure (ITP) on the organs of the thoracic cavity. The systemic arterial and venous systems each consist of an intra- and an extrathoracic part.

5.3.3 Extension of the numerical model

The numerical model has already been extended in order to emulate suction [148]. For the current study, we further extended it in order to account for influences of ITP variations, based on the analysis presented above. Figure 5.2 shows the structure of the extended model. The systemic venous and arterial systems are now divided into an intra- and an extrathoracic part. The resistance of the intra- and extrathoracic veins, namely $R_{sv,it}$ and $R_{sv,et}$, respectively, are used to simulate the collapse of the large vessels when the transmural pressure is negative. Furthermore, we added a venous valve in order to prevent regurgitation of the venous return [101]. The ITP is implemented by adding its value to all pressure values inside the thoracic cavity. Table 5.1 lists the values of all new parameters introduced into the extended model as well as their source. The remaining parameters used in the model were the same as presented in [123].

5.3.4 Simulation of Valsalva maneuver

Figure 5.3A and 5.3C show the input signals to simulate the VM. The ITP was increased manually by 30 mmHg at $t \in [5, 15]$ s, and the HR varied according to clinical data presented in [191]. The amplitude of the ITP for the VM were defined such that the resulting AoP waveform matched those presented in clinical studies [101], [191], [193], [196].

5.3.5 Simulation of arrhythmia

Figure 5.3B and 5.3D show the input signals to simulate arrhythmia. We introduced several PVCs, as they were defined in [90]. For that, we altered the cardiac cycle of the time-varying elastance model of the simulated ventricles and atria. Soon after the end of the systole another ventricular contraction is triggered, while the subsequent diastolic phase is prolonged.

5.3.6 Experiments

For the physiological circulation, the HR was fixed at 70 bpm and increased up to 90 bpm during VM event. The pathological circulation was simulated by decreasing the contractility of the LV to 34% of physiological contractility and increasing the HR to 90 bpm. For each experiment we ran the HMC until steady state was reached and then started either the VM or the PVCs experiment as depicted in Figure 5.3. The numerical model was executed with Matlab/Simulink running Real-Time Windows Target (The Mathworks Inc., Natick, MA, USA) and all signals were recorded at 1 kHz. A glycerol water mixture with viscosity of 2.8 mPa·s was used for all the experiments.

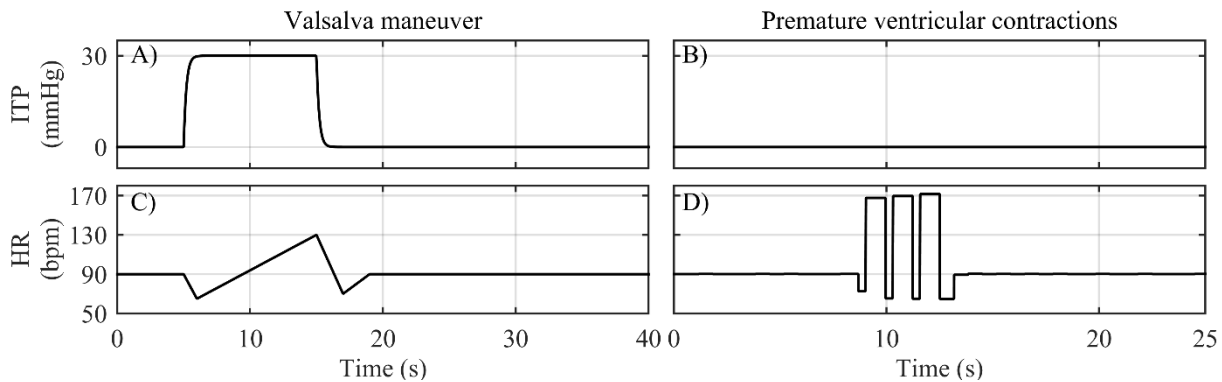


Figure 5.3: Defined values for the parameters that were varied during the experiments. Panels A) and C) show the variation of the intrathoracic pressure (ITP) and the heart rate (HR) during the Valsalva maneuver (VM). Panels B) and D) show the ITP and the HR during the implementation of premature ventricular contractions.

Table 5.1: Numbers and references used for the extended numerical model of the human blood circulation. The extrathoracic unstressed venous volume is a variable input, all other parameters are constant.

Parameter	Description	Value	Units	References
$V_{0sv,0,ei}(t)$	Extrathoracic unstressed venous volume	3088	mL	[97], [197]
$V_{0sv,0,it}$	Intrathoracic unstressed venous volume	162	mL	[97], [197]
$C_{sv,et}$	Extrathoracic venous system compliance	55	mL/mmHg	[191]
$C_{sv,it}$	Intrathoracic venous system compliance	10	mL/mmHg	[191]
H_{it}	Intrathoracic vena cava collapse gain coefficient	0.547	mmHg ² ·s/mL	[123]

5.3.7 Pump control configurations

Three different control configurations (C1 – C3) of a tVAD were tested, as described below. The input to the PRS controller was the simulated LVV signal; the output was the desired pump speed (Figure 5.4A).

1) Constant speed (C1)

For the C1 configuration, the PRS controller was disabled and the tVAD was operated at a constant speed. The speed was set to 4100 rpm, which yielded a CO of 5 L/min at rest.

2) Nominal PRS controller (C2)

For the C2 configuration, we used the PRS controller as presented in [65], i.e., with a sliding window (Figure 5.4B) of three seconds to extract the EDV value. The lower limit for the pump speed was set to 1800 rpm.

3) Modified PRS controller with beat-to-beat EDV detection algorithm (C3)

For the C3 configuration, we modified the signal-processing algorithm of the nominal PRS controller in order to extract the EDV value at every heartbeat. Figure 5.4C depicts the structure of the beat-to-beat EDV extraction algorithm. First, the simulated LVV signal is low-pass filtered with a second-order IIR filter with a cut-off frequency of 2.5 Hz. Second, the derivative of the signal is computed. When the derivative of the LVV signal changes sign, the LVV signal is at a maximum, which corresponds to the EDV. Due to the continuous flow of a tVAD, no isovolumetric contraction occurs and the LVV signal has one distinct maximum. Therefore, the zero detection of the LVV derivative works reliably *in vitro*. The PRS controller structure (Figure 5.4D) remained unchanged, as presented in [65].

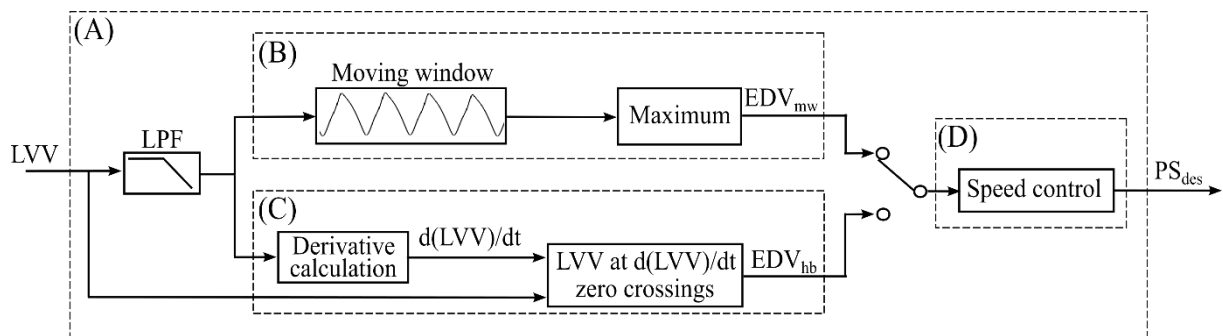


Figure 5.4: Structure of the PRS controller configurations of the tVAD (A). The left ventricular volume (LVV) is processed and the end-diastolic volume is extracted either from the maximum of a moving window (EDV_{mw}) (B) or at every heartbeat (EDV_{hb}) (C). The extracted EDV is fed to the preload responsive speed (PRS) controller algorithm, which computes the desired pump speed (PS_{des}). The detailed structure of (D) is presented in [65].

5.4 Results

Figure 5.5 shows the CO and the AoP of a physiological circulation during the VM (panels A and C) and four PVCs (panels B and D)). The four phases of VM and the four PVCs are separated by dashed lines. After the onset of VM (phase 1) and a sudden AoP increase due to the increase of the ITP, the AoP decreased and made a trough during phase 2, while the CO decreased from 5 L/min to 2.5 L/min. In phase 3, at the end of VM, the AoP dropped suddenly together with the ITP. AoP recovered and increased up to 160 mmHg. After a final oscillation, the AoP returned to its initial value. Accordingly, the CO increased up to approx. 7 L/min in phase 4 and then returned to 5 L/min.

During the PVCs, sudden CO drops can be observed, while the mean AoP decreased from 105 to 90 mmHg. After the last PVC both the CO and the AoP increased slightly above their initial values (end of phase 4) before they returned to their initial values ($t > 20$ s).

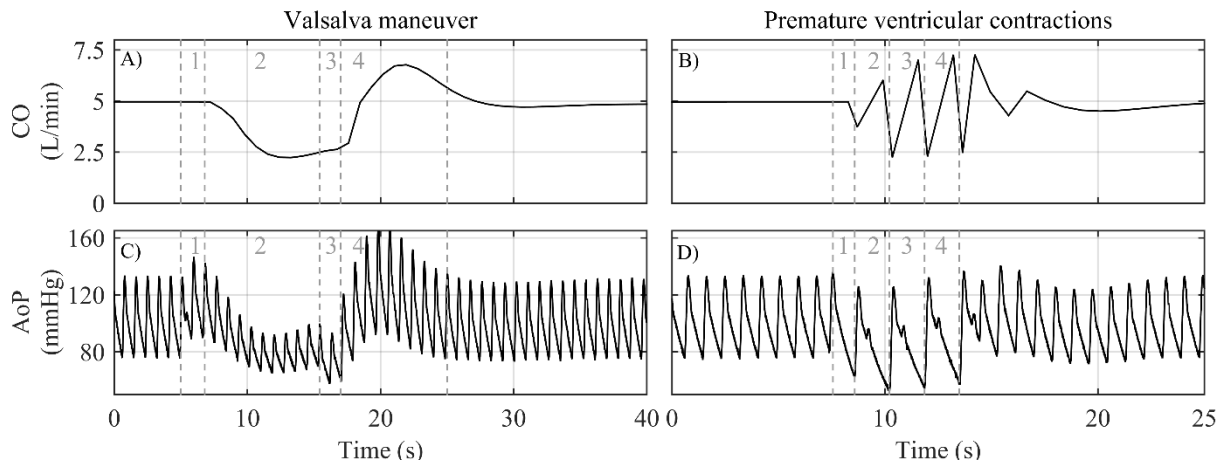


Figure 5.5: Cardiac output (CO) and aortic pressure (AoP) signals of a physiological circulation during the simulated Valsalva maneuver (VM) and premature ventricular contractions (PVCs). Dashed lines indicate the four phases of the VM and the four PVCs.

Figure 5.6 shows the effect of VM (left-hand side) and PVCs (right-hand side) on a pathological circulation assisted with a tVAD operated at a constant speed (C1). The figure shows the pump speed (PS) and flow (PF), the CO, the transmural pump inlet pressure (PIP) and the AoP. The PIP signal shows that suction (negative pressure) occurred during the VM. At the same time, the CO decreased and the AoP pulsatility was diminished. All signals recovered to the steady-state value after the end of the VM. During PVCs, all signals except the pump speed showed strong oscillations, but quickly returned to their steady-state values after the last PVC.

Figure 5.7 shows the effect of the VM and PVCs on a pathological circulation assisted with a tVAD controlled by the nominal PRS controller (C2). During the VM, due to the reduced LVV, the controller reduced the pump speed down to its minimum value of 1800 rpm at $t = 12$ s. The pump flow decreased as well and back flow occurred, while the CO decreased down to 1.5 L/min. The PIP signal shows that no suction occurred, while the mean AoP dropped down to approx. 60 mmHg. During PVCs, the PS slowly adapted to the decreased LVV resulted from the arrhythmic beats. After the end of PVCs, the increased LV feeling led to a PS increase until it returned to steady state. The mean PF, CO and AoP fluctuated according to the PS variations.

5.4 Results

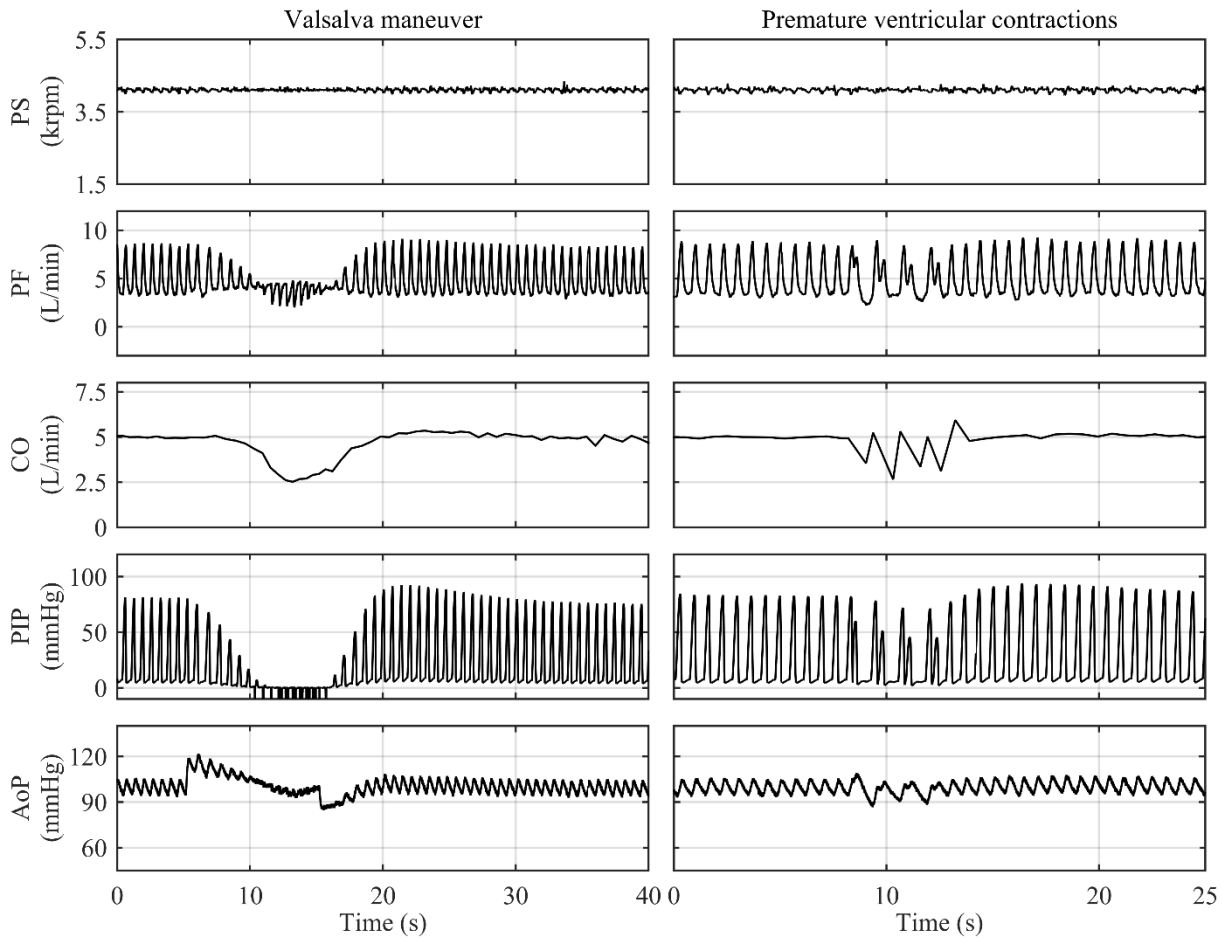


Figure 5.6: Performance of a pathological circulation assisted by a tVAD operated at a constant speed (C1) during the Valsalva maneuver (left-hand side panels) and premature ventricular contractions (right-hand side panels). PS: pump speed, PF: pump flow, CO: cardiac output, PIP: pump inlet pressure, AoP: aortic pressure.

Figure 5.8 shows the effect of the VM and PVCs on a pathological circulation assisted with a tVAD controlled by the modified PRS controller (C3). In this case, the PS adaptation during the VM led to a minimum value of approx. 2500 rpm at $t = 12$ s. The PF decreased as well, but now back flow occurred. The minimum CO observed is 2.5 L/min. The maximum PIP dropped down to approx. 60 mmHg and the mean AoP down to 80 mmHg. A further AoP drop down to 60 mmHg occurred after the end of VM. The PS adapted to the PVCs by decreasing the speed, whereas it increased during the normal contractions ($8 \text{ s} < t < 12.5 \text{ s}$). Pump flow, CO and AoP varied similarly to PS.

Figure 5.9 shows the performance of the EDV detection methods for the configurations C2 and C3 during the experiments. An LVV decrease occurred during the VM (Figure 5.9 – panels A) and C)). Clearly, the EDV detection algorithm of C2 shows a delayed detection during the LVV decrease compared to C3, which detected the EDV accurately at every beat. Panels B) and D) in Figure 5.9 show the irregular LVV waveform during the PVCs. The C3 configuration detected not only the EDV of the normal contraction but also the maximum volume during the premature ventricular contraction. Due to the three-second moving window, the C2 configuration did not capture the sudden EDV drops during PVCs.

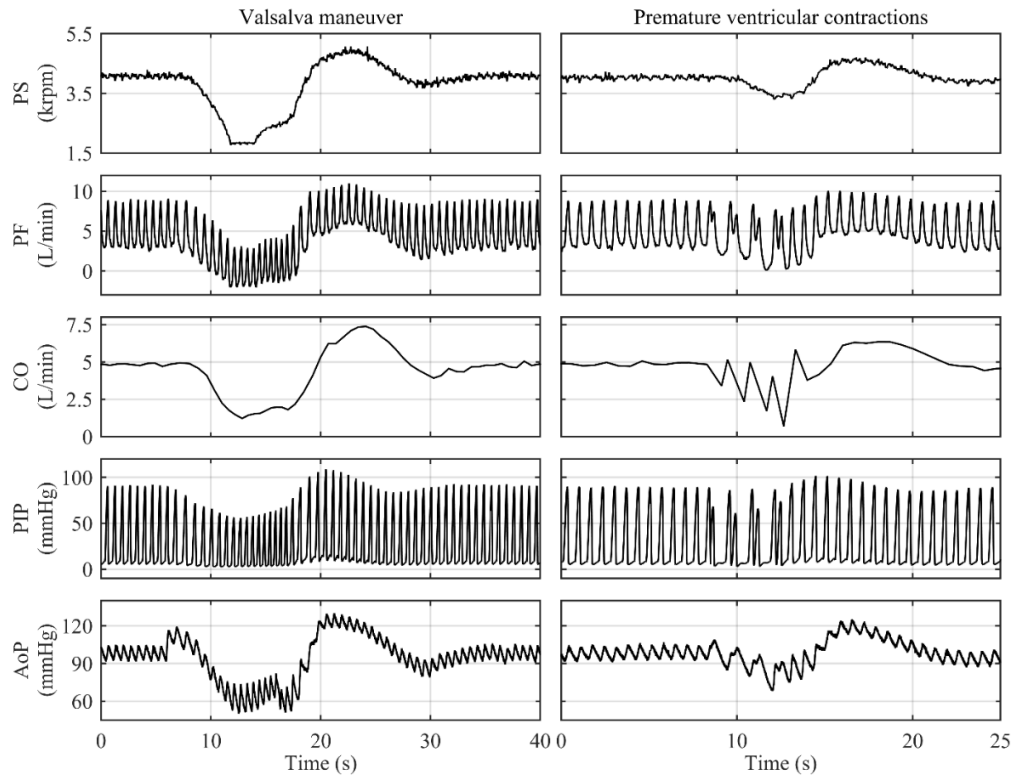


Figure 5.7: Performance of a pathological circulation assisted by a tVAD controlled by the nominal PRS controller (C2) during the Valsalva maneuver (left-hand side panels) and premature ventricular contractions (right-hand side panels). PS: pump speed, PF: pump flow, CO: cardiac output, PIP: pump inlet pressure, AoP: aortic pressure.

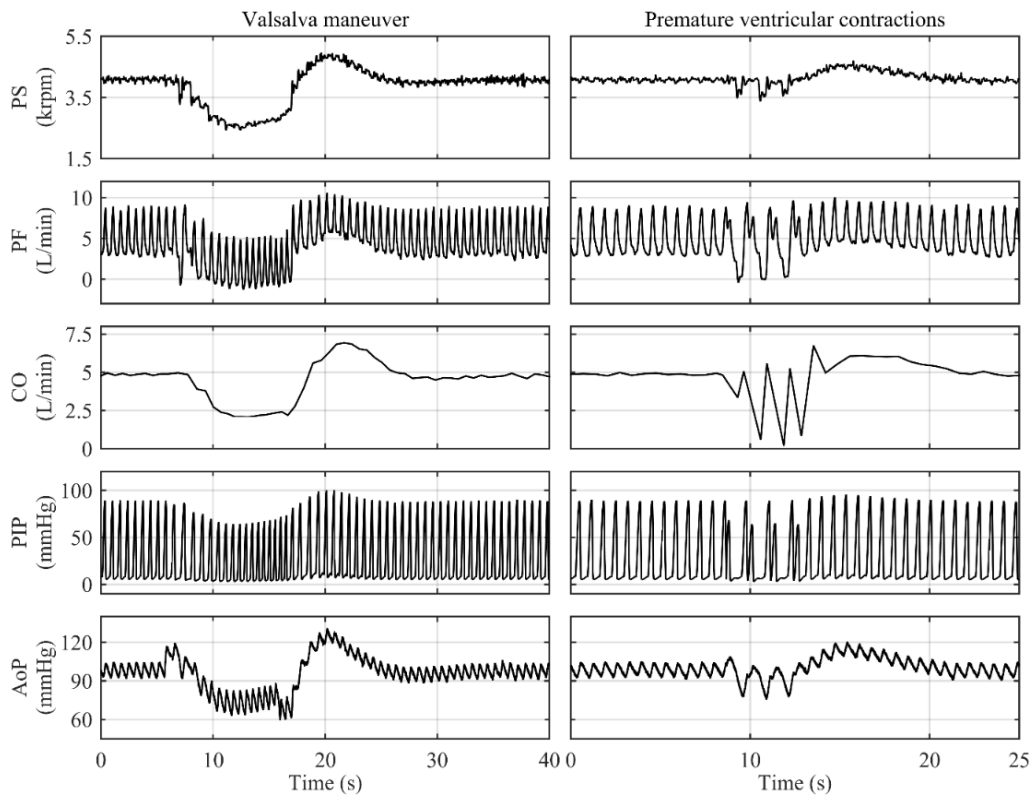


Figure 5.8: Performance of a pathological circulation assisted by a tVAD controlled by the modified PRS controller (C3) during the Valsalva maneuver (left-hand side panels) and premature ventricular contractions (right-hand side panels). PS: pump speed, PF: pump flow, CO: cardiac output, PIP: pump inlet pressure, AoP: aortic pressure.

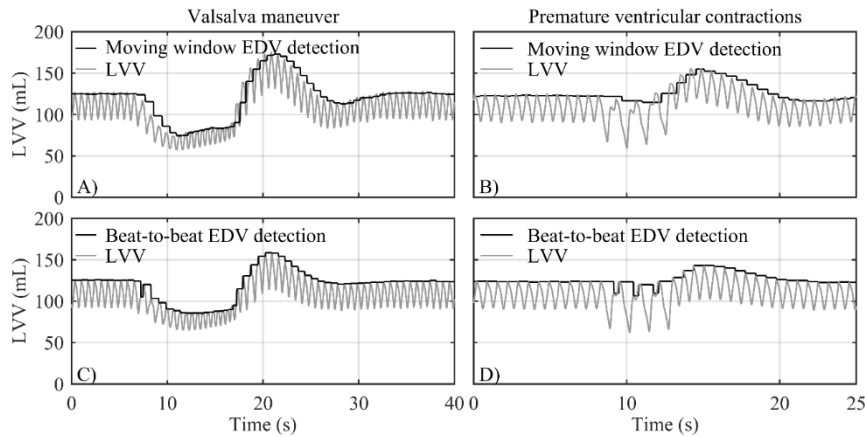


Figure 5.9: Comparison of two algorithms to extract the end-diastolic volume (EDV) from the left ventricular volume (LVV) signal during Valsalva maneuver (panels A) and C)) and premature ventricular contractions (panels B) and D)). Panels A) and B) show the performance of the three-second moving window extraction algorithm used in C2. Panels B) and D) show the performance of the beat-to-beat EDV extraction algorithm used in C3.

5.5 Discussion

In this study, we investigated special pathophysiological situations that can lead to sudden changes of the venous return and therefore, suction or LV overloading. We simulated the VM on our HMC by introducing a change in the ITP. We increased the ITP to 30 mmHg over 10 s, as it is reported from clinical experiments [193], [198], [199]. Such an ITP increase can also occur during daily strain conditions of the patients, such as bowel movement, heavy lifting, coughing and posture changes [196]. The observed AoP signals of the physiological heart matched well with those reported in studies about clinical experiments [193], [196]. The four phases of VM seen in clinical recordings of arterial blood pressure are identified (Figure 5.5).

In the failing circulation without tVAD, a square-wave AoP response would be expected during the VM due to the blood pooling in the congested pulmonary vascular system, i.e. due to sustained LV preload [193], [199]. This was not observed in our experiments with the controlled tVAD support, where the AoP waveform during the VM was similar to that observed in the physiological circulation. This was to be expected, because the pulmonary vascular system was not congested in this case.

PVCs were simulated as described in [90], where the simulated results were validated based on the MIT-BIH arrhythmia database [200]. The moving window method detected the gradual LVV decrease resulting from the consecutive PVCs (Figure 5.7), while the beat-to-beat method was able to capture the sudden LVV changes between the irregular beats (Figure 5.8). No suction occurred during PVCs with neither of the configurations C1, C2, or C3. The case of sustained tachycardia was not included in our experiments, because we focused on the detection of abrupt and temporary hemodynamics changes.

The goal of this study was to investigate whether a beat-to-beat extraction of the EDV is required for a clinical physiological controller, or if a simpler method with a moving window is sufficient. We used the PRS controller [55] as test controller. As it was developed in our group, we could faithfully configure and implement it. However, the results allow drawing conclusions for other physiological controllers, which rely on a certain feature that is extracted from the signal. The controllers presented in [61], [65], [69]–[71], [81], [143], [187] all use one of the two approaches investigated in the current study. Additionally, the presented numerical model can be a useful tool while tuning physiological controllers or defining their sampling rate, as such factors influence the aggressiveness of its response.

For our study, the lack of an implantable, long-term LV volume sensor is not addressed. We acknowledge the use of admittance catheters or sonomicrometry as a short-term, real time volume measurement for in vivo research studies, but these technologies are not suitable to be used in patients for long term. In the clinic, echocardiography or magnetic resonance imaging systems are normally used for the measurement of EDV, but they require computationally expensive post processing. In our group, we focus on the development of an implantable LV volume sensor that will be suitable for clinical applications.

The constant speed operation (C1) and the nominal PRS physiological controller (C2) were compared during the VM and the PVCs (Figure 5.6 and Figure 5.7). The C2 configuration led to a pump speed and flow

decrease during PVCs, which in turn decreased CO and AoP. After the end of the PVCs, a slight overshoot of all signals occurred due to the abrupt venous return recovery. This overshoot was absent in case of C1 and the CO and AoP changes resembled better the physiological ones (Figure 5.5). During the VM, the physiological controller (C2) was able to prevent suction, whereas suction is observed with the constant speed (C1). The pump speed and flow adaptation of C2 led to stronger reduction of the CO during the VM, which is more physiological, but leads to a critically low AoP. The AoP waveform during constant speed operation resembled more that of a pathological circulation as presented in [193], [199], where the overshoot is attenuated.

Two different methods for extracting the index of the PRS controller were evaluated (C2 and C3). Both configurations performed better than the constant speed operation (C1) with respect to suction prevention. C3 outperformed C2 due to its faster response resulting from the beat-to-beat detection. The moving window of C2 introduced a delay (Figure 5.9). Comparing signals during VM between Figure 5.7 and Figure 5.8, it is well visible that with C2 there was a greater drop in pump speed (lower speed limit was reached) than with C3. This lower speed resulted in turn in lower pump flow and CO. Backflow through the pump was higher with C2, thereby presumably increasing the probability for blood damage and thrombus formation due to blood recirculation and stagnation zones [201]. Furthermore, the lower pump flow with C2 led to lower AoP. Such low AoP may cause organ dysfunction and affect the quality of life of the patient. Thus, C2 led to less physiological hemodynamics compared to C3. With C1, the AoP sustained in physiological limits, but suction occurred. These outcomes show that the aggressiveness of a physiological controller may be hard to be identified when aiming to design an optimal controller. Additional algorithms to monitor parallel cases of e.g. suction, backflow, low AoP and adapt the response of the core physiological controller seems to be required for a better performance of a physiological controller.

During the PVCs with C3, the LVV dropped due to the additional contraction of the heart and the shortened diastolic phase. Thus, sudden speed changes occurred (Figure 5.8). Disturbances of the measured signal can lead to misdetection of the EDV with a beat-to-beat algorithm and therefore, undesirable speed changes. Furthermore, such an extraction algorithm is considered to be more complex thus increasing the sensitivity to measurement noise, the probability for wrong feature extraction and ultimately reducing the stability margins of the controller in a clinical implementation. On the other hand, a moving window algorithm is considered quite simple, robust and independent of the HR of the native heart. However, the lack of fast adaptation to short-time acute events can lead to momentarily high flows during premature contractions and intermittent suction events or strong maneuvers. Considering all these results, a trade-off is observed between a fast response, which can more likely prevent over- and underpumping, and a slower response, which is more robust. For a clinical implementation, robustness should be the major goal.

One direct impact of physiological control could be the avoidance of low-flow alarms, which occur frequently in clinical practice. They directly affect the workload of the clinical staff and thus increase treatment costs. Typical everyday activities like coughing, bowel movement, heavy lifting, sleep apnea or even deep breathing can affect ITP and lead to abrupt blood flow changes. With physiological control, the pump flow will be adapted to such activities and the risks of over- and underpumping events can be reduced drastically. The clinical routines for monitoring VAD-patients would need to be revised, as low-flows will, hopefully, not constitute such a critical condition for the patients any more. This can also contribute to reduce the psychological stress of the patients and thus improves their quality of life as well as the workload of the health care professionals. However, the development of a physiological controller that can achieve all this positive impact constitutes a multi-objective task. It seems that a very fast suction prevention may result to non-physiological hemodynamics, thus reducing the positive effect of a controller. Therefore, the statement that a physiological controller is superior to constant speed should be carefully stated and the comparison between them should be based on realistic, clinically frequent scenarios.

The development of a tVAD and its regulatory approval require extensive *in vivo* testing. Because these tests are expensive and ethically problematic, it is very important to gain as much knowledge as possible from *in vitro* tests. Therefore, it is important to test physiological controllers against all possible pathophysiological events that may occur and thereby influence the performance of the controller. With our extended numerical model of the human blood circulation, we propose an additional tool for testing physiological controllers that can contribute to boost the trust in *in vitro* testing and reduce the amount of required *in vivo* trials.

6 Comparison of LVAD Flow Estimators (Paper V)

6.1 Abstract

Various approaches for estimating the flow rate of a rotary blood pump have been proposed for monitoring and control purposes. They have been evaluated under different test conditions and, therefore, a direct comparison between them is difficult. Furthermore, a limited performance has been reported for the areas where the pump flow and motor current present a non-monotonic relationship. In this regard, we selected most approaches that have been presented in literature and added a modified one, resulting in four estimators which are either non-invasive or invasive, i.e., inlet and outlet pump pressure sensors are used. Data from in-vitro and in-vivo studies with the Deltastream pump DP2 were used to compare the estimators under the same test conditions. These data included both constant and varying pre- and afterload, contractility, viscosity, as well as pump speed settings. Bland-Altman plots were used to evaluate the performance of the estimators. The mean error of the overall estimated flow in-vitro ranged from 0.002 to 0.38 L/min and the limits of agreement (LoA) between ± 2 L/min. During negative flows the mean error decreased by about 25% when the pump inlet pressure as an input was added. In vivo, the mean errors increased, while the LoA remained in the same range. An estimator based on pump pressure difference improves the reliability in areas where flow and current relationship is not monotonic. A trade-off between estimation accuracy and number of sensors was identified. The estimation objective and the potential errors should be considered when selecting an estimation approach and designing the pump systems.

6.2 Introduction

The continuous monitoring of the circulation during ventricular assist device (VAD) therapy is considered as very crucial for detecting critical conditions, such as ventricular suction, to allow their prevention or release. Several monitoring techniques have been developed and investigated, which can be divided into invasive and non-invasive techniques. Most of them use one or more of the following signals: pump speed, current, flow, pump inlet and outlet pressure, and left ventricular volume. The first two can be measured directly by the device. Pump speed has been proposed for detecting suction [70], whereas sudden increases in pump current are associated with pump thromboembolic events [202]. Pressure and volume signals require implantable sensors. Several recent studies have focused on the development of implantable and long-term pressure sensors [59],[89], which, however, have not been integrated into the VAD system as yet. Long-term volume sensors are still on a conceptual phase [60]. Thus, a pump flow estimator, which provides reliable hemodynamic information is considered of great importance and may improve the VAD therapy.

The development of a reliable pump flow estimator has been addressed by several groups who conducted in-silico, in-vitro, and in-vivo validation experiments. As early as 1997, Tsukiya et al. [42] investigated the use of pump-intrinsic signals to develop an estimator that uses a static model. The model-based approach was also followed by Kitamura et al. [203] and Granegger et al. [44], who used a model of the brushless direct-current (BLDC) motor that included the dynamic properties of the pump. In the latter study, the authors developed an estimator that outperforms the one clinically used by the HVAD with respect to bandwidth, and their estimation error reported was the smallest thus far. Particularly, that estimator can accurately estimate flow at increased frequencies, which is desirable for several monitoring algorithms, such as when the dynamics of a recovering ventricle have to be monitored. Based on such analytical approaches, Lim et al. [204] performed a dimensional analysis to exploit theoretical principles of fluid mechanics to obtain insights into the relationships among the pump flow, speed, power, differential pressure and the fluid viscosity. In contrast, a group of researchers [45]–[48] used autoregressive exogenous (ARX) models to derive the relationship between pump intrinsic signals and flow to estimate pump flow. Notably, Giridharan et al. [49] developed an Extended Kalman Filter (EKF) based on a method with so-called soft sensors to estimate flow rate and head pressure. Furthermore, in two of the studies mentioned above [44], the blood viscosity was added as an input, as viscosity variations that are not captured affect the performance of the estimators.

6.3 Materials and Methods

All these studies were conducted with various VADs, using different testing environments (in vitro, in vivo) and experiments, while numerous metrics have been used to report the performance of the estimators. While AlOmari et al. [205] summarized most of those studies and their final results, the diversity of the studies did not allow a direct comparison of the various approaches proposed. While most of the estimators have provided good results in silico and in vitro, few have been evaluated in vivo. Furthermore, most studies reported results during steady-state conditions, and only few studies presented varying physiological requirements conditions by varying the pump speed and the viscosity of the circulation [206], [207]. The pump speed was also constant, while current clinical devices, such as the HeartMate 3 (Abbott Laboratories Inc., Chicago, IL, USA), have started to incorporate algorithms that apply speed variations [208]. To the best of our knowledge, no flow estimator has been successfully tested in vivo and under varying physiological requirements and speed settings.

The aim of the current study is to collect most concepts for pump flow estimation that have been presented and to evaluate them: 1) using the same device and testing environment, in vitro and in vivo, and 2) under various conditions, with experiments that include varying physiological requirements and pump speed control modes. The influence of varying physiological requirements, pump speed, and viscosity on the error of the output of the estimator was investigated. The evaluation and comparison focused on different indices of the flow signal as well as on the whole waveform, based on mean absolute error (MAE) values and Bland-Altman plots. Furthermore, we investigated the hypothesis that, in addition to pump-intrinsic signals, using the pump inlet pressure or both inlet and outlet pressures as input signals for estimator approaches, the estimation error can be decreased efficiently.

6.3 Materials and Methods

In the current study, four different approaches for estimating pump flow were evaluated. Figure 6.1 depicts an overview of their structures. Estimators 1 and 2 are non-invasive and have been developed earlier [44], [49]. Estimator 3 constitutes a modification of existing estimators [44],[203], such that the signal of the pump inlet pressure is exploited, which turns it into an invasive flow estimator. Estimator 4 uses both inlet and outlet pressures as inputs.

6.3.1 Pump flow estimators

Estimator 1: BLDC model-based approach [44]

In this approach, a first-order dynamic model of a BLDC motor was used to develop a non-invasive flow estimator. The inputs were the pump-intrinsic signals, i.e., pump current and speed. Figure 6.1A summarizes the structure of the estimator, which is described by equation (6.1):

$$M(\omega(t)) \frac{d\omega(t)}{dt} = T(t) - a_1 Q(t)\omega(t) - a_2 \omega(t) - a_3 \omega(t)^2 \quad (6.1)$$

where $Q(t)$ is the pump flow rate, a_1 , a_2 , a_3 represent the static coefficients, $M(\omega(t))$ corresponds to the dynamic coefficient, while $T(t)$ and $\omega(t)$ represent the mechanical torque and the motor speed, respectively. The mechanical torque $T(t)$ is proportional to the motor current $I(t)$ multiplied by the constant (k_T), i.e., $T(t) = k_T \cdot I(t)$, where $k_T = 13 \times 10^{-3} \text{Nm A}^{-1}$ for the Deltastream DP2 (Xenios AG, Heilbronn, Germany). The coefficients a_1 , a_2 , a_3 , and $M(\omega(t))$ have a physical meaning and must be identified for every different type of rotary pump and for the different viscosities. The coefficient $M(\omega(t))$ also depends on the pump speed. Their values and the method to assess them are presented in the paragraph *Dataset for parameter identification*.

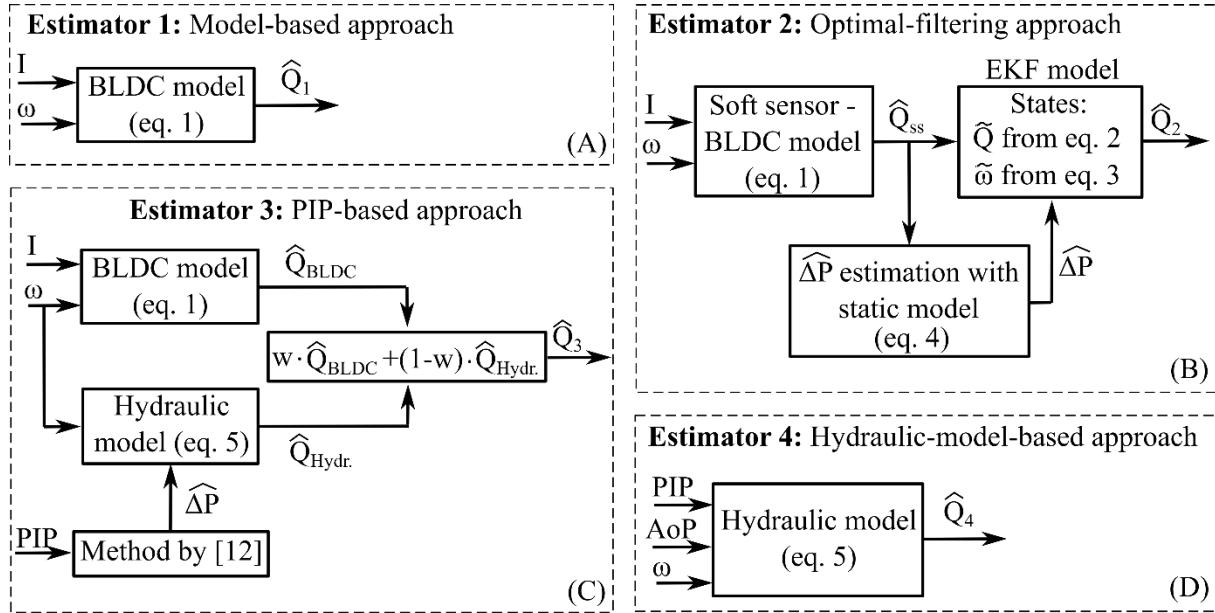


Figure 6.1: Schematic representation of the four estimators evaluated. The respective inputs, outputs, and equations used are depicted. For Estimator 3, the pump inlet pressure (PIP) is used to derive an estimate of the pump pressure difference ($\hat{\Delta P}$) based on [95]. For Estimator 4, the aortic pressure (AoP) is considered to be measured. ω , pump speed; I , pump current; \hat{Q} , estimated pump flow; ss, soft sensor; BLDC, brushless direct current; eq., equation; w , weight factor.

Estimator 2: Optimal filtering approach [49]

Giridharan et al. [49] used an Extended Kalman Filter (EKF) to estimate the pump flow as well as the pump head pressure. Two states were used, the pump flow $\tilde{Q}(t)$ and the pump speed $\tilde{\omega}(t)$. The process model consisted of two first-order differential equations (Equations 6.2 and 6.3) which were adjusted to the Deltastream DP2 blood pump used:

$$\frac{d\tilde{Q}(t)}{dt} = \frac{1}{F} (-\hat{\Delta P}(t) + f_1 \tilde{\omega}(t)^2 - f_2 \tilde{Q}(t) - f_3 \tilde{Q}(t)^2) \quad (6.2)$$

$$\frac{d\tilde{\omega}(t)}{dt} = \frac{1}{J(\tilde{\omega}(t))} (k_T I(t) - g_1(\tilde{\omega}(t)) + g_2 \tilde{\omega}(t) - g_3 \tilde{\omega}(t)^2 - g_4 \tilde{Q}(t) \tilde{\omega}(t)) \quad (6.3)$$

where $f_1, f_2, f_3, k_T, g_1(\tilde{\omega}(t)), g_2, g_3, g_4$ are static coefficients, F and $J(\tilde{\omega}(t))$ are dynamic coefficients, and $\hat{\Delta P}$ is the estimated pump pressure head derived from equation (6.4):

$$\hat{\Delta P}(t) = \begin{cases} h_{1\omega} \omega(t)^2 - h_{2h} \hat{Q}(t)^2 - h_{3h} \hat{Q}(t) & \text{if } \hat{Q}(t) \geq 0 \\ h_{1\omega} \omega(t)^2 - h_{2l} \omega(t)^2 \hat{Q}(t)^2 - h_{3l} \hat{Q}(t) & \text{if } \hat{Q}(t) < 0 \end{cases}, \quad (6.4)$$

where $\omega(t)$ is the measured pump speed and $\hat{Q}(t)$ is the estimated pump flow derived from Equation (1). The $h_{1\omega}, h_{2h}, h_{2l}, h_{3h}$ and h_{3l} are static coefficients. Although the piecewise function described in Equation (4) is continuous, it is not differentiable at the switching point $Q(t) = 0$. Also, it is not defined for the motionless state, where the Deltastream DP2 speed is zero, corresponding to $\omega(t) = 0$, and when the flow is negative. The head pressure $\hat{\Delta P}$ was used as an input of the EKF, together with the estimated pump flow \hat{Q} . Figure 1B illustrates the structure of the EKF. The values of the parameters of the EKF and the method to obtain them are presented in the paragraph *Dataset for parameter identification*.

Estimator 3: Pump inlet pressure (PIP) based approach

The Estimator 3 represents a modification of Estimator 1. Estimator 1 uses the BLDC model, which relies on the strictly monotone relationship between pump flow and current. This relationship depends on the specific pump design. In our study, it presents a non-monotonic behaviour for flows below 0 L/min, which constitutes a drawback of this approach. Figure 6.2 depicts this relationship for various pump speeds. To investigate the potential of a pump inlet pressure measurement to account for this deficiency of Estimator 1, an invasive approach was developed. This approach combines the BLDC model with a hydraulic model of the pump derived by modifying equation (6.4) by adding the dynamic coefficient L and thus yields the piecewise function of Equation (6.5):

$$\tilde{Q}(t) = \begin{cases} \frac{h_{3h} + \frac{L}{\Delta t} - \sqrt{\left(h_{3h} + \frac{L}{\Delta t}\right)^2 + 4 \cdot h_{2h} \cdot \left(h_1 \cdot \omega(t)^2 - \Delta P(t) + \frac{L}{\Delta t} Q(t - \Delta t)\right)}}{-2 \cdot h_{2h}} & \text{if } \Delta P(t) < h_1 \cdot \omega(t)^2 + \frac{L}{\Delta t} Q(t - \Delta t) \\ \frac{h_{3l} + \frac{L}{\Delta t} - \sqrt{\left(h_{3l} + \frac{L}{\Delta t}\right)^2 + 4 \cdot h_{2l} \cdot \omega(t)^2 \cdot \left(h_1 \cdot \omega(t)^2 - \Delta P(t) + \frac{L}{\Delta t} Q(t - \Delta t)\right)}}{-2 \cdot h_{2l} \cdot \omega(t)^2} & \text{if } \Delta P(t) \geq h_1 \cdot \omega(t)^2 + \frac{L}{\Delta t} Q(t - \Delta t) \end{cases}, \quad (6.5)$$

To combine the BLDC and the hydraulic model, a weighting factor was defined and kept constant at $w = 0.8$ for all other in-vitro and in-vivo experiments. The weighting factor was assessed experimentally by using only identification data. It showed that this value is a good compromise between the BLDC model, that has a weak behavior for negative flows, and the hydraulic model, that is adversely affected by not exactly knowing the aortic pressure.

Estimator 3 requires the measured value of the head pressure ΔP . However, our hypothesis included only the pump inlet pressure sensor, as it constitutes the minimum requirement for realizing physiological control techniques and enabling a continuous monitoring of the LV. To obtain the value of ΔP , while measuring the pump inlet pressure, a method developed and evaluated earlier [95] was used to estimate the aortic pressure (AoP). Based on that method, the mean AoP is extracted when the aortic valve opens. The pump inlet pressure was subtracted from this value to derive a surrogate value of the real ΔP . If the aortic valve was closed, Estimator 1 was used. The valve had higher probability to open during low flows. An approach to detect the aortic valve opening based on pump inlet pressure has been proposed in literature [95] but in this study, the measured aortic valve flow was used.

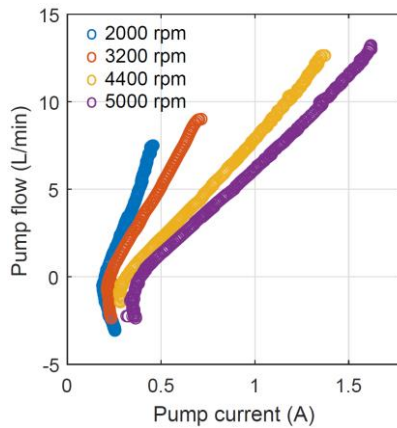


Figure 6.2: Relationship of the flow versus current of the Deltastream DP2 pump for various pump speeds. Data were collected on the hybrid mock circulation [97].

Estimator 4: Hydraulic model

The Estimator 4 was purely model-based, using the hydraulic model of the Deltastream DP2 (Equation (6.5)). Thus, the current-flow relationship does not influence the estimation. A similar approach had been investigated by Pennings et al. [209], but without including the dynamic part of the hydraulic model. In our case, the pump inlet and outlet pressures were assumed to be measured and the flow was estimated by Equation (6.5).

6.3.2 Hybrid mock circulation

The in-vitro experiments for parameter identification and evaluation of the estimators were conducted on a hybrid mock circulation (HMC) developed earlier in our group based on the hardware-in-the-loop (HIL) concept [97]. The HMC used has been extended to accurately mimic different viscosities [92]. It uses an existing numerical model of the human blood circulation [156], which can interact with a physical left VAD (LVAD) through a hydraulic interface that consists of two pressure reservoirs. Instead of a clinical LVAD, we used a non-implantable mixed-flow turbodynamic blood pump, the Deltastream DP2, which was modified to be controlled as desired. More details about the principle of operation of the HMC and the viscosity control is provided within the supplementary material.

6.3.3 Dataset for parameter identification

A set of static and dynamic experiments were conducted in vitro to generate training data for the identification of the coefficients of the flow estimators. For the static experiments, the pump pressure difference over pump flow (HQ) curves were derived at speeds ranging from 1,500 rpm to 6,000 rpm with steps of 500 rpm. Those experiments were conducted at a fixed, controlled viscosity of 3 mPa·s, which corresponds to an HCT value of approximately 31% [92]. The dynamic experiments included the implementation of a chirp signal for the outlet pressure, while keeping the pump inlet pressure at 0 mmHg and the pump speed constant at the values used for the static experiments. The amplitude of the chirp signals varied to cover all areas of the HQ curve, while its frequencies varied from 0.1 to 20 Hz. Based on those experiments (Table 6.1, Dataset A), the static and dynamic coefficients of the estimators were identified using a Nelder-Mead simplex algorithm to find the optimal parameters. Table 6.2 lists the values identified for all parameters used in Equations (1)-(6). A linear interpolation was applied for any coefficients depending on the pump speed.

Table 6.1: Overview of the in-vitro and in-vivo datasets used for parameter identification and validation. The head pressure (ΔP) was varied to derive the data for identifying static and dynamic coefficients of the estimators. The multi-objective controller includes a combination of a physiological controller, an aortic valve opening controller, and a pulsatile speed modulation [95].

Dataset	Environment	Variations	Controller	Purpose	Ref.
A	In vitro	Pressure head ramp (static), Chirp signal for ΔP (dynamic, 0.1 to 20Hz)	Constant speed (1,500 rpm to 6,000 rpm with steps of 500 rpm)	Parameter identification	–
B	In vitro	a) Preload b) Afterload c) Contractility d) Exercise	Constant speed (to achieve 5 L/min at the initial steady-state conditions)	Validation	[63]
C	In vitro	a) Preload b) Afterload c) Contractility	Physiological controller	Validation	[63]

d) Exercise					
D	In vitro	a) Preload b) Afterload c) Contractility d) Exercise	Multi-objective controller	Validation	[95]
E	In vivo w/ constant viscosity	a) Preload b) Afterload	Constant speed & Physiological controller	Validation	[146]
F	In vivo w/ varying viscosity	a) Preload b) Afterload	Constant speed & Physiological controller	Validation	[146]

In-vitro dataset

The validation experiments were conducted earlier at the HMC in two different studies of our group [63],[95], and under various physiological conditions. For both studies, a pathological circulation with a decreased contractility (30% ejection fraction) was mimicked, as proposed by Colacino et al. [156] The experiments included: variations of a) preload, b) afterload, c) contractility and d) a combination of a), b), and c) to mimic exercise conditions. For this purpose, the parameters of unstressed venous volume, systemic vascular resistance, contractility and heart rate were adjusted. We used the signals recorded while operating the pump a) at a constant speed (CS), b) using the systolic pressure (SP) physiological controller [78], or c) using a multi-objective control (MOC) system [95], which combines a physiological controller and an aortic-valve-opening controller with a pulsatile speed modulation. Table 6.1, Datasets B, C, and D summarize all in-vitro experiments used for evaluating the estimators. Further details about the in-vitro experimental setting, the exact hemodynamic values applied, and the physiological controllers used can be found in the supplementary material.

Table 6.2: Static and dynamic parameters identified based on static and dynamic experiments (Table 6.1, Dataset A).

Est.	Static coefficients	Dynamic coefficients	Other parameters
1) BLDC	a_1	M	-
	$= 2.822 \cdot 10^{-7} \frac{\text{Nm}}{\frac{\text{L}}{\text{min}} \text{rpm}}$,	$= \begin{bmatrix} \text{rpm} & \frac{\text{Nm}}{\text{rpm/s}} \cdot 10^{-6} \\ 2000 & -1.626 \\ 2500 & -1.589 \\ 3000 & -1.625 \\ 3500 & -1.660 \\ 4000 & -1.709 \\ 4500 & -1.718 \\ 5000 & -1.746 \\ 5500 & -1.828 \\ 6000 & -1.891 \end{bmatrix}$	
	$a_2 = 6.929 \cdot 10^{-7} \frac{\text{Nm}}{\text{rpm}}$,		
	$a_3 = 9.293 \cdot 10^{-11} \frac{\text{Nm}}{\text{rpm}^2}$		

2) EKF	$f_1 = 6.572 \cdot 10^{-6} \frac{\text{mmHg}}{\text{rpm}^2},$ $f_2 = 2.071 \frac{\text{mmHg}}{\text{L}/\text{min}},$ $f_3 = 1.043 \frac{\text{mmHg}}{(\text{L}/\text{min})^2},$ $g_1 = \begin{bmatrix} \text{rpm} & \text{Nm} \cdot 10^{-3} \\ 2000 & 3.563 \\ 3000 & 3.447 \\ 4000 & 3.480 \\ 5000 & 3.317 \\ 6000 & 3.264 \end{bmatrix},$ $g_2 = 1.087 \cdot 10^{-6} \frac{\text{Nm}}{\text{rpm}},$ $g_3 = 3.280 \cdot 10^{-10} \frac{\text{Nm}}{\text{rpm}^2},$ $g_4 = 2.629 \cdot 10^{-7} \frac{\text{Nm}}{\frac{\text{L}}{\text{min}} \text{rpm}}$	$F = 0.8596 \frac{\text{mmHg}}{\frac{\text{L}}{\text{min}}/s}$ $J = \begin{bmatrix} \text{rpm} & \frac{\text{Nm}}{\text{rpm}/s} \cdot 10^{-6} \\ 2000 & 1.444 \\ 3000 & 1.498 \\ 4000 & 1.560 \\ 5000 & 1.615 \\ 6000 & 1.723 \end{bmatrix}$	Filter settings: $R = \begin{bmatrix} 10^{-4} & 0 \\ 0 & 0.49 \end{bmatrix},$ $Q = \begin{bmatrix} 25 \cdot 10^{-4} & 0 \\ 0 & 22 \cdot 10^{-5} \end{bmatrix},$ $P = \begin{bmatrix} 9 \cdot 10^{-8} & 0 \\ 0 & 40 \end{bmatrix}$
3) PIPB	$h_1 = 5.809 \cdot 10^{-6} \frac{\text{mmHg}}{\text{rpm}^2},$ $h_{2h} = 0.703 \frac{\text{mmHg}}{(\text{L}/\text{min})^2},$ $h_{3h} = 1.791 \frac{\text{mmHg}}{\text{L}/\text{min}},$ $h_{2l} = -4.324 \cdot 10^{-7} \frac{\text{mmHg}}{(\text{L}/\text{min})^2 \text{rpm}^2},$ $h_{3l} = 4.570 \frac{\text{mmHg}}{\text{L}/\text{min}}$	$L = 0.6084 \frac{\text{mmHg}}{\frac{\text{L}}{\text{min}}/s}$	-

BLDC, brushless direct current; EKF, Extended Kalman Filter; PIPB, Pump-inlet pressure-based; R, measurement noise covariance matrix; Q, process noise covariance matrix; P, initial state estimation covariance matrix

In-vivo dataset

A dataset obtained from acute in-vivo experiments [146] was also used for the evaluation of the flow estimators, where the ground truth for the pump flow was available. The experiments had been conducted earlier with pig models and approved by the Cantonal Veterinary Office of Zurich Switzerland under the license number 152/2013. Their purpose was for the evaluation of two physiological controllers and the comparison of their performance with the CS operation [146]. During those experiments, the Deltastream DP2 pump had served as an LVAD, while the same flow probe from the HMC was used to measure the pump flow after being recalibrated with pig blood. The protocol and the equipment of those series of acute experiments are described in detail by Ochsner et al. [146] In summary, the SP, the preload responsive-speed (PRS) controller, and the CS operation were evaluated during pre- and afterload experiments. For the preload experiments, 500 mL of blood were drained and returned to the circulation of the animal using a heart-lung machine. For the afterload experiments, an occlusive balloon catheter was fully inflated, which was placed at the abdominal aorta of the animal. Before the onset of the manipulations, a speed ramp experiment was

6.4 Results

conducted. More information regarding the in-vivo experimental setting, the instrumentation and the PRS controller can be found in the supplementary material.

We used data recorded from one animal of the study [146], which included the pump-intrinsic signals, the pump inlet cannula pressure, and the measured flow to evaluate the estimators. These signals were recorded at 500 Hz. No aortic pressure measurement was available and, therefore, Estimator 4 was excluded from the in-vivo evaluation. Finally, a sum of approximately 8,600 heartbeats were used, 50% of which corresponded to preload variation experiments, 25% to afterload variation experiments, and 25% to speed ramps and rest conditions. As no continuous viscosity was recorded, the first speed ramp experiment was used to identify the pump flow-current relationship used by Estimators 1-2. Monitoring this relationship, we observed that after the first 30% of the heartbeats, a viscosity change occurred due to the fluid changes induced to conduct preload variations. Thus, the in-vivo data were divided such that the influence of HCT changes on the performance of the estimators could be investigated separately. For Estimators 1-3 evaluated in vivo, the same parameters as for the in-vitro evaluation were used. In Table 1, Datasets E and F summarize all in-vivo experiments used for evaluating the estimators.

6.4 Results

In-vitro evaluation

Figure 6.3 depicts the MAE obtained with each estimator over all the experiments included in Datasets B-D (Table 6.1). Estimator 1 presented a performance similar to that of Estimator 3, and when the pump was controlled at a CS or with the SP controller, the MAE values were below 0.6 L/min. With the MOC, the MAE of Estimators 1 and 3 ranged between 0.6 L/min and 1 L/min. In this case, Estimator 4 performed best with an MAE of around 0.5 L/min. However, during the other modes of pump control, the MAE was higher by 0.1-0.3 L/min. The MAE of Estimator 2 was above 0.6 L/min for almost all the experiments.

Figure 6.4 shows the performance of each estimator per sample, during the experiments of Datasets B-D, when estimating the whole pump flow signal, the mean flow, and the flow pulsatility, i.e., the difference between maximum and minimum flows. Using Bland-Altman plots, the mean error (red lines and text), as well as the LoA (yellow lines and text) obtained are presented. Estimator 2 yielded the least mean error when the overall flow was estimated and the LoA reached up to ± 2.03 L/min. Estimators 1 and 3 had slightly increased mean errors, but the LoAs were lower and approximately ± 1.3 L/min. Estimator 4 yielded an even higher mean error of 0.38 L/min, while the LoA equaled 1.65 L/min and -0.88 L/min. Similar trends in the performance of the estimators were observed among the estimators when the mean pump flow was estimated, with Estimator 2 showing the least mean error. In contrast, when the flow pulsatility was estimated, Estimators 2 and 4 showed the worst performance. The flow pulsatility was estimated best by Estimators 1 and 3 with a mean error of -0.13 L/min and -0.2 L/min, respectively.

Figure 6.5 shows the performance of the estimators when they are estimating negative flows. In this case, Estimator 4 yielded the best performance with a mean error of 0.41 L/min, a low LoA of -0.24 L/min and a high LoA of 1.06. Estimator 3 followed with a mean error of -0.65 L/min as well as a high and low LoA of 0.31 and -1.61 L/min, respectively, which were approximately 20%-30% lower than the results furnished by Estimator 1, except for the upper LoA, which was higher. Estimator 2 presented the worst performance during negative flows.

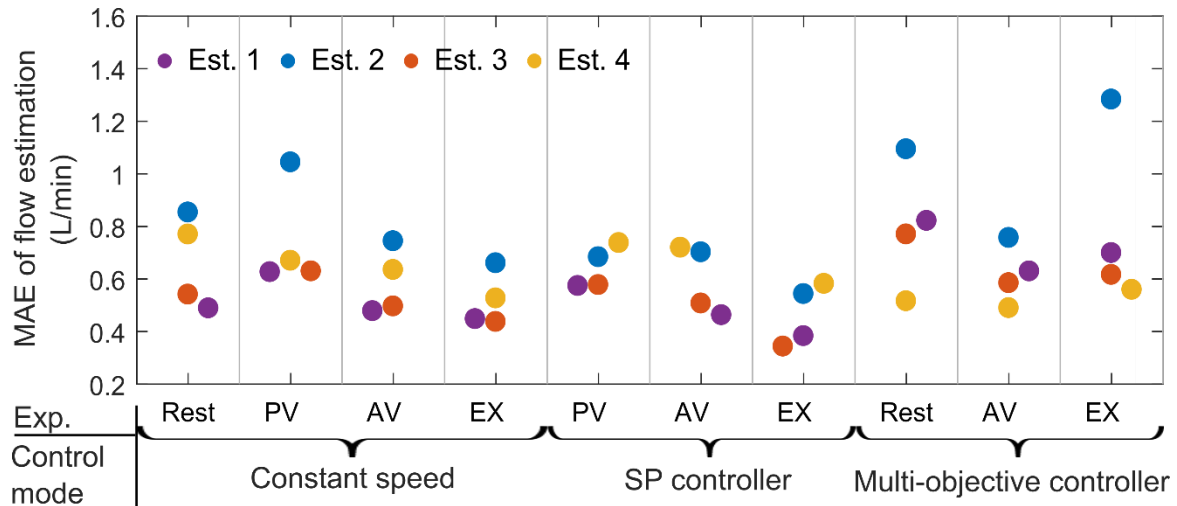


Figure 6.3: Mean absolute errors (MAE) of all the estimators with in-vitro experiments and Datasets B-D. The MAE for each experiment, i.e., preload variation (PV), afterload variation (AV), exercise (EX), and Rest (steady-state conditions) are presented, as well as the control mode of the pump speed for each experiment. SP: systolic pressure.

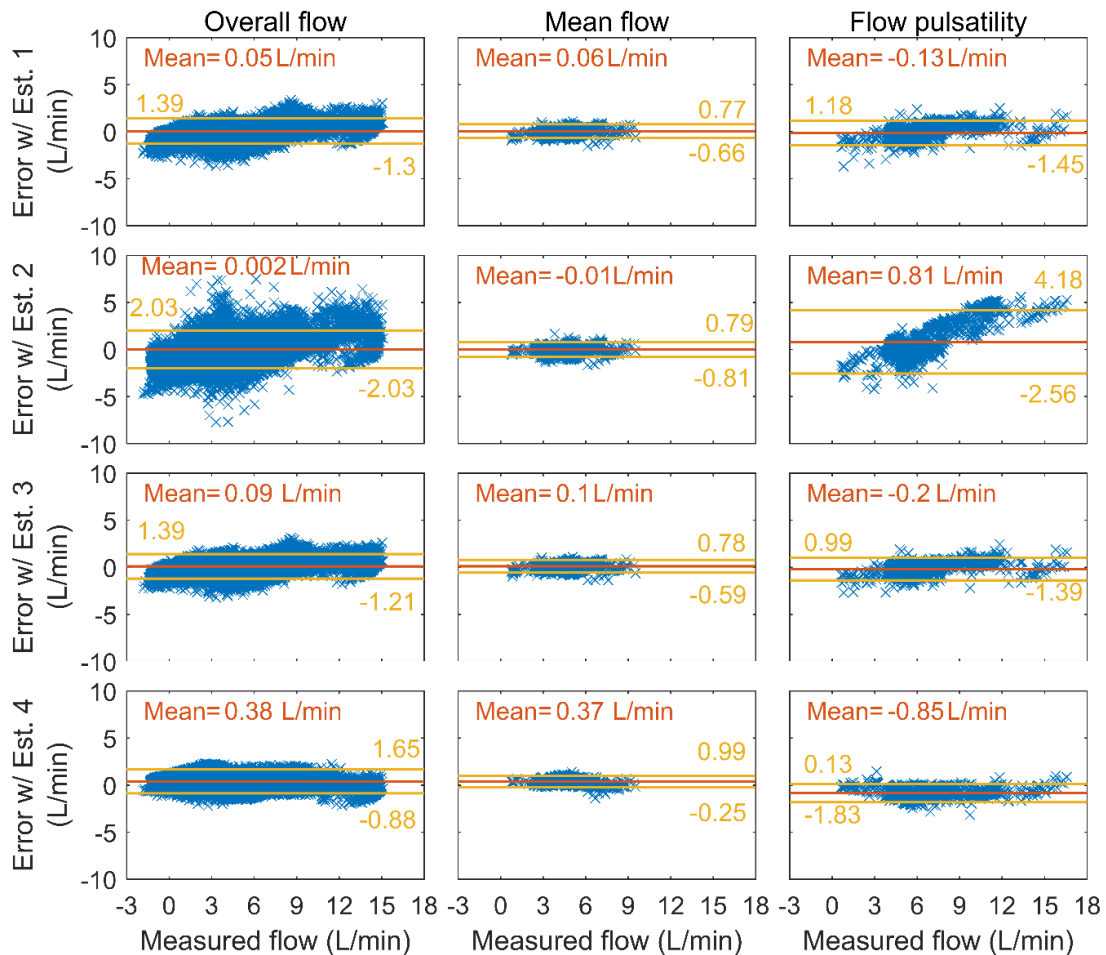


Figure 6.4: Bland-Altman plots for all in-vitro experiments with Estimators 1-4 when the whole flow signal (overall flow), the mean flow, and the flow pulsatility (maximum–minimum) were estimated. The mean values of the estimated error are depicted in red, while the limits of agreements ($mean \pm 1.96 \cdot standard\ deviation$) are depicted in yellow in L/min.

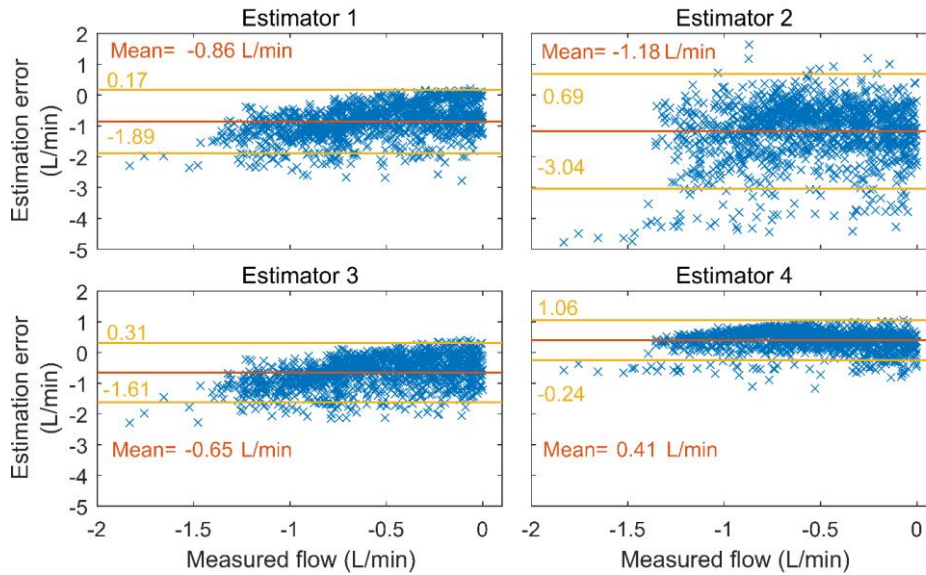


Figure 6.5: Bland-Altman plots for all in-vitro experiments with Estimators 1-4 when the negative flows were estimated. The mean values of the estimated error are depicted in red, while the limits of agreements ($mean \pm 1.96 \cdot standard\ deviation$) are depicted in yellow in L/min.

In-vivo performance

Figure 6.6 presents the performance of Estimators 1-3, during the experiments of Datasets E and F, when the whole pump flow signal, the mean flow, and the flow pulsatility were estimated. Estimator 3 yielded the least mean error when overall and mean flow were estimated, while the LoAs were similar to those of Estimators 1 and 2. When the overall flow was estimated, all estimators produced several errors that exceeded the calculated LoA. The quality of the recorded signals is considered a reason for this behavior. That was also the case during the estimation of the mean flow and of the values close to 0 L/min. Regarding the estimation of flow pulsatility, Estimator 2 yielded a lower mean error and LoA than Estimators 1 and 3.

Figure 6.7 illustrates an example of the influence that a change in viscosity can have on the estimation error. For this purpose, Estimator 1 was selected and evaluated on all the experiments of the pig model (Table 6.1 – Dataset F). The right plot of Figure 6.7 depicts the two different curves that were observed during all experiments for a speed of approximately 3,000 rpm. The shift from the blue to the red curve indicates a decrease in blood viscosity. The indices of mean flow and flow pulsatility are calculated based on the Bland-Altman approach. In this case, the mean error of the mean flow is more than doubled compared to the error shown in Figure 6.6, while the LoAs have also increased. In contrast, the estimation error for the pump flow pulsatility did not differ much from the result shown in Figure 6.6. The viscosity changes affect the performance of Estimator 2 and 3 in the same way and increase their estimation error.

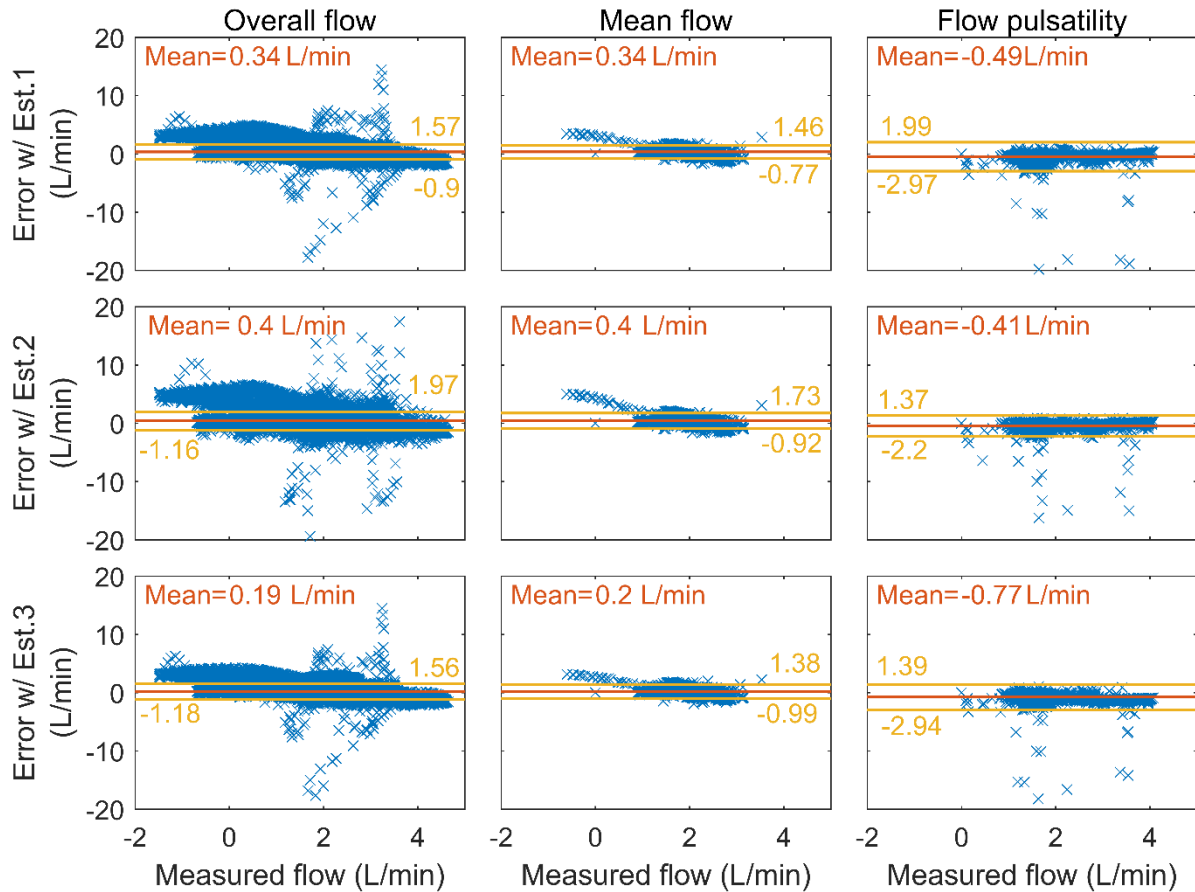


Figure 6.6: Bland-Altman plots for all in-vivo experiments at the same viscosity with Estimators 1-3 when estimating the whole flow signal (overall flow), the mean flow, and the flow pulsatility. The mean values of the estimated errors are depicted in red, while the limits of agreements ($mean \pm 1.96 \cdot standard\ deviation$) are depicted in yellow in L/min.

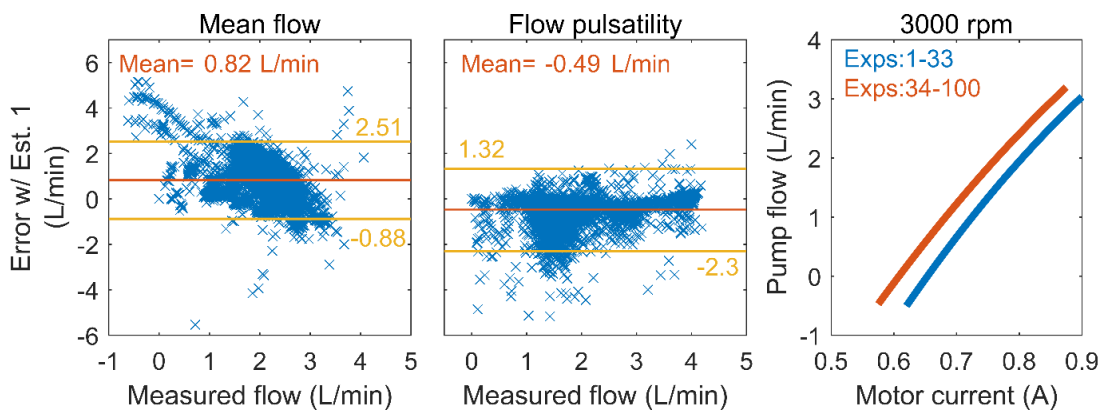


Figure 6.7: Left and middle plots: Bland-Altman plots for all in-vivo experiments at varying levels of viscosity obtained with Estimator (Est.) 1 when estimating the mean flow and the flow pulsatility. The mean values of the estimated errors are depicted in red, while the limits of agreements ($mean \pm 1.96$ standard deviation) are depicted in yellow in L/min. Right plot: The relationship between pump flow and motor current during all in-vivo experiments for a specific pump speed with two viscosities. Experiments (Exps.) 1-33 and 34-100 belong to Dataset F (Table 6.1).

6.5 Discussion

The current manuscript presents the first systematic comparison study among various approaches for the non-invasive and invasive estimation of the VAD flow rate. A single blood pump, a unique HMC, and the same animal model were used, thus allowing the systematic and equal comparison among the estimators. The in-vivo and in-vitro experiments conducted included a wide range of variations of the pump speed settings, the conditions of the circulation, and the viscosity. Thus, various conditions of the pump flow and the input signals, and their respective influences on the estimators' performance were investigated. Among the non-invasive approaches presented in literature, Estimators 1 and 3 with the model-based approach [44] yielded the least error and showed the most reliable performance in the majority of the experiments. Both of them rely on the modelling of the BLDC motor of the pump, which had earlier been proposed by Pillay et al. [210]. The same model is being used by Estimator 2 with the EKF approach, but the incorporation of soft sensors did not cause any improvement. It has to be noted, that the pump models used differ from those used by Giridharan et al. [49] but the in-vitro performance is comparable. Estimator 4 presented an overall better performance when using the MOC (Figure 6.3), presumably due to the lack of the speed derivatives from its inputs, which are much higher in the case of the MOC.

The non-monotonic relationship between pump flow and current was investigated. This relationship has earlier been discussed in literature, as it influences the performance of the estimator of the HeartMate II [209], one of the most frequently implanted VADs, resulting in a wrong estimation below flows of 2 L/min. That behavior is also common in other types of VADs, such as the HVAD (Medtronic Inc., Minneapolis, MN, USA), but the flow value below which the non-monotonic relationship begins varies. The exploitation of the pump inlet pressure seemed to only slightly improve the reliability of the estimators during negative flows. The use of both inlet and outlet pressure sensors, as implemented with Estimator 4, resulted in the most reliable flow estimation during negative flows, as it does not depend anymore on the non-monotonic relationship between pump flow and current (Figure 6.5). Pennings et al. [209] used an approach similar to that of Estimator 4, but with only a static model which was applied in three different devices. Their results also showed the importance of the pump pressure difference as an additional input of the estimator to improve its performance. However, a VAD system that directly measures the pump pressure difference seems to be quite far from implementation. Only devices which can estimate this signal from their levitation concept may benefit from such an approach [211].

Estimating negative flows is considered quite crucial as it indicates an increased workload of the native heart, while more blood damage and hemolysis are induced. Therefore, it is beneficial to monitor negative flows and set the pump speed, manually or automatically, at a setpoint that prevents negative flows. Negative mean pump flow happens rarely and may indicate a device failure. However, negative flows within the heart cycle and especially during the diastolic phase when the pump pressure difference increases. Negative flows may occur when the pump speed remains constant. This can be the case especially for devices with flat pump characteristics.

Clinical studies have shown that current flow estimators used in VADs lack robustness and accuracy [212]. Reyes et al. [212] evaluated the HVAD estimator in vivo. They reported a correlation between measured and estimated pump flow with an R^2 value of 0.92, for flows ranging from -2 L/min to 8 L/min. Granegger et al. [44] proved that their model-based approach outperforms the HVAD estimator when used for estimating the parts of the flow signal with a high-frequency content. This characteristic is important when the estimator is used for monitoring purposes, such as for detecting contractility changes of the LV [213]. A mock circulation which can generate high-frequency pressure signals was used, like in the current study, to generate the appropriate dataset for identification. This characteristic of the mock circulation is very important when the dynamic parameters of the physical models are identified. In contrast to the current study, Granegger et al. [44] did not focus their investigations on the performance of the estimator during negative flows, but they reported the limitation of their approach.

Another study by Slaughter et al. [206] evaluated the estimator of the HeartMate II in VAD patients. In their case, the measured pump flow varied from 2 to 7 L/min and the R^2 value was 0.56. However, for flows between 4 and 6 L/min the error reported was 15% to 20%. No results were reported for flows less than 2 L/min, which is the area where the flow-current relationship of the device becomes non-monotonic [209]. The current study focused especially on low flows and presented the performance as well as the limitations of various approaches. Finally, Giridharan et al. [49] showed that the root mean squared error of their EKF

estimator increased from 0.48 L/min to 0.96 L/min when switching from constant speed to physiological control mode. No such difference was observed in our experiments with the EKF (Figure 6.3).

The in-vivo experiments included manipulations which were also simulated in vitro. The evaluation of the estimators in both environments revealed a poorer performance in vivo and the mean error increased from 0.1 to 0.4 L/min. The errors in the range of 15-20 L/min observed in Figure 6 are related to recordings with sudden current spikes that were present in vivo, presumably due to data logging. Furthermore, the decreased performance can also be explained by the fact that the outflow graft resistance was not incorporated in the hydraulic model. During animal studies, the manual calibration of the flow sensor and the measurement of viscosity may introduce errors, which could be the reason why the in-vivo validation yielded a decreased performance. Not accurately calibrated flow probes may lead to an error of $\pm 10\%$ [206]. Yet, the HMC used was able to control the viscosity accurately and keep it constant, while the flow probes were calibrated for the specific viscosity used [92]. The calibration method of the flow probe of the current study is described in the supplementary material. Therefore, if viscosity is accurately controlled and the flow probes are calibrated, in-vitro testing constitutes a reliable environment for such studies. The uncertainty that exists in vivo due to the varying viscosities is therefore also possible to be investigated in vitro. The flow sensor was not calibrated in vivo with the method used in vitro. That constitutes a limitation of the study and possibly a main reason why the in-vivo performance of the estimators worsened.

The BLDC model-based approach seemed to be quite reliable for pump flow estimation, but only when the relationship between pump flow and current is strictly monotone. A slight improvement was observed by using only the pump inlet pressure only, while using pump inlet and outlet pressure sensors allowed for a more reliable estimation of negative flows. Thus, there may exist a potential for switching estimators based on the current region to derive a more reliable estimation of the overall flow. A model for the outflow graft would be required in case that Estimator 1 is combined with Estimators 3 or 4, such that a more accurate derivation of the pump outlet pressure is derived. The estimation errors in-vivo were higher than in vitro. The estimation errors derived should be considered when using the estimated pump flow for control and monitoring purposes. Pump and motor design affect the performance of the estimators. The decision to incorporate a flow estimator and sensors to a device is suggested to be met at the early stages of development. A trade-off between estimation accuracy and number of sensors was identified. However, the long-term stability limitations of sensors, such as their drift, should also be considered in such a decision.

7 Viscosity Prediction in A Physiologically Controlled VAD (Paper VI)

The content of this chapter is completely taken from [94] and reprinted with permission from:

Petrou, M. Kanakis, S. Boes, P. Pergantis, M. Meboldt, and M. Schmid Daners, "Viscosity prediction in a physiologically controlled ventricular assist devices;," *IEEE Trans Biomed Eng*, © IEEE 2018.

7.1 Abstract

Objective: We present a novel machine learning model to accurately predict the blood-analog viscosity during support of a pathological circulation with a rotary ventricular assist device (VAD). The aim is the continuous monitoring of the hematocrit (HCT) of VAD patients with the benefit of a more reliable pump flow estimation and a possible early detection of adverse events, such as bleeding or pump thrombosis. **Methods:** A large dataset was generated with a blood pump connected to a hybrid mock circulation, by varying the pump speed, the physiological requirements of the modelled circulation and the viscosity of the blood-analog. The pump inlet pressure and the pump intrinsic signals were considered as inputs for the model. Gaussian process yielded models with the best performance, which were then combined using a variant of stacked generalization to derive the final model. The final model was evaluated with unseen testing data from the created data set. **Results:** For these data, the model yielded a mean absolute deviation of 1.81% from the true HCT, while it proved to correctly predict the direction of the HCT change. It showed to be independent of the set speed and the condition of the simulated cardiovascular circulation. **Conclusion:** The accuracy of the prediction model allows to improve the quality of flow estimators and detect adverse events at an early stage. Evaluation of this approach with blood is suggested for further validation. **Significance:** Its clinical application could provide the clinicians with reliable and important hemodynamic information of the patient, and, thus, enhance patient monitoring and supervision.

7.2 Introduction

Ventricular assist devices (VADs) are currently considered a valid alternative for end stage heart failure treatment when heart transplantation is not possible. Survival rates with the widely used rotary VADs (95% of all VAD implantations) remain above 80% and 70% for the first and second years of support, respectively [32]. Despite that, adverse events still occur and affect negatively the quality of life of VAD-patients, while leading to high rehospitalization costs [214]. The constant speed operation is assumed to be a factor that leads to non-physiological hemodynamics, such as suction, which may induce blood damage and, ultimately, lead to adverse events, such as thrombosis. Various concepts for physiological control have been proposed as a method to prevent critical flow conditions [63], such as suction, but the lack of long-term, implantable sensors still hampers their clinical implementation. Furthermore, the lack of reliable telemetric systems for continuous monitoring of the patients after discharge from a healthcare facility hinders the prediction or immediate detection of adverse events, which would allow their treatment at an early stage. Thus, their treatment relies mostly on the awareness of the patients and their caregivers. To counteract this deficiency, non-invasive monitoring algorithms for various hemodynamic information have been proposed [54], [215]–[218]. Their implementation in clinical practice for continuous monitoring of the interaction between the human heart and the VAD can provide the clinical personnel with significant information, leading to a dramatic improvement of the patient outcomes.

Continuous monitoring of blood viscosity, especially in the ambulatory setting, can allow healthcare professionals to monitor the hematocrit (HCT) of the patients, and thus derive information regarding their health status and the interaction of the VAD with the circulation. The connection between HCT and blood viscosity has already been described by Boës et al. [92]. HCT may follow great variations, especially in VAD-supported adolescents [219]. Additionally, current algorithms require the HCT values as input to estimate the pump flow [44], which is used for multiple purposes from the clinicians, such as for adjusting the pump speed

7.3 Materials and Methods

during hospitalization. A wrongly set HCT value may lead to significant errors of estimated flow [62] and influence the clinical observations which rely on pump flow variations due to varying conditions of the circulation. Decrease in pump flow can be caused by pump thrombosis, right heart failure or volume depletion, as in the cases of dehydration or bleeding [220]. In the case of acute gastrointestinal bleeding the estimated flow is reduced both due to hemodynamic effects of blood volume loss and decrease in the preload for the left ventricle and VAD, but also due to the fall of the HCT. In the chronic setting, one of the most common complications is hemolysis, leading to chronic anemia and, therefore, to a decrease in the HCT and, thus, in estimated flow [221]. Therefore, reliable HCT and pump flow estimation is important for the supervision of VAD-patients.

Methods to detect HCT changes have already been developed. In clinical practice, the analysis of the log files of the pump current of the devices constitutes the golden standard to detect changes in blood viscosity and to consider the onset or occurrence of adverse events, such as pump thrombosis [51], [52]. Furthermore, low flow alarms or power spikes are also used for early detection of possible complications [53], but without being able to classify the level of emergency until exact values of HCT are provided. Nowadays, HCT values can only be measured manually by the clinicians during hospitalization of the patient. In research, an advanced approach for sensorless viscosity estimation has been recently presented by Hijikata et al. [54]. However, it has been evaluated only on one operating condition with a fixed pump speed and without taking into consideration the varying physiological requirements of a VAD-assisted pathological circulation. In addition, this approach can only be used for pumps with the same kind of contactless active magnetic bearing.

Pump current variations, which are currently used clinically, may not be solely correlated with changes in viscosity. In case of applied artificial pulsatility, as already implemented clinically at Heartmate III (Abbott Laboratories Inc., Illinois, US), or physiological control, which is considered as a future technology for improving VAD-therapy [55], the pump current will continuously vary due to the varying desired pump speed. Thus, in such cases, only monitoring the pump current will not suffice to monitor changes in viscosity or to detect possible adverse events.

The integration of sensors in VAD systems can substantially improve the monitoring of VAD-patients, while it constitutes a major prerequisite for the clinical implementation of physiological control. Several sensors for VADs are currently under development [56], whereas a left atrial pressure sensor, has been tested with VAD patients as well [57]. Furthermore, the first FDA approved implantable pressure sensor for the pulmonary arterial pressure (CardioMEMS™ HF System, Abbott AG, Illinois, US) has been recently realized and is in clinical use. All these advancements promise the possibility of acquiring more information from the human blood circulation during VAD support in the future and, therefore, implementing better monitoring and control systems [95].

Machine learning models that exploit the availability of data have already been proposed in VAD research [215], [222], presenting their potential for better patient monitoring, such as for detecting an aortic valve opening. Their usage is mainly recommended in cases where the application of analytical approaches is restricted. Furthermore, various medical applications have already implemented such models nowadays, such as in the field of medical imaging [223], and their implementation seems to broaden the potential of autonomous systems. Their application for HCT prediction during VAD support has not yet been investigated.

In the current manuscript, we present a novel machine learning model for the prediction of blood-analog viscosity in a VAD-assisted circulation, considering recent developments in sensor technologies and physiological control [56]. For this model, named as Final Model from now on, pump intrinsic signals and the signal of the pump inlet pressure are required as input. All steps for the development of the Final Model are presented in detail. It was evaluated under various pump speeds and physiological requirements of a pathological circulation assisted by a rotary VAD, using a hybrid mock circulation (HMC) with controlled viscosity. The performance of the Final Model, its limitations and future development are finally discussed.

7.3 Materials and Methods

7.3.1 Overview

Figure 7.1 depicts the workflow followed for the development of the machine learning model, divided into four main parts (A-D) which yielded nine total steps (S1-S9). Part A: An in-vitro experimental setup, i.e., an HMC, was used for the simulation of a VAD-supported pathological circulation and experiments with varying

VAD speed and physiological requirements were conducted (S1). Raw data of interest were recorded, and measured viscosity was converted into HCT based on Merrill et al. [224]. Part B: A list of potential features which can be used as inputs to the model were identified and extracted from the raw data (S2). All data were split randomly into two subsets, named the training (80% of all data) and the testing set (20% of all data), the former to be used for the development of various models and the latter to be used at the very end to evaluate the performance of the proposed models on unseen observations. Part C: Each model was developed based on an iterative procedure. Pre-processing (S3) allowed for the processing of features, such as to expose a structure in the data (e.g. feature normalization). Then, learning algorithms were applied on the new feature vectors (S4), and the hyperparameters were optimized to improve the performance of the models on validation datasets (S5). With ten-fold cross-validation (S6), the performance of different models, which were based on different pre-processing, learning algorithm and hyperparameter combinations, was evaluated, by using a specific, task-sensitive loss function. By iterating steps S3 to S6, the best performing model was identified and evaluated on the testing dataset (S7). Part D: Based on steps S2 to S7, three different models were derived that perform best on different observations of the training dataset, i.e., full, partial or full and partial support observation. Partial support means that the level of VAD support allows an aortic valve opening, which is not the case for full support. The stacking method (S8) was followed to combine the predictions of these three models and develop the Final Model, which was finally evaluated using the testing data (S9). The following paragraphs describe the parts A) to D) from Figure 7.1 in more detail.

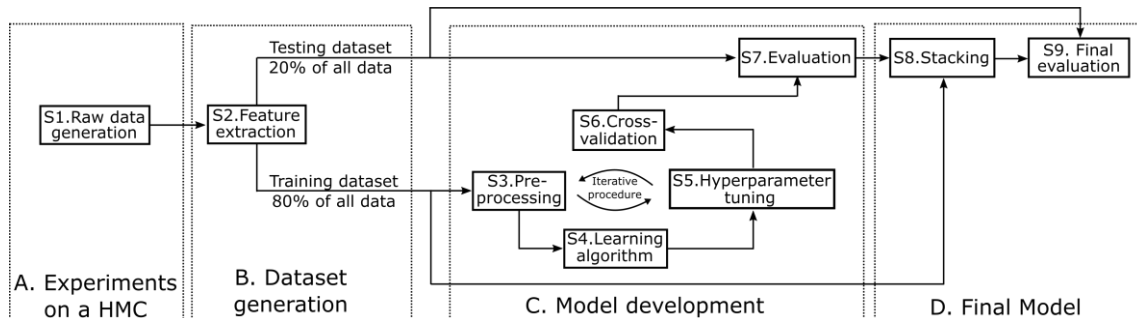


Figure 7.1: Steps (S1-S9) were followed for the development of the Final Model of the study. In part B. features, representing the 80% of the dataset recorded on the hybrid mock circulation (HMC) from part A., are sampled as training dataset, whereas the remaining 20% are used as testing dataset. The training dataset is used within an iterative procedure for the development of each model, which is then evaluated at the end with the testing dataset. Three best performing models, developed using different observations based on the level of pump support, were combined through a modified stacking method, to generate the Final Model, which was finally evaluated with the testing dataset.

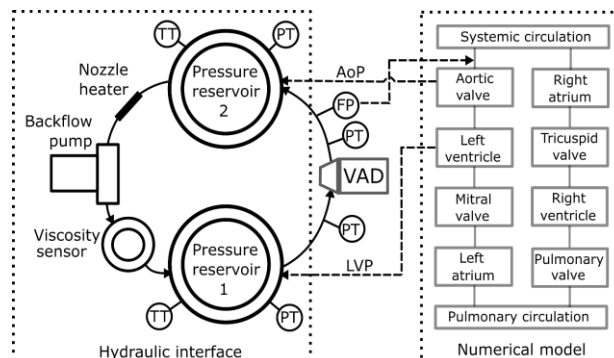


Figure 7.2: Schematic diagram of the hybrid mock circulation (HMC) used in the presented study. The left, dotted box illustrates the hardware part of the HMC with the hydraulic interface. The pressure reservoir 1 corresponds to the left ventricular pressure (LVP) and the pressure reservoir 2 to the aortic pressure (AoP). The right, dotted box depicts the elements of the lumped-parameter numerical model. PT, pressure transducer; TT, temperature transducer; FP, flow probe; VAD, ventricular assist device.

7.3.2 Experiments on a hybrid mock circulation

The experiments for generating the required data were conducted on the HMC presented by Ochsner et al. [97] and extended by Boës et al. [92] to incorporate a viscosity-control system for the working fluid, a water-glycerin mixture. Figure 7.2 illustrates an overview of the HMC, which consists of three main parts and operates based on the hardware-in-the-loop approach. First, the hardware part of the hydraulic circuit (hydraulic interface) consisting of two pressure-regulated reservoirs, which were required to enable a real-time interaction between the VAD and the numerical model of the cardiovascular system. The pressures of the reservoirs, which correspond to the left ventricular and aortic pressures, are applied as computed from the numerical model, through pressurized air and vacuum systems. Further hardware parts are a flow probe (TS410/ME-11PXL, Transonic Systems, Inc., Ithaca, NY) to provide the measured pump flow to the numerical model, a reflux pump (Jabsco 18660 Series, Xylem Inc., NY, USA) to equalize the fluid level of the reservoirs, a viscometer (preliminary development version of inline viscometer DVP-0300, Rheonics, Inc., Winterthur, Switzerland), two nozzle heater bands to heat up the fluid (Düsenheizband Mica 125 W, Brütsch/Rüegger Werkzeuge AG, Urdorf, Switzerland) as well as temperature (TT) (Temperature Probe 590-59AD07-302, Honeywell International, Inc., Freeport, IL, USA) and pressure (PT) (TruWave, Edwards, Lifesciences, Irvine, CA, USA) transducers. Second, the physical model of the VAD that supports the circulation; here, a non-implantable mixed-flow turbodynamic blood pump (Deltastream DP2, Xenios AG, Heilbronn, Germany) was used, indicated in dark grey line. Third, a numerical lumped-parameter model of the cardiovascular system, whose individual parts are depicted in grey boxes in Figure 7.2 and their detailed content has been explained in [97].

The experiments conducted to gather the required training and test data included a variety of combinations of settings related to the pump, the circulation and the water-glycerin mixture. The pump speed was varied between 2000-5000 rpm with steps of 500 rpm, the fluid viscosity such that HCT values varied between 20-40% in increments of 2.5%, the unstressed venous volume increased and decreased by 300 mL with 100 mL steps, and the systemic vascular resistance varied between 0.8-1.4 mm Hg·s/mL with steps of 0.1 mm Hg·s/mL. Thus, various circulation, HCT and pump conditions were simulated, resulting in 3087 different observations. For each experiment, the signals of (i) the pump current, (ii) the pump speed, (iii) the estimated pump flow based on the model-based approach proposed by Granegger et al. [44], and the measured pump flow, (iv) the pump inlet pressure, and (v) the fluid viscosity, which was converted to HCT based on equation from [224], were acquired.

7.3.3 Dataset generation

Prior to extracting features from the raw data which were acquired at a high rate of 1 kHz, all signals were down-sampled to a rate of 200 Hz. Thus, the samples' size is reduced while data information is preserved, as proposed by Karantonis et al. [222]. The down-sampled signal was then low-pass filtered to remove sensor-noise. Then, features were extracted based on feature engineering. However, due to the complex relationship between parameters, such as the afterload, preload and their effect on VADs, exploratory data analysis was also used to enhance the potential list of features that could be used to construct the model. Table 7.1 lists all features initially selected and their selection process, which is described below.

Feature engineering was first used to identify the features required for the prediction of HCT based on domain knowledge. The mean pump current, over a period of five cardiac cycles, was used in this category, as it has been proven clinically to be correlated to viscosity changes [202]. Furthermore, the mean estimated pump flow, mean and maximum pump inlet pressure and pump speed can be correlated with viscosity through the pump characteristics [92].

Statistical analysis was then applied, over a period of five cardiac cycles, to uncover further features with the use of histograms by investigating one parameter of interest at a time. This approach offers a visualization of the change in distribution by simplifying the problem into smaller sub-problems. Figure 7.3 presents an example of such an analysis for two different sensors and the flow estimator for two different HCT values, namely 20% and 40%. During these experiments, pump and circulation settings were fixed. The histograms

show that apart from the pump current none of the mean values of the other features were influenced significantly from changes in HCT. Thus, the mean pump current is proven to be a reasonable potential feature as expected from the feature engineering process. However, the standard deviation of the current changes significantly among the different cases and therefore proves to be another potential feature to be used by the model. Similar procedure was followed for various potential circulation settings.

Considering that HCT value changes are minor within adjacent cardiac cycles, the signals periodicity can be analyzed, such that features in the frequency domain are derived. Figure 7.4 depicts the spectrum of the same experiment as in Figure 7.3. Here, we observed that the current does not provide as much information as it did in statistical analysis, as there are no clear peaks. However, the remaining signals seem to provide significant information for HCT changes, both in the amplitude and occurring frequency and, therefore, constitute additional meaningful features to be investigated.

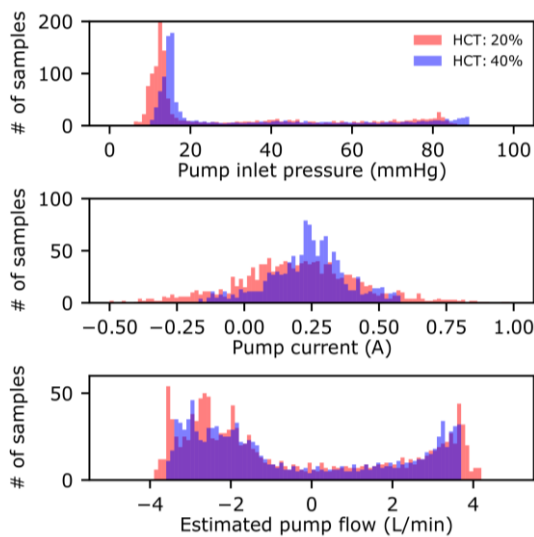


Figure 7.3. Example of statistical analysis for potential features. Data were extracted over five heartbeats for three different hematocrit (HCT) values while pump and circulation settings remained constant.

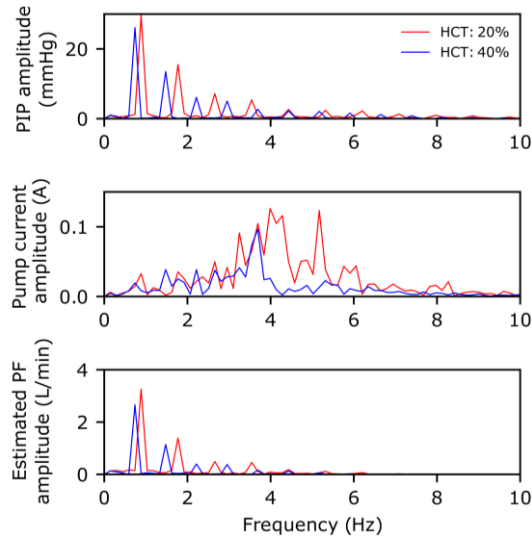


Figure 7.4. Example of frequency analysis for potential features with pump inlet pressure (PIP), pump current and estimated pump flow (PF) signals. Data were extracted over five heartbeats for three different hematocrit (HCT) values while pump and circulation settings remained constant.

Table 7.1: List of potential features

Data source	Features		
	Feature Engineering	Statistical Analysis	Frequency Analysis
Pump current	mean	median, standard deviation	-
Pump inlet pressure	mean, max	median, standard deviation	1st, 2nd, 3rd peak amplitude and corresponding frequency
Estimated pump flow	mean	median, standard deviation	1st, 2nd, 3rd peak amplitude and corresponding frequency
Pump speed	mean	-	-

7.3.4 Model development process

For the model development, the training dataset was used to investigate different learning algorithms as well as appropriate pre-processing (Figure 7.1). The investigated algorithms were ridge regression, support vector regression, artificial/convolutional neural networks, random forest, bagging, boosting algorithms and Gaussian process with different kernels [225], where applicable. Out of the investigated algorithms, Gaussian

process was identified to perform the best, which looks at the extension of the Gaussian distribution to infinite dimensions, i.e., they allow for the generation of data points which are in a domain where any subset follows a Gaussian distribution [226], and was thus used to construct the models described in the manuscript. For the pre-processing, the features were initially normalized to bring all features in the same scale, which is desirable when using Gaussian processes. Highly correlated features were then eliminated to avoid the model becoming unstable prior to training the model. Finally, a combination of greedy forward and backward selection, as well as elimination of features with minimum in class variance was used for the identification of the desired features.

For the validation of the different pre-processing and learning algorithms, ten-fold cross-validation was used and evaluated with an evaluation metric chosen based on information from clinical practice and research. In clinical practice, the HCT input of the flow estimator is recommended to be updated only if changes of $\pm 5\%$ or greater occur [227]. Thus, this limit constitutes the preliminary upper threshold for our study. As an extent, a cost function had to be used which penalizes significantly less the predictions within this limit and more the predictions that are further away from it. Therefore, the hyperparameters chosen must pull the predictions within the defined threshold. One of the most commonly used cost functions for this purpose is the mean squared error (MSE), where the difference between the prediction and the real label is squared, as defined by:

$$MSE = \frac{1}{N} \sum_{i=1}^N (\hat{y}_i - y_i)^2 \quad (7.1)$$

where N represents the total number of predictions, \hat{y}_i the predicted HCT and y_i the measured HCT.

7.3.5 Final Model

Three different models were initially developed using the workflow depicted in Figure 7.1, trained on three different observation type combinations. Namely, Model 1 for observations with partial support, Model 2 with full support, and Model 3 with all observations. However, the aim was to develop a model that predicts well the HCT for any type of observations. To accomplish this, the authors propose a model based on a variant of “Stacked generalization” presented by Wolpert [228]. The proposed model is referred to as stacked generalization using multi-scope models. Figure 7.5 illustrates the structure of this approach, which is described below.

At Level 0, ten new submodels (1.1-1.10, 2.1-2.10, 3.1-3.10) for each of the Models 1-3 were developed. These submodels had the same learning algorithm and hyperparameters as defined for the main Models 1-3, according to the process of Figure 7.1. A ten-fold scheme was implemented to train each submodel, using the data it should be optimized for. Each fold constitutes a $Q \times R$ matrix, where Q is the number of features extracted and R is the number of observations yielded after dividing all observation in ten folds, as well as the corresponding HCT values. For example, for submodel 1.1 of Figure 7.5, the partial support observations of the training dataset were initially divided into ten folds. Then, nine folds, depicted as white squares, were used to train the submodel. The submodel yielded was used to predict the HCT values of the 10th fold, based on the features of the 10th fold, as well as the full support data that were not used for training. The latter step conducted only for submodels 1.1 – 2.10 and its purpose was to avoid any dimension mismatch in the next steps and have predictions from each of the three models for all observations, as submodels 3.1- 3.10 predicted both full and partial support observations. These steps were repeated ten times for each type of models, i.e., Models 1-3, such that all folds were used for training and prediction.

The predicted HCT values from the submodels are illustrated with colored thin rectangles in Level 1 and correspond to arrays of length R. The colored crossed rectangles represent the predictions for the type of data that were not used for training the submodels. As a next step, all arrays seen in Figure 7.5 were averaged column-wise, ensuring that each model yields 1 prediction per observation. Prior to training a new model that uses the predictions of each of the three models to acquire the final prediction pseudorandomization is required. The reason for this is that for the construction of Model 3, all observations were randomized such that each fold is comprised from both partial and full support observations. As an extent, pseudorandomization of the predictions of Models 1 and 2 is performed such as to randomize those predictions in the same manner as for

Model 3. In other words, it ensures that predictions of each observation from the three models are clustered together. These predictions can now be considered as the new feature vector that will be used to train the Final Model. As proposed by Wolpert [228], linear regression as learning algorithm for the Level 1 data was used and the model built can ultimately be considered as a linear combination of the predictions from Models 1-3. Thus, a model that captures the relationship between predictions of partial and full support data from the different models was constructed.

The process described above looks at how to generate the training data and linearly combine the predictions from Models 1-3. In order to make predictions for the test dataset, a similar approach is followed. More specifically, prediction for the trained submodels 1.1-1.10 are averaged and repeated for submodels 2.1-2.10 and 3.1-3.10. These three predictions can be seen as the new feature vector which is then passed into the final model for the final prediction.

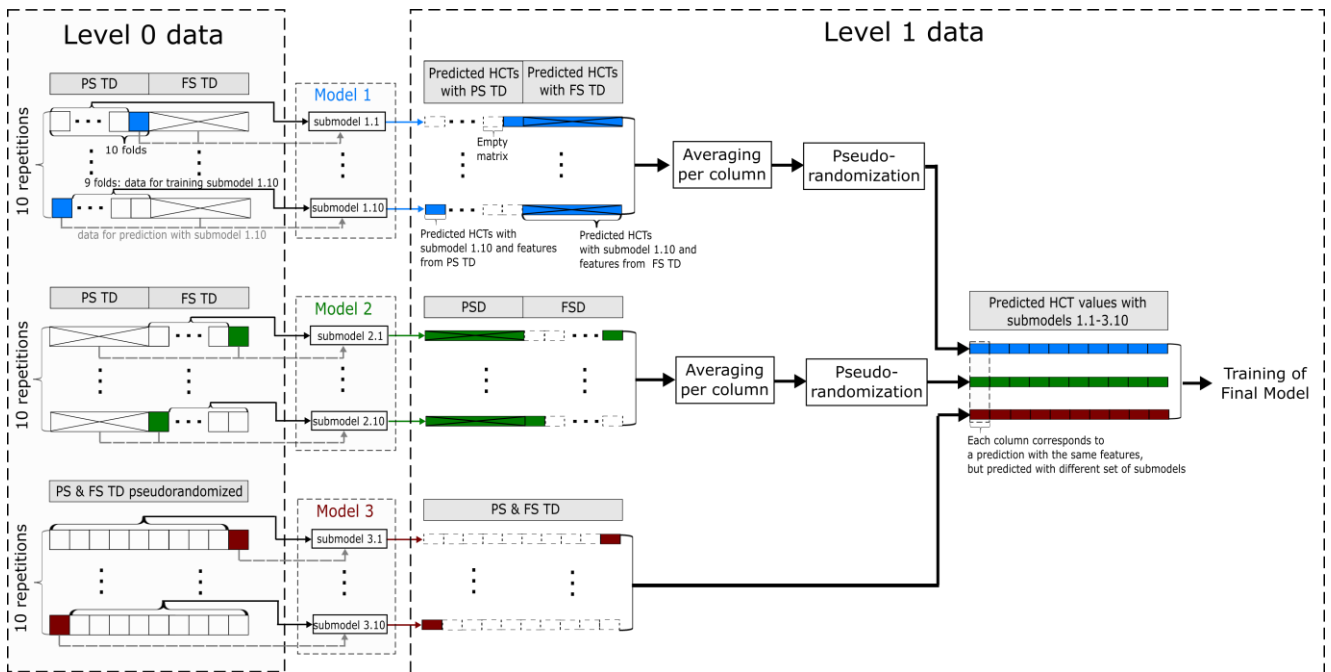


Figure 7.5. Schematic representation of the proposed modified method of stacking generalization using multi-scope models. Partial (PS) and/or full support data (FS) (Level 0 data) of the training dataset (TD) of the study are divided into ten folds. Nine folds are then used to train submodels 1.1-3.10, represented by white squares. The features of the 10th fold (colored squares) and of the PS or FS observations not included in the training step (white crossed rectangles) are used to predict HCT values, which constitute the data of Level 1, depicted in thinner colored rectangles. This step was repeated ten times to train and predict with each fold.

7.4 Results

7.4.1 Models with Gaussian process

Table 7.2 lists the MSE yielded with each model (depicted in Figure 7.5). For all these models, the selected features that were used to accomplish the best performance were: (i) Pump current: mean, median and standard deviation (SD) (ii) Pump inlet pressure: mean, median, SD, maximum, 1st and 3rd peak amplitude and corresponding frequency and the 2nd peak amplitude (iii) Pump flow estimation: mean, SD, 1st, 2nd and 3rd peak amplitude and corresponding frequency (iv) Pump speed: mean. Based on Table 7.2, the mean HCT difference for Models 1-3 is 1.84%, 2.25% and 1.90% respectively, which is less than the 5% threshold of interest. Figure 7.6 presents a visual representation of the results of Model 1 (top - partial support data), Model 2 (middle - full support data) and Model 3 (bottom - partial and full support data) for HCT prediction error over all testing data and HCT values tested. The solid grey line indicates the perfect prediction for every observation, while the dashed lines represent the limit of the clinical standard, i.e., $\pm 5\%$ HCT.

For Model 1, there are 26 predictions out of the 582 experiments that had an error beyond the 5% threshold but less than 10%, and 2 predictions with a prediction error higher than 10%. That is, 4.8% of the predictions were beyond the 5% threshold. Similarly, Model 2 had 10 predictions out of the 126 experiments available between 5% and 10% difference error, 2 predictions between the range of 10% and 15% error difference, and 1 predictions with an error higher than 15%, yielding a 10.4% of the predictions being beyond the 5% threshold. For Model 3, which constitutes a naïve approach to the problem since it takes both partial and full support observations, there are 33 predictions out of the total 708 predictions between 5% and 10% difference error, 5 predictions between the range of 10% and 15% error, and 1 predictions with an error higher than 15%, yielding 5.5% of the predictions being beyond the 5% threshold. However, most of the outliers are from the fully supported observations.

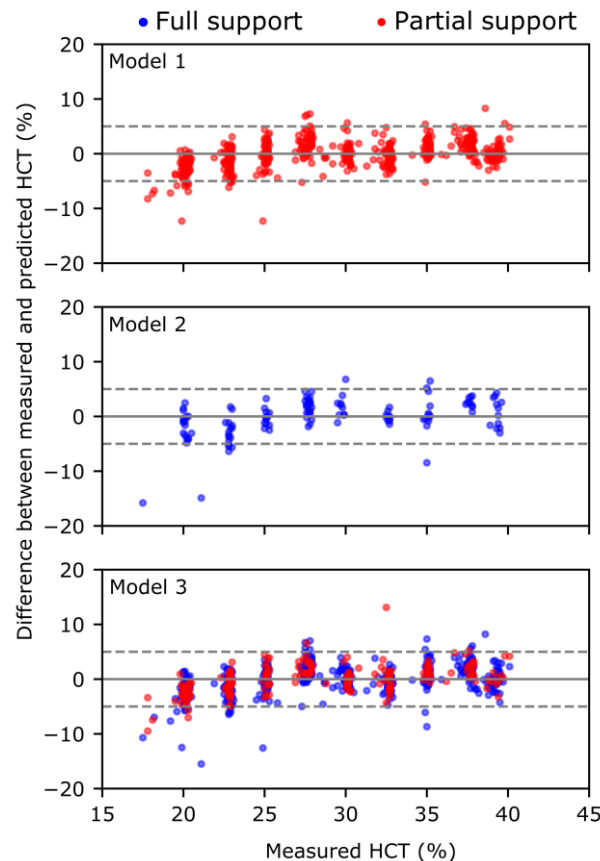


Figure 7.6: Top: Hematocrit (HCT) prediction error for the various HCT values tested with Model 1 (see Figure 7.5), which was optimized for partial support data. Middle: HCT prediction error for the various HCT values tested with Model 2 (see Figure 7.5), which was optimized for full support data. Bottom: HCT prediction error for the various HCT values tested with Model 3 (see Figure 7.5), which was optimized for full and partial support data. In all three cases the prediction results with the testing data are plotted. In all plots, solid grey lines represent the ideal performance of each model, whereas grey dashed-lines represent the limit of $\pm 5\%$ HCT, representing the limit which should enclose the predictions.

7.4.2 Final model: Stacked generalization with multi-scope models

Figure 7.7 – left, depicts all the predictions of the testing dataset when using the Final Model (Figure 5), which produced an HCT difference of 1.81%, (Table 7.2), that is, a 4.8% error decrease from Model 3 for the mean HCT error, or 9.9% decrease of the MSE. Only 29 out of the 708 predictions were out of the 5% limit (dashed grey line), while no prediction errors were beyond the 10% limit. Comparing these results to Model 3 (Figure 6), the Final Model managed to bring the observed outliers closer to the desired performance, as intended. Figure 7.7 – right, depicts a histogram of the prediction errors, which shows the importance of using MSE as an evaluation metric to enforce values to be as close as possible to the perfect prediction, while minimizing outliers.

Table 7.2: List of The Mean Squared Errors (MSE) And Mean Absolute Differences Between True And Predicted Hematocrit (HCT) With The Developed Models

Model	Test error (MSE)	Mean absolute HCT difference (%)
Upper bound	25	5.00
Partial support (Model 1)	5.89	1.84
Full support (Model 2)	10.98	2.25
Partial and Full support (Model 3)	6.98	1.90
Stacked generalization using Multi-scope models (Final Model)	6.32	1.81

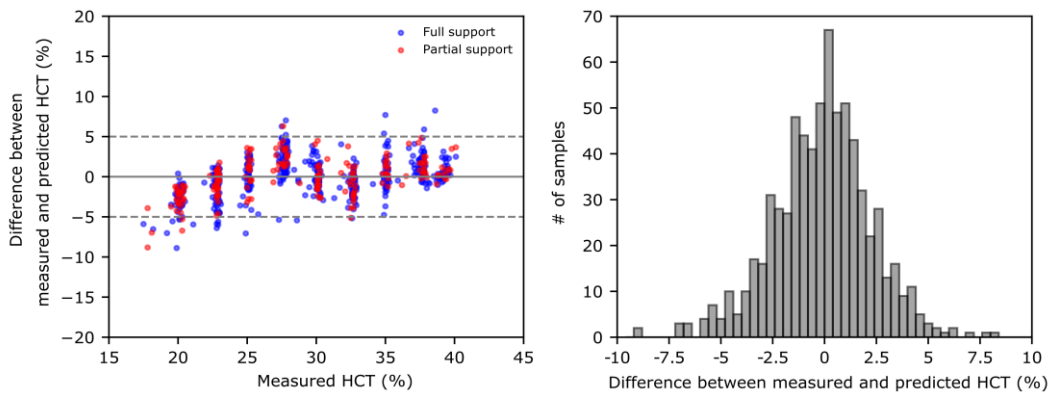
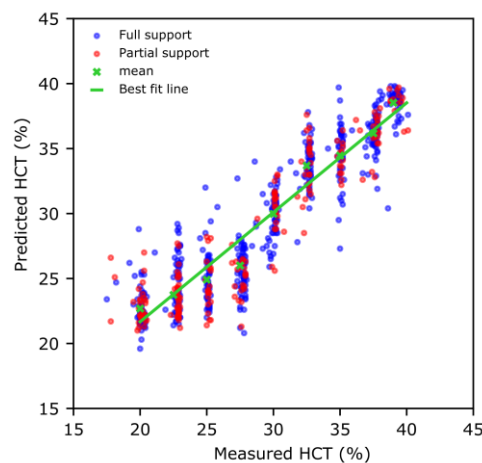
**Figure 7.7.** Left: Hematocrit (HCT) prediction error of the Final Model (see Figure 7.5) for the various HCT values measured within the testing dataset. Solid grey lines represent the ideal performance of each model, whereas grey dashed-lines represent the limit of $\pm 5\%$ HCT, which should enclose the predictions. Right: Histogram of the HCT errors of the Final Model for all unseen observations of the study.

Figure 7.8 depicts a scatter plot of the measured and the predicted HCT values for both partially and fully supported observations, for the investigation of a trend between true and predicted HCT values. Due to the large number of observations with different circulation settings, it can also be seen that for every HCT value investigated there is a noticeable fluctuation. To make the trend more apparent and better explain why the proposed model can be further investigated for health monitoring models, the mean prediction value for each of the HCT clusters has been plotted, as well as a least squares line of the observations. From this, it can be visually identified that the mean prediction for each of the HCT clusters is close to the best fit line proving the performance of the model as well as the trend.

**Figure 7.8.** Correlation between measured and predicted hematocrit (HCT) for all observations of the testing dataset, i.e., with both full and partial support, when using the Final Model. The mean values of the predictions at each measured HCT are depicted and fitted linearly.

7.5 Discussion

A novel model to predict the HCT of VAD patients using features extracted from the pump intrinsic signals and the pump inlet pressure was developed. In vitro experiments under various conditions and controlled viscosities were conducted to train and evaluate the model. The Final Model presented is a modified version of stacked generalization, which allowed for the development of a robust and reliable model by combining the advantages of models optimized for different data based on the level of VAD support. The combination of these models was chosen because of the data imbalance, as there are four times more partial supported observations than fully supported ones. In case of a balanced dataset, the different performance among the models may not be that distinct. However, even then, the proposed modified version of stacked generalization would be considered beneficial as it will provide an added layer of safety maintaining and yield a more stable model.

The Final Model presented an overall absolute HCT difference of 1.81% for a large span of HCT values and for observations that could be associated to different patient conditions. Of course, this enhancement in prediction performance comes at the extent of computational complexity. However, since the application at hand does not require a prediction in every cardiac cycle, which was the motivation behind using five cardiac cycles for the observations, this complexity is considered insignificant compared to the enhancement in reliability and prediction power of the model. Figure 7.8 proved that by collecting data over several beats, a prediction close to the true values can be achieved, independent of variations of the pump speed or of the physiological requirements. Thus, the direction of HCT change will be ultimately predicted correctly, which is of vital importance for the development of health monitoring models.

The model developed has some pros and cons against other methods proposed in literature, with respect to clinical implementation. On the one hand, our model requires a pump inlet pressure sensor, which is not the case for the approach of Hijikata et al. [54]. On the other hand, their method is constrained for VADs which use active magnetic levitation, while our model can be redeveloped and adapted for different VADs as it relies on “learning” the relationships between current, speed, pressure and flow, which are unique for each different device. For this reason, the recording of a sufficiently large dataset is required during the development of such a model. Thus, the convergence of the model can be ensured while possible overfitting can be minimized, the latter being a common problem with machine learning models that leads to poor predictive performance. Considering the interaction required with the algorithm, both approaches do not introduce any additional actions for the clinical personnel apart from the step of decision making, based on the continuously available HCT values.

The error yielded with our model is slightly less than the one presented in the study of Hijikata et al. [54]. They reported a mean absolute difference of viscosity of 0.12 mPas, which can be translated in 1.93% in HCT, according to the equations from Merrill et al. [224]. However, in our case, a good performance of the model under various conditions of the pump and the circulation was proven, while previous studies kept these conditions constant. Furthermore, for the optimization of our model, the MSE was used to enforce measurements to be enclosed within the desired limit, while the study presented in [54] was optimized using the mean absolute error. Thus, no further information regarding the limits enclosing their predictions and the likelihood of exceeding the threshold were provided. The benefit of continuously monitoring HCT with such an error for improving pump flow estimation has already been proven [54].

Exploratory data analysis was followed to enhance the feature space from domain knowledge of the model. Preliminary tests conducted with only features extracted from statistical analysis showed that the developed feature space is not sufficient to capture the complex relationship required for acceptable HCT prediction. The additional features extracted from the frequency domain however proved to significantly enhance the performance of all models, with a significant decrease in the error lower than the set upper threshold. These findings indicate the importance of taking advantage of the periodicity of the VAD signals when developing machine learning models for this application.

The future development of the model proposed mainly concerns its evaluation with blood. In such a case, the same development process would need to be followed, as the pump characteristics differ between blood and water-glycerin [229]. As HMCs that use blood do not exist and patient data with pump inlet pressure measurements are not yet available, only simple blood circuits and acute animal studies can be considered [83]. The implementation of our approach on other clinical rotary VADs constitutes another important investigation

to prove also that the presented approach accounts for any type of rotary VAD.

7.6 Conclusion

With the current study, we presented the development of a model that can predict the HCT of VAD patients, using the pump inlet pressure signal and the pump intrinsic signals as input. This model is robust against variations of the physiological requirements of the circulation and independent of the type of the rotary VAD. It relies on a modified machine learning method and was evaluated in vitro under various experiments. It presented a performance, which would allow a continuous HCT monitoring and a more reliable pump-flow estimation. Furthermore, it has the potential to detect possible adverse events such as bleeding or thrombosis at an early stage, while the patient is discharged from the hospital. Combined with proper, decision-making systems, such a model can greatly help the supervision of VAD patients and release workload from the clinical personnel. Having introduced a model that can successfully predict HCT in an in-vitro setting, the authors strongly consider a further validation with blood in vitro or with a VAD-supported animal circulation, to prove the potential of the HCT prediction in a clinical environment.

7.7 Corrigendum:

In the article titled “Viscosity Prediction in a Physiologically Controlled Ventricular Assist Device” [94] the input viscosity that the flow estimator requires to generate the estimated pump flow was not specified. This input was kept constant at 3 mPa·s over all measurements. Furthermore, an error was identified in the bottom panel of Fig. 3 of this article, where the measured pump flow is plotted instead of the estimated pump flow. Figure R3 below shows the revised plot with the estimated pump flow.

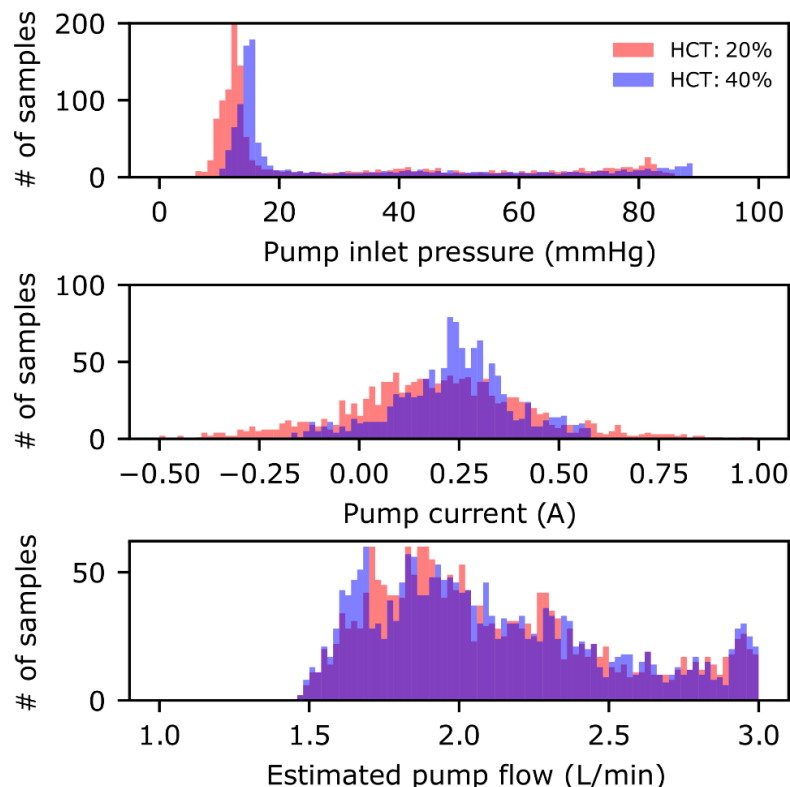


Fig. R3: Example of statistical analysis of potential features. Data were extracted over five heartbeats for two different hematocrit (HCT) values while pump and circulation settings remained constant.

8 A Novel Multi-Objective Physiological Control System for Rotary LVADs (Paper VII)

8.1 Abstract

Various control and monitoring algorithms have been proposed to improve the left-ventricular assist device (LVAD) therapy by reducing the still-occurring adverse events. We developed a novel multi-objective physiological control system that relies on the pump inlet pressure (PIP). Signal-processing algorithms have been implemented to extract the required features from the PIP. These features then serve for meeting various objectives: pump flow adaptation to the perfusion requirements, aortic valve opening for a predefined time, augmentation of the aortic pulse pressure, and monitoring of the LV pre- and afterload conditions as well as the cardiac rhythm. Controllers were also implemented to ensure a safe operation and prevent LV suction, overload, and pump backflow. The performance of the control system was evaluated *in vitro*, under preload, afterload and contractility variations. The pump flow adapted in a physiological manner, following the preload changes, while the aortic pulse pressure yielded a threefold increase compared to a constant-speed operation. The status of the aortic valve was detected with an overall accuracy of 86% and was controlled as desired. The proposed system showed its potential for a safe physiological response to varying perfusion requirements that reduces the risk of myocardial atrophy and offers important hemodynamic indices for patient monitoring during LVAD therapy.

8.2 Introduction

Rotary left-ventricular assist devices (LVADs) have been established as a viable treatment method for heart failure (HF), the leading health problem in developed countries. Despite several decades of development and significant technological improvements [55], LVADs are still associated with life-threatening adverse events, such as pump thrombosis and gastrointestinal bleeding [7]. The constant-speed operation of the clinical LVADs is assumed to be one of the factors that induces some of these adverse events. Operating an LVAD at constant speed may lead to non-physiological and critical blood flow conditions, such as LV suction and overload due to over- and underpumping, respectively, and in the long term may result in adverse events such as right-ventricular failure and pulmonary edema [89].

In clinical practice, no feedback controllers have been implemented to prevent these critical flow conditions. However, some companies have incorporated in their devices feedforward controllers that detect suction, based on the estimated or measured pump flow, and release it by decreasing the pump speed to a predefined setpoint. Additionally, they have implemented algorithms to enable an aortic valve opening or to augment the aortic pulse pressure of the patients. Despite those algorithms, it is believed that a more physiological behavior of an LVAD can be achieved to presumably reduce some of the adverse events and improve the LVAD therapy. For this purpose, the research has focused for many years on the development of such algorithms [78],[87], [89], [215]–[218].

A number of monitoring [215]–[218] and control algorithms [89] have been proposed to monitor the condition of the patient and generate a physiological pump flow. For monitoring, there exist algorithms that focus on the detection of suction events from the minimum pump flow [115], of arrhythmic events from the peak-to-peak pump flow frequency [216], of contractility changes from the pump flow pulse generated [218], or of the open or closed state of the aortic valve from the changes in the pump flow waveform [215]. For generating a physiological pump flow, the algorithms developed mainly focused either on adapting the pump flow to the requirements of the patient or on augmenting the arterial pulsatility. Most pump-flow-adaptation controllers developed aim at estimating the preload condition of the LV and adapting the pump flow according

to the Frank-Starling mechanism [230]. In-vivo experiments have proved the outperformance of such controllers against the constant-speed operation [83]. The pulsatile operation of a rotary LVAD has been investigated extensively. Amacher et al. [85] presented the effect of different periodic speed signals and phase shifts to the heart beat on the hemodynamics of an LVAD-assisted pathological circulation. Most of the monitoring and control algorithms proposed are based on a measured or estimated signal which constitutes the input of a simple control structure to achieve one specific objective, e.g. pump flow adaptation.

More complex algorithms which combine various signals and pursue additional objectives have also been presented in literature. For example, Bullister et al. [71] used the pump inlet and outlet pressure and the heart rate as inputs to their pump flow adaptation controller, while they used separate algorithms to detect suction and pump backflow through the estimated pump flow. Arndt et al. [231] used the pressure difference across the pump and developed a control system that responds to preload changes and detects suction events, while it can operate the LVAD in full or partial support. Karantonis et al. [86] used the pump-speed signal as input for a classification and regression tree to detect five different states of the LV, i.e., backflow, ventricular ejection, closed aortic valve, and intermittent or continuous suction. Amacher et al. [87] presented a more sophisticated approach to compute the optimal waveform of the LVAD speed for an assisted circulation based on a predefined objective function. For their study, a trade-off function between maximum aortic valve flow and minimum stroke work was applied.

In the current study, we present an advanced control and monitoring system which uses the pump inlet pressure to fulfill the following objectives: (1) To adapt the pump flow to the physiological requirements of the LVAD-supported pathological circulation, (2) to increase the aortic pulse pressure, (3) to ensure an opening of the aortic valve for a predefined period, (4) to provide information regarding the pre- and afterload conditions of the LV as well as the cardiac rhythm, and (5) to ensure the safe operation of the control system, such that no LV suction and overload or pump backflow events occur. As, the various objectives of the algorithms may contradict each other and, therefore, their prioritization approach is being elaborated. The control system developed was evaluated in vitro under several preload, afterload, heart rate, and contractility variations. In the following sections, the in-vitro performance of the proposed multi-objective control system and its potential for a clinical environment are presented and discussed.

8.3 Materials and Methods

8.3.1 Hybrid mock circulation

Figure 8.1 depicts the hybrid mock circulation (HMC) where all experiments of the study were conducted. This HMC was earlier developed in our group based on the hardware-in-the-loop (HIL) concept [97]. **Error! Reference source not found.** It uses a validated numerical model of the human blood circulation [123] which interacts with a physical LVAD through a hydraulic interface that consists of two pressure reservoirs. The HIL concept works as follows: The LVAD flow is measured by an ultrasound flow probe (TS410/ME-11PXL, Transonic Systems, Ithaca, NY, USA) and is fed into the numerical model. The model computes in real time the LV and the aortic pressures which are then applied through pneumatics at the pressure reservoirs. The new pressures of the hydraulic interface interact with the LVAD and generate an adjusted flow, which follows the same loop path as described above. The numerical model was implemented in MATLAB/Simulink running with Real-Time Windows Target (The Mathworks Inc., Natick, MA, USA) and executed on a PC equipped with two data acquisition boards (MF624 multifunction I/O card, Humusoft s.r.o., Prague, Czech Republic). All signals were recorded at 1 kHz. Instead of a clinical LVAD, we used a non-implantable mixed-flow turbodynamic blood pump, the Deltastream DP2 (Xenios AG, Heilbronn, Germany), which was modified to be controlled as desired. This HMC has been extended to emulate ventricular suction [148] **Error! Reference source not found.** as well as to accurately mimic different viscosities [92].

8.3.2 Experiments

The experiments were split into three main categories. The first category consisted of separate preload, afterload, and contractility variation experiments. The second consisted of an exercise experiment where preload, afterload, heartrate, and contractility vary in parallel. Table 8.1 summarizes the experiments of these two categories and presents the specific parameters we varied for each of them. For the third category, pre-, afterload, and exercise variations were repeated on circulations with increased and decreased contractility, i.e., 51% and 17%, respectively, with respect to the physiological one, thus mimicking cases of recovery or progression of a heart failure.

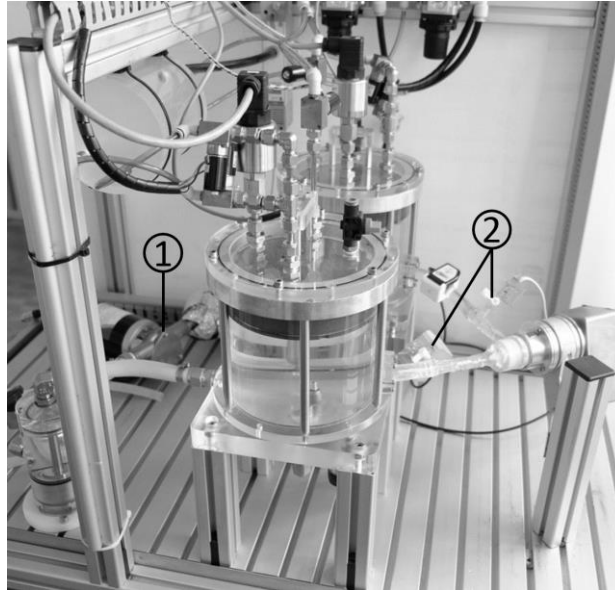


Figure 8.1: Picture of the hybrid mock circulation (HMC) used for the current study. The principle of operation and all components of the HMC were presented in detail by Ochsner et al. [97] Only the reflux pump (1) has been replaced by a flexible impeller pump (Jabsco 18660 Series, Xylem Inc., NY, USA), and pump inlet and outlet disposable pressure transducers (2) (TruWave, Edwards, Lifesciences, Irvine, CA, USA) were added.

8.3.3 Overview of control system

Figure 8.2 depicts a schematic overview of the multi-objective physiological control system presented in the current study. It is divided into three main parts (C1-C3) and all main subsystems are enumerated (blocks 1-11). First, the signals used are being processed to filter or add noise and to extract the required features. Then, estimators are implemented, while the part C3 includes all controllers developed. Each enumerated block includes algorithms which are described in the following subsections and evaluated in the Results section based on the experiments presented in the preceding paragraph.

Table 8.1: Parameters varied during the experiments of our study. All other parameters of the circulation were fixed and equal for each experiment. The contractility is expressed with respect to the physiological one.

Exp	Description	Time (s)	SVR (mmHg·s/mL)	PVR (mmHg·s/mL)	UVV (mL)	HR (bpm)	Contractility (%)
1	Preload variation	[0, 20, 25, 80, 90, 120]	1.11	0.1	[2520, 2520, 2020, 2020, 3025, 3025]	80	34
2	Afterload variation	[0, 20, 25, 80, 90, 120]	[1.1, 1.1, 0.51, 0.51, 1.91]	0.1	2520	80	34
3	Contractility variation	[0, 20, 25, 80, 90, 120]	1.11	0.1	2520	80	[34, 34, 51, 51, 17, 17]
4	Exercise	[0, 20, 30, 120]	[1.1, 1.1, 0.6, 0.6]	[0.1, 0.1, 0.05, 0.05]	[2520, 2520, 2220, 2220]	[80, 80, 100, 100]	[34, 34, 40, 40]

Exp experiment, SVR systemic vascular resistance, PVR pulmonary vascular resistance, UVV unstressed venous volume, HR heart rate.

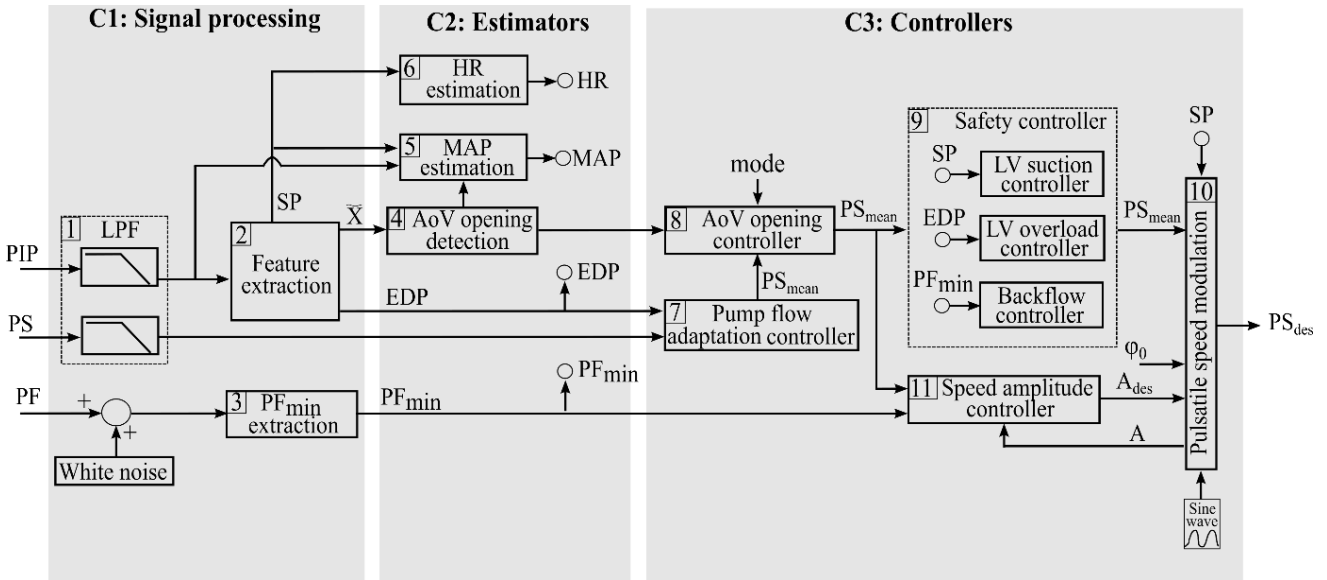


Figure 8.2: Schematic overview of the multi-objective physiological control system proposed in the current study. The input signals of the system are the pump inlet pressure (PIP), the pump speed (PS), and the pump flow (PF). The output is the desired pump speed (PS_{des}). The whole control system is divided into the three main parts named Signal processing (C1), Estimators (C2), and Controllers (C3). Each category consists of the various subsystems illustrated with blocks (1-11). The content of the variable mode is listed in Table 8.2. LPF, low-pass filter; \tilde{X} , features extracted from the filtered PIP; SP, systolic pressure; EDP, end-diastolic pressure; MAP, mean aortic pressure; HR, heart rate; AoV, aortic valve; PF, pump flow; min, minimum; des, desired; A, speed amplitude; and φ_0 , phase shift.

8.3.4 C1. Signal processing

Block 1. Low-pass filtering

Block 1 was implemented to filter the noise from the pump inlet pressure (PIP) signal. The PIP was filtered with a first-order low-pass filter (LPF) with a cut-off frequency of 25 Hz.

Block 2. Feature extraction

Two main indices were extracted from the filtered PIP at every heartbeat, namely the end-diastolic pressure (EDP) and the systolic pressure (SP). In parallel, various features from the PIP and its gradient were extracted to be used for the detection of the state of the aortic valve (block 4) and the MAP estimation

(block 5). The features extracted were chosen to depict the different waveforms of the PIP signal with and without aortic valve opening. For our implementation, the systolic phase of the PIP was segmented, and the histogram amplitude of each part was used as a feature. Additionally, combinations of the minimum, mean, maximum and root-mean square features were derived from the PIP, as proposed by Ooi et al., [232] but with the pump-speed waveform.

Block 3. Minimum pump flow extraction

For the current study, the measured pump flow was used to extract the minimum pump flow (block 3). However, in clinical practice the estimated pump flow could be used instead in order to avoid having to use additional sensors. To account for the estimator error, we added a white noise of 0.5 ± 0.2 L/min to the measured pump flow before we fed it to the backflow (part of the safety controller) and speed amplitude controllers.

8.3.5 C2. Estimators

Block 4. Aortic-valve-opening detection

The features extracted in the signal processing (C1, block 2) were used in a linear discrimination algorithm (LDA) to detect the opening state of the aortic valve (block 4). The LDA was based on the minimization of the total probability of misclassifications. This allows a discrimination function to be determined. By assessing the location of a weighted linear combination of the calculated features relative to a threshold, the sample can be classified in indicating either an open or a closed aortic valve. The algorithm was fitted to in-silico data resulting from Experiments 1 and 2 as listed in Table 8.1 with a 34% contractility with respect to the physiological one.

Block 5. Mean aortic pressure estimation

The mean aortic pressure (MAP) was also estimated for monitoring the afterload of the circulation. To estimate the MAP with the following algorithmic steps, the aortic valve should first be detected as open. Then, based on the PIP gradient, the time close to an aortic valve opening is detected, where the PIP equals the diastolic aortic pressure (AoP_{dias}). Furthermore, as the aortic valve has opened, the SP detected approximates the systolic aortic pressure (AoP_{sys}). Thus, the MAP can be calculated by the known equation $MAP = (2 \cdot AoP_{dias} + AoP_{sys})/3$.

Block 6. Heart rate estimation

The HR is extracted by calculating the time between two consecutive SP detections (block 6).

8.3.6 C3. Controllers

Block 7. Pump-flow-adaptation controller

The last part of the multi-objective physiological control system used the indices extracted from the measured and estimated signals to control the pump speed and generate a physiological pump flow. A purely preload-based approach was used to adapt the pump flow to the requirements of the circulation. The EDP was extracted at every heartbeat and served as an input to a proportional controller which aims at imitating the linear part of the Frank-Starling curve of the physiological heart [233]. The speed was updated according to the equation

$$PS_{des} = PS_{ref} + (EDP - EDP_{ref}) * K_p \quad (1)$$

8.3 Materials and Methods

where PS_{ref} and EDP_{ref} are the pump speed and EDP values defined during calibration, i.e., when the initial PS is defined, while K_p is the proportional gain which equaled 300 rpm/mmHg. For this purpose, in-vitro experiments were repeated while increasing the gain stepwise. The very high gains were defined that led to sustained oscillations during a pump speed increase and very low gains that led to suction during a pump speed decrease. Then, the final gain was selected such that it differed from the “limit” gains at least by a factor of two. Thus, a good performance against suction was achieved while avoiding oscillations.

Block 8. Aortic-valve-opening controller

The knowledge of the state of the aortic valve opening (block 4) was used to adapt the pump speed and influence the state of the aortic valve as desired. The control of the aortic valve opening is based on the user(clinician)-defined open and close thresholds. For example, if the aortic valve is consecutively closed longer than the “closed” threshold, the pump speed is linearly decreased until an aortic valve opening is detected. The pump speed remains low until the aortic valve has opened at least for the time defined by the “open” threshold. The pump speed then returns linearly to the pump speed defined by the pump flow adaptation controller (block 7).

The desired opening time of the aortic valve can lead to quite different responses of the control system presented. For example, assuming a very diseased heart, trying to keep the aortic valve open during exercise conditions may lead to limited perfusion as the heart is not able to pump enough blood through the valve. This condition has been proven clinically by Camboni et al. [234]. To prevent such a condition, we added a pump speed threshold ($PS_{thres} = 4600$ rpm, corresponding to an EDP above 13 mmHg) and applied a different objective of the aortic-valve-opening controller above and below this threshold. Therefore, the open and closed times and the PS ranges within which these times apply are adjustable and lead to various modes of operation of the aortic-valve-opening controller (“mode” input variable).

For our study, three different modes were defined and tested under all experiments described in the Experiments section. Table 8.2 lists these different modes of operation. Mode 1 aims at a regular opening and closing of the valve regardless of the physiological requirements of the circulation. Mode 2 tries to always keep the valve open below the PS_{thres} , whereas it keeps the aortic-valve-opening controller deactivated above the PS_{thres} . Mode 3 aims at keeping the valve open at all times. In the latter case, the PS was set to operate close to a closing status of the aortic valve to limit the loading of the LV when the valve is open.

Table 8.2: Modes of operation of the aortic-valve-opening controller. The pump speed threshold (PS_{thres}) was set at 4600 rpm for all modes. The symbol ∞ indicates the requirement of a continuously open aortic valve.

Mode	Below PS_{thres}		Above PS_{thres}	
	Open time	Close time	Open time	Close time
1	5 s	15 s	5 s	15 s
2	∞	0	AoV controller deactivated	
3	∞	0	∞	0

Block 9. Safety controller

After the aortic-valve-opening controller, a safety controller (block 9) was implemented that ensures a safe operation by preventing pump speeds that may lead to complications, such as LV suction, LV overload, and pump backflow. For the case of suction, the ratio of negative pressures within a heartbeat, named suction index (SI), are detected and fed into a PI controller ($P = 2500$ rpm/SI, $I = 125$ rpm/SI) that lowers the pump speed to remove the suction event. For the detection and release of LV overload, the EDP measurement is being used. A predefined EDP threshold was set at 20 mmHg to indicate overload. The

difference between the measured EDP and the threshold is fed into a PI controller that increases the pump speed to resolve the overload ($P = 250 \text{ rpm/mmHg}$, $I = 12.5 \text{ rpm/mmHg}\cdot\text{s}$). This controller is only activated after 10 consecutive heartbeats with an EDP above 20 mmHg. To detect and release pump backflow events, the minimum pump flow from block 3 is used. A PI controller with the minimum pump flow as input is implemented to achieve a continuously positive pump flow by increasing the pump speed ($P = 30 \text{ rpm}\cdot\text{s/ml}$, $I = 20 \text{ rpm/ml}$). Anti-reset windup techniques were incorporated to all the PID controllers implemented to prevent overshooting due to accumulated error. All gains were tuned according to the method followed for the pump-flow-adaptation controller to have a safe margin against too high or too low gains.

Block 10. Pulsatile speed modulation

The last part of the system aimed at increasing the aortic pulse pressure (AoPP). A sinusoidal PS modulation has been implemented that is synchronized to the heartbeat. The synchronization to the heartbeat was based on the SP per heartbeat detection. Based on results from a previous study about the influence of the phase shift on AoPP [85], a co-pulsating mode with a fixed phase shift of 90% (with respect to SP) was applied. The mean value of the sinusoidal waveform was defined by the pump-flow-adaptation controller or the aortic-valve-opening controller.

Block 11. Speed-amplitude controller

The amplitude of the waveform was controlled such that a positive minimum pump flow was ensured, thus preventing backflow (block 11). An operation close to backflow enabled the maximum AoPP without any possible complications, e.g. blood damage due to backflow. The amount of AoPP achieved depends on the pump characteristics and the contractility of the circulation.

8.3.7 *Prioritization of the controllers*

The various controllers included in the multi-objective control system presented call for contrary responses in certain situations, e.g. when for a specific patient condition not all objectives set are met. For example, it may happen that the PS should be greatly decreased to open the aortic valve to the point that backflow may occur. As such cases, may be inevitable where controllers are in conflict with each other, an adjustable prioritizing concept has been implemented. The safety controller has the first priority, followed by the aortic-valve-opening and the pump-flow-adaptation controllers. By high priority, we define the controller that is most important to define the desired pump speed. If a higher-prioritized controller is active, all lower-prioritized controllers are locked and cannot further influence the mean pump speed. Thus, their output remains the same as the output at the time the higher-prioritized controller became active. This prevents any abrupt speed changes such as when the speed control changes from the first- to the second-priority controller and back.

The prioritization concept is implemented via logic operators. When the safety controller becomes active, it defines the desired pump speed of the LVAD while all other controllers are locked. The locking is implemented by setting the inputs to all other controllers to zero, thus preventing any reaction from these controllers. Compared to a complete deactivation of these controllers, this not only prevents any sudden jump in the desired pump speed, but also any influence from the lower prioritized controllers on the desired speed. Otherwise, the pump speed is defined by the aortic-valve-opening and the pump-flow-adaptation controllers. If the aortic valve status is as desired by the user/clinician, then the pump-flow-adaptation controller regulates the desired pump speed. Else, the aortic-valve-opening controller regulates the pump speed and the pump-flow-adaptation controller is locked.

8.4 Results

8.4.1 Signal processing (C1) and estimators (C2)

The aortic-valve-opening detection algorithm was evaluated over all the experiments of the study (all three categories described in the Experiments section), such that unseen data are included. Each experiment was executed with all three modes of the AoV opening controller, thus leading to a total of 30 different experiments of 120 s each. The accuracy of the algorithm was 82.33% for the open status and 93.46% for the closed status, while the overall accuracy was 86.35%. Furthermore, the detection of the EDP, SP, HR and the estimation of the MAP were evaluated over the same pool of experiments. The mean absolute errors achieved were: 3.61 mmHg for the EDP, 1.38 mmHg for the SP, 1.86 bpm for the HR and 5.34 mmHg for the MAP. Figure 8.3 shows an example of the pump inlet and aortic pressures measured over three heartbeats. The values detected during signal processing and the estimated MAP are depicted (asterisks) together with the real values (circles).

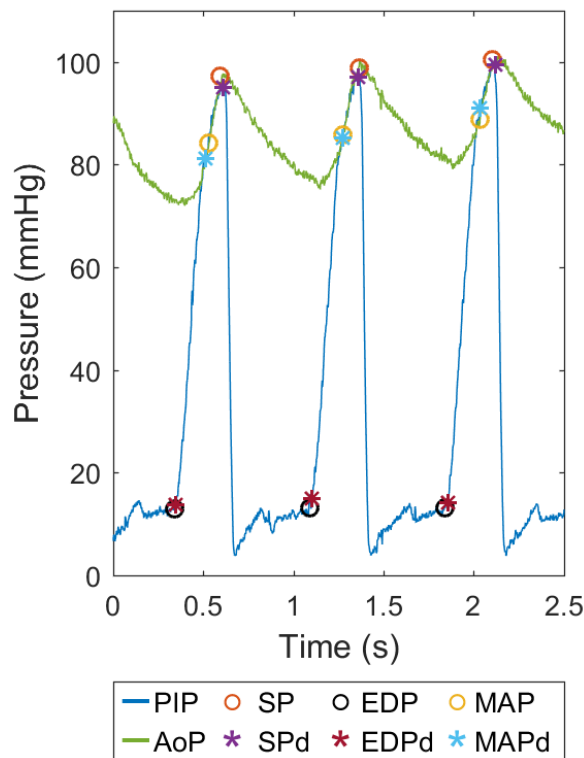


Figure 8.3: Example of detection algorithms during the experiments of the study. The measured signal of pump inlet pressure (PIP) and aortic pressure (AoP) are depicted. The values detected in real-time of the systolic pressure (SPd), the end-diastolic pressure (EDPd), and the mean aortic pressure (MAPd) are indicated by asterisks, while the real values of SP, EDP, and MAP are indicated by circles.

8.4.2 Control system

Figure 8.4 shows the performance of the multi-objective physiological control system during preload and afterload variations. The aortic-valve-opening controller was operated with mode 1. The signals of the pump speed (PS), mean PS (\overline{PS}), mean pump flow (\overline{PF}), cardiac output (CO), pump backflow (backPF), aortic valve flow (AoVF), MAP, AoPP, and EDP are depicted. During preload increase, the \overline{PS} and speed amplitude increased, following the changes of the EDP and leading to a \overline{PF} and MAP increase. However, due to the PS decrease, they all decreased approximately every 15 s to enable an aortic valve opening, which the positive

AoVF clearly shows. During a preload decrease, \overline{PS} decreased due to an EDP decrease and reached the low limit of 2 krpm. This low speed caused backflow and, therefore, the safety controller slightly increased the \overline{PS} after 100 s to release it. To avoid backflow, the pulsatile speed modulation as well had to be deactivated after 95 s. Some backflow still occurred during the experiment when the speed amplitude was varied.

Additionally, Figure 8.4 shows the practical implementation of the prioritization concept of the various controllers during the preload variations. Particularly, from 60 to 80 s, the pump-flow-adaptation controller requires a PS increase due to the increased EDP. However, according to user settings, the aortic valve should stay open. As, the aortic-valve-opening controller has a higher priority than the pump-flow-adaptation, this is the one that defines the pump speed. At $t = 65$ s the LV is overloaded, which activates the safety controller (orange line) to overwrite the aortic-valve-opening controller (purple line) and define the \overline{PS} of the pulsatile speed modulation such that the LV overload is released.

The afterload decrease caused a strong decrease of the MAP. The \overline{PS} and \overline{PF} in turn decreased due to the EDP decrease. Despite that, the CO remained unchanged as the AoVF increased, which yielded an AoPP of around 28 mmHg. The afterload increase increased the MAP and the EDP. Thus the \overline{PS} and the \overline{PF} increased according to the actions of the pump-flow-adaptation controller. The \overline{PF} increase led to an aortic valve closure and the CO decreased slightly. At $t = 100$ s, the \overline{PS} started to decrease to enable an aortic valve opening, as it remained closed for more than 15 s (mode 1). For both experiments, the green, purple, red, and blue \overline{PS} signals show how differently the pump-flow-adaptation controller, the aortic-valve-opening controller, the safety controller, and the pulsatile speed modulation, respectively, control the PS during the experiments.

Figure 8.5 presents the same signals as Figure 8.4, but for Experiments 3 and 4 listed in Table 8.1. During a contractility increase (Exp 3) after $t = 20$ s, the \overline{PS} slightly decreased due to the EDP decrease, while the pulsatile speed modulation was operated with a decreased speed amplitude to prevent backflow. At the same time, the AoVF and AoPP increased while the MAP and CO remained unchanged. When contractility decreased, the LVAD support increased by increasing the \overline{PS} and \overline{PF} , while the speed amplitude of the pulsatile speed modulation was increased. At approximately $t = 80$ s and $t = 100$ s, a prolonged aortic valve closure was detected that led to an LVAD support decrease such that the valve opened, which in turn yielded an EDP greater than 20 mmHg. During exercise, due to the preload increase, the LVAD support increased by increasing the \overline{PS} , the \overline{PF} , and the speed amplitude of the pulsatile speed modulation. Thus, the CO and AoPP increased at 8 L/min and 28 mmHg, respectively, whereas the MAP and EDP remained unchanged. The aortic valve never stayed closed for more than 15 s during exercise. Therefore, no regular reduction in the PS was recorded. If the circulation settings would return to their initial values of resting conditions, the physiological control system would restore the hemodynamics as well. Results that prove this ability of the control system presented are provided within the supplementary material.

Figure 8.6 shows the various performance effects of the multi-objective physiological control system during the exercise experiment, but when an LVAD was regulated which supports a circulation whose contractility decreased from 34% to 17%. The experiment was repeated while operating the aortic-valve-opening controller in all three modes of the aortic-valve-opening controller (Table 8.2). The signals of \overline{PS} , \overline{PF} , AoVF, MAP, and EDP are depicted for each mode. With Mode 1, a regular opening of the aortic valve was achieved. During exercise ($t > 20$ s), the \overline{PS} , the \overline{PF} , and the MAP in turn dropped (between approximately $t \in [30, 50]$ s, $[65, 80]$ s and $[95, 110]$ s) to let the valve open, leading to an EDP above 20 mmHg for a few seconds. When the valve stayed closed, a \overline{PF} of approximately 8 L/min resulted, whereas during the time of an opened aortic valve the \overline{PF} dropped below 5 L/min. With Mode 2, the valve status was not controlled during exercise, as the desired \overline{PS} of the pump flow adaptation controller was above the given PS_{thres} . This mode yielded the higher \overline{PF} and MAP among all modes, while it kept the EDP at around 11 mmHg.

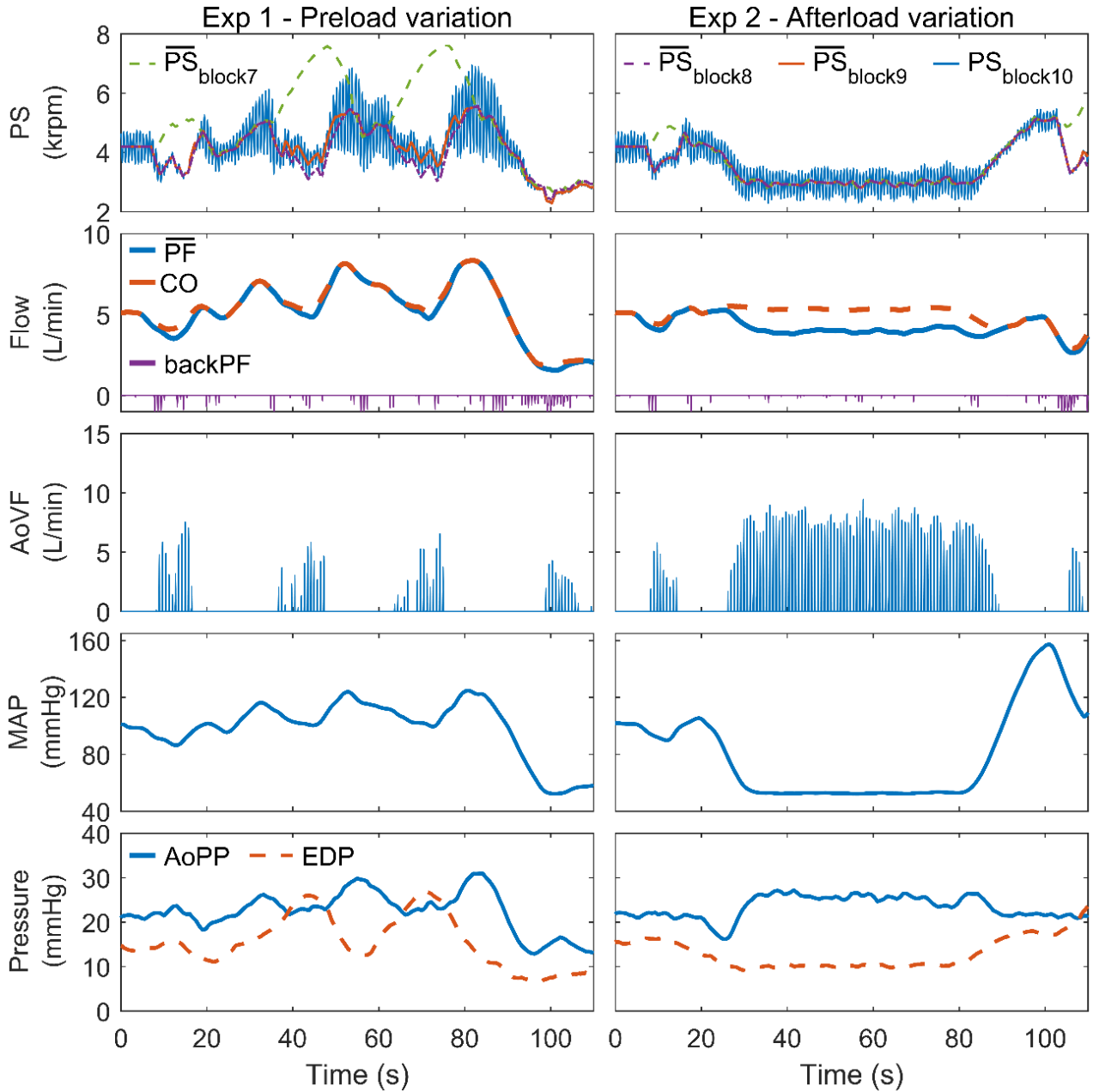


Figure 8.4: Performance results of the multi-objective physiological control system under Experiments (Exp) 1 and 2 (pre- and afterload variations). The aortic-valve-opening controller was operating in Mode 1 (Table 8.2). The signals of pump speed (PS) and mean PS (\overline{PS}), mean pump flow (\overline{PF}), cardiac output (CO), pump backflow (backPF), aortic valve flow (AoVF), mean aortic pressure (MAP), aortic pulse pressure (AoPP), and end-diastolic pressure (EDP) are depicted. The additional $\overline{PS}_{block,i}$ depicted in the two top panels correspond to the outputs of blocks 7-10 as illustrated in Figure 8.2.

Finally, with Mode 3, the valve status was controlled such as to stay always open during the whole experiment, thus leading to an EDP above 20 mmHg during exercise ($t > 20$ s). For this case, the LV overload controller of the safety controller was deactivated in order to better observe the influence of Mode 3 on the EDP. Despite the high EDP, the \overline{PS} did not increase, as it would due to the pump flow adaptation controller, in order to keep the aortic valve open (according to our prioritization). The abrupt \overline{PS} increase and decrease were due to the effort of the multi-objective controller to operate slightly above the \overline{PS} that leads to a closed valve, i.e., to keep the aortic valve open while avoiding an overload of the LV. Despite these \overline{PS} changes, the

\overline{PF} remained almost unchanged except below 5 L/min. The limited perfusion led to very low values of MAP of 60 mmHg.

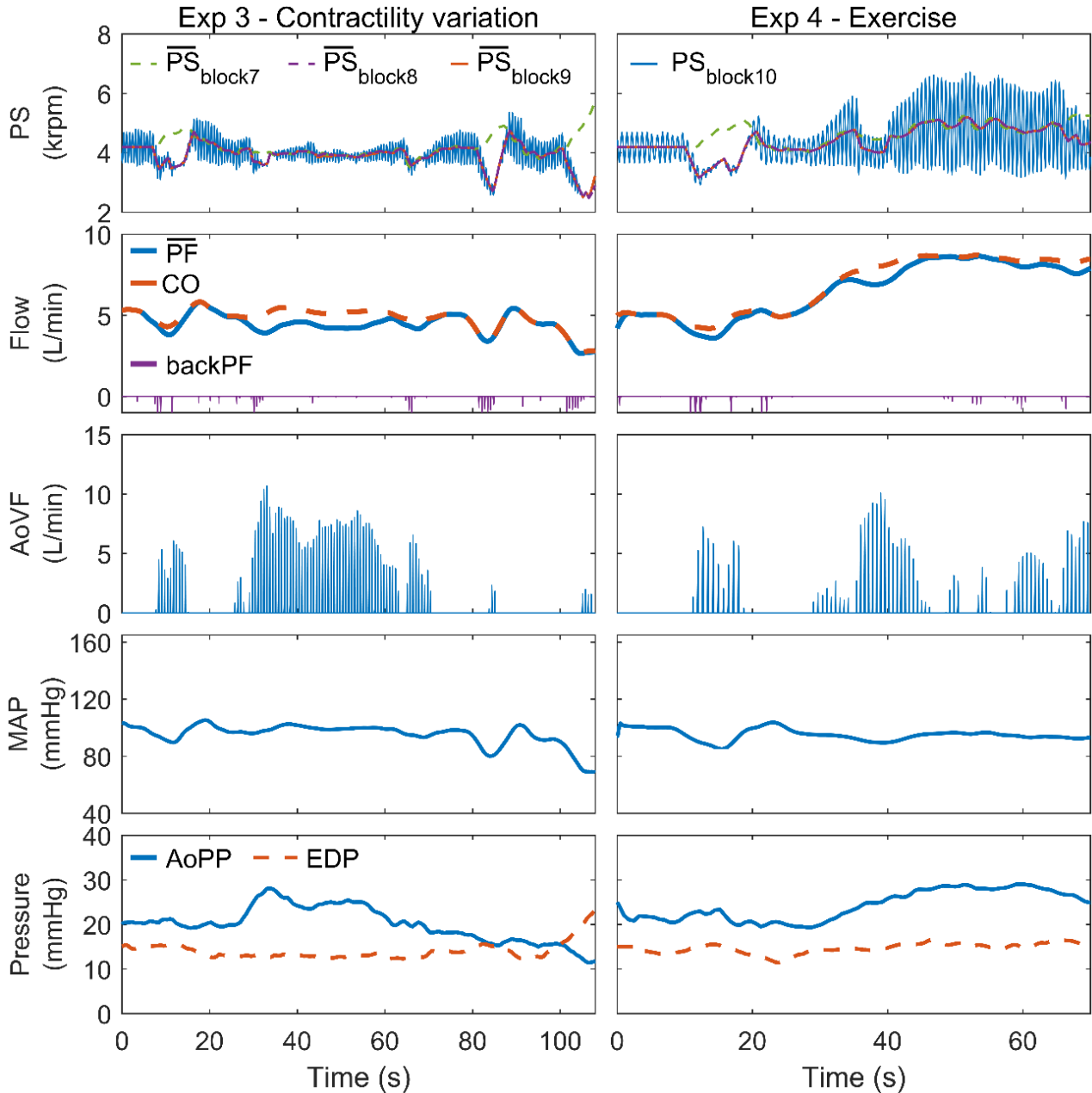


Figure 8.5: Performance results of the multi-objective physiological control system under Experiments (Exp) 3 and 4 (contractility variation and exercise). The aortic-valve-opening controller was operating in Mode 1 (Table 8.2). The signals of pump speed (PS) and mean PS (\overline{PS}), mean pump flow (\overline{PF}), cardiac output (CO), pump backflow (backPF), aortic valve flow (AoVF), mean aortic pressure (MAP), aortic pulse pressure (PP), and end-diastolic pressure (EDP) are depicted. The additional $\overline{PS}_{block,i}$ depicted in the two top panels correspond to the outputs of blocks 7-10 as illustrated in Figure 8.2.

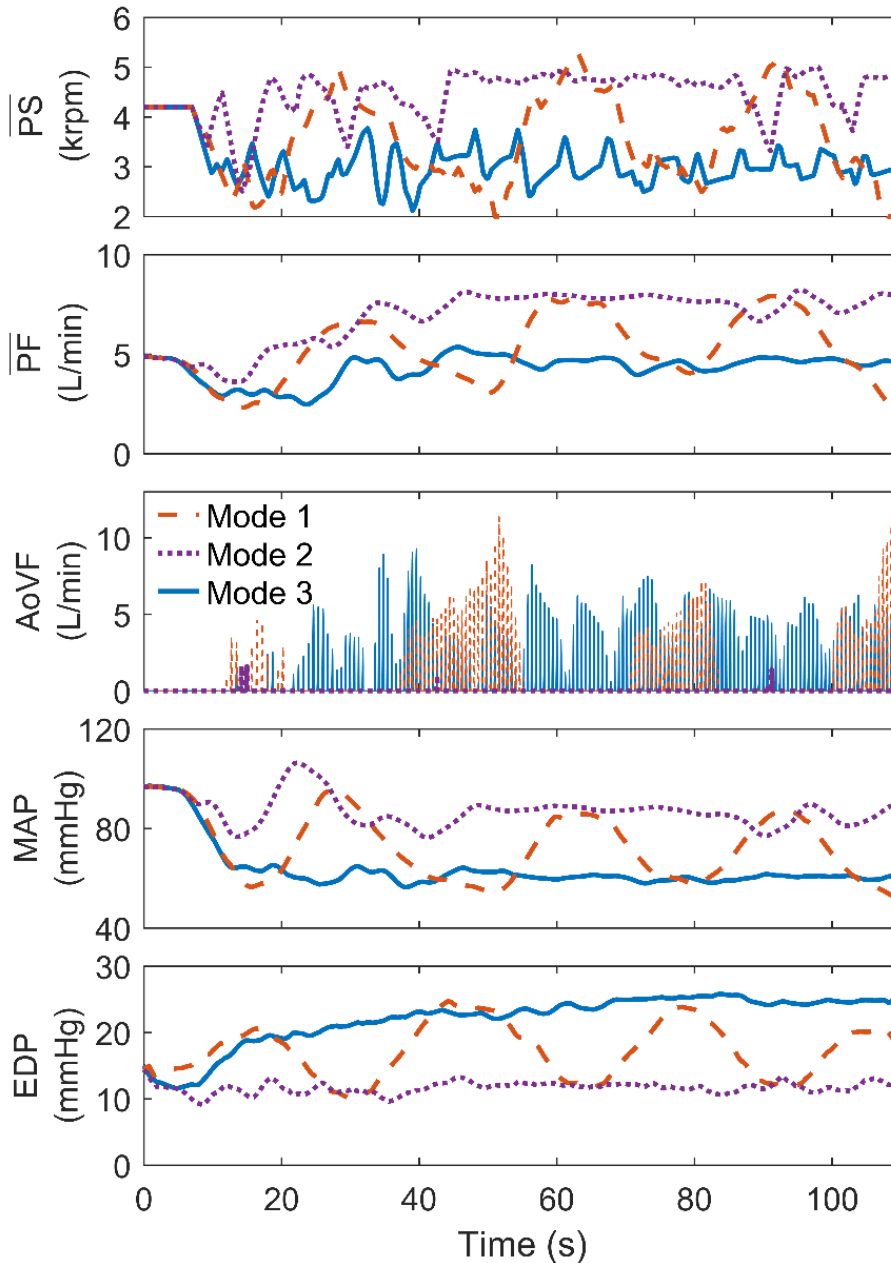


Figure 8.6: Performance results of the multi-objective physiological control system under Experiment 4 (exercise) with a decreased contractility of 17% and when the aortic-valve-opening controller is operated with each of the three modes (Table 8.2). The signals of mean pump speed (\overline{PS}), mean pump flow (\overline{PF}), aortic valve flow (AoVF), mean aortic pressure (MAP), and end-diastolic pressure (EDP) are shown.

8.5 Discussion

The current study presents a novel multi-objective, physiological control system, which, to our knowledge, is the first to incorporate the described functionalities based on a single pressure sensor alone at the inlet of an LVAD. Here, the DP2 was used as an LVAD, but the control system can be implemented in any clinical rotary LVAD after adapting the gains. The controller has been extensively evaluated *in vitro* and has met the set requirements during preload, afterload, and contractility variations. The PS was regulated such that it adapts to varying physiological requirements, augments the AoPP, and enables a controlled aortic valve opening. It was surrounded by algorithms that provided important indices for the monitoring of a pathological circulation assisted by an LVAD, such as the status of the aortic valve, the afterload conditions, and the cardiac rhythm.

Safety features were implemented to ensure a safe operation by overwriting and compensating any failures of the control system. Thus, no suction events occurred, which was not the case during the same pre- and afterload decrease experiments with a constant speed LVAD, as previously presented by Petrou et al. [78] A prioritization concept was successfully implemented to switch among the different controllers. The pump speed signals in Figure 8.4 and Figure 8.5 show the effect of this prioritization.

In our system, an EDP-based pump flow adaptation controller was used. This approach is highly intuitive when it is used to aim at imitating the Frank-Starling mechanism. A similar approach with a proportional controller was presented by Kwan-Gett et al. [117] **Error! Reference source not found.** many years ago, but it was based on the measurement of the left atrial pressure (LAP). A preload-based pressure-control system was recently presented by Stevens et al. [126] and Mansouri et al. [235], but they used EDP together with pump flow. Bullister et al. [71] used the minimum diastolic pressure as an input for a physiological controller, but their approach required the pump outlet pressure data as well. Another preload-based pump flow adaptation controller, which uses the end-diastolic volume, was developed by Ochsner et al. [65] The benefit of preload-based controllers had been described by Tchantchaleishvili et al. [89] and was proven in vitro by Pauls et al. [80] as well as in vivo by Ochsner et al. [83].

A feedback controller that is more dynamic for pulsatile speed modulation is presented here. Thus far, all studies that presented pulsatile speed modulation approaches were based on feedforward approaches and were mainly investigating the influences of phase shift and amplitude [85]. To our knowledge, no experiments under varying physiological requirements have been presented that operate the LVAD in a pulsatile mode. The feedforward approach may lead to backflow when PS is not high enough to overcome the afterload conditions, especially if the LVAD design leads to flat pump characteristics. Ando et al. [174] proposed the counterpulsation as a method to avoid backflow, but it limits the potential increase in AoPP. In the control system presented, we dynamically vary the parameters of the periodic speed waveform and thus achieve the maximum possible AoPP, which here is three times higher than without pulsatile speed modulation, while we limit the negative effects. Despite the backflows observed (Figure 8.4 and Figure 8.5), which resulted from the overshoot of the speed-amplitude controller, the performance can be improved by increasing the desired reference minimum pump flow, for instance. Furthermore, we showed that by using the PIP, we can robustly synchronize the pump speed with the heartbeat, while up to now, ECG was the main approach for synchronization [90].

Despite the effort to increase the AoPP, the authors acknowledge that the amount of pulsatility required and its positive effects remain controversial [236]. Furthermore, an AoPP increase alone cannot guarantee improved hemodynamics, while there are additional indices that need to be investigated, such as the gradient of the AoPP [237]. However, the proposed control system may constitute the basis for a reliable system that can support the efforts to answer the questions concerning the required pulsatility and its benefits without inducing any new problems, such as additional blood damage due to backflow [237].

Various approaches to detect an aortic valve opening have been proposed in literature. Ooi et al. [232] used the pump speed to detect a non-opening state, whereas Granegger et al. [215] used the estimated pump flow to detect the state of the aortic valve. Jansen-Park et al. [238] presented an invasive approach to detect the pump speed that leads to aortic valve closure based on the pump inlet pressure and the pump power. Granegger et al. [215] evaluated their approach even clinically, but with stable hemodynamics. None of these approaches have been evaluated under varying physiological requirements and with contractility changes or together with a pump-flow-adaptation controller. Although the idea of an aortic-valve-opening controller had been proposed earlier, here we present the performance of such a system that would allow the clinician to predefine the opening time of the valve together with additional controllers, such as the pump-flow-adaptation controller.

The opening of the aortic valve constitutes a crucial condition for the LVAD patients as it can prevent aortic valve insufficiency and decrease the possibility of thrombogenicity at the aortic root [239]. Furthermore, a switch of the LVAD operation such that it closes or opens the aortic valve can be related to a switch between maximum unloading to decrease the stroke work, to increase the loading of the LV, and to allow a gradual

8.6 Conclusion

training of the heart muscle. In other words, such a control system would ensure that the patient remains in full or partial support as desired by the clinician. Thus, the risk of myocardial atrophy could be reduced and methods towards the myocardial recovery could be established.

Most of the physiological controllers proposed use gains which have been determined for a specific in-vitro circulation. An inappropriate gain due to interpatient variability may lead to values of PS that are too high and, therefore, cause aortic valve closure or even LV suction. Furthermore, backflow or even LV overload may occur when the PS is set too low. The novel multi-objective, physiological control system presented considers such events and constitutes a potential system for a robust performance even among various circulations.

8.5.1 Limitations

The authors acknowledge that the current study contains certain limitations, which would need to be addressed in the future. (1) So far, no reliable, long-term blood pressure sensor for VADs is available. However, much research is currently in progress in this area and promising results have been presented in literature [89], [240]. Therefore, it is reasonable to investigate the possible benefits of the usage of such a sensor. (2) We applied a white noise to the measured pump flow instead of using an estimator. Pump-flow estimators have already been described extensively in literature and are being used clinically (e.g., Heartmate 3, Abbott Laboratories Inc.). To avoid increasing the size and complexity of the manuscript we preferred not to include such an estimator within the control system presented. (3) Abrupt speed changes resulted from the proposed control system. It can be questionable how these speed accelerations influence the potential blood damage. However, state-of-the-art devices, such as the Heartmate 3, have implemented algorithms in clinical practice that cause fast speed changes to induce wash-out. (4) The implementation of the MAP estimator cannot be accurate during full support, i.e. when the aortic valve is continuously closed. It can be used only during a detected aortic valve opening. (5) The accuracy of the aortic-valve-opening algorithm in a clinical environment should be investigated further. Thus far, a clinical study has shown promising results for such an algorithm [215], while in our study the accuracy was sufficient even during changes of the physiological requirements and the contractility of the circulation. However, cases with mitral or aortic valve insufficiencies should also be considered as they may influence the accuracy of the algorithm. To account for such possible limitations and present a fail-safe behavior, a safety controller such as the one included in our control system is crucial, especially in a clinical environment.

8.6 Conclusion

The latest technological improvements promise the integration of a pressure sensor in an LVAD. This will broaden the possibilities for controlling the LVAD and monitoring the LVAD-supported pathological circulation. The current study shows the potential of the novel multi-objective physiological control system developed that only uses the signal of a pressure sensor at the pump inlet to control the speed of an LVAD. In-vitro results showed that our control system can adapt the pump flow to varying physiological requirements, increase the aortic pulse pressure, regulate the opening of the aortic valve, and ensure a safe operation while offering important hemodynamic variables for monitoring the circulation. To our knowledge, no physiological control system that serves for all these objectives has been presented in literature up to now. As a next step, in-vivo experiments would be required to further evaluate and improve these algorithms.

9 A Versatile HMC for Hydraulic Investigations of Cardiovascular Implants (Paper VIII)

9.1 Abstract

During the development process of active or passive cardiovascular implants, such as ventricular assist devices, or vascular grafts, extensive in-vitro testing is required. Aim of the study was to develop a versatile hybrid mock circulation (HMC) which can also support the development of such implants that have a complex interaction with the circulation. The HMC operates based on the hardware-in-the-loop concept with a hydraulic interface of four pressure-controlled reservoirs allowing the interaction of the implant with a numerical model of the cardiovascular system. Three different conditions were investigated to highlight the versatility and the efficacy of the HMC during the development of such implants: (1) biventricular assist device (BiVAD) support with progressive aortic valve insufficiency, (2) total artificial heart (TAH) support with increasing pulmonary vascular resistance, and (3) flow distribution in a total cavopulmonary connection (TCPC) in a Fontan circulation during exercise. Realistic pathophysiological waveforms were generated with the HMC and all hemodynamic conditions were simulated by only adapting the software. The result of the experiments indicated the potential of physiological control during BiVAD or TAH support to prevent suction or overload events, which may occur during constant speed operation. The HMC constitutes a reliable testing environment for the initial development steps of such devices and their control algorithms. In the Fontan case, the TCPC geometry influences the flow distribution between left (LPA) and right pulmonary artery, which was unbalanced and 10% higher in LPA and led to higher pressures. The HMC together with rapid prototyping methods may enhance the design of anatomic structures and improve their geometry before implantation to achieve better hemodynamics.

9.2 Introduction

The typical development process of active and passive cardiovascular implants, such as ventricular assist devices and vascular grafts, consists of several steps. It starts with the in-silico modeling of the hydraulic properties to virtually test the implant, continues with the in-vitro testing to verify the in-silico results with physical models before testing the device in vivo. In-vivo testing allows the validation of the performance of the implant in animals before proceeding with clinical testing and application. While in terms of pressures and flows in-silico hydraulic models and boundary conditions can be adjusted as desired to mimic a realistic hemodynamic scenario, such an adjustment is more demanding with in-vitro setups, which are required to accurately imitate real conditions.

Conventional hydraulic mock circuits to investigate the hydraulic properties of cardiovascular implants consist of tubes, open and air trapped reservoirs, valves, and cardiac simulators to simulate hemodynamic conditions [241]. However, undesired effects due to the fluid inertance may occur when tubes and valves are used, especially in the case of in-vitro imitation of the cardiovascular system, which constitutes a very dynamic and complex environment. Thus, realistic waveforms of pressure and flow characteristics cannot be achieved at high fidelity. Furthermore, the versatility of such mock circuits is limited since hardware changes are required whenever different conditions are to be tested. Systems are thus required to evaluate different cardiovascular implants efficiently and in a versatile way with realistic hemodynamic waveforms.

Such systems have been presented earlier for the evaluation of left ventricular assist devices (LVADs). Besides others [242]–[244], Ochsner et al. [97] used air- and vacuum-pressure regulated reservoirs to mimic the left ventricular (LVP) and the aortic pressures (AoP), which are computed by a numerical model of the cardiovascular system. This hybrid mock circulation (HMC) and operates based on the hardware-in-the-loop (HIL) approach. It can be used to evaluate LVADs and their control algorithms. In HMCs all components of the cardiovascular system are simulated numerically. The reservoirs, which are the main hardware parts of the

system, form the interface between the numerical model of the cardiovascular system and the LVAD. The numerical model can be of almost unlimited complexity, for instance to mimic any desired input impedance of the arterial vasculature [245], which cannot be achieved with a conventional hardware-based system. Furthermore, if any physiologic feedback control mechanisms of compliances, resistances, etc. are desired, the HIL interface provides advantages in terms of complexity: While with the numerical model the compliance value can be easily adjusted, in hardware-based loops the amount of air in an air-trapped reservoir needs to be adjusted using a pneumatically controlled system for each reservoir.

In this study, the technology of the HMC developed earlier with two pressure reservoirs [97] was extended to four reservoirs and the numerical model adapted according to the specific investigation. This versatile HMC allows to test complex active and passive cardiovascular implants, such as biventricular assist devices (BiVADs), total artificial hearts (TAHs), and total cavopulmonary connections (TCPCs) for Fontan patients, i.e., patients with a single-functional ventricle who underwent the Fontan procedure, i.e., the surgery where the caval veins are directly connected to the pulmonary arteries to palliate their symptoms yielding a TCPC. Currently, 10% to 30% of LVAD recipients develop right-ventricular (RV) failure [246], and in many cases a BiVAD support treatment is followed. The outcomes of BiVAD support with rotary blood pumps has been worse than with LVAD support [32], [247]. The fluid balance between the pulmonary and the systemic circulation is challenging with two pumps running at constant speeds. Therefore, appropriate test setups to investigate new control methods of physical devices in an early development phase are required to verify in-silico methods to control and adapt the two pumps to each other and to the physiologic requirements of the circulation.

When the biventricular failure is treated with a TAH [248], the hydraulic performance of the device and its interaction with the cardiovascular system are crucial and should be evaluated at an early development phase using appropriate in-vitro facilities. The lack of neurohumoral cardiac response during TAH support constitutes a challenge for any physiologic adaptation of the device to the demands of the patient [249] and the control of the left/right fluid balance remains a challenging topic [250]. Finally, in the case of Fontan patients with a TCPC, no power is added to the blood on the sub-pulmonary side and any pressure drop due to the geometry of the TCPC impedes a sufficient venous return [251]. Simulated flow fields and pressure losses in the TCPC need to be validated in vitro with realistic flows and vascular impedances.

The versatile HMC developed can be employed for evaluating the performance of BiVADs and TAHs and their control algorithms, when interacting with the cardiovascular system. Furthermore, it allows the assessment of the influence of the TCPC geometry on Fontan hemodynamics, such as the resulting pressure losses, under various pathophysiological conditions.

9.3 Materials and Methods

In all three test cases presented, the same hardware setup was used and only the software part, i.e., the numerical model of the cardiovascular system, was adapted. Both hardware and software parts are described below in detail.

9.3.1 Hardware

Figure 9.1 depicts a schematic overview of the hardware parts of the HMC developed, which is divided into the hydraulic and the pneumatic system. The hydraulic system consists of four pressure reservoirs (PR1-PR4) whose pressures are controlled as desired by using pressurized air and vacuum, while pressure sensors are used for the feedback signals (PN2009, IFM Electronic GmbH, Essen, Germany). Additional hardware includes four ultrasound flow probes (CO.55/190, Sonotec Ultraschallsensorik Halle GmbH, Halle, Germany), four pressure transducers for monitoring inline pressures (TruWave, Edwards, Lifesciences, Irvine, CA, USA), and three reflux pumps (two Jabsco 18660 Series, Xylem Inc., NY, USA and one S-pump, Xenios AG, Heilbronn, Germany). The pneumatic system consists of one vacuum pump (ZL112-K15LOUT-E26L-Q, SMC Pneumatics, Tokyo, Japan), one vacuum chamber and proportional solenoid valves, one inlet valve (PVQ33-5G-23-01F, SMC Pneumatics) for connecting each reservoir with the compressed air from the network supply, and two outlet valves (PVQ33-5G-40-01F, SMC Pneumatics) for connecting each reservoir with the vacuum chamber. These valves were controlled to achieve the desired pressures in the respective four reservoirs.

The methods to control the pressure of the reservoirs via pressurized air and vacuum as well as to control the fluid level of the reservoirs by making use of the reflux pumps in the hydraulic part have been described earlier in detail [97]. The HMC operates as follows: The volume flow rates are measured and fed into the numerical model, which computes the pressures to be applied to the reservoirs in real time. These pressures of the hydraulic interfaces are applied to the active or passive cardiovascular implant tested and produce new volume flow rates, which are fed back to the numerical model, causing the loop to continue.

9.3.2 Software

Figure 9.2 presents the three different numerical models of the cardiovascular systems used in each test of this study. Each model consists of four main parts, the left heart (red), the right heart (blue), the pulmonary circulation (light gray) and the systemic circulation (dark gray). The arterial and venous systems were simulated by five- and three-element Windkessel models, respectively, resulting in different arterial input impedances. In the case of the testing of the TAH configuration, no active ventricular models were employed. The lumped parameter models for the BiVAD and TAH cases were adopted from Colacino et al. [123] Based on that model, control mechanisms for the unstressed venous volume, the systemic venous and arterial resistances, as well as the pulmonary arterial resistance were implemented. For the univentricular cardiovascular system, the model was derived from Granegger et al. [252], which also included control mechanisms for the systemic and pulmonary arterial resistance as well as the unstressed venous volume. Furthermore, heart rate and maximum elastance control mechanisms were incorporated, analogously to those described by Colacino et al. [123] A detailed description of the model is provided in the supplementary material. The numerical models were implemented in MATLAB/Simulink running with Real-Time Windows Target (The Mathworks Inc., Natick, MA, USA). Two data acquisition boards (MF634 multifunction I/O card, Humusoft s.r.o., Prague, Czech Republic) were used for the in- and outputs of analog signals.

9.3.3 Active cardiovascular implant

The HVAD (Medtronic Inc., Minneapolis, MN, USA) was used as an active cardiovascular implant for our study. Two HVADs were used for both the BiVAD and the TAH configuration experiments. To control the HVAD speed as desired, an in-house speed controller was developed. The control unit was based on a control board (LAUNCHXL-F28069M, Texas Instruments, Dallas, TX, USA) with two DC drive stage modules (BOOSTXL-DRV8305EVM, Texas Instruments, Dallas, TX, USA) for the two motors of the pump. The control algorithm of the HVAD motor was realized by using sensorless field-oriented control. The control unit was communicating with the data acquisition card of the HMC, thus setting the desired pump speed and recording the values of the actual speed and current. The speed can be set in the range of 1800 – 4000 rpm, similarly to the original control system. In both BiVAD and TAH configuration experiments, the HVAD speed desired was either set at a constant value or dynamically controlled with a physiologic controller.

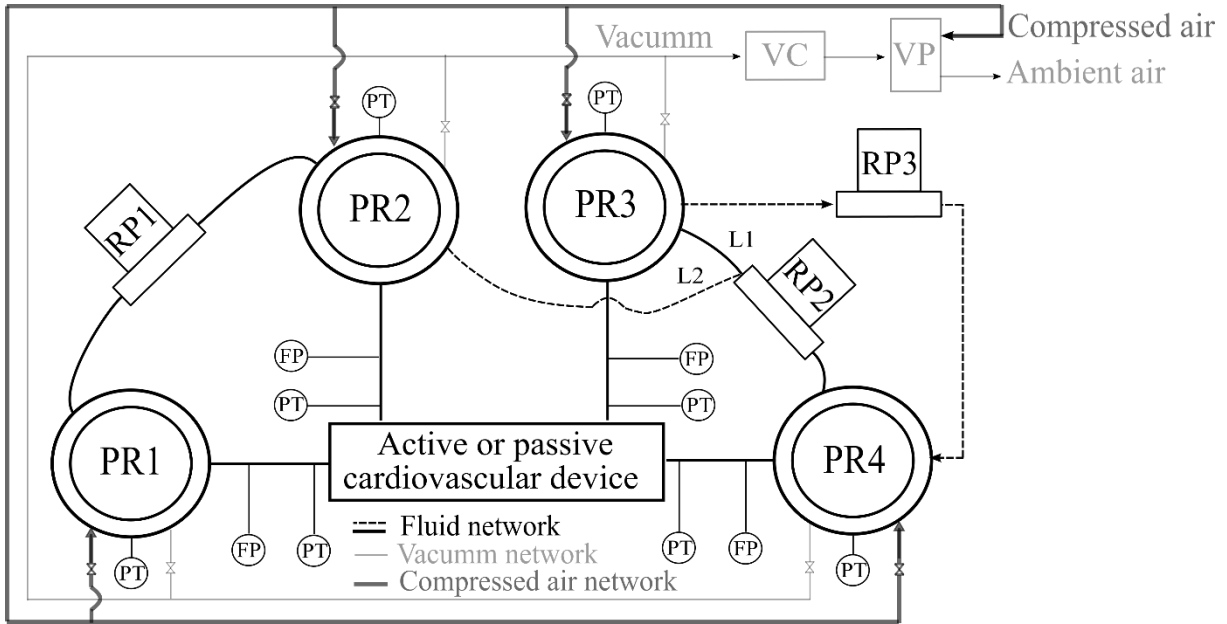


Figure 9.1: Scheme of the hardware parts of the versatile hybrid mock circulation developed. It consists of four pressure reservoirs (PR1-PR4), three reflux pumps (RP1-RP3), one vacuum chamber (VC), one vacuum pump (VP), eight pressure transducers (PTs) and four flow probes (FPs). For the Fontan experiment, the dashed line (L2) replaces the solid line (L1). The RP3 is only used during the Fontan experiment.

9.3.4 Test case 1: BiVAD support during aortic valve insufficiency

A pathological circulation of an adult patient with biventricular failure was simulated with reduced RV and LV ejection fractions of 30% and 20%, respectively [247]. Both ventricles were supported with an HVAD whose speed was adjusted to yield a cardiac output (CO) of 5 L/min. Figure 9.3 - left depicts the HVAD configuration on the HMC. A resistance element was added at the outflow of the RVAD to reduce the flow by increasing the pressure head across the pump while keeping the operating speed between 1800 and 4000 rpm [246].

The pressure in the reservoirs PR1 – PR4 represented the pulmonary arterial (PAP), the right ventricular (RVP), the left ventricular (LVP) and the aortic pressures (AoP), respectively. In this study we simulated the implantation of the RVAD into the RV, unlike another possibility that is commonly reported, which features an RVAD implantation in the right atrium [246]. To investigate the fluid balance between the systemic and the pulmonary vasculature during BiVAD support, we simulated a transition from mild to severe aortic insufficiency (AI), which seems to occur in a large number of patients supported by continuous-flow VADs [253]. For this purpose, the resistance of the aortic valve was adapted during baseline conditions to result in regurgitant fractions of less than 30% and greater than 50%, respectively [254].

This transition experiment was conducted twice. First, both HVADs were operated at a constant speed such that 5 L/min were supplied to the pulmonary and the systemic circulation in the baseline condition, where LAP and RAP were 12.5 mmHg and 2.7 mmHg, respectively. For the second case, both HVADs were controlled to keep either preloads in a physiologic range. This algorithm was implemented to control the end-diastolic pressure (EDP) by a simple proportional controller, which increased the HVAD speed with increasing preload, as presented earlier [95] and described in equation (1):

$$N_{des} = k_{edp} (EDP - EDP_{ref}) + N_{ref}, \quad (1)$$

where k_{edp} is the proportional gain (rpm/mmHg), EDP_{ref} is the set point EDP (mmHg) defined during calibration, i.e., while adjusting the reference speed N_{ref} (rpm).

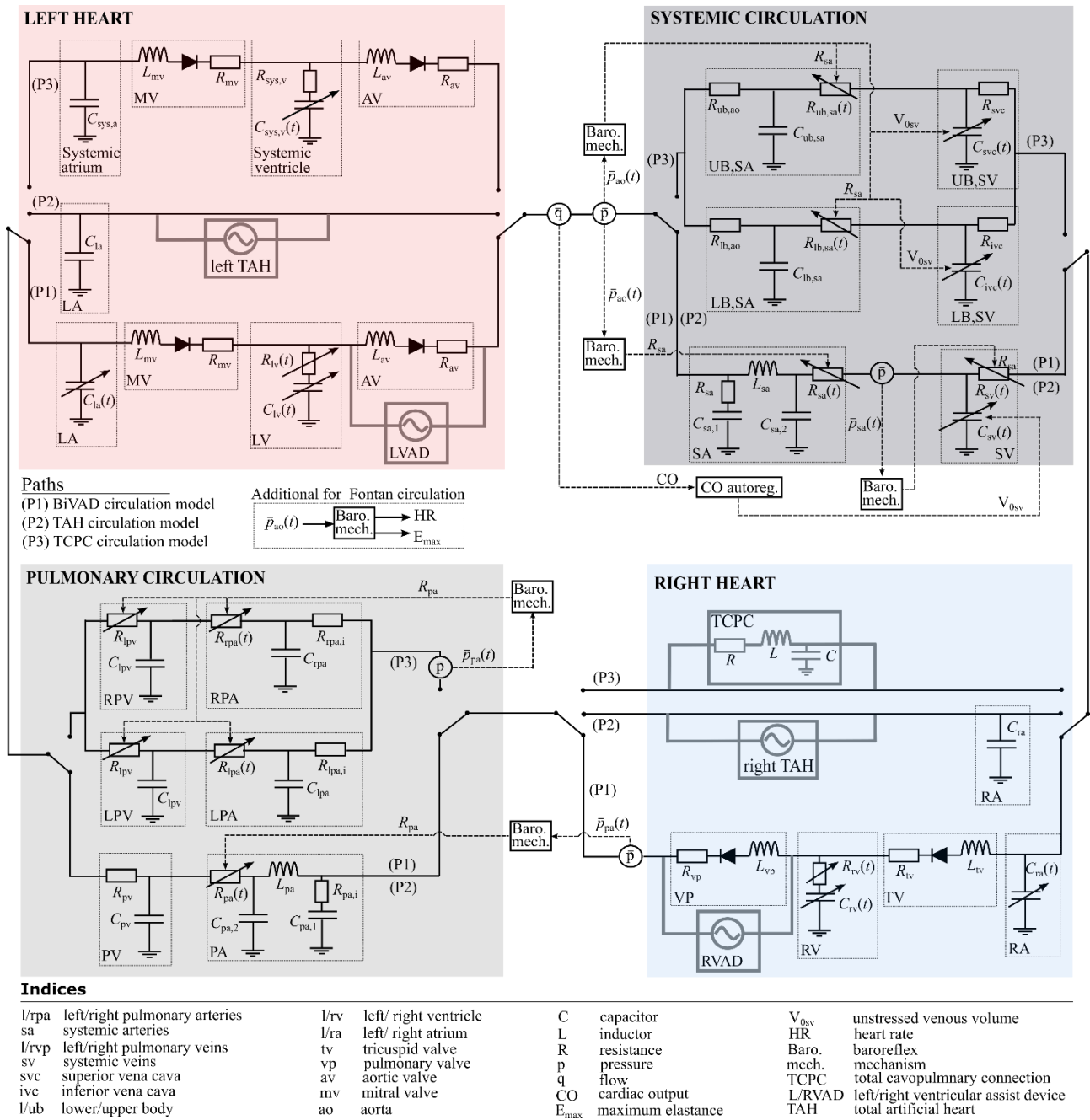


Figure 9.2: Electric analog of the numerical models of the cardiovascular system used in this study. Path 1 (P1) corresponds to the biventricular assist device (BiVAD) test case, Path 2 (P2) to the total artificial heart (TAH) test case, and Path 3 (P3) to the total cavopulmonary connection (TCPC) test case. Grey lines indicate the interfaces of the respective devices to the numerical model. The additional control mechanisms for heart rate and maximum elastance are only used for the Fontan circulation based on Granegger et al. [252].

9.3.5 Test case 2: TAH-configuration support during increase of the pulmonary vascular resistance

The model of the circulatory system employed in Test case 1 was also used for Test case 2, but without a simulation of the ventricles. Thus, the pressures in PR1 – PR4 represented the pulmonary arterial, the central venous, the pulmonary venous, and the aortic pressures, respectively. The two HVADs were now serving as a TAH configuration, thus pumping from a passive left or right atrium to the aorta or the pulmonary artery, respectively. A five-fold PVR increase from 0.1 to 0.5 mmHg·s/mL was applied [255] to simulate the clinical condition of pulmonary hypertension, which may occur in VAD patients [256] and lead to fluid imbalance

9.4 Results

problems. This experiment was conducted under two different control cases of the HVADs. First, they were operated at a constant speed, such that a pump flow and CO of 5 L/min resulted. Then, the experiment was repeated while the HVADs were controlled to keep the preloads in a physiologic range by controlling the LAP and RAP, i.e., by applying the control structure of equation (1) and by replacing the EDP with LAP and RAP, respectively. Figure 9.3 - left also depicts the HVAD configuration used on the HMC for this test case.

9.3.6 Test case 3: TCPC flow distribution during rest and exercise

A rigid model of a TCPC was used as a passive cardiovascular implant. The geometry was derived from a patient who followed Fontan completion. For this purpose, cardiovascular magnetic resonance (CMR) imaging datasets were acquired from the patient. The TCPC geometry was 3D-printed with a polymer material (Polyamide 12). The 3D-printed TCPC geometry was evaluated when coupled with a numerical model of a univentricular cardiovascular system, which had been developed previously [252]. That model includes closed-loop baroreflex and metabolic reflexes (as illustrated in Figure 9.2) to simulate exercise. Increased power loss in the TCPC during exercise conditions has been reported to greatly influence the clinical outcomes of Fontan patients [98] and thus requires investigation to develop new solutions. In our study, a baseline condition at rest was compared to an exercise level of three metabolic equivalents of tasks (METs) by recording the pressures and flow distribution within the TCPC. Figure 9.3 - right depicts the implementation of the TCPC on the HMC developed.

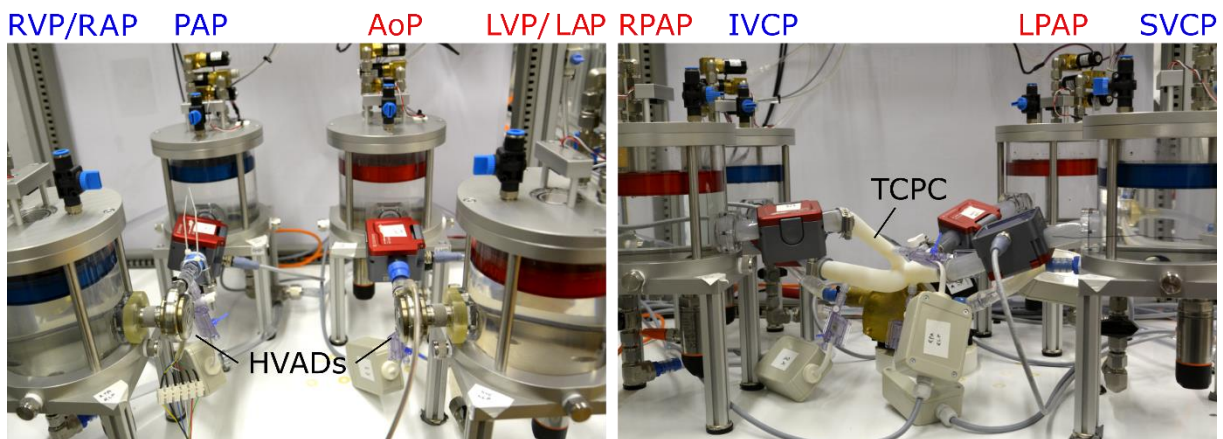


Figure 9.3: Left: Picture of the hybrid mock circulation (HMC) during the BiVAD and TAH configuration experiments with the two HVADs installed. Right: Picture of the HMC during the Fontan experiments with the 3D printed total cavopulmonary connection (TCPC). RVP, right ventricular pressure; RAP, right atrial pressure; AoP, aortic pressure; LVP, left ventricular pressure; LAP, left atrial pressure; RPAP, right pulmonary arterial pressure; IVCP, inferior vena cava pressure; LPAP, left pulmonary arterial pressure; SVCP, superior vena cava pressure.

9.4 Results

9.4.1 Test case 1: BiVAD support during aortic valve insufficiency

Error! Reference source not found. and **Error! Reference source not found.** show the in-vitro results obtained during BiVAD support with mild and severe AI with and without physiologic control. **Error! Reference source not found.** depicts the signals of the measured pump speed (PS) and pump flow (PF) as well as the simulated flows through the aortic and pulmonary valves. Figure 5 depicts the pressure-volume (PV) loops for the left and the right ventricles. During constant-speed BiVAD support, the AI progression led to an increase in LV preload, with an LV EDP elevation from 15 to 24 mmHg, respectively. That preload increase, in turn led to an LVAD PF increase from 6.2 to 7.5 L/min, but the corresponding CO decreased from 4.9 to 4 L/min due to the increased regurgitant flow. The RVAD PF decreased by 1 L/min due to the RV

preload decrease, which resulted from the blood volume shift to the pulmonary circulation as well as the afterload increase. The RVAD speed remained at 2200 rpm and as a result, excessive unloading with negative pressures and consequent RV suction occurred (as depicted by the RV PV loops in blue in Figure 9.5). In the case of physiologically controlled pumps, the PS of the LVAD increased to 3300 rpm and the RVAD PS decreased to 2000 rpm during the AI progression. Negative pressures were also observed in Figure 9.5 in the RV PV loops in black and red. The reason for those was the limited ability of the pneumatic pressure controllers [97] of the hydraulic interface to accurately apply a positive pressure close to 0 mmHg to the pressure tanks. Yet, they were not corresponding to suction. The LVEDP increased from 15 to 19 mmHg at a CO of 4.9 and 4.5 L/min, respectively. The LVAD PF increased to 9.5 L/min, while the RVAD PF decreased to 4.5 L/min. The pressure-volume loops of the RV changed marginally, showing a slight preload decrease.

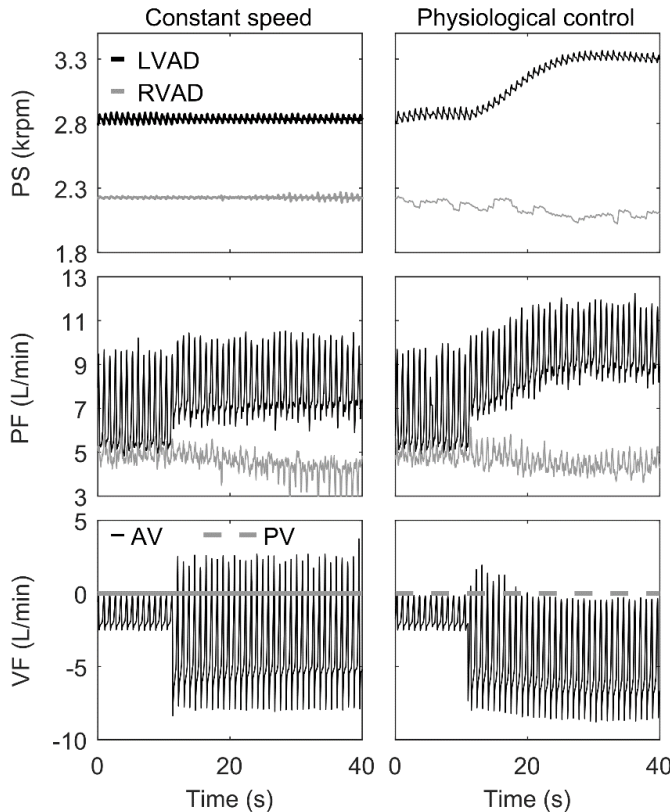


Figure 9.4: Measured and simulated signals during the biventricular support test case. The signals of the measured pump speed (PS) and flow (PF) as well as the simulated valve flows (VF) of the aortic and pulmonary valve (AV and PV, respectively) are depicted.

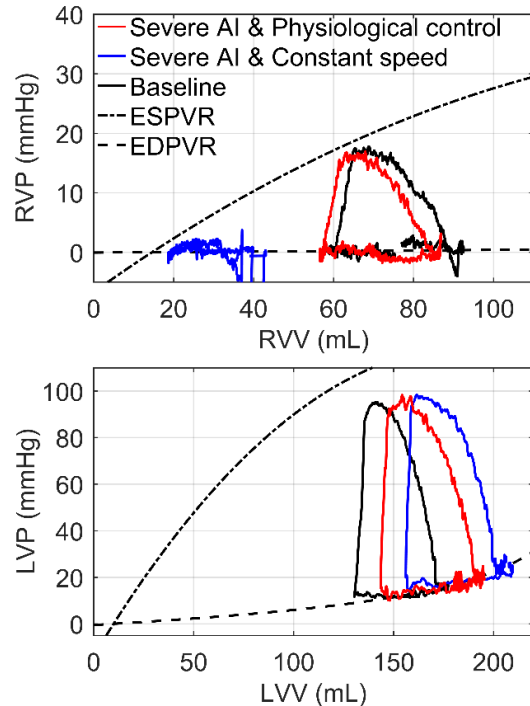


Figure 9.5: Pressure-volume loops of the right (RVP-RVV) and left ventricles (LVP-LVV) during the biventricular support test case. Loops during mild and severe aortic insufficiency (AI) are depicted. The end-diastolic and end-systolic pressure volume relationships are also illustrated (EDPVR and ESPVR, respectively).

9.4.2 Test case 2: TAH-configuration support during increase of the pulmonary vascular resistance

Error! Reference source not found. depicts the in-vitro performance of the TAH configuration consisting of two HVADs during a PVR increase. The measured signals of the PS and PF are presented together with those of the LAP, AoP, RAP and PAP. In the constant-speed case, the RVAD flow decreased due to the PVR increase and the lack of speed adaptation, which led to a preload decrease for the LVAD. The LVAD speed did not decrease and, therefore, negative LAPs occurred at $t > 25$ sec. With physiologic control, the LVAD speed decreased by approximately 400 rpm and the RVAD speed increased by 200 rpm after the PVR increased, thus keeping an equal pump flow between the LVAD and the RVAD. The RAP and LAP remained almost constant, whereas the AoP decreased and the PAP increased.

9.4.3 Test case 3: TCPC flow distribution during rest and exercise

Figure 9.7 depicts the in-vitro results of the univentricular circulation at the transition from rest (1MET) to moderate exercise (3METs) conditions. At rest, the flow of the inferior vena cava (IVC) was three times greater than the one of the superior vena cava (SVC). Due to the asymmetric geometry of the TCPC, the left pulmonary arterial (LPA) flow equaled 2.4 L/min and was 0.5 L/min higher than the right pulmonary arterial (RPA) flow. The IVC and SVC pressures were equal, while the LPA pressure was 0.5 mmHg higher than the RPA pressure. These differences were also observed during the exercise condition: The IVC flow increased by 1.5 L/min, but remained three times larger than the one of the SVC. The difference between LPA and RPA slightly increased up to 0.8 L/min, while the LPA flow equaled 3.6 L/min, thus keeping the flow ratio equal to that observed in rest conditions, i.e., approximately 55% for LPA and 45% for RPA flow. The SVC and IVC pressures increased by approximately 2 mmHg and they remained equal with each other. At the bottom of Figure 9.7, the LVP and AoP are presented. The signals show that the HR increased from around 75 bpm at rest to around 105 bpm during exercise.

During all the experiments, the root mean-square errors between the pressures computed by the numerical models and the pressures applied within the pressure reservoirs remained below 3 mmHg.

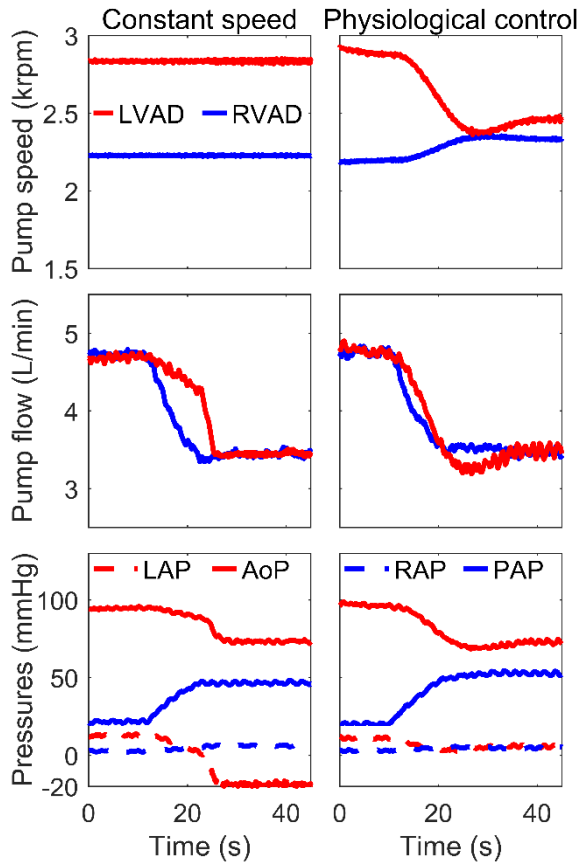


Figure 9.6: In vitro performance of a TAH configuration consisting of two HVADs and operating either at constant speed or with physiological control during an increase of pulmonary vascular resistance. The signals of the pump speeds and flows as well as of the pulmonary venous (PVP), the aortic (AoP), the central venous (CVP), and pulmonary arterial (PAP) pressures are depicted.

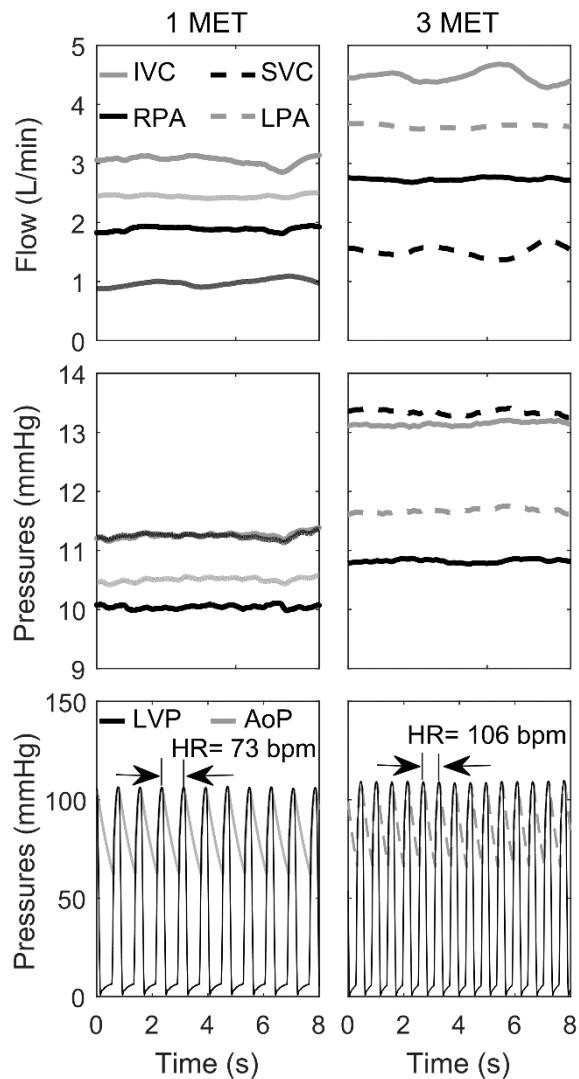


Figure 9.7: In vitro results of the TCPC when interacting with the simulated Fontan circulation under 1 (left) and 3 (right) Metabolic equivalents of task (METs). The flows and pressures for the inferior and superior vena cava (IVC and SVC, respectively), as well as the left and right pulmonary arteries (LPA and RPA, respectively) are depicted. The left ventricular and the aortic pressures (LVP and AoP, respectively) are also shown in the bottom plots, as well as the heart rate (HR) increase from rest to exercise.

9.5 Discussion

In this study, a new HMC was presented that allows the evaluation of the performance of complex active and passive cardiovascular implants. It is able to accurately apply the pressures computed by numerical models to the hydraulic interface used, thus enabling a reliable interaction between the implant and the model. It offers a high flexibility during testing, as various clinical scenarios can be simulated simply by varying parameters of the model while avoiding hardware interventions. Thus, the performance of active implants and their control algorithms as well as that of passive implants can be evaluated before in-vivo testing. The flexibility and

9.5 Discussion

versatility of this HMC was proven with three test cases which required only software adjustments and the exchange of the device to be evaluated.

The principle of operation of the HMC developed is considered superior to existing approaches. The Donovan mock circulation, which is the best-known conventional system, was developed in 1975 and was recently used to evaluate the SynCardia TAH in vitro [257]. It constitutes a pure hardware system that does not use any numerical model of the cardiovascular system. In contrast, in semi-hybrid systems, some of the components of the cardiovascular system are represented by physical components, such as tubes and tanks to mimic resistances, inertances and compliances. Timms et al. [241] introduced such a system to evaluate BiVAD cases. The ventricles are imitated by pneumatically-actuated chambers, equipped with solenoid valves that control the inflow and outflow of the pressurized air. A passive diastolic filling of the ventricles is simulated by venting these valves. As a result, the system relies on the inherent compliance of the trapped air, which may limit the generation of high-frequency, physiologic waveforms. Arterial and pulmonary Windkessel components were similarly imitated by proportional-controlled pinch valves to adjust resistances and air-trapped reservoirs with adaptable air volume to adjust the compliances. Tubes and connections are inevitable in such a system. The fluid inertia, which is an important contributor to vascular input impedances [258], thus cannot be adjusted as desired. Similar approaches have been presented by Schampaert et al. [259], who implemented positive-displacement pumps to represent the ventricles and a polyurethane tube to mimic the elastic aortic properties or by Ruiz et al. [260], who used rubber bellows actuated by positive displacement pumps to model the atria and ventricles. Such semi-hybrid systems have also been used to evaluate a mechanical circulatory support (MCS) device for the Fontan circulation [261].

In mock loops employing physical models of heart valves, an adjustment of the desired regurgitant fraction of an insufficient valve is cumbersome since it must be mechanically induced. In our setup, the resistance of the valves towards backflow was numerically adjusted (by a change of a parameter in software) in such a way that the amount of regurgitation matched the one recorded clinically [254]. Furthermore, suction events with a realistic morphology in pump signals cannot be achieved in passive mock loops, which in our case was possible by using an approach developed earlier [148]. However, investigation and testing of devices under such conditions is crucial since these are realistic worst-case scenarios, for instance bearings of rotary blood pumps. Otherwise, such events can only be tested with less realistic environments or in-vivo trials.

Clinical-use cases during BiVAD and TAH support were investigated in the HMC presented; namely experiments with AI progression during BiVAD support and PVR increase during TAH support. When operating these devices in constant speed, the problem of the fluid imbalance between systemic and pulmonary circulation was reproduced. Such conditions may lead to suction and pulmonary or systemic venous congestion. The conditions simulated matched well the published results of animal experiments under BiVAD support with and without physiologic control [250]. We showed that the implementation of simple physiologic controllers can mitigate the risk of suction or congestion and create more physiologic conditions during BiVAD and TAH therapy. However, long-term, implantable pressure sensors are required for any clinical implementation of these advancements, whose development is still ongoing [56], [240].

The investigation of TCPC properties under realistic hemodynamic conditions, for instance at rest and exercise, is necessary to verify the results of in-silico studies with computational fluid dynamics [98]. The combination of closed-loop baroreflex functionality and physical hydraulic properties of complex geometric TCPC structures provides a unique insight into their interaction. Employing rapid prototyping techniques, TCPC geometries of MR/CT images can be manufactured [98], and pressures as well as flow distributions within the TCPC can be investigated at a fast pace under various conditions. Therefore, the HMC offers a novel, reliable testing environment for passive cardiovascular implants and the assessment of their hydraulic properties in combination with their physiologic effects.

Apart from the cases presented, the HMC developed can be used for other experiments, such as evaluating artificial or mechanical valves, other grafts with multiple in- and/or outlets (e.g. prosthetic replacements of the aortic arch) as well as for evaluating the use of MCS devices in Fontan patients or the BiVAD case with an RVAD pumping from the right atrium to the pulmonary artery. In general, this versatile HMC can be used for any case where one to four pressures interact with a device.

9.5.1 Limitations

A main limitation of this study is the lack of validation of the numerical models used with clinical observations. We used a model described by Colacino et al. [123], which has been validated for investigating

the interaction between a physiologic heart and its pre- and afterload. Studies were focused on LVAD-supported cases. By modifying that model, a new validation is required for the circulation with biventricular failure, TAH support, and the Fontan circulation. However, due to the lack of clinical data, this constitutes a challenging topic. Only for the circulation with biventricular failure was it possible to find clinical data [247] as well as for the simulation of AI [254], and the effort was to match the model with these values. Despite that, reasonable qualitative results were obtained which matched previous animal studies [250]. Future work should be focused on validating these numerical models such that they constitute a reliable testing environment which behaves more similarly to the in-vivo setting.

9.6 Conclusion

With its unique versatility and flexibility, the HMC presented constitutes a valuable tool for researchers that supports the development and investigation of complex active or passive cardiovascular implants such as TAHs and TCPCs. Its principle of operation allows for the generation of realistic pathophysiologic signal waveforms and the simulation of various clinical conditions. Thus, new devices and their control algorithms can be evaluated extensively at an early stage of development. Further research is required to prove the fidelity of the numerical models used. However, the conditions simulated were reasonable and proved the importance of physiologic control during BiVAD and TAH support to prevent unphysiologic flow conditions, which may occur during a constant-speed operation. The combination of rapid testing of TCPC geometries with such an HMC was realized to reveal unequal flow distributions and high pressure drops at the TCPCs. Such information is crucial and may support to optimize the TCPC design before the implantation.

10 Conclusion and Outlook

10.1 Conclusion

This thesis describes the development of a novel multi-objective control and monitoring system for VADs which only relies on the pump inlet pressure. This system consists of various control and monitoring algorithms. The ones that have already been proposed with different methods were compared extensively.

First, the feasibility study of a pump-flow-adaptation controller, the SP controller was presented in Chapter 2. The controller was evaluated *in vitro* and proved its potential to enable a physiological adaptation of the speed of a turbodynamic VAD to the perfusion requirements of a VAD patient. Thus, over- and underpumping were eliminated. Its performance remained robust against excessive simulated sensor drift.

The SP controller was then compared with another five, promising pump-flow-adaptation controllers and the clinical standard of the CS operation. For this purpose, a reliable testing method was developed to allow a fair comparison among the controllers. Various physiological conditions and sensor drift cases were simulated *in vitro*. All controllers presented a better preload sensitivity than the CS operation. The SP controller was the most robust against sensor drift among the pressure-based controllers. However, it presented a high sensitivity to contractility variations, which may occur during long-term support and would require the recalibration of the controller to still avoid underpumping. The volume-based PRS controller, also developed in our group, behaved as desired when contractility variations and sensor drift were applied.

Acute animal studies with eight pig models were conducted to validate the promising *in-vitro* performance of the SP controller in a clinical environment. Additionally, the PRS controller was also included in the *in-vivo* study. Both controllers performed robustly *in vivo* and adapted the pump flow according to the Frank-Starling law of the heart, thus reducing the risk for suction and overload.

The acute pathophysiological events of Valsalva maneuver and PVCs were accurately simulated *in vitro*. The response of the PRS controllers was analyzed during such events. A very fast and aggressive response presented a high efficacy in preventing suction but may lead to low arterial pressures and backflow. Thus, the need for additional control system was indicated.

The development of a pump flow estimator was investigated to provide the control input for preventing backflow events as well as additional hemodynamic information. The first comparison study with all approaches published was conducted *in vitro* with various physiological conditions mimicked. The influence of the pump design on the performance of the estimators was identified. A new estimator, which consists a modification of an existing one and exploits the pump inlet pressure measurement was developed. This estimator proved to be less influenced by the pump type and improved the estimation of the minimum pump flow. However, all estimators presented a high sensitivity to viscosity changes.

A novel model that can predict the viscosity and, in turn, the HCT of VAD patients, was successfully developed using a modified machine learning method. This model used the pump inlet pressure signal and the pump-intrinsic signals as inputs. An *in-vitro* evaluation proved its robustness against variations of the physiological requirements of the circulation and its independency of the type of the turbodynamic VAD. Its performance promises a continuous HCT monitoring and a more reliable pump-flow estimation. Furthermore, such a model can be used to detect possible adverse events such as bleeding or thrombosis at an early stage, while the patient is discharged from the hospital. Thus, the supervision of VAD patients can be greatly enhanced, and the efficacy of the therapy may improve.

The development of a novel multi-objective control and monitoring system that consists of various algorithms which only rely on the pump inlet pressure was presented in Chapter 8. *In-vitro* experiments proved this system can adapt the pump flow to varying physiological requirements, increase the aortic pulse pressure, regulate the opening of the aortic valve, ensure a safe operation by preventing critical flow conditions, while offering important hemodynamic variables for monitoring the circulation. Despite contradiction in some objectives, the system presented a harmonic collaboration among the various algorithms. Thus, it broadens the potential for VAD control and allows a reliable investigation of the potential of physiological control in a

10.1 Conclusion

clinical environment in the future. To the best knowledge of the author, no physiological control system that serves for all these objectives has been presented in literature up to now.

An HMC with unique versatility and flexibility was developed. Such a testing environment is considered a valuable tool for researchers and industry that supports the development and investigation of complex active or passive cardiovascular implants, such as BiVADs, and TCPCs, respectively. Its principle of operation allows the simulation of various clinical conditions and the generation of realistic pathophysiological signal waveforms. Physiological control systems for BiVADs and TAHs were developed and tested on the HMC, proving the importance of control to prevent unphysiological flow conditions, which may occur during constant speed operation. This HMC can greatly support the optimization of the TCPC design pre-implantation by rapid prototyping and testing of TCPC geometries until sufficient hemodynamic performance is achieved.

10.2 Outlook

The future steps of this thesis can be divided into two main directions. One is the development of additional systems that will increase the monitoring and control possibilities of the multi-objective system developed. The author has already worked towards this direction and proposes the use of the pump inlet pressure to detect changes in contractility and relaxation properties of the LV. Animal and human studies have proven this possibility but for unsupported hearts. Very well controlled animal studies are required to prove this when a VAD is implanted. Additionally, the author has conducted the first steps towards the development of a cardiac output estimator. Using the recorded signals from the animal studies conducted in our group, the reliability of such an estimator can be investigated. Furthermore, the machine learning model for detecting the aortic valve opening has been further researched, compared with other from literature and improved. This new model needs to be incorporated in the system developed to increase the reliability of the aortic valve opening controller. The flow estimator and the HCT prediction model were also not incorporated in the final system and this constitutes future work. Especially for the HCT prediction model, its performance during online prediction remains to be evaluated.

The second direction includes the evaluation of the multi-objective system developed in a clinical environment. Although the SP controller has been already tested with animal models, further experiments with contractility variations are recommended to investigate its sensitivity to contractility in vivo. The flow estimators were tested with animal data, but not the HCT prediction model. For this purpose, a controlled study with blood is required to validate the model in a clinical environment. The model would have to be retrained. Different VADs are also recommended to be used to prove its independency of the pump type and their pump flow estimators. The evaluation of the multi-objective control system with animal models constitutes the biggest step forward. The control of the aortic valve opening constitutes an important part of the system and its performance should be carefully validated in vivo. Additionally, as the development of the pressure sensor within Zurich Heart Project progresses, chronic animal trials can be considered.

In this thesis, various, promising pump-flow-adaptation controllers were tested. Having developed a unique environment and protocol for testing such controllers, the performance of other approaches can be evaluated.

Only a part of the multi-objective control system was used to enable physiological control for the BiVAD support case. The implementation of the whole system for both left and right VADs and the investigation of their potential in such a case constitutes an interesting study. The HMC developed offers the appropriate environment for these investigations. Furthermore, it allows for testing the hydraulic performance of new and existing TAH prototypes, which so far have been tested in less sophisticated in-vitro environments. The HMC was used for one case with TCPC. A thorough study with optimized TCPC geometries that have been suggested by Children's National Medical Center, Washington, DC [98] may validate their findings and their CFD simulations. Additional studies with new technologies for Fontan patients, such as Fontan pumps and grafts with new materials can be conducted on the HMC developed.

References

- [1] E. Policy, “Radcliffe Cardiology,” vol. 9, no. 1, pp. 1–3, 2013.
- [2] G. Sunagawa, D. J. Horvath, J. H. Karimov, N. Moazami, and K. Fukamachi, “Future Prospects for the Total Artificial Heart,” *Expert Rev. Med. Devices*, vol. 4440, no. February, 2016.
- [3] E. L. Wu, M. C. Stevens, J. P. Pauls, and U. Steinseifer, *First-generation ventricular assist devices*, vol. di. Elsevier Inc., 2018.
- [4] P. M. Portner *et al.*, “First human use of an electrically powered implantable ventricular assist system,” *Artif Organs*, vol. 9, no. 3, 1985.
- [5] M. S. Slaughter *et al.*, “Advanced heart failure treated with continuous-flow left ventricular assist device,” *N Engl J Med*, vol. 361, no. 23, pp. 2241–2251, 2009.
- [6] P. Rose, Eric A; Gelijns, Annetine C; Moskowitz, Alan J; Heitjan, Daniel F; Stevenson, Lynne W; Dembitsky, Walter; Long, James W; Ascheim, Deborah D; Tierney, Anita R; Levitan, Ronald G; Watson, John T; Meier, “Long-Term Use of a Left Ventricular Assist Device,” *N. Engl. J. Med.*, vol. 345, no. 20, pp. 1435–1443, 2001.
- [7] J. K. Kirklin *et al.*, “Seventh INTERMACS annual report: 15,000 patients and counting,” *J. Hear. Lung Transplant.*, vol. 34, no. 12, pp. 1495–1504, 2015.
- [8] P. Jilma-Stohlawetz *et al.*, “Acquired von Willebrand factor deficiency caused by LVAD is ADAMTS-13 and platelet dependent,” *Thromb. Res.*, vol. 137, pp. 196–201, 2016.
- [9] J. G. Rogers, R. R. Bostic, K. B. Tong, R. Adamson, M. Russo, and M. S. Slaughter, “Cost-Effectiveness Analysis of Continuous Flow Left Ventricular Assist Devices as Destination Therapy,” *Circ. Heart Fail.*, 2011.
- [10] J. K. Kirklin *et al.*, “Eighth annual INTERMACS report: Special focus on framing the impact of adverse events,” *J. Hear. Lung Transplant.*, vol. 36, no. 10, pp. 1080–1086, 2017.
- [11] G. Foster, *Third-generation ventricular assist devices*. Elsevier Inc., 2018.
- [12] J. G. Rogers *et al.*, “Intrapericardial Left Ventricular Assist Device for Advanced Heart Failure,” *N. Engl. J. Med.*, vol. 376, no. 5, pp. 451–460, 2017.
- [13] M. R. Mehra *et al.*, “A Fully Magnetically Levitated Circulatory Pump for Advanced Heart Failure,” *N. Engl. J. Med.*, vol. 376, no. 5, pp. 440–450, 2017.
- [14] “International Society of Heart and Lung Transplantation.” [Online]. Available: <https://www.ishlt.org/registries>.
- [15] S. F. Marasco, R. Summerhayes, M. Quayle, D. McGiffin, and M. Luthe, “Cost comparison of heart transplant versus left ventricular assist device therapy at one year,” *Clin Transpl.*, 2016.
- [16] U. P. Jorde *et al.*, “Results of the destination therapy post-food and drug administration approval study with a continuous flow left ventricular assist device: A prospective study using the INTERMACS registry (interagency registry for mechanically assisted circulatory support,” *J. Am. Coll. Cardiol.*, vol. 63, no. 17, pp. 1751–1757, 2014.
- [17] M. Guglin and L. Miller, “Myocardial recovery with left ventricular assist devices,” *Curr. Treat. Options Cardiovasc. Med.*, vol. 14, no. 4, pp. 370–383, 2012.
- [18] B. A. Bruckner *et al.*, “Regression of fibrosis and hypertrophy in failing myocardium following mechanical circulatory support,” *J. Hear. Lung Transplant.*, vol. 20, no. 4, pp. 457–464, 2001.
- [19] M. L. Ogletree-Hughes, L. B. Stull, W. E. Sweet, N. G. Smedira, P. M. McCarthy, and C. S. Moravec, “Mechanical unloading restores beta-adrenergic responsiveness and reverses receptor downregulation in the failing human heart,” *Circulation*, vol. 104, pp. 881–886, 2001.
- [20] P. M. Heerd *et al.*, “Chronic unloading by left ventricular assist device reverses contractile dysfunction and alters gene expression in end-stage heart failure,” *Circulation*, vol. 102, no. 22, pp. 2713–9, 2000.
- [21] E. J. Birks *et al.*, “Remission from stage D heart failure (RESTAGE-HF): early results from a prospective multi-center study of myocardial recovery,” *J. Hear. Lung Transplant.*, vol. 34, no. 4, pp. S40–S41, 2015.
- [22] M. Guglin and L. W. Miller, “Left Ventricular Assist Device as Destination Therapy,” vol. 1, no. 2, pp. 75–84, 2014.
- [23] R. J. Gordon *et al.*, *Prospective, multicenter study of ventricular assist device infections*, vol. 127, no. 6. 2013.

References

- [24] J. G. Allen *et al.*, “Quality of life and functional status in patients surviving 12 months after left ventricular assist device implantation,” *J. Hear. Lung Transplant.*, vol. 29, no. 3, pp. 278–285, 2010.
- [25] A. D. Enriquez, B. Calenda, P. U. Gandhi, A. P. Nair, A. C. Anyanwu, and S. P. Pinney, “Clinical impact of atrial fibrillation in patients with the HeartMate II left ventricular assist device,” *J. Am. Coll. Cardiol.*, vol. 64, no. 18, pp. 1883–1890, 2014.
- [26] S. D. Gregory, D. Timms, N. Gaddum, D. G. Mason, and J. F. Fraser, “Biventricular assist devices: A technical review,” *Ann. Biomed. Eng.*, vol. 39, no. 9, pp. 2313–2328, 2011.
- [27] R. L. Kormos *et al.*, “Right ventricular failure in patients with the HeartMate II continuous-flow left ventricular assist device: Incidence, risk factors, and effect on outcomes,” *J. Thorac. Cardiovasc. Surg.*, vol. 139, no. 5, pp. 1316–1324, 2010.
- [28] S. Lee *et al.*, “Effects of the HeartMate II continuous-flow left ventricular assist device on right ventricular function,” *J. Hear. Lung Transplant.*, vol. 29, no. 2, pp. 209–215, 2010.
- [29] M. Argiriou *et al.*, “Right heart failure post left ventricular assist device implantation,” *J. Thorac. Dis.*, vol. 6 Suppl 1, pp. S52–9, 2014.
- [30] S. W. Pak *et al.*, “Prevalence of de novo aortic insufficiency during long-term support with left ventricular assist devices,” *J. Hear. Lung Transplant.*, vol. 29, no. 10, pp. 1172–1176, 2010.
- [31] J. A. Morgan *et al.*, “Management of Aortic Valve Insufficiency in Patients Supported Left Ventricular Assist Devices,” *ATS*, vol. 94, no. 5, pp. 1710–1712, 2012.
- [32] J. K. Kirklin *et al.*, “Eighth annual INTERMACS report: Special focus on framing the impact of adverse events,” *J. Hear. Lung Transpl.*, vol. 36, no. 10, pp. 1080–1086, 2017.
- [33] Z. T. Demirozu, W. B. Etheridge, R. Radovancevic, and O. H. Frazier, “Results of HeartMate II left ventricular assist device implantation on renal function in patients requiring post-implant renal replacement therapy,” *J. Hear. Lung Transplant.*, vol. 30, no. 2, pp. 182–187, 2011.
- [34] H. Schima, K. Dimitrov, and D. Zimpfer, “Debate,” *Curr. Opin. Cardiol.*, vol. 31, no. 3, pp. 337–342, 2016.
- [35] S. R. Patel and U. P. Jorde, “Creating adequate pulsatility with a continuous flow left ventricular assist device: just do it!,” *Curr. Opin. Cardiol.*, vol. 31, no. 3, pp. 329–336, 2016.
- [36] S. Islam, E. Islam, C. Cevik, H. Attaya, M. Otahbachi, and K. Nugent, “Aortic stenosis and angiodysplastic gastrointestinal bleeding: Heyde’s disease,” *Hear. Lung J. Acute Crit. Care*, vol. 41, no. 1, pp. 90–94, 2012.
- [37] M. S. Slaughter, “Hematologic effects of continuous flow left ventricular assist devices,” *J. Cardiovasc. Transl. Res.*, vol. 3, no. 6, pp. 618–624, 2010.
- [38] S. Dassanayaka, M. S. Slaughter, and C. R. Bartoli, “Mechanistic pathway(s) of acquired von willebrand syndrome with a continuous-flow ventricular assist device: In vitro findings,” *ASAIO J.*, vol. 59, no. 2, pp. 123–129, 2013.
- [39] A. Aggarwal *et al.*, “Incidence and management of gastrointestinal bleeding with continuous flow assist devices,” *Ann. Thorac. Surg.*, vol. 93, no. 5, pp. 1534–1540, 2012.
- [40] O. Wever-Pinzon *et al.*, “Pulsatility and the risk of nonsurgical bleeding in patients supported with the continuous-flow left ventricular assist device heartmate II,” *Circ. Hear. Fail.*, vol. 6, no. 3, pp. 517–526, 2013.
- [41] B. E. Braunwald, C. J. Frahm, J. Ross, J. R. With, and F. A. Bullock, “STUDIES ON STARLING ’ S LAW OF THE HEART . V . LEFT There is general agreement that the force of variations in ventricular filling and thus to permit contraction developed by strips of cardiac muscle an examination of Starling ’ s law of the heart . is a,” no. 50, pp. 1882–1890, 1961.
- [42] T. Tsukiya, T. Akamatsu, K. Nishimura, T. Yamada, and T. Nakazeki, “Use of motor current in flow rate measurement for the magnetically suspended centrifugal blood pump,” *Artif. Organs*, vol. 21, no. 5, pp. 396–401, 1997.
- [43] T. Kitamura *et al.*, “Physical model-based indirect measurements of blood pressure and flow using a centrifugal pump,” *Artif. Organs*, 2000.
- [44] M. Granegger, F. Moscato, F. Casas, G. Wieselthaler, and H. Schima, “Development of a pump flow estimator for rotary blood pumps to enhance monitoring of ventricular function,” *Artif. Organs*, vol. 36, no. 8, pp. 691–699, 2012.
- [45] A. Tanaka, M. Yoshizawa, K. I. Abe, H. Takeda, T. Yambe, and S. I. Nitta, “In vivo test of pressure head and flow rate estimation in a continuous-flow artificial heart,” in *Artificial Organs*, 2003.
- [46] M. Yoshizawa *et al.*, “Sensorless estimation of pressure head and flow of a continuous flow artificial heart based on input power and rotational speed,” *ASAIO J.*, 2002.

- [47] D. M. Karantonis, S. L. Cloherty, D. G. Mason, P. J. Ayre, and N. H. Lovell, "Noninvasive pulsatile flow estimation for an implantable rotary blood pump.," *Conf. Proc. IEEE Eng. Med. Biol. Soc.*, 2007.
- [48] A. H. Alomari *et al.*, "Non-invasive estimation of pulsatile flow and differential pressure in an implantable rotary blood pump for heart failure patients," *Physiol. Meas.*, 2009.
- [49] P. A. Giridharan, M. Skliar, M. Skliar, and G. A. Giridharan, "Physiological Control of Blood Pumps Using Intrinsic Pump Parameters: A Computer Simulation Study," *Artif. Organs*, 2006.
- [50] M. Granegger, F. Moscato, F. Casas, G. Wieselthaler, and H. Schima, "Development of a pump flow estimator for rotary blood pumps to enhance monitoring of ventricular function," *Artif. Organs*, 2012.
- [51] S. S. Najjar *et al.*, "An analysis of pump thrombus events in patients in the HeartWare ADVANCE bridge to transplant and continued access protocol trial," *J Hear. Lung Transpl.*, vol. 33, no. 1, pp. 23–34, 2014.
- [52] J. M. Stulak, S. Sharma, and S. Maltais, "Management of pump thrombosis in patients with left ventricular assist devices," *Am J Cardiovasc Drugs*, vol. 15, no. 2, pp. 89–94, 2015.
- [53] A. D. DeVore, R. J. Mentz, and C. B. Patel, "Medical management of patients with continuous-flow left ventricular assist devices," *Curr Treat Options Cardiovasc Med*, vol. 16, no. 2, p. 283, 2014.
- [54] W. Hijikata, J. Rao, S. Abe, S. Takatani, and T. Shinshi, "Sensorless Viscosity Measurement in a Magnetically-Levitated Rotary Blood Pump," *Artif organs*, vol. 39, no. 7, pp. 559–568, 2015.
- [55] M. Schmid Daners *et al.*, "Left Ventricular Assist Devices: Challenges Toward Sustaining Long-Term Patient Care," *Ann Biomed Eng*, pp. 1–16, 2017.
- [56] V. Tchanchaleishvili *et al.*, "Clinical Implications of Physiologic Flow Adjustment in Continuous-Flow Left Ventricular Assist Devices," *ASAIO J*, vol. 63, no. 3, pp. 241–250, 2017.
- [57] L. Hubbert, J. Baranowski, B. Delshad, and H. Ahn, "Left Atrial Pressure Monitoring With an Implantable Wireless Pressure Sensor After Implantation of a Left Ventricular Assist Device.," *ASAIO J*, vol. 63, no. 5, pp. e60–e65, 2017.
- [58] M. Guglin, B. George, S. Branam, and A. Hart, "CardioMEMS™ in LVAD Patients : A Case Series," pp. 1–6, 2016.
- [59] S. Stauffert and C. Hierold, "Novel Sensor Integration Approach for Blood Pressure Sensing in Ventricular Assist Devices," *Procedia Eng.*, vol. 168, pp. 71–75, 2016.
- [60] S. A. Dual *et al.*, "R-Wave Magnitude: a Control Input for Ventricular Assist Devices," in *Proceedings of the 8th International Workshop on Biosignal Interpretation*, 2016.
- [61] A.-H. H. AlOmari *et al.*, "Developments in control systems for rotary left ventricular assist devices for heart failure patients: a review.," *Physiol. Meas.*, vol. 34, no. 1, pp. R1-27, 2013.
- [62] C. Reyes *et al.*, "Accuracy of the HVAD pump flow estimation algorithm," *ASAIO J*, vol. 62, no. 1, pp. 15–19, 2016.
- [63] A. Petrou, J. Lee, S. Dual, G. Ochsner, M. Meboldt, and M. Schmid Daners, "Standardized Comparison of Selected Physiological Controllers for Rotary Blood Pumps: In Vitro Study," *Artif. Organs*, vol. 00, no. 3, 2017.
- [64] M. Mansouri *et al.*, "Preload-based Starling-like control of rotary blood pumps: An in-vitro evaluation," *PLoS One*, vol. 12, no. 2, pp. 1–15, 2017.
- [65] G. Ochsner *et al.*, "A Physiological Controller for Turbodynamic Ventricular Assist Devices Based on a Measurement of the Left Ventricular Volume.," *Artif. Organs*, vol. V, no. 26, pp. 1–6, 2013.
- [66] M. C. Stevens *et al.*, "Frank-starling control of a left ventricular assist device," *2011 Annu. Int. Conf. IEEE Eng. Med. Biol. Soc.*, pp. 1335–1338, 2011.
- [67] N. R. Gaddum *et al.*, "Starling-like flow control of a left ventricular assist device: In vitro validation," *Artif. Organs*, vol. 38, no. 3, pp. E46–E56, 2014.
- [68] M. A. Bakouri, R. F. Salamonsen, A. V Savkin, A.-H. H. Alomari, E. Lim, and N. H. Lovell, "A Sliding Mode-Based Starling-Like Controller for Implantable Rotary Blood Pumps," *Artif. Organs*, vol. 38, no. 7, pp. 587–593, 2014.
- [69] A. Arndt, P. Nüsser, B. P. Lampe, and J. Müller, "Physiological Control of a Rotary Left Ventricular Assist Device: Robust Control of Pressure Pulsatility with Suction Prevention and Suppression," vol. 25/7, no. 2, pp. 775–778, 2009.
- [70] Y. Wang, S. C. Koenig, M. S. Slaughter, and G. a. Giridharan, "Rotary Blood Pump Control Strategy for Preventing Left Ventricular Suction," *ASAIO J*, vol. 61, no. 1, pp. 21–30, 2015.
- [71] E. Bullister, S. Reich, and J. Sluetz, "Physiologic Control Algorithms for Rotary Blood Pumps Using Pressure Sensor Input," *Artif. Organs*, vol. 26, no. 11, pp. 931–938, 2002.

References

- [72] F. Casas, N. Ahmed, and A. Reeves, "Minimal sensor count approach to fuzzy logic rotary blood pump flow control.," *ASAIO J.*, vol. 53, no. 2, pp. 140–146, 2007.
- [73] F. Casas, A. Orozco, W. a. Smith, J. a. De Abreu-García, and J. Durkin, "A fuzzy system cardio pulmonary bypass rotary blood pump controller," *Expert Syst. Appl.*, vol. 26, pp. 357–361, 2004.
- [74] A. Verbeni *et al.*, "An Innovative Adaptive Control Strategy for Sensorized Left Ventricular Assist Devices.," *IEEE Trans. Biomed. Circuits Syst.*, vol. 8, no. 5, pp. 1–9, 2014.
- [75] S. Choi, J. R. Boston, and J. F. Antaki, "Hemodynamic Controller for Left Ventricular Assist Device Based on Pulsatility Ratio," *Artif. Organs*, vol. 31(2), no. 2, pp. 114–125, 2007.
- [76] G. A. Giridharan, G. M. Pantalos, K. J. Gillars, S. C. Koenig, and M. Skliar, "Physiologic Control of Rotary Blood Pumps: An In Vitro Study," *ASAIO J.*, vol. 50, no. 5, pp. 403–409, 2004.
- [77] Y. Wu, P. Allaire, G. Tao, H. Wood, D. Olsen, and C. Tribble, "An Advanced Physiological Controller Design for a Left Ventricular Assist Device to Prevent Left Ventricular Collapse," *Artif. Organs*, vol. 27, no. 10, pp. 926–930, 2003.
- [78] A. Petrou *et al.*, "A Physiological Controller for Turbodynamic Ventricular Assist Devices Based on Left Ventricular Systolic Pressure," *Artif Organs*, vol. 40, no. 9, pp. 842–855, Sep. 2016.
- [79] E. Lim *et al.*, "Hemodynamic Response to Exercise and Head-Up Tilt of Patients Implanted With a Rotary Blood Pump: A Computational Modeling Study," *Artif. Organs*, vol. 39, no. 2, pp. E24–E35, 2015.
- [80] J. P. Pauls, M. C. Stevens, N. Bartnikowski, J. F. Fraser, S. D. Gregory, and G. Tansley, "Evaluation of Physiological Control Systems for Rotary Left Ventricular Assist Devices: An In-Vitro Study," *Ann. Biomed. Eng.*, 2016.
- [81] M. Mansouri, R. F. Salamonsen, E. Lim, R. Akmeliawati, and N. H. Lovell, "Preload-Based Starling-Like Control for Rotary Blood Pumps: Numerical Comparison with Pulsatility Control and Constant Speed Operation," *PLoS One*, 2015.
- [82] S. D. Gregory *et al.*, "In Vivo Evaluation of Active and Passive Physiological Control Systems for Rotary Left and Right Ventricular Assist Devices," no. 4, 2016.
- [83] G. Ochsner *et al.*, "In Vivo Evaluation of Physiologic Control Algorithms for Left Ventricular Assist Devices Based on Left Ventricular Volume or Pressure," *ASAIO J.*, vol. 63, no. 5, pp. 568–577, 2017.
- [84] H. Schima *et al.*, "First clinical experience with an automatic control system for rotary blood pumps during ergometry and right-heart catheterization," *J. Hear. Lung Transplant.*, vol. 25, no. 2, pp. 167–173, 2006.
- [85] R. Amacher, G. Ochsner, and M. Schmid Daners, "Synchronized pulsatile speed control of turbodynamic left ventricular assist devices: review and prospects.," *Artif. Organs*, vol. 38, no. 10, pp. 867–75, 2014.
- [86] D. M. Karantonis, E. Lim, D. G. Mason, R. F. Salamonsen, P. J. Ayre, and N. H. Lovell, "Noninvasive activity-based control of an implantable rotary blood pump: Comparative software simulation study," *Artif. Organs*, vol. 34, no. 2, pp. 34–45, 2010.
- [87] R. Amacher *et al.*, "Numerical Optimal Control of Turbo Dynamic Ventricular Assist Devices," *Bioengineering*, pp. 22–46, 2014.
- [88] M. Granegger *et al.*, "Interaction of a Transapical Miniaturized Ventricular Assist Device With the Left Ventricle : Hemodynamic Evaluation and Visualization in an Isolated Heart Setup," *Artif. Organs*, vol. 00, no. 00, 2016.
- [89] V. Tchanchaleishvili *et al.*, *Clinical implications of physiological flow adjustment in continuous-flow left ventricular assist devices*. 2016.
- [90] R. Amacher, G. Ochsner, A. Ferreira, S. Vandenberghe, and M. Schmid Daners, "A robust reference signal generator for synchronized ventricular assist devices," *IEEE Trans Biomed Eng*, vol. 60, no. 8, pp. 2174–2183, 2013.
- [91] A. Petrou *et al.*, "Response of a physiological controller for ventricular assist devices during acute patho-physiological events: an in vitro study," *Biomed. Eng. / Biomed. Tech.*, vol. 0, no. 0, 2017.
- [92] S. Boës, G. Ochsner, R. Amacher, A. Petrou, M. Meboldt, and M. Schmid Daners, "Control of the Fluid Viscosity in a Mock Circulation," *Artif. Organs*, vol. 15, no. 12, 2017.
- [93] A. Petrou, D. Kuster, J. Lee, M. Meboldt, and M. Schmid Daners, "Comparison of flow estimators for ventricular assist devices: an in-vitro and in-vivo study," *Submitt. ASAIO J*, 2018.
- [94] A. Petrou, M. Kanakis, S. Boes, P. Pergantis, M. Meboldt, and M. Schmid Daners, "Viscosity prediction in a physiologically controlled ventricular assist devices:," *IEEE Trans Biomed Eng*, 2018.
- [95] A. Petrou, M. Monn, M. Meboldt, and M. Schmid Daners, "A Novel Multi-objective Physiological

- Control System for Rotary Left Ventricular Assist Devices,” *Ann Biomed Eng*, pp. 1–12, 2017.
- [96] A. Petrou, M. Granegger, M. Meboldt, and M. Schmid Daners, “A versatile hybrid mock circulation for hydraulic investigations of active and passive cardiovascular implants,” *Submitt. ASAIO J*, 2018.
- [97] G. Ochsner *et al.*, “A novel interface for hybrid mock circulations to evaluate ventricular assist devices,” *IEEE Trans. Biomed. Eng.*, vol. 60, no. 2, pp. 507–516, 2013.
- [98] D. Siallagan *et al.*, “Virtual surgical planning, flow simulation and 3D electro-spinning of patient-specific grafts to optimize Fontan hemodynamics,” *J. Thorac. Cardiovasc. Surg.*, vol. 21287, 2017.
- [99] N. H. Cohrs *et al.*, “A Soft Total Artificial Heart—First Concept Evaluation on a Hybrid Mock Circulation,” *Artif. Organs*, vol. 41, no. 10, pp. 948–958, 2017.
- [100] M. Rebholz, R. Amacher, A. Petrou, M. Meboldt, and M. Schmid Daners, “High-frequency operation of a pulsatile VAD – a simulation study,” *Biomed. Eng. / Biomed. Tech.*, vol. 0, no. 0, pp. 1–10, 2016.
- [101] A. C. Guyton and J. E. Hall, *Textbook of medical physiology*. Saunders London, 2011.
- [102] G. F. Mendez and M. R. Cowie, “The epidemiological features of heart failure in developing countries: a review of the literature,” *Int J Cardiol*, vol. 80, no. 2, pp. 213–219, 2001.
- [103] J. J. V McMurray *et al.*, “ESC Guidelines for the diagnosis and treatment of acute and chronic heart failure 2012,” *Eur J Hear. Fail*, vol. 14, no. 8, pp. 803–869, 2012.
- [104] J. Garbade, M. J. Barten, H. B. Bittner, and F.-W. Mohr, “Heart Transplantation and Left Ventricular Assist Device Therapy: Two Comparable Options in End-Stage Heart Failure?,” *Clin Cardiol*, vol. 36, no. 7, pp. 378–382, 2013.
- [105] D. Timms, “A review of clinical ventricular assist devices,” *Med Eng Phys*, vol. 33, no. 9, pp. 1041–1047, 2011.
- [106] D. Mancini and P. C. Colombo, “Left Ventricular Assist Devices: A Rapidly Evolving Alternative to Transplant,” *J Am Coll Cardiol*, vol. 65, no. 23, pp. 2542–2555, 2015.
- [107] E. M. Schumer, M. S. Ising, and M. S. Slaughter, “The current state of left ventricular assist devices: challenges facing further development,” *Expert Rev Cardiovasc Ther*, vol. 13, pp. 1–9, 2015.
- [108] M. Argiriou *et al.*, “Right heart failure post left ventricular assist device implantation,” *J Thorac Dis*, vol. 6, no. Suppl 1, p. S52, 2014.
- [109] N. Moazami *et al.*, “Does pulsatility matter in the era of continuous-flow blood pumps?,” *J Hear. Lung Transpl.*, 2014.
- [110] A.-H. H. AlOmari *et al.*, “Non-invasive measurements based model predictive control of pulsatile flow in an implantable rotary blood pump for heart failure patients,” in *Conference Proceeding IEEE Mediterranean of Control and Automation*, 2011, pp. 491–496.
- [111] Y. Chang, B. Gao, and K. Gu, “A model-free adaptive control to a blood pump based on heart rate.,” *ASAIO J.*, vol. 57, no. 4, pp. 262–267, 2011.
- [112] G. J. Endo, K. Kojima, K. Nakamura, Y. Matsuzaki, and T. Onitsuka, “The meaning of the turning point of the index of motor current amplitude curve in controlling a continuous flow pump or evaluation of left ventricular function,” *Artif Organs*, vol. 27, no. 3, pp. 272–276, 2003.
- [113] D. M. Karantonis, E. Lim, D. G. Mason, R. F. Salamonsen, P. J. Ayre, and N. H. Lovell, “Noninvasive Activity-based Control of an Implantable Rotary Blood Pump: Comparative Software Simulation Study,” *Artif Organs*, vol. 34, no. 2, pp. E34–E45, 2010.
- [114] E. Lim *et al.*, “A method for control of an implantable rotary blood pump for heart failure patients using noninvasive measurements,” *Artif Organs*, vol. 35, no. 8, pp. E174–E180, 2011.
- [115] M. Vollkron, H. Schima, L. Huber, R. Benkowski, G. Morello, and G. Wieselthaler, “Development of a reliable automatic speed control system for rotary blood pumps,” *J Hear. Lung Transpl.*, vol. 24, no. 11, pp. 1878–1885, 2005.
- [116] N. R. Gaddum *et al.*, “Starling-Like Flow Control of a Left Ventricular Assist Device: In Vitro Validation,” *Artif Organs*, vol. 38, no. 3, pp. E46–E56, 2014.
- [117] C. S. Kwan-Gett, M. J. Crosby, A. Schoenberg, S. C. Jacobsen, and W. J. Kolff, “Control systems for artificial hearts.,” *ASAIO J*, vol. 14, no. 1, pp. 284–290, 1968.
- [118] A. Arndt, P. Nüsser, K. Graichen, J. Müller, and B. Lampe, “Physiological control of a rotary blood pump with selectable therapeutic options: control of pulsatility gradient,” *Artif Organs*, vol. 32, no. 10, pp. 761–771, 2008.
- [119] Y. Wang, S. C. Koenig, M. S. Slaughter, and G. A. Giridharan, “Rotary blood pump control strategy for preventing left ventricular suction,” *ASAIO J*, vol. 61, no. 1, pp. 21–30, 2015.
- [120] I. Saito *et al.*, “Preliminary study of physiological control for the undulation pump ventricular assist

References

- device,” in *Proc 32nd Annu Int Conf IEEE Eng Med Biol Soc*, 2010, pp. 5218–5221.
- [121] M. Mansouri, R. F. Salamonsen, E. Lim, R. Akmeliawati, and N. H. Lovell, “Preload-Based Starling-Like Control for Rotary Blood Pumps: Numerical Comparison with Pulsatility Control and Constant Speed Operation,” *PLoS One*, vol. 10, no. 4, p. e0121413, Apr. 2015.
- [122] E. Bullister, S. Reich, and J. Sluetz, “Physiologic control algorithms for rotary blood pumps using pressure sensor input,” *Artif Organs*, vol. 26, no. 11, pp. 931–938, 2002.
- [123] F. M. Colacino, F. Moscato, F. Piedimonte, M. Arabia, and G. a. Danieli, “Left Ventricle Load Impedance Control by Apical VAD Can Help Heart Recovery and Patient Perfusion: A Numerical Study,” *ASAIO J.*, vol. 53, no. 3, pp. 263–277, 2007.
- [124] F. Moscato, M. Vollkron, H. Bergmeister, G. Wieselthaler, E. Leonard, and H. Schima, “Left ventricular pressure--volume loop analysis during continuous cardiac assist in acute animal trials,” *Artif Organs*, vol. 31, no. 5, pp. 369–376, 2007.
- [125] R. Klabunde, *Cardiovascular physiology concepts*. Lippincott Williams & Wilkins, 2011.
- [126] M. C. Stevens *et al.*, “Frank-starling control of a left ventricular assist device,” in *Conf Proc IEEE Eng Med Biol Soc*, 2011, pp. 1335–1338.
- [127] M. A. Bakouri, R. F. Salamonsen, A. V Savkin, A.-H. H. AlOmari, E. Lim, and N. H. Lovell, “A Sliding Mode-Based Starling-Like Controller for Implantable Rotary Blood Pumps,” *Artif Organs*, vol. 38, no. 7, pp. 587–593, 2014.
- [128] J. P. Pauls, M. C. Stevens, N. Bartnikowski, J. F. Fraser, S. D. Gregory, and G. Tansley, “Evaluation of Physiological Control Systems for Rotary Left Ventricular Assist Devices: An In-Vitro Study,” *Ann Biomed Eng*, pp. 1–11, 2016.
- [129] F. Casas, A. Orozco, W. A. Smith, J. A. De Abreu-Garcia, and J. Durkin, “A fuzzy system cardio pulmonary bypass rotary blood pump controller,” *Expert Syst Appl*, vol. 26, no. 3, pp. 357–361, 2004.
- [130] G. A. Giridharan, G. M. Pantalos, K. J. Gillars, S. C. Koenig, and M. Skliar, “Physiologic control of rotary blood pumps: an in vitro study,” *ASAIO J.*, vol. 50, no. 5, pp. 403–409, 2004.
- [131] Y. Wu, P. Allaire, G. Tao, H. Wood, D. Olsen, and C. Tribble, “An advanced physiological controller design for a left ventricular assist device to prevent left ventricular collapse,” *Artif Organs*, vol. 27, no. 10, pp. 926–930, 2003.
- [132] R. W. Troughton *et al.*, “Direct left atrial pressure monitoring in severe heart failure: long-term sensor performance,” *J Cardiovasc Transl Res*, vol. 4, no. 1, pp. 3–13, 2011.
- [133] D. Goldstein and M. Oz, *Cardiac assist devices*. Wiley-Blackwell, 2000.
- [134] P. Naiyanetr, F. Moscato, M. Vollkron, P. Zrunek, G. Wieselthaler, and H. Schima, “Cardiac Contractility Assessment in Rotary Blood Pump Recipients Derived from Pump Flow,” in *Proc. World Congr. of Int Federation of Medical and Biological Eng*, 2009, pp. 434–437.
- [135] P. Naiyanetr *et al.*, “Estimation of cardiac contractility during rotary blood pump support using an index derived from left ventricular pressure,” in *IFMBE Proceeding EMBEC08, “4th European Medical & Biological Engineering Conference, IFMBE European Conference on Biomedical Engineering,”* 2009, pp. 1885–1888.
- [136] M. A. Quiñones, W. H. Gaasch, and J. K. Alexander, “Influence of acute changes in preload, afterload, contractile state and heart rate on ejection and isovolumic indices of myocardial contractility in man.,” *Circulation*, vol. 53, no. 2, pp. 293–302, 1976.
- [137] G. Konieczny, Z. Opilski, T. Pustelny, A. Gacek, P. Gibinski, and R. Kustos, “Results of experiments with fiber pressure sensor applied in the polish artificial heart prosthesis,” *Acta Phys Pol A*, vol. 118, no. 6, pp. 1183–1185, 2010.
- [138] M.-D. Zhou, C. Yang, Z. Liu, J. P. Cysyk, and S.-Y. Zheng, “An implantable Fabry-Pérot pressure sensor fabricated on left ventricular assist device for heart failure,” *Biomed Microdevices*, vol. 14, no. 1, pp. 235–245, 2012.
- [139] J. a. Potkay, “Long term, implantable blood pressure monitoring systems,” *Biomed. Microdevices*, vol. 10, no. 3, pp. 379–392, 2008.
- [140] W. T. Abraham *et al.*, “Safety and accuracy of a wireless pulmonary artery pressure monitoring system in patients with heart failure,” *Am Hear. J.*, vol. 161, no. 3, pp. 558–566, 2011.
- [141] M. C. Stevens, S. Wilson, A. Bradley, J. Fraser, and D. Timms, “Physiological control of dual rotary pumps as a biventricular assist device using a master/slave approach,” *Artif. Organs*, vol. 38, no. 9, pp. 766–74, 2014.
- [142] K. Reesink *et al.*, “Suction due to left ventricular assist: implications for device control and management,” *Artif organs*, vol. 31, no. 7, pp. 542–549, 2007.

- [143] F. Moscato, M. Arabia, F. M. Colacino, P. Naiyanetr, G. a Danieli, and H. Schima, “Left ventricle afterload impedance control by an axial flow ventricular assist device: a potential tool for ventricular recovery.,” *Artif. Organs*, vol. 34, no. 9, pp. 736–44, 2010.
- [144] H. Schima *et al.*, “First clinical experience with an automatic control system for rotary blood pumps during ergometry and right-heart catheterization,” *J Hear. Lung Transpl.*, vol. 25, no. 2, pp. 167–173, 2006.
- [145] V. Tchanchaleishvili *et al.*, “Clinical implications of physiological flow adjustment in continuous-flow left ventricular assist devices.,” *ASAIO J*, 2016.
- [146] G. Ochsner *et al.*, “In vivo Evaluation of Physiological Control Algorithms for LVADs based on Left Ventricular Volume or Pressure.,” *ASAIO J*, 2017.
- [147] E. Lim *et al.*, “Hemodynamic Response to Exercise and Head-Up Tilt of Patients Implanted With a Rotary Blood Pump: A Computational Modeling Study,” *Artif organs*, vol. 39, no. 2, pp. E24–E35, 2015.
- [148] G. Ochsner, R. Amacher, and M. Schmid Daners, “Emulation of Ventricular Suction in a Hybrid Mock Circulation,” pp. 3108–3112, 2013.
- [149] C. Göbel *et al.*, “Development of the MEDOS/HIA DeltaStream extracorporeal rotary blood pump,” *Artif. Organs*, vol. 25, no. 5, pp. 358–365, 2001.
- [150] R. F. Salamonsen *et al.*, “Theoretical Foundations of a Starling-Like Controller for Rotary Blood Pumps,” *Artif Organs*, vol. 36, no. 9, pp. 787–796, 2012.
- [151] L. Guzzella, *{A}nalysis and synthesis of single-input-single-output control systems*, 1. Zürich: Vdf Hochschulverlag an der ETH Zürich, 2007.
- [152] A. Barbone *et al.*, “Comparison of Right and Left Ventricular Responses to Left Ventricular Assist Device Support in Patients With Severe Heart Failure,” pp. 670–676, 2001.
- [153] L. Brancato, G. Keulemans, T. Verbelen, B. Meyns, and R. Puers, “An implantable intravascular pressure sensor for a ventricular assist device,” *Micromachines*, vol. 7, no. 8, pp. 1–17, 2016.
- [154] R. W. Troughton *et al.*, “Direct Left Atrial Pressure Monitoring in Severe Heart Failure: Long-Term Sensor Performance,” *J. Cardiovasc. Transl. Res.*, vol. 4, no. 1, pp. 3–13, 2011.
- [155] C. Jenkins, S. Moir, J. Chan, D. Rakhit, B. Haluska, and T. H. Marwick, “Left ventricular volume measurement with echocardiography: A comparison of left ventricular opacification, three-dimensional echocardiography, or both with magnetic resonance imaging,” *Eur. Heart J.*, vol. 30, no. 1, pp. 98–106, 2009.
- [156] F. M. Colacino, “Left ventricle load impedance control by apical VAD can help heart recovery and patient perfusion; a numerical study,” 2007.
- [157] P. Naiyanetr, “A Review of Cardiac Contractility Indices during LVAD Support,” no. Lvv, pp. 103–106, 2012.
- [158] L. Fresiello, B. Meyns, A. Di Molfetta, and G. Ferrari, “A model for the cardiorespiratory response to aerobic exercise in healthy and heart failure conditions,” *Front Physiol*, vol. 7, p. 189, 2016.
- [159] K. Reesink *et al.*, “Suction Due to Left Ventricular Assist: Implications for Device Control and Management,” *Artif Organs*, vol. 31, no. 7, pp. 542–549, 2007.
- [160] M. Vollkron, H. Schima, L. Huber, and G. Wieselthaler, “Interaction of the Cardiovascular System with an Implanted Rotary Assist Device: Simulation Study with a Refined Computer Model,” *Artif. Organs*, vol. 26(4), no. 4, pp. 349–359, 2002.
- [161] J. R. Boston, J. F. Antaki, and M. a Simaan, “Hierarchical Control of Heart-Assist Devices,” *IEEE Robot. Autom. Mag.*, vol. 10, no. March, pp. 54–64, 2003.
- [162] K. W. Gwak, J. F. Antaki, B. E. Paden, and B. Kang, “Safety-enhanced optimal control of turbodynamic blood pumps,” *Artif. Organs*, vol. 35, no. 7, pp. 725–732, 2011.
- [163] S. H. Jansen-Park *et al.*, “A monitoring and physiological control system for determining aortic valve closing with a ventricular assist device,” *Eur. J. Cardio-thoracic Surg.*, vol. 46, no. 3, pp. 356–360, 2014.
- [164] H. Konishi *et al.*, “Controller for an Axial Flow Blood Pump,” *Artif. Organs*, vol. 20, no. 6, pp. 618–620, 1996.
- [165] K. Ohuchi *et al.*, “Control Strategy for Rotary Blood Pumps,” *Artif. Organs*, vol. 25, no. 5, pp. 366–370, 2001.
- [166] M. Oshikawa, K. Araki, G. Endo, H. Anai, and M. Sato, “Sensorless controlling method for a continuous flow left ventricular assist device,” *Artif Organs*, vol. 24, no. 8, pp. 600–605, 2000.

References

- [167] R. F. Salamonsen *et al.*, “Exercise Studies in Patients With Rotary Blood Pumps: Cause, Effects, and Implications for Starling-Like Control of Changes in Pump Flow,” *Artif. Organs*, vol. 37, no. 8, pp. 695–703, 2013.
- [168] D. G. Mason, A. K. Hilton, and R. F. Salamonsen, “Reliable Suction Detection for Patients With Rotary Blood Pumps,” *ASAIO J.*, vol. 54, no. 4, pp. 359–366, 2008.
- [169] O. Voigt, R. J. Benkowski, and G. F. Morello, “Suction detection for the MicroMed DeBakey Left Ventricular Assist Device.,” *ASAIO J.*, vol. 51, no. February, pp. 321–328, 2005.
- [170] M. Vollkron, H. Schima, L. Huber, R. Benkowski, G. Morello, and G. Wieselthaler, “Advanced suction detection for an axial flow pump.,” *Artif. Organs*, vol. 30, no. 9, pp. 665–70, 2006.
- [171] R. F. Salamonsen, E. Lim, J. Moloney, N. H. Lovell, and F. L. Rosenfeldt, “Anatomy and Physiology of Left Ventricular Suction Induced by Rotary Blood Pumps,” *Artif. Organs*, vol. 39, no. 4, p. n/a-n/a, 2015.
- [172] Y. Wang and M. a Simaan, “A suction detection system for rotary blood pumps based on the Lagrangian support vector machine algorithm.,” *IEEE J. Biomed. Heal. informatics*, vol. 17, no. 3, pp. 654–63, 2013.
- [173] A. Yuhki, E. Hatoh, M. Nogawa, M. Miura, Y. Shimazaki, and S. Takatani, “Detection of suction and regurgitation of the implantable centrifugal pump based on the motor current waveform analysis and its application to optimization of pump flow,” *Artif. Organs*, vol. 23, no. 6, pp. 532–537, 1999.
- [174] M. Ando *et al.*, “A novel counterpulsation mode of rotary left ventricular assist devices can enhance myocardial perfusion,” *Int J Artif Organs*, vol. 14, no. 3, pp. 185–191, 2011.
- [175] M. Arakawa *et al.*, “Novel control system to prevent right ventricular failure induced by rotary blood pump,” *J. Artif. Organs*, vol. 17, no. 2, pp. 135–141, 2014.
- [176] Y. Kishimoto *et al.*, “Development of a novel drive mode to prevent aortic insufficiency during continuous-flow LVAD support by synchronizing rotational speed with heartbeat,” *J. Artif. Organs*, vol. 16, no. 2, pp. 129–137, 2013.
- [177] T. Pirbodaghi, A. Weber, S. Axiak, T. Carrel, and S. Vandenberghe, “Asymmetric speed modulation of a rotary blood pump affects ventricular unloading,” *Eur. J. Cardio-thoracic Surg.*, vol. 43, no. 2, pp. 383–388, 2013.
- [178] K. G. Soucy *et al.*, “Rotary pump speed modulation for generating pulsatile flow and phasic left ventricular volume unloading in a bovine model of chronic ischemic heart failure,” *J. Hear. Lung Transplant.*, vol. 34, no. 1, pp. 122–131, 2015.
- [179] E. Tuzun *et al.*, “The effects of continuous and intermittent reduced speed modes on renal and intestinal perfusion in an ovine model.,” *ASAIO J.*, vol. 60, no. 1, pp. 19–24, 2014.
- [180] A. Umeki *et al.*, “Change in myocardial oxygen consumption employing continuous-flow LVAD with cardiac beat synchronizing system, in acute ischemic heart failure models,” *J. Artif. Organs*, vol. 16, no. 2, pp. 119–128, 2013.
- [181] S. Choi, J. F. Antaki, J. R. Boston, and D. Thomas, “A Sensorless Approach to Control of a Turbodynamic Left Ventricular Assist System,” *IEEE Trans. Control Syst. Technol.*, vol. 9, no. 3, pp. 473–482, 2001.
- [182] K.-W. Gwak, “Application of extremum seeking control to turbodynamic blood pumps.,” *ASAIO J.*, vol. 53, no. 4, pp. 403–409, 2007.
- [183] P. S. Olegario *et al.*, “Outflow Control for Avoiding Atrial Suction in a Continuous Flow Total Artificial Heart,” *Artif. Organs*, vol. 27, no. 1, pp. 92–98, 2003.
- [184] R. F. Salamonsen, D. G. Mason, and P. J. Ayre, “Response of rotary blood pumps to changes in preload and afterload at a fixed speed setting are unphysiological when compared with the natural heart.,” *Artif. Organs*, vol. 35, no. 3, pp. E47-53, 2011.
- [185] E. M. Schumer, M. S. Ising, and M. S. Slaughter, “The current state of left ventricular assist devices: challenges facing further development,” *Expert Rev. Cardiovasc. Ther.*, vol. 9072, no. November, pp. 1–9, 2015.
- [186] A. Xie, K. Phan, and T. D. Yan, “Durability of continuous-flow left ventricular assist devices: a systematic review,” *Ann Thorac Surg*, vol. 3, no. 6, p. 547, 2014.
- [187] E. Lim *et al.*, “A method for control of an implantable rotary blood pump for heart failure patients using noninvasive measurements.,” *Artif. Organs*, 2011.
- [188] F. Moscato, M. Arabia, P. Naiyanetr, G. a Danieli, and H. Schima, “Control of a rotary blood pump for defined ventricular unloading: A potential tool for ventricular recovery,” *World Congr. Med. Phys. Biomed. Eng. Sept. 7 - 12, 2009, Munich, Ger.*, vol. 25/7, pp. 502–505, 2009.

- [189] E. Lim *et al.*, “A cardiovascular mathematical model of graded head-up tilt,” *PLoS One*, vol. 8, no. 10, p. e77357, 2013.
- [190] E. Lim *et al.*, “Parameter-optimized model of cardiovascular--rotary blood pump interactions,” *IEEE Trans. Biomed. Eng.*, vol. 57, no. 2, pp. 254–266, 2010.
- [191] F. Liang and H. Liu, “Simulation of hemodynamic responses to the Valsalva maneuver: an integrative computational model of the cardiovascular system and the autonomic nervous system,” *J Physiol Sci*, vol. 56, no. 1, pp. 45–65, 2006.
- [192] D. L. Timms, S. D. Gregory, M. C. Stevens, and J. F. Fraser, “Haemodynamic modeling of the cardiovascular system using mock circulation loops to test cardiovascular devices,” in *Engineering in Medicine and Biology Society, EMBC, 2011 Annual International Conference of the IEEE*, 2011, pp. 4301–4304.
- [193] E. P. Sharpey-Schafer, “Effects of Valsalva’s manoeuvre on the normal and failing circulation,” *BMJ*, vol. 1, no. 4915, p. 693, 1955.
- [194] P. SAMET, “Hemodynamic sequelae of cardiac arrhythmias,” *Circulation*, vol. 47, no. 2, pp. 399–407, 1973.
- [195] J. D. MacDougall, R. S. McKelvie, D. E. Moroz, D. G. Sale, N. McCartney, and F. Buick, “Factors affecting blood pressure during heavy weight lifting and static contractions,” *J APPL PHYSIOL*, vol. 73, no. 4, pp. 1590–1597, 1992.
- [196] A. D. Ten Harkel, J. J. Van Lieshout, E. J. Van Lieshout, and W. Wieling, “Assessment of cardiovascular reflexes: influence of posture and period of preceding rest,” *J APPL PHYSIOL*, vol. 68, no. 1, pp. 147–153, 1990.
- [197] J. J. Bergan and N. Bunke-Paquette, *The vein book*. Oxford University Press, 2014.
- [198] G. M. Felker, P. S. Cuculich, and M. Gheorghade, “The Valsalva maneuver: a bedside ‘biomarker’ for heart failure,” *Am J Med*, vol. 119, no. 2, pp. 117–122, 2006.
- [199] W. C. Little, W. K. Barr, and M. H. Crawford, “Altered effect of the Valsalva maneuver on left ventricular volume in patients with cardiomyopathy,” *Circulation*, vol. 71, no. 2, pp. 227–233, 1985.
- [200] A. L. Goldberger *et al.*, “Physiobank, physiotookit, and physionet components of a new research resource for complex physiologic signals,” *Circulation*, vol. 101, no. 23, pp. e215–e220, 2000.
- [201] M. Behbahani *et al.*, “A review of computational fluid dynamics analysis of blood pumps,” *Eur J Appl Math*, vol. 20, no. 04, p. 363, Mar. 2009.
- [202] U. P. Jorde *et al.*, “Identification and management of pump thrombus in the HeartWare left ventricular assist device system,” *JACC Hear. Fail*, vol. 3, no. 11, pp. 849–856, 2015.
- [203] T. Kitamura *et al.*, “Physical model-based indirect measurements of blood pressure and flow using a centrifugal pump,” *Artif. Organs*, vol. 24, no. 8, pp. 589–593, 2000.
- [204] E. Lim, D. M. Karantonis, J. A. Reizes, S. L. Cloherty, D. G. Mason, and N. H. Lovell, “Noninvasive average flow and differential pressure estimation for an implantable rotary blood pump using dimensional analysis,” *IEEE Trans. Biomed. Eng.*, 2008.
- [205] A.-H. H. AlOmari *et al.*, “Developments in control systems for rotary left ventricular assist devices for heart failure patients: a review,” *Physiol. Meas.*, 2013.
- [206] M. S. Slaughter *et al.*, “Intraoperative Evaluation of the HeartMate II Flow Estimator,” *J. Hear. Lung Transplant.*, vol. 28, no. 1, pp. 39–43, 2009.
- [207] G. A. Giridharan *et al.*, “Left Ventricular Volume Unloading with Axial and Centrifugal Rotary Blood Pumps,” *ASAIO J.*, vol. 61, no. 3, pp. 292–300, 2015.
- [208] K. Bourque *et al.*, “Design Rationale and Pre-Clinical Evaluation of the HeartMate 3 Left Ventricular Assist System for Hemocompatibility,” *ASAIO J.*, vol. 62, no. 4, pp. 375–383, 2016.
- [209] K. A. Pennings *et al.*, “Pump flow estimation from pressure head and power uptake for the HeartAssist5, HeartMate II, and HeartWare VADs,” *Asaio J*, vol. 59, no. 4, pp. 420–426, 2013.
- [210] P. Pillay and R. Krishnan, “Modeling, Simulation, and Analysis of Permanent-Magnet Motor Drives, Part II: The Brushless DC Motor Drive,” *IEEE Trans Biomed Eng*, vol. 25, no. 2, pp. 274–279, 1989.
- [211] A. Arndt, P. Nüsser, and B. Lampe, “Fully Autonomous Preload-Sensitive Control of Implantable Rotary Blood Pumps,” vol. 34, no. 9, pp. 726–735, 2010.
- [212] C. Reyes *et al.*, “Accuracy of the HVAD Pump Flow Estimation Algorithm,” *ASAIO J.*, vol. 62, no. 1, pp. 15–19, 2016.
- [213] P. Naiyanetr, F. Moscato, M. Vollkron, D. Zimpfer, G. Wieselthaler, and H. Schima, “Continuous assessment of cardiac function during rotary blood pump support: A contractility index derived from

- pump flow,” *J Hear. Lung Transpl.*, 2010.
- [214] J. G. Rogers, R. R. Bostic, K. B. Tong, R. Adamson, M. Russo, and M. S. Slaughter, “Cost-effectiveness analysis of continuous flow left ventricular assist devices as destination therapy,” *Circ Hear. Fail.*, p. 100-111, 2011.
- [215] M. Granegger *et al.*, “Continuous Monitoring of Aortic Valve Opening in Rotary Blood Pump Patients,” *IEEE Trans. Biomed. Eng.*, vol. 63, no. 6, pp. 1201–1207, 2016.
- [216] F. Moscato, M. Granegger, M. Edelmayer, D. Zimpfer, and H. Schima, “Continuous monitoring of cardiac rhythms in left ventricular assist device patients,” *Artif. Organs*, vol. 38, no. 3, pp. 191–198, 2014.
- [217] F. Moscato, M. Granegger, P. Naiyanetr, G. Wieselthaler, and H. Schima, “Evaluation of Left Ventricular Relaxation in Rotary Blood Pump Recipients Using the Pump Flow Waveform: A Simulation Study,” *Artif Organs*, pp. 470–478, 2011.
- [218] P. Naiyanetr, F. Moscato, M. Vollkron, D. Zimpfer, G. Wieselthaler, and H. Schima, “Continuous assessment of cardiac function during rotary blood pump support: A contractility index derived from pump flow,” *J Hear. Lung Transpl.*, vol. 29, no. 1, pp. 37–44, 2010.
- [219] P. E. Allaire, H. G. Wood, R. S. Awad, and D. B. Olsen, “Blood flow in a continuous flow ventricular assist device,” *Artif organs*, vol. 23, no. 8, pp. 769–773, 1999.
- [220] A. M. Scandroglio *et al.*, “Diagnosis and treatment algorithm for blood flow obstructions in patients with left ventricular assist device,” *J Am Coll Cardiol*, vol. 67, no. 23, pp. 2758–2768, 2016.
- [221] J. N. Katz, B. C. Jensen, P. P. Chang, S. L. Myers, F. D. Pagani, and J. K. Kirklin, “A multicenter analysis of clinical hemolysis in patients supported with durable, long-term left ventricular assist device therapy,” *J Hear. Lung Transpl.*, vol. 34, no. 5, pp. 701–709, 2015.
- [222] D. M. Karantonis, N. H. Lovell, P. J. Ayre, D. G. Mason, and S. L. Cloherty, “Identification and classification of physiologically significant pumping states in an implantable rotary blood pump,” *Artif organs*, vol. 30, no. 9, pp. 671–679, 2006.
- [223] G. Carneiro, J. C. Nascimento, and A. Freitas, “The segmentation of the left ventricle of the heart from ultrasound data using deep learning architectures and derivative-based search methods,” *IEEE Trans Image*, vol. 21, no. 3, pp. 968–982, 2012.
- [224] E. W. Merrill, E. R. Gilliland, G. Cokelet, H. Shin, A. Britten, and R. E. Wells, “Rheology of blood and flow in the microcirculation,” *Eur J Appl Physiol*, vol. 18, no. 2, pp. 255–260, 1963.
- [225] C. M. Bishop, *Pattern recognition and machine learning*. springer, 2006.
- [226] M. Ebden, “Gaussian Processes: A Quick Introduction.”
- [227] “HeartWare, Inc.” 2012.
- [228] D. H. Wolpert, “Stacked generalization,” *Neural Networks*, vol. 5, pp. 241–259, 1992.
- [229] K. A. Mann, S. Deutsch, J. M. Tarbell, D. B. Geselowitz, G. Rosenberg, and W. S. Pierce, “An experimental study of Newtonian and non-Newtonian flow dynamics in a ventricular assist device,” *J Biomech Eng*, vol. 109, no. 2, pp. 139–147, 1987.
- [230] R. F. Salamonsen *et al.*, “Theoretical Foundations of a Starling-Like Controller for Rotary Blood Pumps,” *Artif. Organs*, vol. 36, no. 4, pp. 787–796, 2012.
- [231] A. Arndt, P. Nüsser, and B. Lampe, “Fully Autonomous Preload-Sensitive Control of Implantable Rotary Blood Pumps,” *Artif organs*, vol. 34, no. 9, pp. 726–735, 2010.
- [232] H. L. Ooi, S. C. Ng, E. Lim, R. F. Salamonsen, A. P. Avolio, and N. H. Lovell, “Robust aortic valve non-opening detection for different cardiac conditions,” *Artif. Organs*, vol. 38, no. 3, 2014.
- [233] A. C. Guyton, “Textbook of medical physiology,” *Acad. Med.*, vol. 36, no. 5, p. 556, 1961.
- [234] D. Camboni *et al.*, “Left ventricular support adjustment to aortic valve opening with analysis of exercise capacity,” *J Cardiothorac Surg*, vol. 9, no. 1, p. 93, 2014.
- [235] M. Mansouri, R. F. Salamonsen, E. Lim, R. Akmeiliawati, and N. H. Lovell, “Preload-based starling-like control for rotary blood pumps: Numerical comparison with pulsatility control and constant speed operation,” *PLoS One*, vol. 10, no. 4, pp. 1–16, 2015.
- [236] H. Schima, K. Dimitrov, and D. Zimpfer, “Debate: creating adequate pulse with a continuous flow ventricular assist device: can it be done and should it be done? Probably not, it may cause more problems than benefits!,” *Curr. Opin. Cardiol.*, vol. 31, no. 3, pp. 337–342, 2016.
- [237] A. Üндar, “Myths and truths of pulsatile and nonpulsatile perfusion during acute and chronic cardiac support,” *Artif organs*, vol. 28, no. 5, pp. 439–443, 2004.
- [238] S.-H. Jansen-Park *et al.*, “A monitoring and physiological control system for determining aortic valve closing with a ventricular assist device,” *Eur J Cardiothorac Surg*, p. ezu006, 2014.

- [239] J. A. Crestanello, D. A. Orsinelli, M. S. Firstenberg, and C. Sai-Sudhakar, “Aortic valve thrombosis after implantation of temporary left ventricular assist device,” *Interact. Cardiovasc. Thorac. Surg.*, vol. 8, no. 6, pp. 661–662, 2009.
- [240] S. Staufert and C. Hierold, “Novel Sensor Integration Approach for Blood Pressure Sensing in Ventricular Assist Devices,” vol. 168, pp. 71–75, 2016.
- [241] D. Timms, M. Hayne, K. McNeil, and A. Galbraith, “A complete mock circulation loop for the evaluation of left, right, and biventricular assist devices,” *Artif organs*, vol. 29, no. 7, pp. 564–572, 2005.
- [242] M. Darowski *et al.*, “A new hybrid (hydro-numerical) model of the circulatory system,” *Bull PolAcad Sci - Tech Sci*, vol. 61, no. 4, pp. 993–1003, 2013.
- [243] B. J. E. Misgeld, D. Rüschen, S. Schwandtner, S. Heinke, M. Walter, and S. Leonhardt, “Robust decentralised control of a hydrodynamic human circulatory system simulator,” *Biomed Signal Process Control*, vol. 20, pp. 35–44, 2015.
- [244] F. Nestler, A. P. Bradley, S. J. Wilson, D. L. Timms, O. H. Frazier, and W. E. Cohn, “A hybrid mock circulation loop for a total artificial heart,” *Artif organs*, vol. 38, no. 9, pp. 775–782, 2014.
- [245] N. Westerhof, J.-W. Lankhaar, and B. E. Westerhof, “The arterial windkessel,” *Med Biol Eng Comput*, vol. 47, no. 2, pp. 131–141, 2009.
- [246] T. Krabatsch, “Biventricular Circulatory Support with Two Implantable Continuous-Flow Pumps,” in *Mechanical Circulatory Support in End-Stage Heart Failure*, Springer, 2017, pp. 305–311.
- [247] T. Krabatsch *et al.*, “Biventricular circulatory support with two miniaturized implantable assist devices,” *Circulation*, vol. 124, no. 11 suppl 1, pp. S179–S186, 2011.
- [248] S. M. Sale and N. G. Smedira, “Total artificial heart.,” *Best Pr. Res Clin Anaesthesiol*, vol. 26, no. 2, pp. 147–165, Jun. 2012.
- [249] Y. Abe *et al.*, “Physiological control of a total artificial heart: conductance-and arterial pressure-based control,” *J Appl Physiol*, vol. 84, no. 3, pp. 868–876, 1998.
- [250] S. D. Gregory *et al.*, “In vivo evaluation of active and passive physiological control systems for rotary left and right ventricular assist devices,” *Artif organs*, vol. 40, no. 9, pp. 894–903, 2016.
- [251] D. A. de Zélicourt and V. Kurtcuoglu, “Patient-Specific Surgical Planning, Where Do We Stand? The Example of the Fontan Procedure,” *Ann. Biomed. Eng.*, vol. 44, no. 1, pp. 174–186, 2016.
- [252] M. Granegger, M. Schweiger, M. Schmid Daners, M. Meboldt, and M. Hübler, “Cavopulmonary mechanical circulatory support in Fontan patients and the need for physiologic control: A computational study with a closed-loop exercise model,” *Int. J. Artif. Organs*, 2018.
- [253] S. V. Deo, V. Sharma, Y. H. Cho, I. K. Shah, and S. J. Park, “De Novo Aortic Insufficiency During Long-Term Support on a Left Ventricular Assist Device,” *ASAIO J.*, vol. 60, no. 2, pp. 183–188, 2014.
- [254] W. A. Zoghbi *et al.*, “Recommendations for evaluation of the severity of native valvular regurgitation with two-dimensional and Doppler echocardiography,” *J Am Soc Echocardiogr*, vol. 16, no. 7, pp. 777–802, 2003.
- [255] H. A. Khalil *et al.*, “Continuous flow total artificial heart: modeling and feedback control in a mock circulatory system.,” *ASAIO J*, vol. 54, no. 3, pp. 249–255, 2008.
- [256] D. Zimpfer *et al.*, “Post-transplant survival after lowering fixed pulmonary hypertension using left ventricular assist devices,” *Eur. J. Cardio-thoracic Surg.*, vol. 31, no. 4, pp. 698–702, 2007.
- [257] J. R. Crosby *et al.*, “Physiological characterization of the SynCardia total artificial heart in a mock circulation system.,” *ASAIO J.*, vol. 61, no. 3, pp. 274–281, 2015.
- [258] N. Stergiopulos, B. E. Westerhof, and N. Westerhof, “Total arterial inertance as the fourth element of the windkessel model.,” *Am J Physiol*, vol. 276, no. 1 Pt 2, pp. H81–H88, Jan. 1999.
- [259] S. Schampaert, K. Pennings, M. J. G. de Molengraft, N. H. J. Pijls, F. N. de Vosse, and M. C. M. Rutten, “A mock circulation model for cardiovascular device evaluation,” *Physiol Meas*, vol. 35, no. 4, p. 687, 2014.
- [260] P. Ruiz, M. A. Rezaenia, A. Rahideh, T. R. Keeble, M. T. Rothman, and T. Korakianitis, “In vitro cardiovascular system emulator (bioreactor) for the simulation of normal and diseased conditions with and without mechanical circulatory support,” *Artif organs*, vol. 37, no. 6, pp. 549–560, 2013.
- [261] M. D. Rodefeld *et al.*, “Cavopulmonary assist for the univentricular Fontan circulation: von Karman viscous impeller pump,” *J Thorac Cardiovasc Surg*, vol. 140, no. 3, pp. 529–536, 2010.